Effect of K_2O, Cr_2O_3, H_2O and CO_2 on the partial melting behaviour of spinel lherzolite in system CaO-MgO-Al_2O_3-SiO_2±K_2O±Cr_2O_3±H_2O±CO_2 at 11 kbar

by

Liu (Louie), Xi

A thesis submitted for the degree of

Doctor of Philosophy

of the Australian National University

Canberra

March 2003

Declaration

This thesis contains the results of research done at the Research School of Earth Sciences, Australian National University from March 1999 to March 2003. Except where mentioned in the text or the acknowledgments, the research described in the thesis is my own. No part of this thesis has been submitted to any other university.

Liu (Louie), Xi

Canberra, February 2003

Acknowledgments

I would like to thank my wife, Huichun Peng, for her continuous support to my studying, her maintenance of the home and her looking after my son. I would like to thank my boy, Yixiang Liu, for being such a good boy and for his sacrifice of being accompanied and holiday when he grows up. Being abroad is tough, but they successfully overcame all pressure. Also I want to thank my brother and my sisters who took care of my parents when I was so far away from hometown for such a long time.

Special thanks go to my supervisor, Dr Hugh StC O'Neill, who took the trouble sending me email and then letter to bring me to the beautiful country, Australia. Without his effort, it were possible that I would never come to the big stage of international world and be known by the international scientific community. Also I would like to thank him for his understanding, encouragement, support and guidance throughout all these years. His great effect in helping me to write this thesis is also sincerely acknowledged.

Thanks to Professor David Green, Dr Jorg Hermann, Dr Andrew Berry, Dr Sue Kesson, Professor Jianping Li (visitor at RSES from Chinese Academy of Sciences), Dr Yaxley Gregory, Dr Stephen Eggins, Professor Max Schmidt (visitor at RSES from ETH), Dr Stephan Klemme, Professor David Ellis (the ANU geology department), Professor Qingchen Wang (Chinese Academy of Sciences), Dr Liangyue Cao (Australian Bureau of Agricultural and Resource Economics), Dr John Mavrogenes and Dr Uli Troitzsch (the ANU geology department) for serious discussions and constructive suggestions, reading early versions of part of the thesis, supplies of special computer programs (Magma2, Tripplot, Mass-balance and Falloon-program), supplies of experimental material (ruby disc), or showing me experimental techniques like FTIR and X-ray diffraction. Dr. Andrew Berry also helped me a lot in preparing this thesis.

Many thanks to the RSES high-pressure team Bill Hibberson, Dean Scott, Nick Ware and Mike Shelley. They showed me, step by step and hand by hand, how to do the piston-cylinder experiments, how to prepare the sample for electron probe and ICP-MS, and how to get the analysis numbers. When I messed around in the lab, they were always kind and ready to solve the problems I created.

Also I would like to thank Frank Brink and Dr Roger Heady at EMU of ANU for their maintenance of the Cambridge Instrument and the JOEL 6400 electron probe. They said that they would settle down at EMU a bed for me; their project, however, had not been completed when I finished my time down there.

Thanks to Dr Ian Jackson and Harry Kokkonen at the RSES geophysics group for their permission of using their lab to prepare the thin sections for FTIR analyses. Harry also helped in preparing some of the samples.

I would like to thank Alistair Hack, Silvano Sommacal, Linda Glass, Wilfred Lus, Dr Ulrich Faul, Dr Tomoaki Morishita, Naomi Douglas, Dagmar Kelly and more for the happy time of playing together soccer and Australian Touch, and for their friendship. We had good times and good fun. It was a pity that nobody here likes playing basketball.

Thanks to my Chinese friends, Chinese Australian friends and Australian friends out of the school. Their presence in the past helped making my life here very enjoyable.

This work was carried out under an A. E. Ringwood Memorial Scholarship and an Australian International Postgraduate Researcher Scholarship.

Abstract

Magmatism happening on the earth and other planets mainly involves SiO_2, TiO_2, Al_2O_3, Cr_2O_3, Fe_2O_3, FeO, MgO, CaO, Na_2O, K_2O, H_2O and CO_2. It is reasonably approximated by the partial melting behaviour of the system CaO-MgO-Al_2O_3-SiO_2 (CMAS) which has been extensively studied. The effects of FeO and Na_2O on this process have been studied in the systems CMAS-FeO* and CMAS-Na_2O, respectively. The geochemical behaviour of other oxides in the partial melting process, however, has not been rigorously studied so far. The current study is intended to partially address this issue, and my attention has been mainly focused on the phase assemblage of spinel lherzolite plus melt (olivine (Ol) + spinel (Sp) + orthpyroxene (Opx) + clinopyroxene (Cpx) + melt (Melt)).

In this PhD study, high temperature-high pressure experiments have been carried out in the systems CMAS ± K_2O (Chapter 2), CMAS-Cr_2O_3-K_2O (Chapter 3) and CMAS-H_2O-CO_2 (Chapter 4) at 11 kbar and from 1200 °C to 1380 °C using piston-cylinder apparatus. Due to the inaccuracy of literature data in the system CMAS-Na_2O (CMASN), some experiments have also been conducted in this system. During this study, new experimental techniques have been developed and successfully applied. The major analytical techniques used in this study are electron microprobe, infrared spectroscopy, scanning electron microprobe, X-ray diffraction and laser-ablation ICP-MS.

The study in the system CMAS ± K_2O (Chapter 2) at 11 kbar suggests that partial melting for a spinel lherzolite occurs over a wide temperature range (~ 60 degrees from ~ 1260 °C to ~ 1320 °C), produces a wide range of melt composition (from quartz tholeiite at low temperatures to olivine basalt at high temperatures) and occurs according to different melting reactions. The major changes of the partial melting reaction caused by the addition of K_2O into the system CMAS are that spinel joins olivine to be in a reaction relationship with melt, and Opx replaces Cpx to be the number one contributor to the partial melting process at high K_2O concentrations.

The extrapolated result at 0 wt% K_2O (i. e., the isobarically invariant point of the system CMAS), a temperature of ~ 1319 °C with a melt composition of 49.09 wt% SiO_2, 20.14 wt% Al_2O_3, 15.45 wt% MgO and 15.33 wt% CaO, from the experiments displaying a spinel-lherzolite phase assemblage in the system CMAS + K_2O, is fully confirmed by reversal experiments using the extrapolated melt composition, with and

without the addition of olivine. This identifies a new experiment method (the K_2O-method) which potentially can be applied to indirectly determine melt compositions in low variance phase assemblages.

The study in the system CMAS ± K_2O has also been extended to locate several other isobarically invariant points at 11 kbar, namely Sp + Opx + Cpx + anorthite (An) + Melt at ~ 1320 °C in the system CMAS, Fo + Sp + Opx + Cpx + sanidine (San) +Melt at ~ 1240 °C, Sp + Opx + Cpx + An + San + Melt at ~ 1230 °C and Opx + Sp + An + San + sapphirine (Sapph) + Melt at ~ 1230 °C in the system CMAS-K_2O. The coexisting of An with San observed here provides valuable data for the thermodynamic modelling of plagioclase, which has only had limited success.

The K_2O method designed and justified in the study in the system CMAS ± K_2O has been successfully applied in my study in the system CMAS + Cr_2O_3 (Chapter 3). This technique not only helps to overcome the isobarically pseudo-invariant nature of the partial melting process of spinel lherzolite in this system, but also helps to modify the melt so that it becomes quenchable. In order to ensure most chromium is Cr^{3+}, Fe_2O_3 is used as external hydrogen fugacity buffer in the experiments. With these experimental techniques, the effect of Cr_2O_3on partial melting is successfully studied for the first time.

During the partial melting process Cr_2O_3 tends to retain in the solid phases and the distribution coefficient of Cr_2O_3 observed here is 0.84 between Ol and Melt, 165.8 between Sp and Melt, 7.2 between Opx and Melt, and 8.7 between Cpx and melt. These numbers suggest that Cr^{3+} is extremely compatible during partial melting process. The effect of chromium on the melt compositions, therefore, is not readily apparent from the melts themselves.

My experiments in the system CMAS + Cr_2O_3 indicate that Cr_2O_3 increases the solidus of the system. Interestingly, this effect is not linear with the Cr_2O_3 content of the bulk composition but is very strong at low Cr_2O_3 contents, very weak at median Cr_2O_3 contents and very strong again at high Cr_2O_3 contents. This phenomenon is comparable to the effect of Cr_2O_3 on the subsolidus phase transformation between spinel lherzolite and garnet lherzolite.

The phase relationship of pyroxenes in the system CMAS-Cr_2O_3 at 11 kbar is very different to that of the system CMS. In the CMAS-Cr_2O_3 system, low Ca-Cpx and high Ca-Cpx can not coexist at high temperatures, and the stable pyroxene combination is Opx and a supercritical Cpx, the latter of which decreases its Ca content rapidly but continuously, as temperature increases.

Cr_2O_3 also changes the melt composition. It substantially decreases the Al_2O_3 content but strongly increases the MgO content. It increases the SiO_2 content at a relatively weaker level. Its effect on the CaO content, however, is negligible. As Cr_2O_3 increases, thus, the CaO/Al_2O_3 ratio of the melt increases sharply and the melt progressively becomes more Di-normative. Another interesting effect of Cr_2O_3 on the melt composition is that a small amount of Cr_2O_3 makes the melt Qz-normative but more Cr_2O_3 does not make the melt more Qz-normative. Instead, the melt moves towards Hy and remains only marginally Qz-normative.

The excellent agreement (high SiO_2, high CaO/Al_2O_3, high Di component and Hy-normative) between the experimentally produced melts at high Cr_2O_3 conditions in the system CMAS-Cr_2O_3 and the melt inclusions in Sp and Ol from mid-ocean ridge basalt and oceanic island basalt suggests that the upper mantle from which magma is generated is very refractory. The much lower Di component of the most primitive MORBs documented to date possibly indicates that these melts might have been modified by high pressure fractional crystallisation of Cpx. The much lower Di component of the experimentally produced melts using natural rock compositions in the literature, however, suggests that the starting compositions used in the experiments were too fertile (poor in Cr_2O_3).

The effect of H_2O and CO_2 on the partial melting process of the Earth's upper mantle is a long standing problem. Due to some special experimental difficulties and the problem associated with determining the volatile contents of small amount of melt, no literature data published so far provides a complete data set for a study on the effect of fluids. In my study in the system CMAS-H_2O-CO_2 (Chapter 4), high quality experimental data has been successfully obtained and the effect of H_2O and CO_2 can be rigorously parameterised.

The study in the system CMAS-H_2O-CO_2 suggests that H_2O has a strong effect on the solidus of spinel lherzolite: 1 wt% H_2O depresses the solidus by ~ 38 degrees. The effect of CO_2 on the solidus, however, is negligible.

The effect of H_2O on melt composition is 1 wt% H_2O decreases MgO by 1.49 wt% and CaO by 0.39 wt%, but increases Al_2O_3 by 0.67 wt% and SiO_2 by 0.11%. This effect should make the melt corundum-normative and quartz-normative at high water contents. The literature studies at H_2O-free conditions and at H_2O-saturated conditions, therefore, have been linked together as a full picture by my study.

The effect of CO_2 on the melt composition is much stronger than and generally opposite to that of H_2O: the increase of SiO_2 caused by 5 wt% H_2O, for example, can be fully cancelled by 1 wt% CO_2. The effect of CO_2 on the melt composition, however,

is not constant but increases with the H_2O content of the melt. At CO_2-rich conditions, nepheline-normative melt may be produced.

Remarks on the structure of the thesis

The chapters of this thesis have been structured as separate scientific papers with the exception of Chapter 1 and Chapter 5, the former being an introduction to this thesis and the latter a concluding section summarising the most important results of this thesis. As a result, repetitions may occur, especially in the introductory sections and in the reference sections.

Contents

Chapter 1

Introduction

Basaltic magmatism is a fundamental geological process on the Earth and other terrestrial planets. In the case of the Earth, the major source of the basaltic magma is the upper mantle, which consists, at successive depths, of plagioclase lherzolite (olivine, orthopyroxene, clinopyroxene and plagioclase) at low pressure, spinel lherzolite (olivine, orthopyroxene, clinopyroxene and spinel) at medium pressure, and garnet lherzolite (olivine, orthopyroxene, clinopyroxene and garnet) at high pressure. When mantle lherzolite ascends due to mantle convection, adiabatic decompression is expected to produce magma over a range of pressures by a near-fractional melting process.

Potentially, the product magma provides a valuable probe of the earth's deep interior which can not be directly sampled. Unfortunately, the magma-generating process is highly complicated. The major components involved are SiO_2, TiO_2, Al_2O_3, Cr_2O_3, Fe_2O_3, FeO, MgO, CaO, Na_2O, K_2O, H_2O and CO_2. Due to the large number of components involved and the range of pressures and temperatures, compared to the small number of participating minerals and melt, the magma-generating process has a large number of degrees of freedom. Further complications are caused by processes such as magma-mixing, fractional crystallisation and crustal contamination (Hess, 1989). Direct observation made on the natural igneous rock in the field, therefore, can only provide ambiguous results about the initial magma-generating process.

Partial melting experiments at high temperatures and high pressures, however, provide a powerful method of studying the magma-generating process. In principle, there are two ways to undertake the experiments.

Partial melting experiments can be conducted with complex multi-component compositions intended to simulate the composition of the upper mantle (Table 1). These experiments have the advantage of being close to compositions found in natural lherzolites, so that the experimental results may be directly comparable to the observations made in the nature, without significant extrapolation. There are, however, disadvantages. With such natural rock compositions, there are so many degrees of

Table 1 Experimental partial melting study in complex systems

Ref.	P(kbar)	T(°C)	Compositions	Notes
Green, 1973	10-20	900-1200	pyrolite-40* + H_2O	forward
Nicholls & Ringwood, 1973	0.001-30	1000-1400	Ol tholeiite/SiO_2-saturated tholeiite ± H_2O	inverse
Millhollen et al., 1974	10-36	950-1550	peridotite mylonite containing 5.7% H_2O	forward
Mysen & Boettcher, 1975a, b	7.5-30	700-1220	4 lherzolites ± H_2O ± CO_2	forward
Nehru & Wylle, 1975	20	900-1250	peridotite containing 5.7% H_2O	forward
Green, 1976	10-20	1060-1200	Calculated melt composition from Green (1973)	inverse
Mysen & Kushiro, 1977	20-35	1350-1750	2 peridotites	forward
Bender et al., 1978	0.001-15	1205-1350	basalt 572-1-1	inverse
Jaques & Green, 1980	0-15	1100-1550	HP*/TP*-40	forward
Stolper, 1980	10-20	1250-1450	basalt ALV-519-4-1 + Ol + Opx	inverse
Wendlandt & Mysen, 1980	15-30	1100-1600	PHN 1611 + CO_2	forward
Sen, 1982	9	1210-1350	77PAII-1	forward
Fujii & Bougault, 1983	0.001-15	1150-1350	basalt ARP74 10-16	inverse
Takahashi & Kushiro, 1983	0.001-30	1050-1600	HK 66	forward
Elthon & Scarfe, 1984	10-30	1170-1500	basalt NT-23	inverse
Fujii & Scarfe, 1985	10	1250-1310	3 peridotites and 3 basalts	forward
Takahashi & Scarfe, 1985	0.001-70	1200-1800	KLB-1 and PHN1611	forward
Takahashi, 1986	0.001-140	1100-2150	KLB-1	forward
Falloon & Green, 1987	10	1230-1420	4 peridotites	forward
Longhi & Pan, 1987	0.001	1025-1245	16 melt compositions	inverse
Tormey et al., 1987	0.001-2	1152-1243	3 MORBs	inverse
Falloon et al., 1988	2-30	1180-1450	HP, TP and 10 melts from Jaques & Green (1980)	both
Kushiro, 1990	12-20	1100-1250	lherzolite + tholeiitic basalt/boninite	forward
Foden & Green, 1992	0.001-10	950-1260	basalt 41632 ± H_2O	inverse
Grove et al., 1992	0.001-10	1126-1265	6 basalts ± Ol	inverse
Kinzler & Grove, 1992	9-16	1220-1360	10 basalts + Opx/Ol addition	inverse
Gaetani & Grove, 1993	0.001-2	?	basalt 135-839b-15R-2 ± H_2O	inverse
Sisson & Grove, 1993a	2	925-1132	5 natural mafic rocks + mineral addition + H_2O	inverse
Sisson & Grove, 1993b	1	1020-1100	volcanic rocks 79-35g, 82-66, 1140 mf and H_2O	inverse
Baker & Stolper, 1994	10	1270-1390	MM3	forward
Baker et al., 1994	0.001-10	1140-1360	basalts 82-94A, 75SH-70, and 85-44 ± H_2O	inverse
Gaetani et al., 1994	0.001-2	1005-1210	basalts 135-839b-15R-2 and 63-67cm ± H_2O	inverse
Zhang & Herzberg, 1994	50-225	1650-2375	KLB-1	forward
Baker et al., 1995	10	1150-1330	MM3	forward
Hirose & Kawamoto, 1995	10	1100-1350	KLB-1 + H_2O	forward
Herzberg & Zhang, 1996	50-225	1650-2375	KLB-1	forward
Klingenberg & Kushiro, 1996	0.001-5	1242-1405	2 peridotitic compositions	forward
Kushiro, 1996	5-30	1175-1500	PHN1611	forward
Falloon et al., 1997	10	1220-1315	4 peridotites + 2 melts from Baker et al. (1995)	both
Hirose, 1997	10	950-1050	KLB-1+ H_2O	forward
Kawamoto & Holloway, 1997	50-110	950-1100	KLB-1 + H_2O	forward
Kinzler, 1997	15-23	1355-1511	6 synthetic peridotites	forward
Gaetani & Grove, 1998	12-20	1100-1345	4 basalts + 3 peridotites ± H_2O	forward
Hirose & Kushiro, 1998	5-20	1240-1350	PHN1611	forward
Robinson et al., 1998	15	1264-1388	MORB-pyrolite; Tinaquillo peridotite	forward
Walter, 1998	25-70	1415-1950	KR4003	forward
Wagner & Grove, 1998	10-22	1350-1500	estimated primitive tholeiite for Kilauea	inverse
Falloon et al., 1999a	10-15	1250-1550	MM3 and 4 melt compositions	both
Falloon et al., 1999b	0.001-27	1160-1540	8 melt compositions, MM3 and TP-40	both

Table 1 continued

Niida & Green, 1999	4-32	925-1100	MPY-40 + H_2O	forward
Falloon & Danyushevsky, 2000	15-25	1350-1600	harzburgite, TP-40, boninite, 1 melt composition	forward
Herzberg et al., 2000	50-97	1650-2000	KLB-1	forward
Pickering-Witter & Johnston, 2000	10	1270-1390	4 peridotitic compositions	forward
Falloon et al., 2001	10	1310-1500	TP, TP-40, MPY and 6 melt compositions	both
Muntener & Grove, 2001	12	1030-1250	basalt 85-44 and 85-41c + H_2O	inverse
Schwab & Johnston, 2001	10	1245-1390	5 peridotitic compositions	forward
Longhi, 2002	24-34	?	8 melt compositions	inverse
Pichavant et al., 2002	7.5-18	1200-1290	basalt STV 301	inverse

pyrolite-40*: pyrolite – 40% Ol; HP*, Hawaii peridotite; TP*, Tinaquillo peridotite. TP-40, Tinaquillo peridotite – 40% Ol; MPY-40, MPY – 40% Ol. ?: no details available. inverse: crystallising approach; forward, melting approach. References lists are from 1973 on.

Table 2 Experimental partial melting study in simple systems

Ref.	**P(kbar)**	**T(°C)**	**Compositions**	**Notes**
Kushiro, 1969	20	975-1715	CMS ± H_2O	inverse
Yoder, 1971	10	?	CMAS-H_2O	H_2O-saturated
Kushiro, 1972a	0.001	1365-1530	CMS	inverse
Kushiro, 1972b	8-60	900-1590	CMAS-Na_2O ± H_2O	H_2O-saturated
Kushiro, 1972c	10-20	1325-1535	CMAS ± Na_2O	lherzolite
Kushrio, 1974	15	?	CMAS-Na_2O-H_2O ± K_2O	inverse
Presnall, 1976	8.7-14	1302-1400	CMAS	inverse
Presnall, 1978	0.001-20	1263-1690	CMAS	inverse
Eggler, 1978	< 30	?	CMAS-Na_2O-CO_2	inverse
Presnall et al., 1979	0.001-20	1240-1443	CMAS	lherzolite
Longhi & Boudreau, 1980	0.001	1378-1455	CMS	inverse
Sen & Presnall, 1984	10	1260-1570	CMAS	inverse
Longhi, 1987	0.001	1240-1371	CMAS	inverse
Liu & Presnall, 1989	0.001	1361-1377	CMAS	inverse
Liu & Presnall, 1990	20	1350-1770	CMAS	inverse
Libourel, 1991	0.001-15	?	CMAS-Cr_2O_3	inverse
Shi & Libourel, 1991	0.001	1160-1275	CMAS-FeO	different-fO_2
Walter & Presnall, 1994	7-35	1225-1594	CMAS-Na_2O	lherzolite
Gudfinnsson & Presnall, 1996	24-34	1495-1615	CMAS	lherzolite
Sisson et al., 1997	12-28	?	CMAS-Na_2O-H_2O	Am-lherzolite?
Herzberg & Zhang, 1997	50	1750-1850	CMAS and CMAS-Fe*	inverse
Milholland & Presnall, 1998	30	1400-1820	CMAS	inverse
Herzberg & Zhang, 1998	30-150	1800-2225	CMAS and MS	inverse
Dalton & Presnall, 1998a	60	1380-1505	CMAS-CO_2	carbonated lherzolite
Dalton & Presnall, 1998b	30-70	1245-1430	CMAS-CO_2	carbonated lherzolite
Gudfinnsson & Presnall, 2000	7-28	1260-1530	CMAS-FeO	lherzolite
Conceicao & Green, 2000	5-20	1200-1400	MAS-FeO-K_2O	inverse
Liu & Presnall, 2000	20	1340-1540	CMAS	inverse
Weng & Presnall, 2001	51	1850-1930	CMS	inverse

inverse, crystallising approach to bracket the targets; lherzolite, melting approach. Fe*, Fe^0, Fe^{2+} and Fe^{3+}. ?: no details available. References listed here are from 1969 on.

freedom that it is difficult to relate an effect to a particular component. Also it is not possible to rigorously extrapolate the experimental results to different temperatures, pressures or compositions.

Alternatively, partial melting experiments can be conducted with simplified compositions (Table 2). These experiments have the advantage of simplicity. It is usually easy to determine the effect of a particular component on the partial melting process. These experiments also produce valuable thermodynamic data for the participating phases. There are, however, disadvantages associated with this approach. The simplified compositions may be sufficiently different from the compositions of natural lherzolites, so that application of the experimental results to nature may require substantial extrapolation which may not be valid, especially when components which are absent in the simple systems have a strong effect on the melting phase relationships. Another disadvantage is that the large number of phases in a desired phase assemblage may not be easy to experimentally observe due to the low variability of the simplified system.

This study follows the second experimental approach, and includes partial melting experiments in the systems CaO-MgO-Al_2O_3-SiO_2 (CMAS), CMAS-K_2O, CMAS-Cr_2O_3 (-K_2O) and CMAS-H_2O-CO_2 (-trace Na_2O) at 11 kbar. It also contains a couple of partial melting experiments in the system CMAS-Na_2O and a few reversal experiments in the system CMAS. My main effort has been directed to the partial melting behaviour of the phase assemblage of spinel lherzolite.

An experimental pressure of 11 kbar was chosen due to several reasons. First, 11 kbar closely approximates the lowest pressure at which primary melt is in equilibrium with the upper mantle (Presnall et al., 1979; Sen, 1982; Presnall & Hoover, 1984, 1987; Melt Seismic Team, 1998; Dunn & Forsyth, 2001). Second, spinel lherzolite is a stable phase assemblage in all the chemical systems studied here and comparison among these systems is simple. Third, numerous partial melting studies have been carried out with natural lherzolite compositions at ~ 11 kbar and comparison between the simplified and the natural systems is facilitated (see Table 1 for references).

The CaO-MgO-Al_2O_3-SiO_2 (CMAS) system closely matches the composition and mineralogy of both the upper mantle source and the product magma. The magma-generating process, therefore, can be closely approximated by the partial melting behaviour of the CMAS system. Literature data on this topic shows some discrepancies (solidus temperature and melt composition; Kushiro, 1972c; Presnall et al., 1979; Walter & Presnall, 1994), so that partial melting experiments in the system CMAS were

firstly conducted to resolve these discrepancies. It was found that the desired spinel lherzolite phase assemblage plus melt can not be experimentally produced due to the isobarically invariant nature of the system at this condition. Hence a small amount of K_2O was added to the system to split the isobarically invariant point (the K_2O method), allowing the spinel lherzolite phase assemblage plus melt to be successfully observed over a large temperature interval. The results were then regressed and extrapolated to 0 wt% K_2O to derive data for the CMAS system. The extrapolated results agree with some literature data but disagree with others. Reversal experiments with and without olivine-addition, thus, were undertaken to check the new data and established indirectly that the K_2O method is successful. The partial melting experiments in the system CMAS-K_2O were also extended to high K_2O contents and several isobarically invariant points were experimentally constrained.

In order to understand the effect of additional components, the complexity of the study system must be increased.

Chromium is potentially important in the partial melting process of the upper mantle due to its abundance (O'Neill & Palme, 1998), its strong geochemical effect on subsolidus phase relationships (O'Neill, 1981; Nickel, 1986; Li et al., 1995; Klemme & O'Neill, 2000) and preliminary experimental results at supersolidus conditions (Irvine, 1977; Libourel, 1991). Previous experimental study on the effect of Cr_2O_3 has been of limited success. Our preliminary experiments (not reported in this thesis) in the system CMAS-Cr_2O_3 suggested that the partial melting process for a spinel lherzolite phase assemblage is isobarically pseudo-invariant and that the melt is unquenchable. The K_2O method hence was applied to later experiments (reported in Chapter 3 of this thesis) to solve these problems. An Fe_2O_3 sleeve was used in these experiments to ensure that chromium was present as Cr^{3+}. This is the first time that the effect of chromium on the partial melting process has been successfully studied.

The explosive nature of volcanoes is one of the most obvious phenomena, illustrating the importance of volatiles, like H_2O and CO_2, in the magma-generating process. Due to the degassing of magmas at low pressures, the geochemical behaviour of H_2O and CO_2 in the partial melting process can only be studied by high temperature-high pressure experiments. Most previous experimental studies have been conducted under H_2O/CO_2-oversaturated conditions which probably never occur in the nature (Pan et al., 1991; Bell & Rossman, 1992; Zhang & Zindler, 1993; Jambon, 1994; O'Neill & Palme, 1998). Further, the data sets are incomplete due to the difficulty of quantifying H_2O and CO_2. In this study, a small amount of H_2O and CO_2 was added into the system

CMAS and experiments were carried out at H_2O/CO_2 undersaturated conditions. Phase compositions were determined by electron microprobe and FTIR spectroscopy, allowing all components in the study system to be quantified. With this data set, the geochemical behaviour of H_2O and CO_2 in the partial melting process of a spinel lherzolite phase assemblage can be determined. Also, the results can be used to evaluate nominally H_2O/CO_2-free partial melting experiments in the literature which were obviously affected by H_2O and CO_2, associated with the diffusion of hydrogen and graphite through noble metal capsules.

References

Baker, M. B. & Stolper, E. M. (1994). Determining the composition of high-pressure mantle melts using diamond aggregates. Geochimica. et. Cosmochimica. Acta 58, 2811-2827.

Baker, M. B., Grove, T. L. & Price, R. (1994). Primitive basalts and andesites from the Mt. Shasta region, N. California: products of varying melt fraction and water content. Contrib. Mineral. Petrol. 118, 111-129.

Baker, M. B., Hirschmann, M. M., Ghiorso, M. S. & Stolper, E. M. (1995). Compositions of near-solidus peridotite melts from experiments and thermodynamics calculation. Nature 375, 308-311.

Bell, D. R. & Rossman, G. (1992). Water in earth's mantle: The role of nominally anhydrous minerals. Science 255, 1391-1397.

Bender, A., Hodges, F. N. & Bence, A. E. (1978). Petrogenesis of basalts from the Project FAMOUS area. Earth Planet. Sci. Lett. 41, 277-302.

Conceicao, R. V. & Green, D. H. (2000). Behaviour of the cotectic curve En-Ol in the system leucite-olivine-quartz under dry conditions to 2.0 GPa. Geochem. Geophys. Geosyst. 1, 2000GC000071.

Dalton, J. A. & Presnall, D. C. (1998a). The continuum of primary carbonatitic-kimberlitic melt compositions in equilibrium with lherzolite: data from the system CaO-MgO-Al_2O_3-SiO_2-CO_2 at 6 GPa. J. Petrol. 39, 1953-1964.

Dalton, J. A. & Presnall, D. C. (1998b). Carbonatitic melts along the solidus of model lherzolite in the system CaO-MgO-Al_2O_3-SiO_2-CO_2 from 3 to 7 GPa. Contrib. Mineral. Petrol. 131, 123-135.

Dunn, R. & Forsyth, D. (2001). Short-period Love waves reveal the transition from broad mantle upwelling to the narrow crustal magmatic system beneath the southern East Pacific Rise. EOS Trans. Am. Geophys. Union 82, 1113.

Eggler, D. H. (1978). The effect of CO2 upon partial melting of peridotite in the system Na_2O-CaO-Al_2O_3-MgO-SiO_2-CO_2 to 35 kb, with an analysis of melting in a peridotite-H_2O-CO_2 system. Am. J. Sci. 278, 305-343.

Elthon, D. & Scarfe, C. M. (1984). High-pressure phase equilibria of a high-magnesia basalt and the genesis of primary oceanic basalts. Am. Mineral. 69, 1-15.

Falloon, T. J. & Green, D. H. (1987). Anhydrous partial melting of MORB pyrolite and other peridotite compositions at 10 kbar: Implications for the origin of MORB glasses. Miner. Petrol. 37, 181-219.

Falloon, T. J., Green, D. H., Hatton, C. J. & Harris, K. L. (1988). Anhydrous partial melting of a fertile and depleted peridotite from 2 to 30 kbar and application to basalt petrogenesis. J. Petrol. 29, 1257-1282.

Falloon, T. J., Green, D. H., O'Neill, H.St.C. & Hibberson, W. O. (1997). Experimental tests of low degree peridotite partial melt compositions: implications for the nature of anhydrous near-solidus peridotite melts at 1 GPa. Earth Planet. Sci. Lett 152, 149-162.

Falloon, T. J., Green, D. H., Jacques, A. L. & Hawkins, J. W. (1999a). Refractory magmas in back-arc basin settings-experimental constraints on the petrogenesis of a Lau Basin example. J. Petrol. 40, 255-277.

Falloon, T. J., Green, D. H., Danyushevsky, L. V & Faul, U. H. (1999b). Peridotite melting at 1.0 and 1.5 GPa: an experimental evaluation of techniques using diamond aggregates and mineral mixes for determination of near-solidus melts. J. Petrol. 40, 1343-1375.

Falloon, T. J. & Danyushevsky L. V. (2000). Melting of refractory mantle at 1.5, 2 and 2.5 GPa under anhydrous and H_2O-undersaturated conditions: implications for the petrogenesis of high-Ca boninites and the influences of subduction components on mantle melting. J. Petrol. 41, 257-283.

Falloon, T. J., Danyushevsky, L. V. & Green, D. H. (2001). Peridotite melting at 1 GPa: reversal experiments on partial melt compositions produced by peridotite-basalt sandwich experiments. J. Petrol. 42, 2363-2390.

Foden, J. D. & Green, D. H. (1992). Possible role of amphibole in the origin of andesite: some experimental and natural evidence. Contrib. Mineral. Petrol. 109, 479-493.

Fujii, T. & Bougault, H. (1983). Melting relations of a magnesian abyssal tholeiite and the origin of MORBs. Earth Planet. Sci. Lett. 62, 283-295.

Fujii, T. & Scarfe, C. M. (1985). Composition of liquids coexisting with spinel lherzolite at 10 kbar and the genesis of MORBs. Contrib. Mineral. Petrol. 131, 323-346.

Gaetani, G. A., Grove, T. L. & Bryan, W. B (1993). The influence of water on the petrogenesis of subduction-related igneous rocks. Nature 365, 332-334.

Gaetani, G. A., Grove, T. L. & Bryan, W. B. (1994). Experimental phase relations of basaltic andesite from Hole 839b under hydrous and anhydrous conditions. In: Hawkins, J., Parsons, L., Allan, J. et al. (eds) Proc. ODP Sci. Results 135. Ocean Drilling Program, College Station TX, 557-564.

Gaetani, G. A. & Grove, T. L. (1998). The influence of water on melting of peridotite. Contrib. Mineral. Petrol. 131, 323-346.

Green, D. H. (1973b). Experimental melting studies on a model upper mantle composition at high pressure under water-saturated and water-undersaturated conditions. Earth Planet Sci. Lett. 19, 37-53.

Green, D. H. (1976). Experimental testing of equilibrium partial melting of peridotite under saturated, high pressure conditions. Can. Mineral. 14, 255-268.

Grove, T. L., Kinzler, R. J. & Bryan, W. B. (1992). Fractionation of mid-ocean ridge basalt (MORB). In: J. P. Morgan, D. K. Blackman & J. M. Sinton (ed.) " Mantle flow and melt generation at mid-ocean ridges", 281-310. Geophys. Monogr. Ser., vol. 71. AGU. Washington, D. C.

Gudfinnsson, G. H. & Presnall, D. C. (1996). Melting relations of model lherzolite in the system $CaO-MgO-Al_2O_3-SiO_2$ at 2.4-3.4 GPa and the generation of komatiites. J. Geophy. R. 101, 27701-27709.

Gudfinnsson, G. H. & Presnall, D. C. (2000). Melting behaviour of model lherzolite in the system $CaO-MgO-Al_2O_3-SiO_2-FeO$ at 0.7-2.8 GPa. J. Petrol. 41, 1241-1269.

Herzberg, C. T. & Zhang, J. (1996). Melting experiments on anhydrous peridotite KLB-1: compositions of magmas in the upper mantle and transition zone. J. Geophys. Res. 101, 8271-8295.

Herzberg, C. & Zhang, J. (1997). Melting experiments on komatiite analog compositions at 5 GPa. American. Minera. 82, 354-367.

Herzberg, C. & Zhang, J. (1998). Melting experiments in the systems $CaO-MgO-Al_2O_3-SiO_2$ and $MgO-SiO_2$ at 3 to 15 GPa. Am. Mineral. 83, 491-500.

Herzberg, C. T., Raterron, P. & Zhang, J. (2000). New experimental observations on the anhydrous solidus for peridotite KLB-1. Geochem. Geophys. Geosyst. 1, 2000GC000089.

Hess, P. C. (1989). Origins of igneous rocks. Harvard Press, Cambridge, MA.

Hirose, K.& Kawamoto, T. (1995). Hydrous partial melting of lherzolite at 1 GPa: the effect of H_2O on the genesis of basaltic magmas. Earth Planet. Sci. Lett. 133, 463-473.

Hirose, K. (1997). Melting experiments on lherzolite KLB-1 under hydrous conditions and generation of high-magnesian andesitic melts. Geology 25, 42-44.

Hirose, K. & Kushiro, I. (1998). The effect of melt segregation on polibaric mantle melting: estimation from the incremental melting experiments. Phys. Earth Planet. Int. 107, 111-118.

Irvine, T. N. (1977). Chromite crystallisation on the join Mg_2SiO_4-$CaMgSi_2O_6$-$CaAl_2Si_2O_8$-$MgCr_2O_4$-SiO_2. Carnegie Inst. Yearbook 76, 465-472.

Jambon, A. (1994). Earth degassing and large-scale geochemical cycling of volatile elements. In: Carroll, M. R. & Holloway, J. R. (eds) Volatiles in magmas. Mineralogical Society of America, Reviews in Mineralogy 30, 479-517.

Jaques, A. L. & Green, D. H. (1980). Anhydrous melting peridotite at 0-15 kbar pressure and the genesis of tholeiitic basalts. Contrib. Mineral. Petrol. 73, 287-310.

Kawamoto, T. & Holloway, J. R. (1997). Melting temperature and partial melt chemistry of H2O-saturated mantle peridotite to 11 gigapascals. Science 276, 240-243.

Kinzler, R. J. & Grove, T. L. (1992). Primary magmas of mid-ocean ridge basalts 1. Experiments and methods. Ibid 97 (B5), 6885-6906.

Kinzler, R. J. (1997). Melting of mantle peridotite at pressures approaching the spinel to garnet transition: application to mid ocean ridge basalt petrogenesis. J. Geophys. Res. 102, 853-874.

Klemme, S. & O'Neill, H. St. C. (2000). The effect of Cr on the solubility of Al in orthopyroxene: experiments and thermodynamic modelling. Contrib. Mineral. Petrol. 140, 84-98.

Klingenberg, B. M. E. T. & Kushiro, I. (1996). Melting of a chromite-bearing harzburgite and generation of boninitic melts at low pressures under controlled oxygen fugacity. Lithos 37, 1-13.

Kushiro, I. (1969). The system forsterite-diopside-silica with and without water at high pressures. Am. J. Sci. 267A, 269-294.

Kushiro, I. (1972a). Determination of liquidus relations in synthetic silicate systems with electron probe analysis: The system forsterite-diopside-silica at 1 atmosphere. Am. Mineral. 57, 1260-1271.

Kushiro, I. (1972b). Effect of water on the composition of magmas formed at high pressures. J. Petrol. 13, 311-334.

Kushiro, I. (1972c). Partial melting of synthetic and natural peridotites at high pressures. Yb. Carnegie Instn. Wash. 71, 357-362.

Kushiro, I. (1974). Melting of hydrous upper mantle and possible generation of andesitic magma: an approach from synthetis systems. Earth Planet. Sci. Let. 22, 294-299.

Kushiro, I. (1990). Partial melting of mantle wedge and evolution of island arc crust. J. Geophys. Res. 95, 15929-15939.

Kushiro, I. (1996). Partial melting of a fertile mantle peridotite at high pressure: an experimental study using aggregates of diamond. In: Basu, A. & Hart, S. (ed.), "Earth Processes: Reading the Isotopic Clock". Geophysical monograph 95, 109-122. American Geophysical Union.

Li, J. P., O'Neill, H. St. C. & Seifert, F. (1995). Subsolidus phase relations in the system MgO-SiO_2-Cr-O in equilibrium with metallic Cr, and their significance for the petrochemistry of chromium. J. Petrol. 36, 107-132.

Libourel, G. (1991). Chromium in basalts: an experimental study. EOS Trans. Am. Geophys. Union 72, 547.

Liu, T. C. & Presnall, D. C. (1989). Diopside-tridymite liquidus boundary line in the system Mg_2SiO_4-$CaMgSi_2O_6$-SiO_2 at atmospheric pressure. Am. Mineral. 74, 1032-1037.

Liu, T. C. & Presnall, D. C. (1990). Liquidus phase relationships on the join anorthite-forsterite-quartz at 20 kbar with applications to basalt petrogenesis and igneous sapphirine. Contrib. Miner. Petrol. 104, 735-742.

Liu, T. C. & Presnall, D. C. (2000). Liquidus phase relations in the system CaO-MgO-Al_2O_3-SiO_2 at 2.0 GPa: applications to basalt fractionation, eclogites, and igneous sapphirine. J. Petrol. 41, 3-20.

Longhi, J. & Boudreau, A. E. (1980). The orthoenstatite liquidus field in the system forsterite-diopside-silica at one atmosphere. Am. Mineral. 65, 563-573.

Longhi, J. (1987). Liquidus equilibrium and solid solution in the system $CaAl_2Si_2O_8$-$CaSiO_3$-SiO_2 at low pressure. Am. J. Sci. 287, 265-331.

Longhi, J. & Pan V. (1987). A reconnaisance study of phase boundaries in low-alkali basaltic liquids. J. Petrol. 29, 115-147.

Longhi, J. (2002). Some phase equilibrium systematics of lherzolite melting: I. Geochem. Geophys. Geosyst. 3, 2001GC000204.

Melt Seismic Team (1998). Imaging the deep seismic structure beneath a mid-ocean ridge: the melt experiment. Science 280, 1215-1218.

Miholland, C. S. & Presnall, D. C. (1998). Liquidus phase relations in the CaO-MgO-Al_2O_3-SiO_2 system at 3.0 GPa; the aluminous pyroxene thermal divide and high-pressure fraction of picritic and komatiitic magmas. J. Petrol. 39, 3-27.

Millhollen, G. L., Irving, A. J. & Wyllie, P. J. (1974). Melting interval of peridotite with 7.5 percent water to 30 kilobars. J. Geol. 82, 575-587.

Muntener, O., Kelemen, P. B. & Grove, T. L. (2001). The role of H_2O during crystallization of primitive arc magmas under uppermost mantle condition and genesis of igneous pyroxenites: an experimental study. Contrib. Mineral. Petrol. 141, 643-658.

Mysen, B. O. & Boettcher, A. L. (1975a). Melting of a hydrous mantle. I. Phase relations of natural peridotite at high P and T and with controlled addition of water, carbon dioxide and hydrogen. J. Petrol. 16, 520-548.

Mysen, B. O. & Boettcher, A. L. (1975b). Melting of a hydrous mantle. II. Geochemistry of crystals and liquids formed by anatexis of mantle peridotite at high pressure and high temperature as a function of controlled activities of water, hydrogen and carbon dioxide. J. Petrol. 16, 549-593.

Mysen, B. O. & Kushiro, I. (1977). Compositional variations of coexisting phases with degrees of melting of peridotite in the upper mantle. Am. Mineral. 62, 843-865.

Nehru, C. E. & Wyllie (1975). Compositions of glasses from St. Paul's peridotite partially melted at 20 kilobars. J. Geol. 83, 455-471.

Nicholls, I. A. & Ringwood, A. E. (1973). Effects of water on olivine stability in tholeiite and the production of silica-saturated magmas in the island-arc environment. J. Geol. 81, 285-300.

Nickel, K. G. (1986) Phase equilibria in the system SiO_2-MgO-Al_2O_3-CaO-Cr_2O_3 (SMACCr) and their bearing on spinel/garnet lherzolite relationships. Neues Jahrbuch fur Mineralogie, Abhandlungen 155, 259-287.

Niida, K. & Green, D. H. (1999). Stability and chemical composition of pargasitic amphibole in MORB pyrolite under upper mantle conditions. Contrib. Mineral. Petrol. 135, 18-40.

O'Neill, H. St. C. (1981). The transition between spinel lherzolite and garnet lherzolite, and its use as a geobarometer. Contr. Mineral. Petrol. 77, 185-194.

O'Neill, H. St. C. & Palme, H. (1998). Compositions of the Silicate Earth: Implications for accretion and core formation. In: Jackson, I. (ed.) " The Earth's Mantle: Composition, Structure and Evolution", 3-126. Cambridge University Press. Cambridge.

Pan, V., Holloway, J. R. & Hervig, R. L. (1991). The pressure and temperature dependence of carbon dioxide solubility in tholeiitic basalt melts. Geochimica et Cosmochimica Acta 55, 1587-1595.

Pichavant, M., Mysen, B. O. & Macdonald, R. (2002). Source and H_2O content of high-MgO magmas in island arc settings: An experimental study of a primary calc-alkaline basalt from St. Vincent, Lesser Antillers arc. Geochimica et Cosmochimica Acta 66: 2193-2209.

Pichering, J. W. & Johnston, A. D. (2000). The effects of variable bulk composition on the melting systematics of fertile peridotitic assemblages. Contrib. Mineral. Petrol. 140, 190-211.

Presnall, D. C. (1976). Alumina content of enstatite as a geobarometer for plagioclase and Sp-lherzolites. Am. Mineral. 61, 582-588.

Presnall, D. C., Dixon, S. A., Dixon, J. R., O'Donnell, T. H., Brenner, N. L., Schrock, R. L. & Dycus, D. W. (1978). Liquidus phase relations on the joint diopside-forsterite-anorthite from 1 atm. to 20 kbar: their bearing on the generation and crystallization of basaltic magma. Contr. Miner. Petrol. 66, 203-220.

Presnall, D. C., Dixon, J. R., O'Donnell T. H. & Dixon, S. A. (1979). Generation of mid-ocean ridge tholeiites. J. Petrol. 20, 3-36.

Presnall, D. C. & Hoover, J. D. (1984). Composition and depth of origin of primary mid-ocean ridge basalts. Contrib. Mineral. Petro. 87, 170-178.

Presnall, D. C. & Hoover, J. D. (1987). High pressure phase equilibrium constraints on the origin of mid-ocean ridge basalts. In: Mysen, B. O. (ed.), "Magmatic Processes: Physicochemical Principles". Geochemical Soc. Spec. Pub. 1, 75-89.

Robinson, J. A. C., Wood, B. J. & Blundy, J. D. (1998). The beginning of melting of fertile and depleted peridotite at 1.5 GPa. Earth Planet. Sci. Lett 155, 97-111.

Schwab, B. E. & Johnston, A. D. (2001). Melting systematics of modally variable, compositionally intermediate peridotites and the effects of mineral fertility. J. Petrol. 42, 1789-1811.

Sen, G. (1982). Composition of basaltic liquids generated from a partially depleted lherzolite at 9 kbar pressure. Nature 299, 336-338.

Sen, G. & Presnall, D. C. (1984). Liquidus phase relationships on the join anorthite-forsterite-quartz at 10 bar with applications to basalt petrogenesis. Contr. Miner. Petrol. 85, 404-408.

Shi, P. & Libourel, G. (1991). The effects of FeO on the system CMAS at low pressure and implications for basalt crystallization processes. Contrib. Mineral. Petrol. 108, 129-145.

Sisson, T. W. & Grove, T. L (1993a). Experimental investigations of the role of H_2O on calc-alkaline differentiation and subduction zone magmatism. Contrib. Mineral. Petrol. 113, 143-166.

Sisson, T. W. & Grove, T. L (1993b). Temperatures and H_2O contents of low-MgO high-alumina basalts. Contrib. Mineral Petrol. 113, 167-184.

Sisson, T. W., Hankins, W. B. & Presnall, D. C. (1997). Melting of amphibole lherzolite investigated in the system CMASN-H2O (abstract). EOS Trans. Am. Geophys. Union 78 suppl. 46, F835.

Stolper, E. (1980). A phase diagram for mid-ocean ridge basalts: preliminary results and implications for petrogenesis. Contrib. Mineral. Petrol. 74, 13-27.

Takahashi, E. & Kushiro, I. (1983). Melting of a dry peridotite at high pressures and basalt magma genesis. Am. Mineral. 68, 859-879.

Takahashi, E. & Scarfe, C. M. (1985). Melting of peridotite to 14 GPa and the genesis of komatiite. Nature 315, 566-568.

Takahashi, E. (1986). Melting of a dry peridotite KLB-1 up to 14 GPa: Implications on the origin of peridotitic upper mantle. J. Geophys. Res. 91, 9367-9382.

Tormey, D. R., Grove, T. L. & Bryan, W. B. (1987). Experimental petrology of normal MORB near the Kane fracture zone, 22-25oN, mid-Atlantic ridge. Contrib. Mineral. Petrol. 96, 121-139.

Wagner, T. P. & Grove, T. L. (1998). Melt/harzburgite reaction in the petrogenesis of tholeiitic magma from Kilauea volcano, Hawaii. Contrib. Mineral. Petrol. 131, 1-12.

Walter, M. J. & Presnall, D. C. (1994). Melting behaviour of simplified lherzolite in the system CaO-MgO-Al_2O_3-Na_2O from 7 to 35 kbar. J. Petrol. 35, 329-359.

Walter, M. J. (1998). Melting of garnet peridotite and the origin of komatiite and depleted lithosphere. J. Petrol. 39, 29-60.

Wendtland, R. F.& Mysen, B. O. (1980). Melting phase relations of natural peridotite + CO_2 as a function of degree of partial melting at 15 and 30 kbar. Am. Mineral. 65, 37-44.

Weng, Y. H. & Presnall, D. C. (2001). The system diopside-forsterite-enstatite at 5.1 GPa: a ternary model for melting of the mantle. Can. Mineral. 39, 239-266.

Yoder, H. S. (1971). The join diopside-pyrope-H2O at 10 kbar: its bearing on the melting of peridotite, the ACF metamorphic facies, and the gedrite-hornblende miscibility gap. Yb. Carnegie Instn. Wash. 69, 176-181.

Zhang, J. & Herzberg, C. (1994). Melting experiments on anhydrous peridotite KLB-1 from 5.0-22.5 GPa. J. Geophy. R. 99 (B9), 17729-17742.

Zhang, Y. & Zindler, A. (1993). Distribution and evolution of carbon and nitrogen in Earth. Earth and Planetary Science Letters 117, 331-345.

Chapter 2

Partial melting of spinel lherzolite in the system CaO-MgO-Al_2O_3-SiO_2±K_2O at 11 kbar

1. Introduction

The simplest chemical system that contains all the major phases of the peridotitic upper mantle (olivine, orthopyroxene, clinopyroxene. and an aluminous phase, either plagioclase, spinel or garnet, depending on pressure) is CaO-MgO-Al_2O_3-SiO_2 (CMAS). This simple system has been used to investigate the basic phase relations of partial melting in the upper mantle (O'Hara, 1968; Kushiro, 1972; Presnall et al., 1979; Longhi, 1987; Gudfinnsson & Presnall, 1996; Milholland & Presnall, 1998; Herzberg & Zhang, 1998; Presnall, 1999; Liu & Presnall, 2000). However, with a typical four-phase lherzolite assemblage, the initial melting in CMAS is isobarically invariant; that is, the chemical potentials of all four components (CaO, MgO, Al_2O_3 and SiO_2) in the melt are completely defined; for example, the following four reactions specify the chemical potentials:

$$CaO + 1.5Mg_2Si_2O_6 = CaMgSi_2O_6 + Mg_2SiO_4 \quad (1)$$
Melt Opx Cpx Ol

$$MgO + 0.5Mg_2Si_2O_6 = Mg_2SiO_4 \quad (2)$$
Melt Opx Ol

$$SiO_2 + Mg_2SiO_4 = Mg_2Si_2O_6 \quad (3)$$
Melt Ol Opx

and, in the Sp-lherzolite stability field,

$$Al_2O_3 + Mg_2SiO_4 = MgAl_2O_4 + 0.5Mg_2Si_2O_6 \quad (4)$$
Melt Ol Sp Opx

Because all chemical potentials are known, the composition of the melt in equilibrium with all four solid phases is particularly valuable in constructing thermodynamic models

of silicate melts. Unfortunately, the isobarically invariant melt composition is difficult to determine experimentally, because this assemblage only exists over an infinitely narrow temperature interval at a given pressure.

The traditional way around this problem is to bracket the isobaric invariant point by varying the experimental starting composition, to produce four-phase isobarically univariant assemblages (i.e. three solid phases plus melt as in Fo+Opx+Sp+Melt). Not only does this require a large number of experiments, but it is tedious to demonstrate equilibrium (Presnall et al., 1978; Liu & Presnall, 1990), particularly since the solid phases (especially the pyroxenes) are multicomponent solid solutions with the potential to be out of equilibrium as regards their compositions. This method also requires some extrapolation to the isobaric invariant point, since this point is only bracketed.

Alternatively, it is possible to rely on experimental imperfections, such as temperature gradients or chemical impurities (e.g., some Na_2O in the starting material or H_2 diffusing through the Pt capsule to produce H_2O present in the experimental charge) to increase the effective variance of the system and obtain melt in equilibrium or quasi-equilibrium with four solid phases, which can then be analysed directly. This approach has been adopted by Presnall and his colleagues (Presnall et al., 1979; Gudfinnsson & Presnall et al., 1996; Milholland & Presnall, 1998; Liu & Presnall, 2000). Although this seems empirically to work well for system CMAS, this may not always be the case, and indeed I have encountered insuperable difficulties in applying this approach to determining the effect of Cr_2O_3 on melting in system CMAS-Cr_2O_3. Relying on imperfections to obtain a result is also intellectually unsatisfying, and there is the question of how much the imperfections affect results.

In this paper I report a logical improvement to this approach, which is to introduce another component into the system deliberately. The system is then studied as a function of the concentration of this component, such that the composition of the CMAS isobaric invariant melt can be obtained by extrapolating to zero concentration of the added component. I chose K_2O as the additional component (the K_2O-method hereafter), as it is almost completely incompatible in all the solid phases (Ol, Opx, Cpx, Sp) at my chosen pressure of 11 kbar. Having the extra component entering only the melt phase makes the extrapolation to the pure CMAS system simple. Also, K_2O is an important major-element constituent in several mantle-derived magma types (kimberlites, shoshonites and so on), so that the data generated in this study in the system CMAS-K_2O as a by-product of my main purpose should be of some petrological value.

I show that the method produces a result in good agreement with the previous work of Presnall and his colleagues (Presnall, 1976; Presnall et al., 1979; Walter & Presnall, 1994), although the improved accuracy of the present method allows for some refinement of previous results.

2. Experimental and analytical techniques

Four types of experiments were performed:

1. Conventional direct partial melting experiments (DEs) in the system CMAS
2. Sandwich experiments using the K_2O-method (KEs), in which the solid assemblage Fo+Opx+Cpx+Sp was placed at the top and bottom of the capsule, with a K_2O-containing melt composition as the "filling"
3. Reversal experiments (REs-1) to study the crystallisation of the CMAS melt composition deduced from the KEs
4. Reversal experiments (REs-2) with Fo added. All but one of these (C-1789) used the sandwich configuration

2.1 Starting materials

Table 1 summarises the starting materials used in this study. Compositions were made from high-purity oxides (SiO_2, Al_2O_3 and MgO) and carbonates ($CaCO_3$ and K_2CO_3). An important strategy was to use pre-synthesised Opx and Cpx with compositions similar to those expected in the run products.

Mix9 was prepared by combining a crystalline mixture of pure forsterite (Fo) and a crystalline mixture of Sp+Opx+Cpx in a proportion of 1:5 by weight. The Fo was synthesised at 1400°C, 1atm for 69 hours; the mixture with Sp : Opx : Cpx in a ratio of 1 : 2 : 2 in weight was made in a 5/8" piston-cylinder press using a 3.5mm diameter Pt capsule and a talc/pyrex assembly at 1280°C, 11 kbar and 48 hours. The phase proportion in the final Mix9 was close to 1 : 1 : 2 : 2 (Fo : Sp : Opx : Cpx).

Crystalline mixture SEM02-1 containing Fo : Sp : Opx : Cpx = 1 : 1 : 1 : 1 (by weight) was made by crystallising the decarbonated oxide mix at 1300°C, 11 kbar and 48 hours in a Pt capsule.

Mixtures SEM02-3, SEM02-4, SEM02-8 and SEM02-6 were melted at 1400°C, 1atm and 20 minutes and then quenched to glass.

Table 1: Starting compositions used in this study

	Mix9	SEM02-1	SEM02-3	SEM02-4	SEM02-10	SEM02-8	SEM02-6	SEM02-13
	cryst.	cryst.	glass	glass	glass	glass	glass	glass
SiO_2	42.12	36.95	48.71	49.37	57.69	59.33	49.09	57.13
Al_2O_3	18.34	22.63	18.97	20.20	20.80	23.13	20.12	17.89
MgO	32.46	35.06	16.60	13.52	6.20	2.57	15.45	11.72
CaO	7.08	5.36	14.72	13.91	6.81	4.99	15.33	4.48
K_2O	0.00	0.00	1.00	3.00	8.49	10.00	0.00	8.79

Mix9 contains Fo:Sp:Opx:Cpx in the proportion 1:1:2:2 where Fo is forsterite, Sp spinel, Opx orthopyroxene and Cpx clinopyroxene. Fo was synthesised at 1400ºC, 1 bar for 69 hrs, while Sp+Opx+Cpx were synthesised together at 1280ºC, 11 kbar for 48 hrs.
SEM02-1 contains Fo:Sp:Opx:Cpx in the proportion of 1:1:1:1, made up as for Mix9.
SEM02-3 and SEM02-4 from 116-3 (Walter & Presnall, 1994), first normalised to 99 or 97 wt% and then 1 or 3 wt% K_2O added, respectively.
SEM02-10 is the melt composition from C-1585.
SEM02-8 is the melt composition from earlier KEs extrapolated to 10 wt% K_2O (See Fig. 4) However, it was found to contain more Al_2O_3 than that in the equilibrium melt, crystallizing sapphirine (see text for details).
SEM02-6 is the melt composition from the KEs extrapolated to 0 wt% K_2O (See Fig. 3), used as the starting material in the REs.
SEM02-13 contains 80% melt + 5% San + 15% Fo in which the composition of melt and San (Sanidine) is from C-1708.

All mixtures were checked for compositions with electron microprobe (Ware, 1991). Mix9 was later stored in an oven at 110°C while other starting materials were stored in another oven at 150°C.

2.2 Piston-cylinder assemblies

All experiments were made in a conventional 1/2" piston-cylinder apparatus (Boyd & England, 1960). The salt-pyrex pressure assembly used in the preliminary DEs was described by Klemme & O'Neill (1997), except that, because of the generally lower pressure and temperature regime of this study, fired pyrophyllite replaced the MgO spacer underneath the capsule and mullite was used instead of high-purity alumina for the thermocouple tube. However, concerns about the possible effect of H_2 diffusion into the Pt capsule causing contamination of the runs by H_2O led me to make some modifications for the assembly used in the KEs and the REs.

In the KEs and the REs, the Pt capsule was held in an Fe_2O_3 sleeve, which was in turn surrounded by an alumina sleeve. At each end of the alumina sleeve, a ruby disc (0.5 mm thick) separated the Fe_2O_3 sleeve from other parts of the assembly. This structure prevents the Fe_2O_3 sleeve from being reduced by the graphite heater, or contaminating the thermocouple. Alumina spacers and then MgO spacers were positioned next to both ruby discs, to enhance the mechanical stability of the assembly. The thermocouple was protected by a combination of high-purity alumina tubing in the hot part of the assembly (~ 4 mm long), followed by mullite tubing above this. The Fe_2O_3 sleeve was made by cold pressing in a steel die and then sintered at 850°C, 1 atm for 3 hours, using acetone as a binder.

These salt-pyrex assemblies have low friction and no pressure correction is required, considering the high temperatures and long run times used in this study (Green et al., 1966; Bose & Ganguly, 1995; Klemme & O'Neill, 1997).

2.3 Experimental procedures

For each experiment, 8-10 mg starting materials was loaded into a Pt capsule. The capsules used in the DEs were stored at 110°C for 6-8 hours before welding. The Pt capsules for the KEs and the REs were stored at 150°C for 6-8 hours and then held in a steel block which had been pre-heated to 750°C while they were welded (Robinson et al., 1998).

All experiments were performed using the 'piston-out' method, i. e., the pressure was first raised to a few kilobars, then the temperature was increased to ca. 450°C to

soften the pyrex sleeve. The pressure was then increased up to ca. 0.5 kbar higher than the desired pressure, the temperature was increased to the nominal temperature of the run and finally the pressure was lowered to the required pressure (Johannes et al., 1971). The pressures were continuously monitored and adjusted, if necessary. The continual adjustment of pressure allowed each run to be controlled within ±0.2 kbar of the nominal pressure. Temperature was measured and controlled with $Pt_{94}Rh_6$-$Pt_{70}Rh_{30}$ thermocouple (type B) which was previously calibrated against the melting point of gold at 1 atm; possible pressure effects on the emf of the thermocouple were neglected. The tip of the thermocouple, the upper ruby disc and the whole Pt capsule containing the experimental charge were all carefully placed in the approximately 5 mm long hot spot of the experimental assembly. Although temperature during experiments was controlled to ± 1°C, the true temperature uncertainties are estimated to be approximately ±5 to 10°C, mainly due to slight differences in sample position and power density through the graphite heater. Such an uncertainty is consistent with the variations in melt composition and other experimental parameters observed in these experiments. For a discussion of the superior merits of type B thermocouples over other Pt/Rh thermocouples or W/Re thermocouples at temperatures near 1300°C, see Klemme and O'Neill (2000b).

2.4 Analytical methods

At the end of a run, the sample was sectioned longitudinally, mounted in epoxy and polished using a series of diamond pastes. Run products were carbon-coated and analysed on a Cameca electron microprobe at RSES, ANU and/or on a JEOL 6400 scanning electron microprobe in energy dispersive mode (EDS) at the Electron Microprobe Unit (EMU) at ANU. Coexisting phases in all run products were carefully identified by back-scattered electron imaging. Beam current was 1 nA, accelerating voltage was 15 keV and ZAF correction was applied in all analyses (Ware, 1991). A beam spot size of 1 μm was used for all crystalline phases while both 1 μm and 10 μm beam spot sizes were used for glass analyses. Calibration was based on optimisation to a large number of standards; to check this calibration and also as a monitor of any drift between analysing sessions, I repeatedly analysed three internationally recognised glass standards, GOR132G, T1G and KL2G, which have comparable compositions to the phases present in this study (Jochum et al., 2000). The 185 analyses over 24 analytical sessions are summarised in Table 2. There is excellent agreement between my electron probe analyses and the recommended values.

Table 2: Comparison of electron probe analyses and recommended values for secondary standards

	GOR132G		KL2G		T1G	
	71*	Rec. V.	57	Rec. V.	56	Rec. V.
SiO_2	46.08(0.26)*	45.98(0.30)	51.33(0.20)	51.37(0.10)	59.56(0.22)	59.28(0.20)
TiO_2	0.32(0.08)	0.29(0.01)	2.70(0.09)	2.67(0.05)	0.77(0.07)	0.74(0.01)
Al_2O_3	11.10(0.22)	11.02(0.10)	13.51(0.11)	13.43(0.10)	17.17(0.12)	17.23(0.10)
Cr_2O_3	0.38(0.08)	0.36(0.01)	0.05(0.07)	0.05(0.00)	0.04(0.05)	0.00(0.00)
FeO	10.21(0.20)	10.21(0.10)	10.78(0.22)	10.97(0.10)	6.49(0.16)	6.51(0.04)
MnO	0.17(0.08)	0.15(0.00)	0.18(0.10)	0.17(0.00)	0.11(0.07)	0.13(0.00)
MgO	22.17(0.27)	22.64(0.10)	7.37(0.07)	7.44(0.06)	3.71(0.07)	3.79(0.04)
CaO	8.57(0.13)	8.51(0.09)	11.19(0.13)	11.07(0.10)	7.13(0.10)	7.17(0.05)
Na_2O	0.98(0.06)	0.81(0.01)	2.42(0.08)	2.33(0.04)	3.06(0.13)	3.18(0.03)
K_2O	0.03(0.04)	0.03(0.00)	0.46(0.05)	0.49(0.01)	1.96(0.06)	1.97(0.02)

71*: the number of electron probe analyses. 46.08(0.26) should be read as 46.08 ± 0.26. Analysis was normalised to 100 wt% before the average and the standard deviation were calculated. For the recommended values, Rec. V., normalised results to 100 wt% are used to facilitate comparison. The standard deviation of the recommended values, however, is directly from Jochum et al (2000).

Besides the major oxides CaO, MgO, Al_2O_3, SiO_2 and K_2O expected in the run products, I also routinely analysed for FeO, Cr_2O_3 and Na_2O in all phases. Either diffusion of Fe through the Pt capsule from the Fe_2O_3 sleeve or a leak in the capsule could result in FeO contamination. Na_2O appears to be a good indicator of the purity of the starting materials. It concentrates in the melt, and 0.1-0.3 wt% was found in the glasses in this study, depending on the proportion of melt to solid in the experiment. Such a concentration is close to the limit of detection by EDS, and since it has a minimal effect on the phase relations (Walter & Presnall, 1994; Chapter 4 of this thesis) this Na_2O will henceforth be ignored.

Lithium and boron have potentially been cryptic contaminants of previous piston-cylinder studies, as these elements have not been amenable to microbeam analysis until recently. Li salts are sometimes used in noble-metal fabrication processes, and B could come from the pyrex glass (it apparently diffuses readily through Pt). To check for any such contamination, Li and B were measured in the glasses in runs C-1422, C-1448 and C-1565 (see Table 3 for experimental conditions) by LA-ICP-MS at RSES, ANU. The Li contents were 4.1±0.2 ppm, 4.1±0.1 ppm and 2.8±0.4 ppm, respectively. The B contents were slightly higher at 53±2, 54±2 and 52.3±7 ppm. Such levels should have a negligible effect on phase relations.

2.5 Fe_2O_3 sleeve and H_2O contamination

Following Robinson et al. (1998), Fe_2O_3 sleeves were used as hydrogen getters surrounding the Pt capsule in all experiments apart from the first few reported in this

study (the DEs). The idea is that an oxidised substance like Fe_2O_3 should react with H_2, which may be produced in the piston-cylinder assembly by contaminant moisture reacting with the graphite heater, for example. This should minimise the ingress of H_2 into the Pt capsule by diffusion, where it can react with silicates (e.g., alloying some Si into the Pt in FeO-free systems), thus forming H_2O. According to Robinson et al. (1998), the use of Fe_2O_3 sleeves coupled with careful drying of capsules before and during welding can reduce the water content in experimental melts from ~ 1 wt% to ~ 0.1 wt%.

The Fe_2O_3 sleeves after two experiments (C-1417 and C-1566; see Table 3 for experimental conditions) were checked by powder X-ray diffraction at the Geology Department, ANU and were found to be > 99 wt% Fe_2O_3. This does not mean that the sleeves were unnecessary, however, as analysis of the Pt capsules (using the Cameca electron microprobe in WDS mode at RSES, ANU) showed metallic Fe diffusing into the capsule. An example is given in Fig. 1 (1340°C, 11 kbar, 72 hours). While Fe metal reached the middle point of the capsule wall, the experimental charge remained untouched. However, longer run times or higher temperatures would result in Fe reaching the inner wall of the capsule, hence the need to analyse Fe routinely in run products.

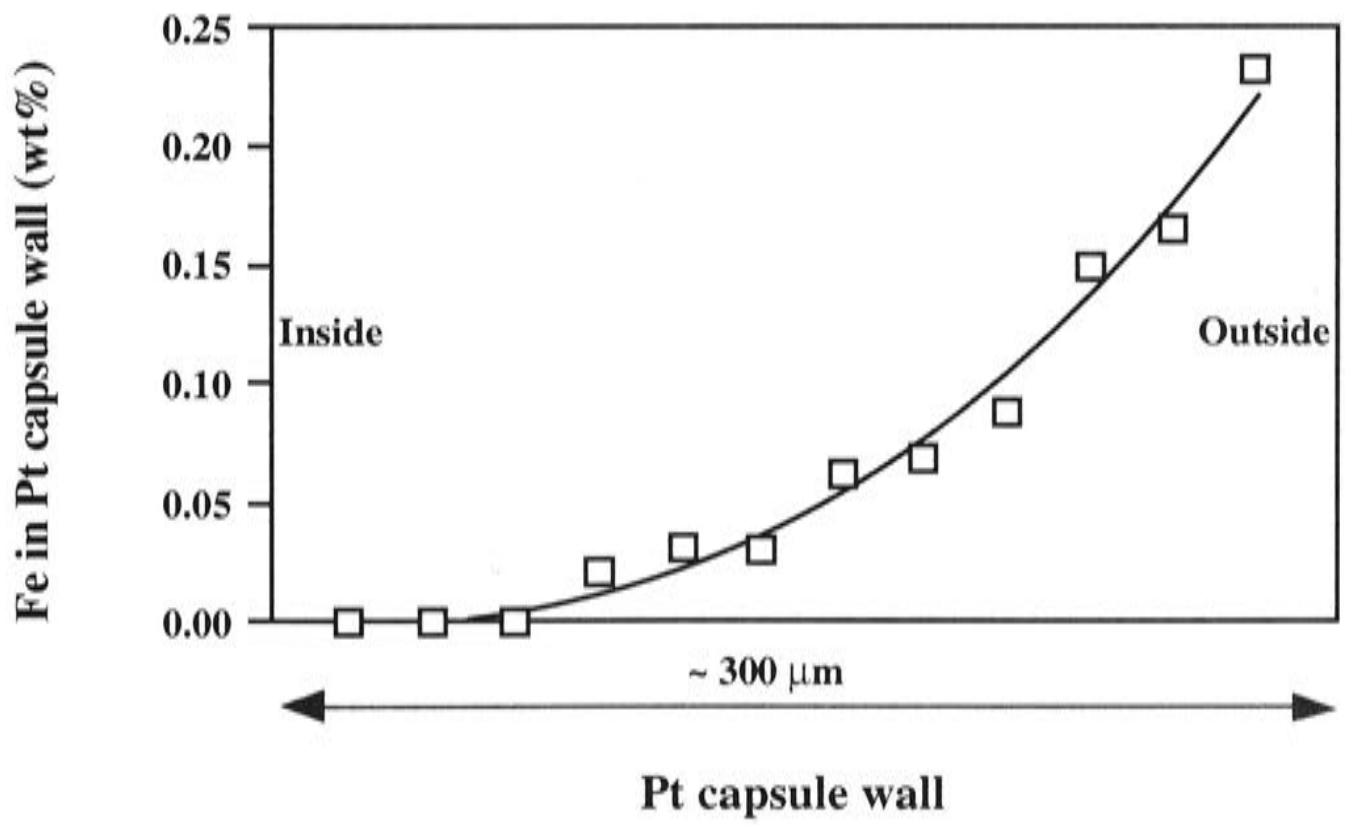

Fig. 1 Profile of metal Fe diffusion into Pt capsule wall. Experimental conditions: 11 kbar, 1340°C, 72 hours. Curve is fitted by eyes.

C-1621 contains only melt (see Table 3 for experimental conditions) and it is ideal for using transmission infrared spectroscopy to determine the water content. Details of this procedure as implemented in this study will be reported in Chapter 4 of this thesis. The average water content from seven analyses is 120 ppm, which is substantially lower than the 0.1% reported by Robinson et al. (1998) and the 1100 ppm by Falloon et al. (1999); Baker et al (1996) and Falloon et al. (2001) estimated an even larger amount, 0.5-1%, in their nominally anhydrous experiments. If the same total of H_2O as in run C-1621 were concentrated into the melt phase in those runs with smaller proportions of melt, the H_2O concentrations might be higher than in C-1621, but it seems unlikely that levels of H_2O in any run with the Fe_2O_3 sleeves would exceed 0.1%.

2.6 Attainment of equilibrium

There is a fundamental dilemma to be addressed in designing experiments aimed at obtaining the compositions of partial melts at modest degrees of melt fraction. To optimise equilibration between melt and crystals, it is obviously advantageous to have the melt distributed between the crystals, to maximise the mutual contact. This is the usual texture formed in simple experiments (the DEs of this study) with less than about 20 to 30% melt, in the absence of a temperature gradient. However, maximising the contact between melt and crystals also maximises the probability of quench modification by precipitation on the rims of crystals. In addition, melt so distributed is difficult to analyse accurately since melt pockets are small and irregularly shaped. This latter problem becomes worse as the melt fraction decreases. The experimental solution to these problems has been to devise ways of separating the melt from the crystals, as in sandwich experiments (as in this study and Stolper, 1980; Takahashi & Kushiro, 1983; Fujii & Scarfe, 1985; Falloon & Green, 1987, 1988; Robinson et al., 1998) or by extraction into diamond aggregates or similar (Johnson & Kushiro, 1992; Kushiro & Hirose, 1992; Baker et al., 1992; Hirose & Kawamoto, 1995; Hirose, 1997). Another possible tactic is to exploit the temperature gradient present in many high pressure experiments, particularly in multi-anvil experiments, to separate melt towards the hot end of the capsule (Takahashi, 1986). However, the inevitable consequence of any separation must be to impair the chances of attaining equilibrium between melt and crystals.

The problems that this can cause are well illustrated in this study by two experiments, C-1580 and C-1576 (Table 3; see Fig. 2a), in which the initial composition chosen for the "filling" part of the sandwich turned out not to be in equilibrium with the

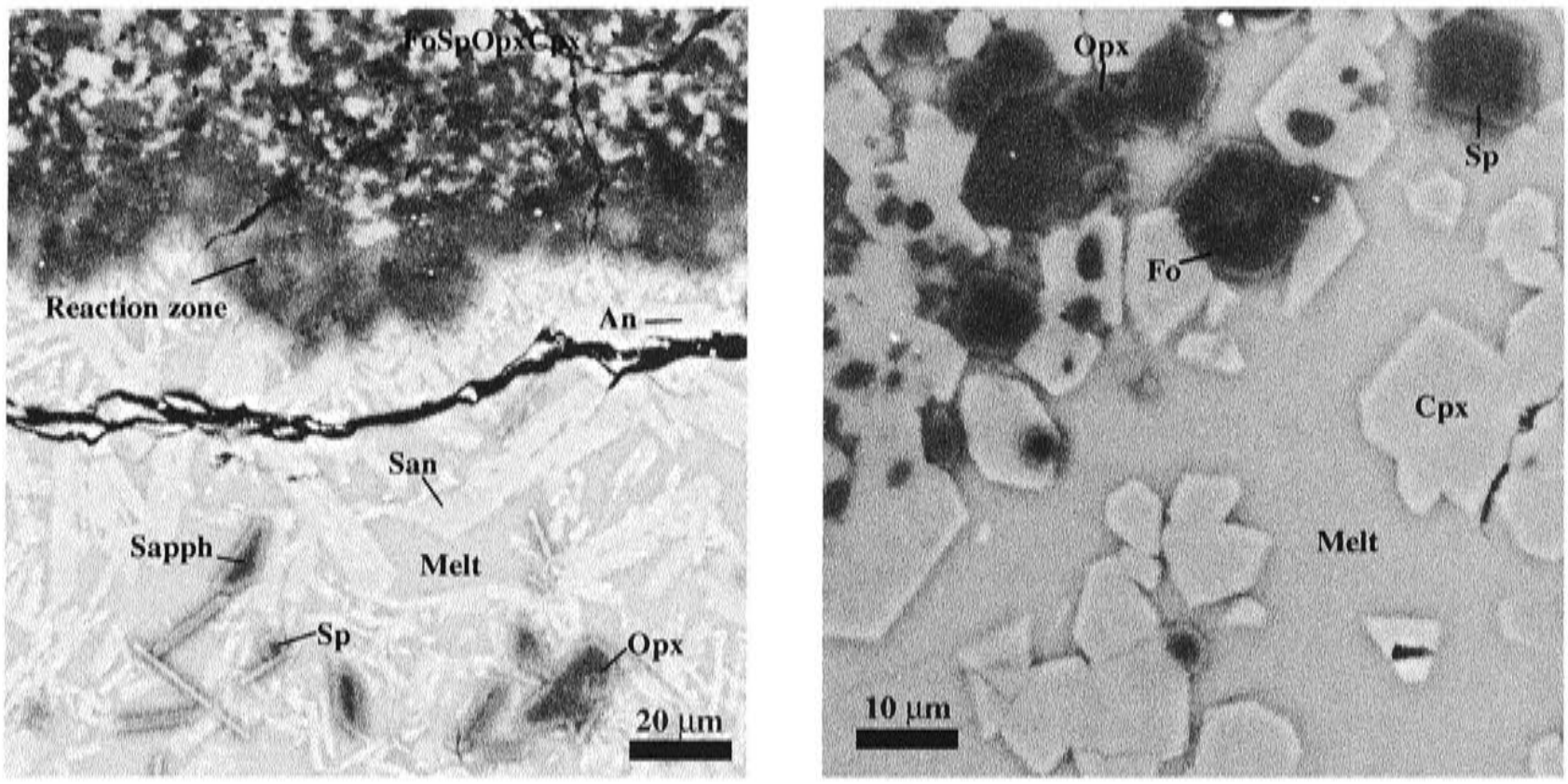

(a) (b)

Fig. 2 Electron back-scatter images showing the texture of experiments C-1576 (a) and C-1448. See Table 3 for experimental conditions and Table 4 for phase compositions.

Fo+Opx+Cpx+Sp assemblage at the ends of the sandwich (the "bread"), despite the long run times used in these experiments. Instead, the run products consisted of three zones: the initial Fo+Opx+Cpx+Sp assemblage, which in these two runs appears also not to have re-equilibrated completely as regards the pyroxene compositions (particularly Opx, see Table 4); the "filling" part, which consists of melt plus crystallised An+Sapph+San plus, in the lower temperature experiment (C-1576), Sp+Opx, the latter of which has a quite different composition to the Opx in the Fo+Opx+Cpx+Sp assemblage; and, thirdly, a narrow reaction zone of Opx, no more than 20μ wide, between the two other zones (more on this topic later). These textures are shown in Fig. 2a; for comparison, the texture developed in a successfully equilibrated sandwich experiments is given in Fig. 2b. The conspicuous inability of the melts in the "filling" to re-equilibrate with the solid Fo+Opx+Cpx+Sp assemblage in these two runs may be due to their high SiO_2, hence high viscosity.

The large difference in the composition of Opx in the different zones of C-1576 is instructive. Since the composition of a solid solution phase depends on its chemical environment, it is unlikely to be the same in the two different parts of a sandwich experiment unless these parts are in equilibrium. I therefore paid particular attention in this study to analysing pyroxene compositions in the "filling" part of the sandwich experiment, to check that they were indeed the same within analytical error as in the "bread" layers. Some crystallisation in the "filling" part is inevitable unless the initial glass composition is exactly that expected at equilibrium; in fact, as regards attainment

of equilibrium, no crystallisation in the "filling" would produce an ambiguous result, in the same way that "no reaction" in the determination of a subsolidus univariant reaction could indicate either full equilibrium at the P-T condition or merely sluggish reaction kinetics.

Clearly, a key aspect of any partial melting experiment in which the melt is separated from the crystals must be to demonstrate that the melt really is in equilibrium with these crystals. I will point out a few other runs in which I believe such equilibrium was not obtained, based on the two following criteria (as discussed above): 1) careful examination of the interface between the melt-rich part and the crystal-rich part; and 2) comparison of compositions of solid-solution phases in the two parts. Conversely, these same two criteria argue that equilibrium was indeed obtained in the great majority of the sandwich experiments reported here. Application of these criteria may not be possible in diamond-aggregate or similar types of melt extraction experiments, in which case the results from these experiments must be viewed with a degree of caution.

Several lines of evidence indicate that local equilibrium was approached closely in the experiments of this study. In addition to being the same in the different parts of the sandwich, the compositions of Opx and Cpx both show good homogeneity: the most heterogeneous oxide component, Al_2O_3, in the most heterogeneous phase, Cpx, generally has a variation of < 0.5 wt% one standard deviation, which is comparable to that observed in other simple-system experiments. The amounts of Al_2O_3 in both Opx and Cpx show small but smooth variations with temperature, and are in good agreement with the results of previous studies (see below). Similarly, the average difference between the calculated temperatures using the geothermometer of Nickel et al (1985) and the nominal experimental temperatures is only 23 °C, suggesting that the CaO contents of Opx and Cpx are in equilibrium.

The achievement of local equilibrium in this work is expected because the duration of my experiments is generally longer than that used in previous comparable studies. The results of previous near-liquidus experiments in the system CMAS (Presnall et al., 1978; Sen & Presnall, 1984; Liu & Presnall, 1990) suggested that a period of several hours is all that is required to establish reversals of phase boundaries. Walter & Presnall's (1994) experiments in the system CMAS-Na_2O found that 48 hours was long enough for the attainment of equilibrium at solidus temperatures. Most of my run durations are longer than this.

3. Experimental results

Table 3 summarises the starting materials, the run conditions, the techniques used, and the results in terms of phases present, for each experiment. The compositions of these phases are given in Table 4. Calculated temperatures from the two-pyroxene geothermometer of Nickel et al (1985) for those experiments containing both Opx and Cpx are shown in Table 3. There is a good correlation between calculated and experimental temperatures, although with a systematic offset towards the calculated temperatures being higher at low experimental temperatures, with a mean difference of 23°C (Fig. 5).

The initial DEs bracket the solidus in the system CMAS between 1300°C (C-1555) and 1310°C. The run at 1300°C contains a small amount of melt (too small to analyse). The melt may have been produced as a result of H_2 diffusion into the capsule during the run, producing a trace of water by reducing SiO_2 to Si, which alloys into Pt (Chen & Presnall, 1975). At slightly higher temperature (1310°C, C-1556), one phase (Cpx) disappears in agreement with the phase rule. I did not observe the four solid phases coexisting with melt over a range of temperature (~ 20 degrees), as did Presnall (1976) and Presnall et al (1979). This is consistent with only small amounts of chemical impurities (like H_2O) in my run products, and also minimal temperature gradients.

Fourteen experiments were carried out using the K_2O-addition method (KEs). The full Sp-lherzolite assemblage coexisting with melt is observed in seven experiments between 1260 and 1310°C. The temperatures of these KEs are plotted against the K_2O contents of the melts in Fig. 3. The relationship is linear, at least to 8 wt% K_2O and 1270°C. Extrapolating K_2O to zero gives a solidus temperature of 1319°C for the system CMAS. The change of melt composition with K_2O is shown in Fig.4. On a simple oxide weight percent (wt%) basis, SiO_2 increases linearly with K_2O, MgO and CaO both decrease linearly, and Al_2O_3 remains approximately constant, although in detail it appears to go up then down, with a maximum at ~ 6 wt% K_2O. The melt composition at the solidus in the CMAS system is found by extrapolation to zero K_2O, as for the solidus temperature: I obtain SiO_2 49.09, Al_2O_3 20.14, MgO 15.45 and CaO 15.33 wt%. The compositions of both Opx and Cpx at the CMAS solidus can be deduced similarly (see Table 5).

I then tested these results by making up a glass with this composition and locating its liquidus and solidus (REs-1). The experiment at 1340°C was above the

Table 3: Experimental conditions and phase assemblages

Run no.	Starting material	Fe_2O_3	ST	Temp. (°C)	T (hrs)	Phase assemblage	K_2O-melt	T-NBK85
DEs								
C-1111	Mix9	No	No	1330	48	Fo+Sp+Opx+Melt		
C-1556	Mix9	No	No	1310	56	Fo+Sp+Opx+Melt		
C-1555	Mix9	No	No	1300	56	Fo+Sp+Opx+Cpx+Melt(tr)		1316
KEs								
C-1417	SEM02-1+SEM02-3	Yes	Yes	1330	60	Fo+Sp+Melt	0.59	
C-1423	SEM02-1+SEM02-3	Yes	Yes	1320	55	Fo+Sp+Melt	0.63	
C-1422	SEM02-1+SEM02-3	Yes	Yes	1310	55	Fo+Sp+Opx+Cpx+Melt	0.73	1337
C-1461	SEM02-1+SEM02-4	Yes	Yes	1310	75	Fo+Sp+Opx+Cpx+Melt	2.31	1326
C-1448	SEM02-1+SEM02-4	Yes	Yes	1300	70	Fo+Sp+Opx+Cpx+Melt	4.08	1331
C-1460	SEM02-1+SEM02-4	Yes	Yes	1290	75	Fo+Sp+Opx+Cpx+Melt	4.76	1315
C-1447	SEM02-1+SEM02-4	Yes	Yes	1280	70	Fo+Sp+Opx+Cpx+Melt	6.20	1332
C-1574	SEM02-1+SEM02-8	Yes	Yes	1270	93	Fo+Sp+Opx+Cpx+Melt	8.35	1310
C-1585[#]	SEM02-1+SEM02-8	Yes	Yes	1240/1260	72/123	Fo+Sp+Opx+Cpx+Melt	8.49	1300
C-1779	SEM02-1+SEM02-13	Yes	Yes	1250	217	Sp+Opx+Cpx+San+Melt+Fo[?]	10.09	1251
C-1701	SEM02-1+SEM02-10	Yes	Yes	1240	117	Sp+Opx+Cpx+An+Melt+Fo[?]	9.17	1295
C-1708	SEM02-1+SEM02-10	Yes	Yes	1230	195	Sp+Opx+Cpx+An+San+Melt	10.12	1238
C-1580[*]	SEM02-1+SEM02-8	Yes	Yes	1250	159	Fo+Sp+Opx+Cpx		
						An+San+Sapph+Melt	9.33	
C-1576[*]	SEM02-1+SEM02-8	Yes	Yes	1230	98	Fo+Sp+Opx+Cpx		

						Sp+Opx+An+San+Sapph+Melt 8.98	
REs-1							
C-1621	SEM02-6	Yes	No	1340	24	Melt	
C-1639	SEM02-6	Yes	No	1320	54	Sp+Opx+Cpx+Melt	1337
C-1565	SEM02-6	Yes	No	1320	26	Sp+Opx+Cpx+An+Melt	1336
C-1566	SEM02-6	Yes	No	1310	48	Opx+Cpx+An+Melt(tr)	1318
REs-2							
C-1769	Fo+SEM02-6	Yes	Yes	1340	24	Fo+Melt	
C-1767	Fo+SEM02-6	Yes	Yes	1320	62	Fo+Opx+Melt	
C-1781	Fo+SEM02-6	Yes	Yes	1315	91	Fo+Sp+Opx+Cpx+Melt	1326
C-1768*	Fo+SEM02-6	Yes	Yes	1315	66	Fo+Sp+Opx+Cpx	1356
						Sp+Opx+Cpx+An	1321
C-1789	Fo+SEM02-6	Yes	No	1300	104	Fo+Sp+Opx+Cpx	1305

Fe_2O_3, Fe_2O_3 external sleeve was always used always together with hot block-welding technique.
ST Sandwich Technique.
T-NBK85, temperature (°C) calculated from the two-pyroxene thermometer for CMAS of Nickel et al (1985).
DEs, Direct partial melting experiments in system CMAS; KEs, partial melting experiments using the K_2O-method; REs, Reversal crystallisation experiments. Fo, forsterite; Sp, spinel; Opx, orthopyroxene; Cpx, clinopyroxene; An, K_2O-bearing anorthite; San, sanidine; Sapph, sapphirine; tr, only trace amount present; $Fo^?$, residual Fo only.
* disequilibrium between the different layers of the sandwich.
# the temperature in this experiment was first held at 1240°C for 72 hours and then adjusted to 1260°C for 123 hours.

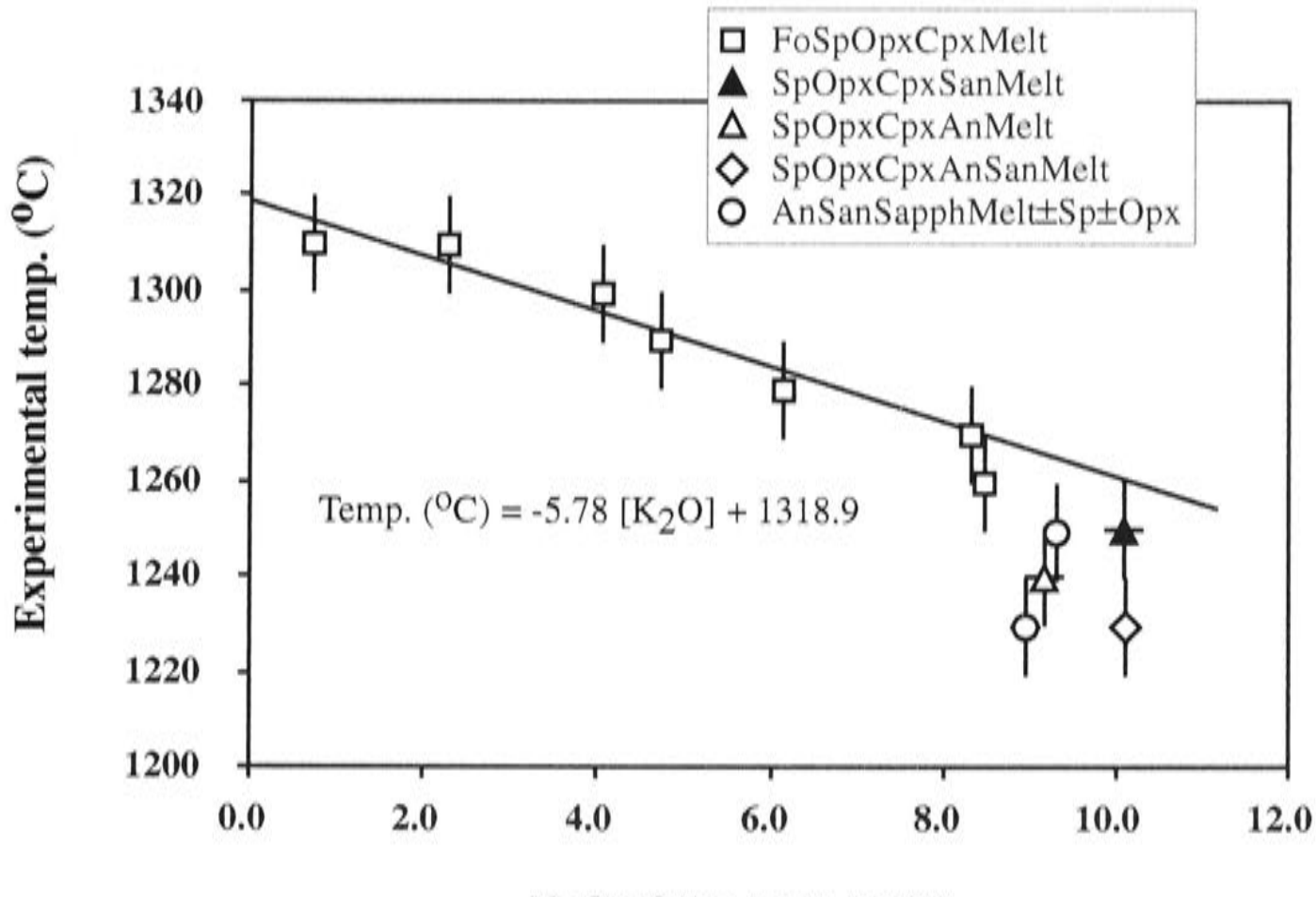

Fig. 3 Relationship between nominal experimental temperature and K_2O content of melt for the KEs. Experimental temperature uncertainty is assumed to be 10 degrees. A strong linear correlation between nominal experimental temperature and K_2O content of the melt is observed at low K_2O contents (< 8.5 wt%) for the Sp-lherzolite phase assemblage. Hence the experiments at low K_2O content (< 7 wt%) are used in the regression to derive the solidus temperature for the Sp-lherzolite phase assemblage of system CMAS at 11kbar system. By extrapolating K_2O to 0, a solidus temperature of 1319°C is derived.

liquidus, while two runs at 1320°C (C-1639 and C-1565) crystallised Sp+Opx+Cpx±An, with the residual melt being close to that in the starting material (Table 4). The compositions of the pyroxenes in C-1639 are in good agreement with the forward experiments, while those in C-1565, with a shorter run time and An present, have slightly higher Al_2O_3 (Table 4). These experiments confirm directly the peritectic nature of the melting reaction, since Fo was not crystallised. They also imply that the solidus of the phase assemblage Sp+Opx+Cpx+An is only slightly lower than that of the phase assemblage Fo+Sp+Opx+Cpx, in agreement with Kushiro (1972). Thus the run at 1310°C (C-1566) is almost completely crystallised. Although in one experiment (C-1565) melt coexists with four crystalline phases, the temperature interval over which this occurs is clearly very narrow (an infinitely narrow temperature interval is expected from the phase rule).

The REs-1 demonstrate empirically that simple crystallization experiments cannot adequately reverse the partial melting equilibrium when this is peritectic, as here, (i.e., the melt is in reaction relationship with Fo). Accordingly, I tried reversal crystallization experiments with added Fo. These experiments (called REs-2) directly

Table 4: Composition data from electron microprobe analyses. For run conditions and other messages, see Table 3.

		CaO	MgO	Al_2O_3	SiO_2	K_2O
DEs						
C-1111, 1330°C	Fo(10)	0.28(0.03)	57.16(0.11)	0.00(0.00)	42.57(0.11)	-
	Sp(7)	0.11(0.06)	28.43(0.10)	71.45(0.11)	0.00(0.00)	-
	Opx(8)	2.16(0.16)	34.78(0.33)	9.25(0.20)	53.82(0.20)	-
	Melt(8)	13.97(0.28)	16.16(0.45)	20.74(0.19)	49.13(0.12)	-
C-1556, 1310°C	Fo(14)	0.28(0.06)	56.78(0.12)	0.17(0.05)	42.67(0.16)	-
	Sp(13)	0.10(0.06)	28.91(0.14)	70.83(0.13)	0.16(0.12)	-
	Opx(22)	2.10(0.14)	35.03(0.19)	8.46(0.39)	54.41(0.27)	-
	Melt(14)	14.34(0.27)	15.73(0.36)	20.14(0.31)	49.79(0.25)	-
C-1555, 1300°C	Fo(12)	0.30(0.05)	56.79(0.18)	0.20(0.06)	42.72(0.14)	-
	Sp(14)	0.10(0.08)	28.99(0.17)	70.70(0.18)	0.22(0.14)	-
	Opx(20)	2.11(0.13)	34.86(0.21)	8.48(0.39)	54.55(0.30)	-
	Cpx(21)	18.63(0.29)	20.73(0.30)	8.81(0.29)	51.84(0.26)	-
	Melt*					
KEs						
C-1417, 1330°C	Fo(14)	0.32(0.03)	56.72(0.13)	0.00(0.00)	42.96(0.12)	-
	Sp(15)	0.12(0.03)	28.46(0.09)	71.42(0.09)	0.00(0.00)	-
	Melt(24)	14.17(0.07)	15.47(0.11)	20.36(0.06)	49.41(0.14)	0.59(0.02)
C-1423, 1320°C	Fo(12)	0.33(0.04)	56.96(0.11)	0.00(0.00)	42.72(0.12)	-
	Sp(17)	0.08(0.04)	28.42(0.11)	71.51(0.11)	0.00(0.00)	-
	Melt(12)	14.64(0.07)	14.91(0.07)	20.40(0.08)	49.43(0.11)	0.63(0.02)
C-1422, 1310°C	Fo(18)	0.31(0.03)	56.78(0.11)	0.00(0.00)	42.91(0.11)	-
	Sp(13)	0.13(0.08)	28.35(0.09)	71.52(0.10)	0.00(0.00)	-
	Opx(19)	2.47(0.41)	34.36(0.32)	8.60(0.34)	54.57(0.27)	-
	Cpx(19)	18.22(0.40)	21.15(0.26)	8.67(0.42)	51.96(0.30)	-
	Melt(19)	14.60(0.07)	14.30(0.07)	20.39(0.10)	49.98(0.11)	0.73(0.03)
C-1461, 1310°C	Fo(8)	0.29(0.03)	56.72(0.04)	0.00(0.00)	42.99(0.06)	-
	Sp(8)	0.08(0.04)	28.56(0.12)	71.28(0.10)	0.08(0.04)	-
	Opx(21)	2.23(0.17)	34.84(0.30)	8.34(0.42)	54.59(0.33)	-
	Cpx(21)	18.44(0.35)	21.00(0.40)	8.39(0.34)	52.17(0.26)	-
	Melt(15)	12.87(0.14)	12.75(0.13)	20.55(0.16)	51.52(0.13)	2.31(0.07)
C-1448, 1300°C	Fo(9)	0.30(0.05)	56.71(0.19)	0.09(0.13)	42.89(0.15)	-
	Sp(8)	0.14(0.06)	28.51(0.07)	71.25(0.16)	0.10(0.09)	-
	Opx(19)	2.19(0.30)	34.80(0.36)	8.50(0.40)	54.51(0.37)	-
	Cpx(19)	18.30(0.47)	20.90(0.42)	8.58(0.43)	52.22(0.35)	-
	Melt(20)	11.19(0.13)	10.09(0.11)	21.47(0.12)	53.17(0.15)	4.08(0.09)
C-1460, 1290°C	Fo(7)	0.30(0.03)	56.71(0.09)	0.03(0.06)	42.96(0.09)	-
	Sp(13)	0.11(0.07)	28.45(0.12)	71.15(0.24)	0.30(0.19)	-
	Opx(20)	2.10(0.26)	34.99(0.32)	8.19(0.39)	54.72(0.24)	-

Table 4: continued

	Cpx(23)	18.71(0.38)	20.76(0.45)	8.28(0.45)	52.24(0.39)	-
	Melt(14)	10.43(0.11)	9.36(0.23)	21.60(0.21)	53.85(0.17)	4.76(0.15)
C-1447, 1280°C	Fo(6)	0.28(0.05)	57.00(0.18)	0.00(0.00)	42.73(0.21)	-
	Sp(6)	0.08(0.04)	28.47(0.13)	71.32(0.21)	0.13(0.11)	-
	Opx(15)	2.19(0.30)	34.83(0.54)	8.33(0.58)	54.64(0.38)	-
	Cpx(15)	18.28(0.45)	21.17(0.62)	8.27(0.56)	52.29(0.38)	-
	Melt(11)	8.93(0.17)	7.33(0.14)	21.74(0.35)	55.83(0.28)	6.17(0.11)
C-1574, 1270°C	Fo(11)	0.27(0.07)	56.46(0.14)	0.36(0.11)	42.91(0.11)	-
	Sp(12)	0.09(0.04)	29.09(0.13)	70.43(0.30)	0.39(0.25)	-
	Opx(18)	2.19(0.29)	34.97(0.32)	8.28(0.56)	54.56(0.40)	-
	Cpx(17)	18.86(0.58)	20.70(0.52)	8.31(0.49)	52.13(0.43)	-
	Melt(13)	6.35(0.13)	5.12(0.09)	20.93(0.12)	59.25(0.18)	8.35(0.12)
C-1585, 1260°C	Fo(7)	0.27(0.03)	56.58(0.14)	0.29(0.09)	42.86(0.16)	-
	Sp(9)	0.05(0.03)	29.05(0.11)	70.58(0.10)	0.31(0.07)	-
	Opx(15)	1.74(0.15)	35.16(0.24)	8.12(0.42)	54.98(0.32)	-
	Cpx(17)	18.97(0.56)	20.79(0.48)	8.09(0.46)	52.16(0.34)	-
	Melt(14)	6.81(0.14)	6.20(0.12)	20.80(0.09)	57.69(0.18)	8.49(0.11)
C-1779, 1250°C	Sp(13)	0.04(0.04)	28.70(0.12)	71.04(0.18)	0.21(0.08)	-
	Opx(22)	1.79(0.17)	34.62(0.22)	9.36(0.52)	54.24(0.33)	-
	Cpx(18)	20.03(0.45)	19.16(0.43)	9.67(0.48)	51.14(0.31)	-
	San(15)	2.81(0.43)	0.00(0.00)	20.81(0.38)	62.29(0.42)	14.08(0.40)
	Melt(22)	5.44(0.15)	4.22(0.17)	22.16(0.12)	58.08(0.30)	10.09(0.20)
C-1701, 1240°C	Sp(12)	0.07(0.05)	28.69(0.11)	70.99(0.27)	0.25(0.18)	-
	Opx(19)	1.71(0.10)	34.66(0.19)	9.30(0.45)	54.33(0.29)	-
	Cpx(3)**	18.91(1.08)	20.21(1.83)	9.97(1.71)	50.78(2.22)	0.14(0.16)
	An(6)	15.21(0.34)	0.77(0.18)	31.14(0.38)	49.69(0.31)	3.20(0.28)
	Melt(12)	6.15(0.16)	4.39(0.15)	20.77(0.18)	59.53(0.28)	9.17(0.12)
C-1708, 1230°C	Sp(14)	0.05(0.05)	28.73(0.16)	71.00(0.17)	0.22(0.13)	-
	Opx(22)	1.86(0.17)	34.74(0.19)	8.93(0.45)	54.47(0.33)	-
	Cpx(22)	20.27(0.42)	19.03(0.33)	9.55(0.38)	51.15(0.26)	-
	An(8)	14.09(0.65)	0.63(0.28)	30.46(0.49)	50.80(0.64)	4.02(0.54)
	San(20)	3.10(0.38)	0.00(0.00)	21.14(0.40)	61.95(0.42)	13.81(0.38)
	Melt(10)	5.41(0.11)	3.90(0.09)	21.04(0.11)	59.54(0.23)	10.12(0.11)
C-1580, 1250°C	Solid region					
	Fo(12)	0.24(0.08)	56.48(0.26)	0.28(0.15)	42.99(0.20)	-
	Sp(11)	0.09(0.06)	28.63(0.10)	71.12(0.13)	0.16(0.10)	-
	Opx(16)	2.08(0.29)	34.82(0.39)	8.67(0.58)	54.53(0.42)	-
	Cpx(17)	18.94(0.69)	20.58(0.57)	8.58(0.39)	51.91(0.39)	-
	Glass region					
	An(9)	12.45(0.93)	0.41(0.27)	28.59(0.67)	52.98(0.93)	5.58(0.77)
	San(9)	2.66(0.16)	0.00(0.00)	20.38(0.14)	62.83(0.17)	13.82(0.18)
	Sapph(9)	0.28(0.14)	23.99(0.41)	57.14(0.64)	18.59(0.78)	-
	Melt(14)	4.20(0.10)	3.23(0.11)	20.05(0.07)	63.19(0.21)	9.33(0.17)

Table 4: continued

C-1576, 1230°C	Solid region					
	Fo(14)	0.24(0.04)	56.49(0.19)	0.22(0.06)	43.06(0.16)	-
	Sp(13)	0.10(0.04)	28.60(0.13)	71.07(0.11)	0.23(0.07)	-
	Opx-1(10)	2.04(0.31)	34.83(0.43)	8.72(0.49)	54.41(0.38)	-
	Cpx(14)	18.69(0.57)	20.54(0.53)	8.65(0.45)	52.12(0.43)	-
	Glass region					
	Sp(9)	0.10(0.05)	28.70(0.11)	70.99(0.14)	0.21(0.05)	-
	Opx-2(6)	0.72(0.04)	33.40(0.48)	14.11(0.54)	51.76(0.13)	-
	An(5)	12.52(1.02)	0.15(0.03)	29.73(0.89)	52.44(1.10)	5.51(0.84)
	San(8)	3.23(0.33)	0.05(0.06)	21.18(0.31)	62.13(0.43)	13.41(0.26)
	Sapph(9)	0.26(0.04)	24.51(0.49)	54.82(0.65)	20.40(0.39)	-
	Melt(12)	3.47(0.11)	2.55(0.11)	18.61(0.12)	66.39(0.26)	8.98(0.10)
REs-1						
C-1621, 1340°C	Melt(8)	15.60(0.12)	15.06(0.09)	19.88(0.12)	49.46(0.16)	-
C-1639, 1320°C	Sp(6)	0.14(0.07)	28.84(0.14)	70.78(0.15)	0.25(0.14)	-
	Opx(13)	2.36(0.26)	34.31(0.38)	9.04(0.43)	54.29(0.22)	-
	Cpx(16)	18.19(0.51)	21.22(0.42)	9.07(0.41)	51.52(0.36)	-
	Melt(8)	15.42(0.16)	14.28(0.14)	20.45(0.09)	49.85(0.10)	-
C-1565, 1320°C	Sp(9)	0.24(0.14)	28.98(0.17)	70.31(0.38)	0.48(0.37)	-
	Opx(16)	2.35(0.21)	34.26(0.27)	9.82(0.62)	53.57(0.48)	-
	Cpx(31)	18.20(0.41)	20.99(0.36)	9.78(0.46)	51.04(0.36)	-
	An(11)	20.24(0.13)	0.74(0.18)	34.65(0.35)	44.37(0.26)	-
	Melt(14)	15.51(0.24)	14.13(0.12)	20.76(0.08)	49.60(0.14)	-
C-1566, 1310°C	Opx(14)	2.33(0.07)	35.06(0.25)	7.47(0.68)	55.14(0.43)	-
	Cpx(15)	18.63(0.33)	21.19(0.39)	7.99(0.64)	52.19(0.36)	-
	An(9)	20.26(0.14)	0.88(0.17)	34.66(0.28)	44.21(0.26)	-
	Melt*					
REs-2						
C-1769, 1340°C	Fo(13)	0.30(0.04)	56.54(0.14)	0.21(0.07)	42.95(0.17)	-
	Melt(16)	14.38(0.12)	16.70(0.09)	19.37(0.07)	49.55(0.12)	-
C-1767, 1320°C	Fo(12)	0.29(0.05)	56.51(0.22)	0.14(0.09)	43.07(0.17)	-
	Opx(21)	2.30(0.17)	34.82(0.33)	7.74(0.77)	55.14(0.42)	-
	Melt(19)	15.14(0.11)	15.41(0.11)	19.90(0.11)	49.54(0.13)	-
C-1781, 1315°C	Fo(13)	0.26(0.05)	56.53(0.13)	0.18(0.08)	43.03(0.10)	-
	Sp(12)	0.10(0.06)	28.63(0.06)	71.08(0.16)	0.19(0.10)	-
	Opx(22)	2.25(0.15)	34.34(0.25)	9.19((0.45)	54.22(0.25)	-
	Cpx(22)	18.47(0.47)	20.87(0.43)	9.14(0.41)	51.52(0.31)	-
	Melt(16)	15.35(0.12)	14.82(0.07)	20.35(0.12)	49.48(0.15)	-
C-1768, 1310°C	Fo(14)	0.26(0.05)	56.49(0.14)	0.14(0.06)	43.10(0.13)	-
	Sp(8)	0.05(0.04)	28.44(0.12)	71.51(0.13)	0.00(0.00)	-
	Opx-1(13)	2.26(0.14)	34.34(0.18)	9.11(0.38)	54.28(0.19)	-
	Cpx-1(14)**	17.54(0.89)	21.53(1.08)	9.47(0.83)	51.46(0.49)	-

Table 4: continued

	Glass region					
	Sp(10)	0.20(0.07)	28.51(0.10)	70.79(0.26)	0.50(0.21)	-
	Opx-2(22)	2.45(0.21)	34.61(0.24)	7.87(0.44)	55.07(0.34)	-
	Cpx-2(15)	18.55(0.36)	21.00(0.34)	8.48(0.25)	51.96(0.23)	-
	An(18)	19.85(0.17)	0.74(0.21)	35.21(0.32)	44.19(0.23)	-
C-1789, 1300°C	Fo(11)	0.30(0.06)	56.54(0.13)	0.16(0.04)	42.99(0.14)	-
	Sp*					
	Opx(17)	2.19(0.46)	34.80(0.45)	8.87(0.40)	54.14(0.41)	-
	Cpx(17)	18.81(0.34)	20.25(0.26)	9.70(0.53)	51.24(0.37)	-

The numbers in parentheses after the name of the phase are the number of successful analyses performed on that phase. Data reading: 0.28(0.03) is 0.28 ± 0.03. All analyses were normalised to 100 wt% before averages and standard deviation were calculated. *: phase is confirmed but too small to analyse. ** phase is confirmed but only poor quality analyses are available.

constrain the solidus of the Sp-lherzolite phase assemblage in the system CMAS at 11 kbar to be ~ 1315±10 °C. The experiment at this temperature, C-1781, produced four crystalline phases plus melt; however, the melt composition is slightly less magnesian than the composition deduced from the KEs (Table 5), and is intermediate between this composition and that in equilibrium with Opx+Cpx+Sp+An. The Al_2O_3 content of the pyroxenes is also slightly higher than in other comparable runs. This raises the question of whether equilibrium between Fo and the "filling" part of the sandwich was truly established. Clearly equilibrium was not established in a similar experiment at the slightly lower temperature of 1310°C, C-1768; here the "filling" crystallized completely to Sp+Opx+Cpx+An, with An separated from Fo by a narrow reaction zone of Opx+Cpx+Sp. The further implications of this experiment for the interpretation of results from melt-extraction experiments (like the diamond-aggregate technique) will be discussed below.

Table 5 compares the result of this study to previous work in CMAS at similar pressures in the literature. There is a difference of 30 degrees between the solidus as determined here and the solidus defined by run 116-3 in Presnall (1976), which contains Fo+Opx+Cpx+Sp+Melt at 1350°C and 11 kbar. However, another run with the same starting composition reported by Presnall et al. (1979), their 122-8 at 1327°C and 11 kbar, contained Fo+Opx+Melt and is therefore above the solidus, which would be in agreement with my result. There is also good agreement as regards the solidus melt composition and the solidus pyroxene compositions. It may be noted that Presnall (1976) reported 8.4±0.2 wt% Al_2O_3 for his Opx based on five analyses, but noted two outliers at 9.6 and 5.5 wt% Al_2O_3, indicating that his Opx was somewhat heterogenous in composition. The higher amount (9.49 wt%) later reported by Walter and Presnall

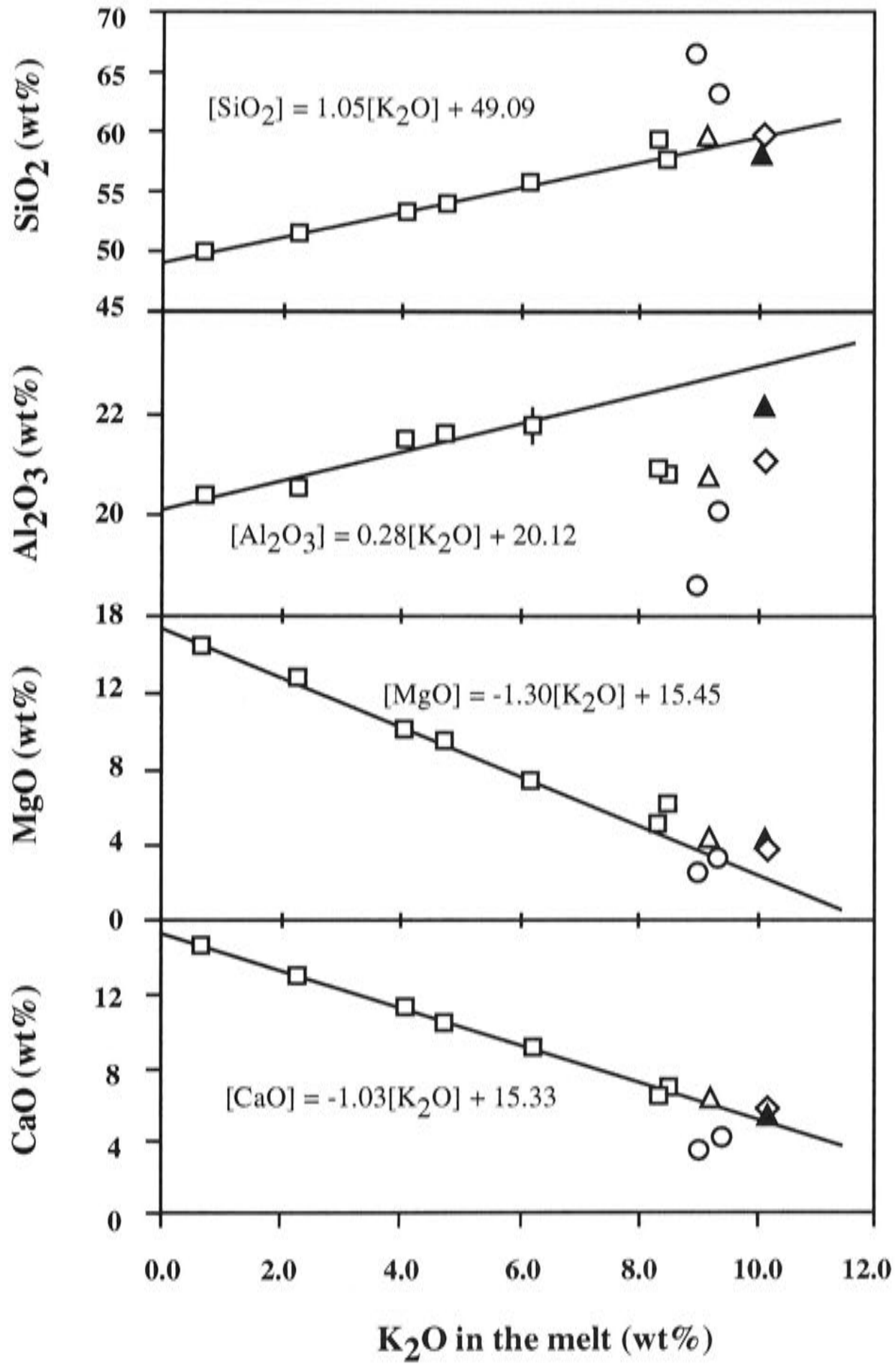

Fig. 4 Variation diagram showing oxide trends for melts in the KEs. Symbols: the same as in Fig. 3. One standard deviation of the oxide content is only occasionally larger than the symbols, as shown. The diagram suggests a strong linear correlation between SiO_2-K_2O, Al_2O_3-K_2O, MgO-K_2O and CaO-K_2O at low K_2O contents (< 8.5 wt%). Hence the experiments at low K_2O content (< 7 wt%) are used in the regression to derive the solidus melt composition of a simplified spinel lherzolite in system CMAS. By extrapolating the K_2O content to 0, a solidus melt composition, SiO_2 49.09, Al_2O_3 20.12, MgO 15.45 and CaO 15.33, is derived. This melt composition was used as the starting material (SEM02-6 in Table 1) for the REs. By extrapolating the K_2O content to 10, I derived a melt composition which was used as the sandwiched starting material (SEM02-8 in Table 1) in some experiments at high K_2O content (Table 3).

(1994) following their re-analysis of this experiment may be due to including high-Al_2O_3 outliers. The solidus temperature and melt composition reported by Kushiro (1972) at 10 kbar agrees slightly less well, the main difference in melt composition

being in CaO (Table 5). Kushiro (1972) also reports data for the phase assemblage Sp+Opx+Cpx+An+Melt; in agreement with this study, this isobaric invariant point occurs at essentially the same temperature at a melt composition only ~ 1 wt % lower in MgO than Fo+Sp+Opx+Cpx+Melt.

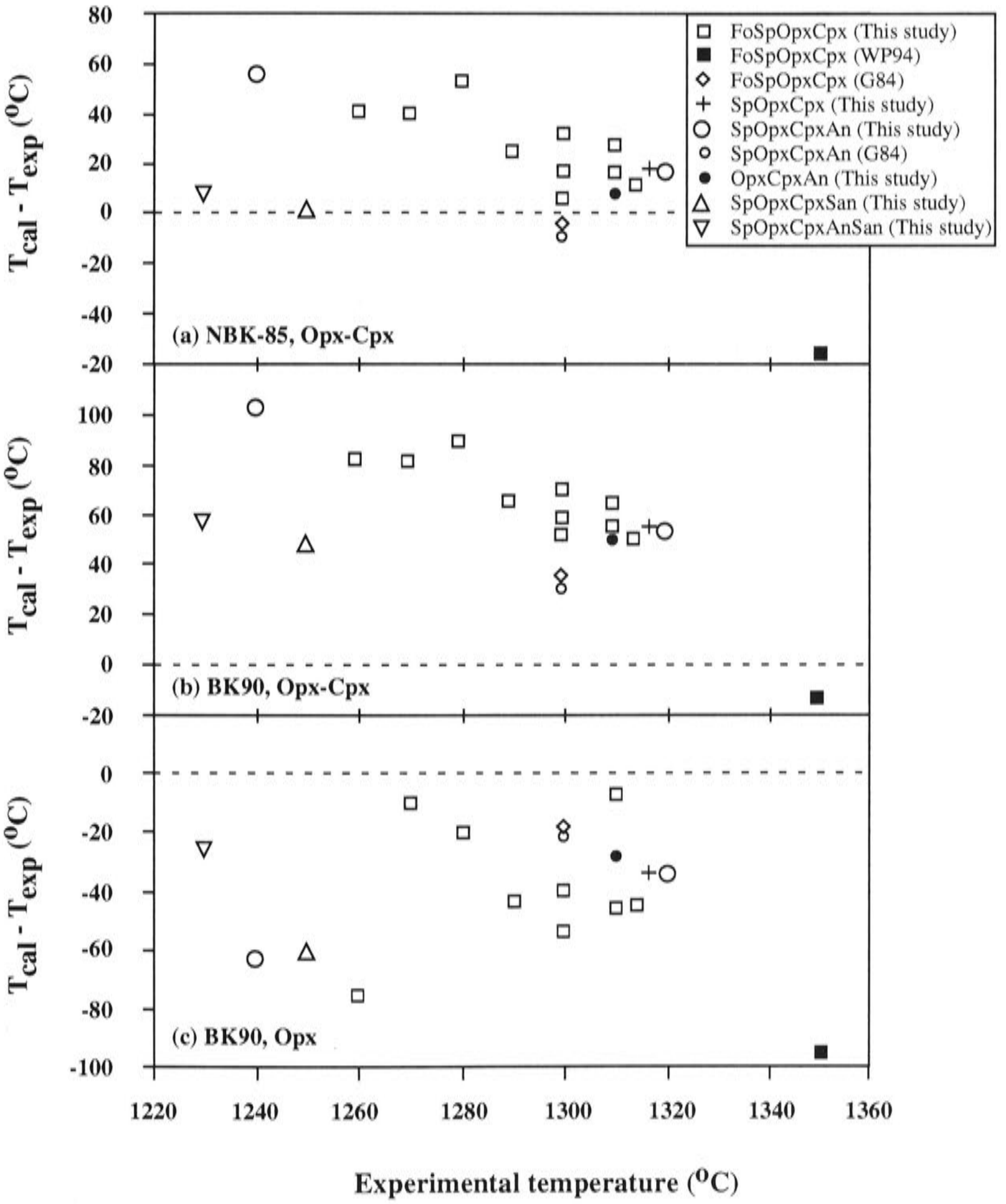

Fig. 5 Temperature difference between the calculated temperature and the nominal experimental temperature (11 kbar). In (a) the Opx-Cpx geothermometer of Nickel et al (1985) is used, in (b) the Opx-Cpx geothermometer of Brey & Kohler (1990; formula 9) is used while in (c) the Opx geothermometer of Brey & Kohler (1990; formula 10) is used. In order to show the data clearly, some data are slightly shifted horizontally.

Table 5: Compositions of Melt, Opx and Cpx in the system CMAS at 10 or 11 kbar in the isobaric invariant assemblages Fo+Sp+Opx+Cpx+Melt and Sp+Opx+Cpx+An+Melt: comparison with literature data

		Phase assemblage Fo+Sp+Opx+Cpx+Melt						Phase assemblage Sp+Opx+Cpx+An+Melt	
Run #	from KEs at K_2O=0	C-1781	116-3	116-3	116-3	1-K72		C-1565	2-K72
Source	This study	This study	P76	P79	WP94	K72		This study	K72
T	1319°C	1315°C	1350°C	1350°C	1350°C	1350°C		1320°C	1345°C
P	11	11	11	11	11	10		11	10
Melt	SiO_2	49.09	49.48(0.15)		49.13(0.37)	49.30(0.1)	50.10	49.60(0.14)	50.91
	Al_2O_3	20.12	20.35(0.12)		19.72(0.33)	19.20(0.1)	20.93	20.76(0.08)	21.37
	MgO	15.45	14.82(0.07)		15.69(0.41)	16.80(0.1)	16.00	14.13(0.12)	14.82
	CaO	15.33	15.35(0.12)		15.47(0.12)	14.90(0.1)	12.98	15.51(0.24)	12.90
Opx	SiO_2	54.54	54.22(0.25)	54.00(0.3)		53.90(0.65)		53.57(0.48)	
	Al_2O_3	8.57	9.19(0.45)	8.51(0.2)		9.49(0.65)		9.82(0.62)	
	MgO	34.47	34.34(0.25)	35.16(0.2)		34.60(0.25)		34.26(0.27)	
	CaO	2.43	2.25(0.15)	2.33(0.1)		2.17(0.1)		2.35(0.21)	
Cpx	SiO_2	51.97	51.52(0.31)			51.40(0.4)		51.04(0.36)	
	Al_2O_3	8.66	9.14(0.41)			9.50(0.65)		9.78(0.46)	
	MgO	21.06	20.87(0.43)			20.20(0.5)		20.99(0.36)	
	CaO	18.30	18.47(0.47)			19.30(0.25)		18.20(0.41)	

P76, Presnall (1976); P79, Presnall et al. (1979); WP94, Walter & Presnall (1994); K72, Kushiro (1972). Data from the literature have been renormalised to 100%.

I then attempted to locate the isobaric invariant point in the system CMAS-K_2O, by exploring lower temperatures. I expected to locate an isobaric invariant point at which sanidine would join Fo+Opx+Cpx+Sp in equilibrium with melt. My first attempt consisted of two runs, C-1580 (1250°C) and C-1576 (1230°C), with the same initial melt composition SEM02-08 as used at 1260 and 1270°C. However, this melt composition crystallised An+Sapph+San at 1260°C, joined at 1250°C by Sp and Opx, the latter with very high Al_2O_3 (14 wt%). This assemblage was clearly out of equilibrium with the Fo+Opx+Cpx+Sp layers, with a narrow reaction zone of about 10 - 20μm separating the two assemblages (see Fig. 2a).

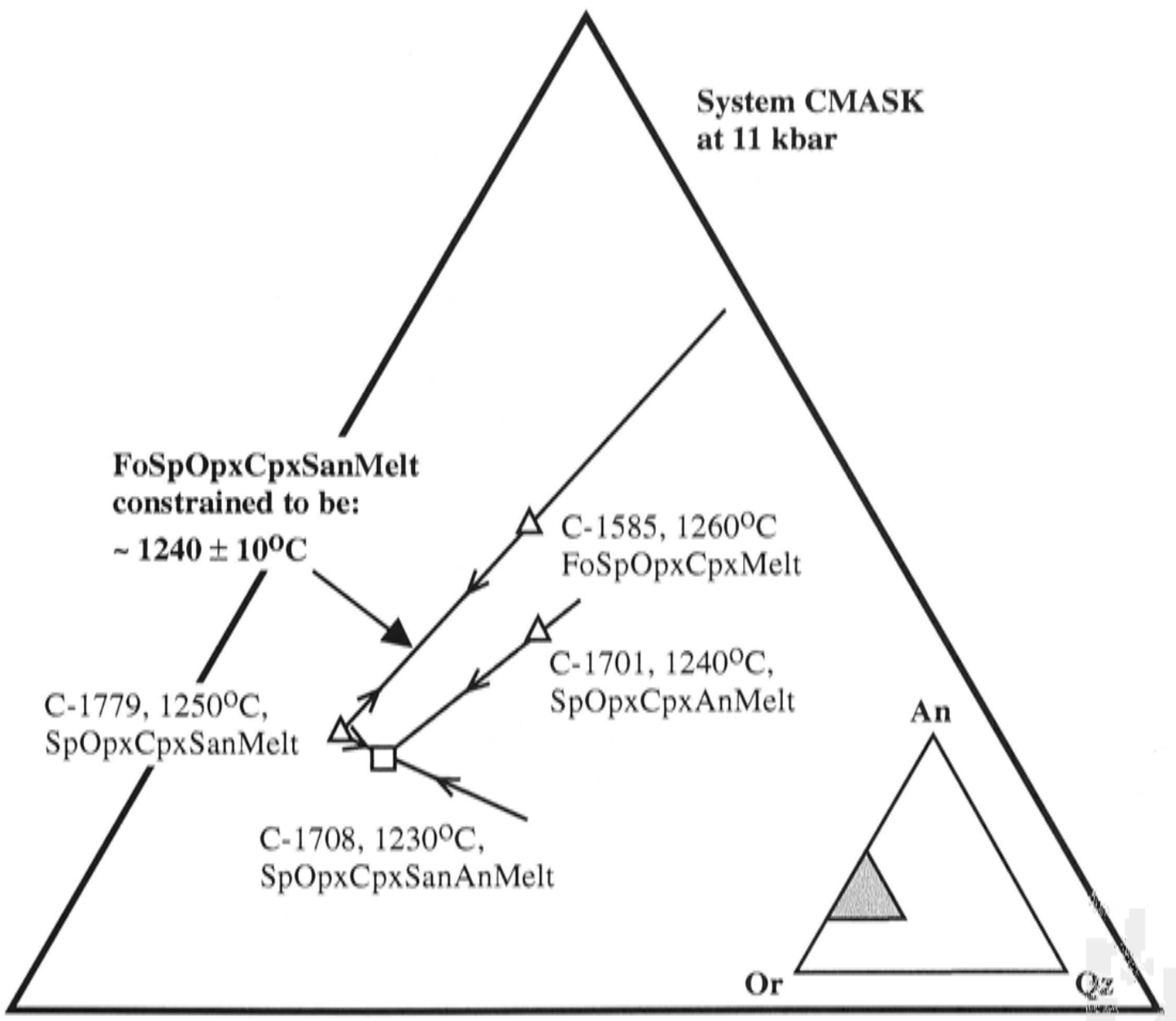

Fig. 6 Defining brackets for the isobariaclly invariant point FoSpOpxCpxSanMelt of the system CMAS-K_2O at 11 kbar. The melt composition of this invariant point locates between C-1779 (on univariant line SpOpxCpxSanMelt) and C-1585 (on univariant line FoSpOpxCpxAnMelt). Arrows show temperature change direction which is constrained by my experimental observation or by the method of Presnall (1986). The solidus of this invariant point should be lower than 1250°C but slightly higher than the solidus (1230°C) of another invariant point SpOpxCpxSanAnMelt.

With this experience, I tried again with a new initial melt composition (SEM02-10). This time equilibrium was approached throughout the charge, but Fo was reacted

out, producing Sp+Opx+Cpx+An+Melt (with a trace of residual Fo) in C-1701 at 1240°C, and the isobarically invariant assemblage Sp+Opx+Cpx+An+San+Melt in C-1708 at 1230°C. A third attempt with another initial melt composition (SEM02-13) produced Sp+Opx+Cpx+San+Melt with a trace of residual Fo in C-1779 at 1250°C.

These and the higher-temperature results in the system CMAS-K_2O are summarized in Fig. 6, a projection from Fo+Di onto the An-Or-Qz plane. Although I failed to locate the isobaric invariant point Fo+Sp+Opx+Cpx+San+Melt at 11 kbar directly, this point, which is eutectic-like on this projection, must occur at a melt composition between runs C-1585 at 1260°C and C-1779 at 1250°C, at a slightly lower temperature (i.e., ~1240±10 °C).

4. Discussions

4.1 Compositions of Opx and Cpx

The compositions of both Opx and Cpx in the experimental run products vary in two ways, namely their CaO and their Al_2O_3 contents.

CaO in pyroxenes

The partitioning of CaO between Opx and Cpx is the basis of the two-pyroxene geothermometry, the main means of estimating temperatures of equilibration in lherzolitic assemblages. To compare my data with previous work in the system CMAS, I have used the formulation of Nickel et al. (1985) to calculate temperatures from my experimental run products (Table 3 and Fig. 5(a)). The calculated temperatures are in good agreement with nominal experimental temperatures, although in detail there is a weak systematic tendency for the former to be higher at low experimental temperatures. The average difference between the calculated temperature and the nominal experimental temperature for the experiments reported here is just 23 degrees with a standard deviation of 17 degrees. I also tested two other pyroxene geothermometers, equations (9) and (10) of Brey & Köhler (1990). Eqn. (9), which uses the exchange of Ca between Opx and Cpx, yields higher calculated temperatures, with an average difference of 65°C between the calculated temperatures and the experimental temperatures (Fig. 5(b)). Conversely, eqn. (10), which only uses the amount of Ca in Opx co-existing with Cpx, gives lower calculated temperatures, with an average difference of –39 degrees (Fig. 5(c)). These equations were intended for use with

chemically complex natural systems, but were formulated as simply as possible for ease of use. Figs. 5b and 5c indicate that this simplicity may result in a loss of accuracy; consequently, more rigorous albeit tediously complicated two-pyroxene geothermometers could potentially give better results.

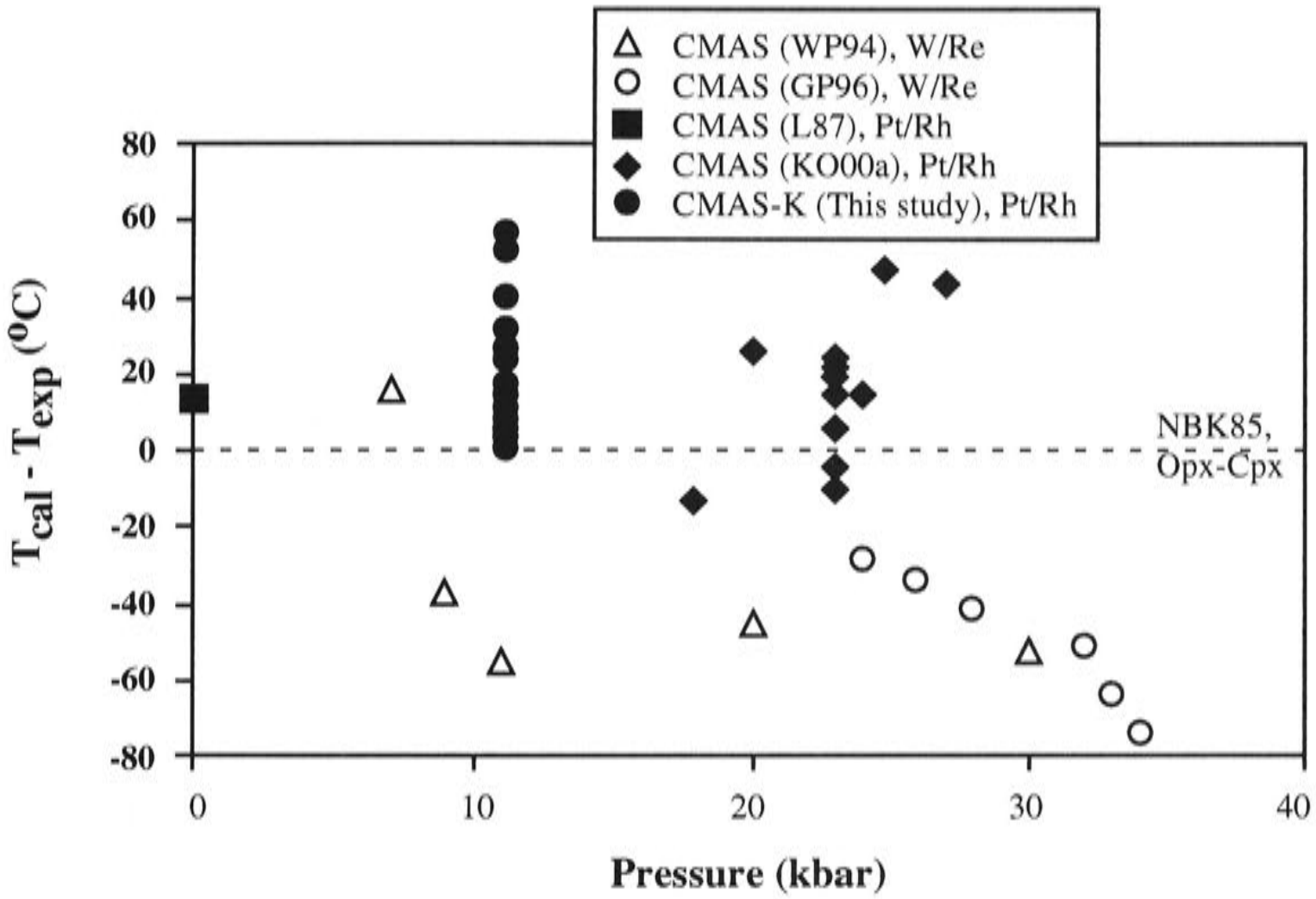

Fig. 7 Comparison of temperature measurement using Pt/Rh thermocouples and W/Re thermocouples in experiments in the system CMAS and the system CMAS-K_2O. Temperature is calculated using the Opx-Cpx geothermometer of Nickel et al. (1984). When Pt/Rh thermocouples used, similar temperature measurement was observed (This study; KO00a, Klemme & O'Neill, 2000a; L87, Longhi, 1987). The W/Re gave out higher nominal experimental temperature (WP94, Walter & Presnall, 1994; Gudfinnsson & Presnall, 1996). Apparently, the Pt/Rh thermocouples are independent to pressure while the W/Re thermocouples may be pressure-dependent.

Shown in Fig. 7 are differences between observed and calculated temperatures using the geothermometer of Nickel et al (1985) for experiments in the system CMAS at pressures from 1 atm to 34 kbar, from Longhi (1987), Walter & Presnall (1994), Gudfinnsson & Presnall (1996) and Klemme & O'Neill (2000a), and this study (CMAS±K_2O). Similar diagrams using the two geothermometers of Brey & Köhler (1990), their eqns (9) and (10), are shown in Fig. 8, with the addition of the CMAS-Na_2O data from Walter and Presnall (1994). These plots raise a number of issues regarding potential problems with the experimental database on the CMAS system, in addition to the problem with the geothermometers. One consideration is the choice of thermocouple. The Nickel et al. (1985) and Brey and Köhler (1990) geothermometers are based on experiments by these authors using type B Pt/Rh thermocouples, as in this

study, whereas the data from Presnall and co-workers were obtained using W/Re thermocouples. Thus the discrepancy with increasing pressure seen in Fig. 7 and Fig. 8 may be due to error in the pressure-dependence of the Brey-Köhler gethermometers, or to differences in the effect of pressure on the emf of Pt/Rh thermocouples compared to W/Re thermocouples.

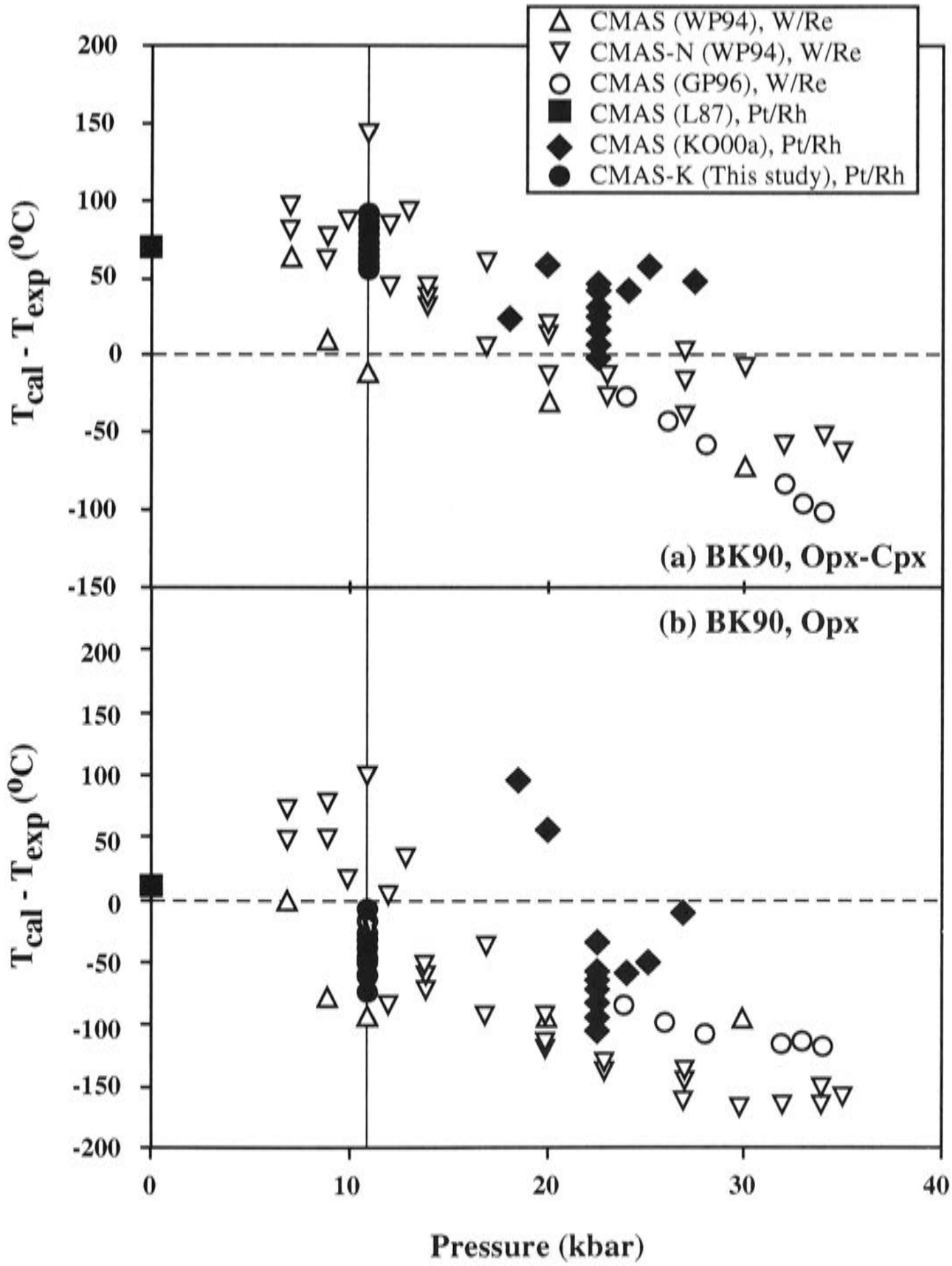

Fig. 8 Comparison of temperature measurement using Pt/Rh thermocouples and W/Re thermocouples in experiments in the system CMAS and the system CMAS-Na_2O: the Opx-Cpx geothermometer of Brey & Kohler (1990) used in (a) and the Opx geothermometer of Brey & Kohler (1990) used in (b). WP94, Walter & Presnall, 1994; GP96, Gudfinnsson & Presnall, 1996; L87, Longhi, 1987; KO00a, Klemme & O'Neill, 2000a. A protective N_2 flow was used to protect the W/Re thermocouples in the low pressure experiments (< 11 kbar) in the system CMAS-Na_2O, so that these experiments gave out similar nominal experimental temperatures to those using Pt/Rh thermocouples.

A further complicating issue is the possibility of oxidation of W/Re thermocouples at lower pressures. To guard against this, Walter & Presnall (1994) used a nitrogen flow at low pressures (≤ 11 kbar) for their experiments in the system CMAS-Na_2O, but this precaution does not appear to have been used in the earlier experiments of Presnall and co-workers in the system CMAS (re-analysed in Walter and Presnall, 1994). (Oxidation of W/Re thermocouples is thought not to be a problem at higher pressures, since collapse of the alumina tubing around the thermocouple wires should prevent oxidation). The calculated temperatures from the lower pressure experiments with W/Re thermocouples with the N_2 flow agree quite well with the experiments using Pt/Rh thermocouples. However, those low pressure experiments using W/Re thermocouples but without a N_2 flow (system CMAS) have lower calculated temperatures, consistent with thermocouple drift caused by oxidation.

Al_2O_3 of pyroxenes in Sp-lherzolite

The alumina contents of Opx and Cpx in the Sp-lherzolite assemblage are controlled by the reactions:

$$\underset{\text{Opx}}{Mg_2Si_2O_6} + \underset{\text{Sp}}{MgAl_2O_4} = \underset{\text{Opx}}{MgAl_2SiO_6} + \underset{\text{Fo}}{Mg_2SiO_4} \qquad (5)$$

and

$$\underset{\text{Cpx}}{CaMgSi_2O_6} + \underset{\text{Sp}}{MgAl_2O_4} = \underset{\text{Cpx}}{CaAl_2SiO_6} + \underset{\text{Fo}}{Mg_2SiO_4} \qquad (6)$$

Previous work has shown that these equilibria are insensitive to pressure but strongly dependent on temperature, Al_2O_3 increasing with temperature (Obata, 1976; Fujii, 1977; Herzberg, 1978; Danckwerth & Newton, 1978; Lane & Ganguly, 1980; Gasparik, 1984; Sen, 1985). Recently Klemme & O'Neill (2000a) refitted existing experimental data for reaction (5) together with their new data.

The alumina contents of Opx coexisting with Fo+Sp in the systems CMAS and CMAS-K_2O agree well with previous work (Fig. 9(b)), except for the data of Gudfinnsson & Presnall (1996), which plot at slightly lower values.

The Al_2O_3 contents of Cpx show a very similar trend (Fig. 9(a)), but with a little more scatter. This extra scatter may be due to a slight pressure effect on this

equilibrium, as seen in the experiments of Gasparik (1984). The partitioning of Al between Opx and Cpx does not vary with temperature (i.e., the temperature-dependences of the Al isopleths are similar in Opx and Cpx), as demonstrated in Fig. 10. In experiments in the system CMAS-Na_2O, the Cpx might be expected to have additional Al from a jadeite component ($NaAlSi_2O_6$). To test this, I also plotted (Fig. 10b) the data for the CMAS-Na_2O system (Walter and Presnall, 1994) with the molar amount of Al associated with Na subtracted. Remarkably, this results in a greatly increased scatter in the plot, indicating that my expectation of increased Al associated with Na must be incorrect.

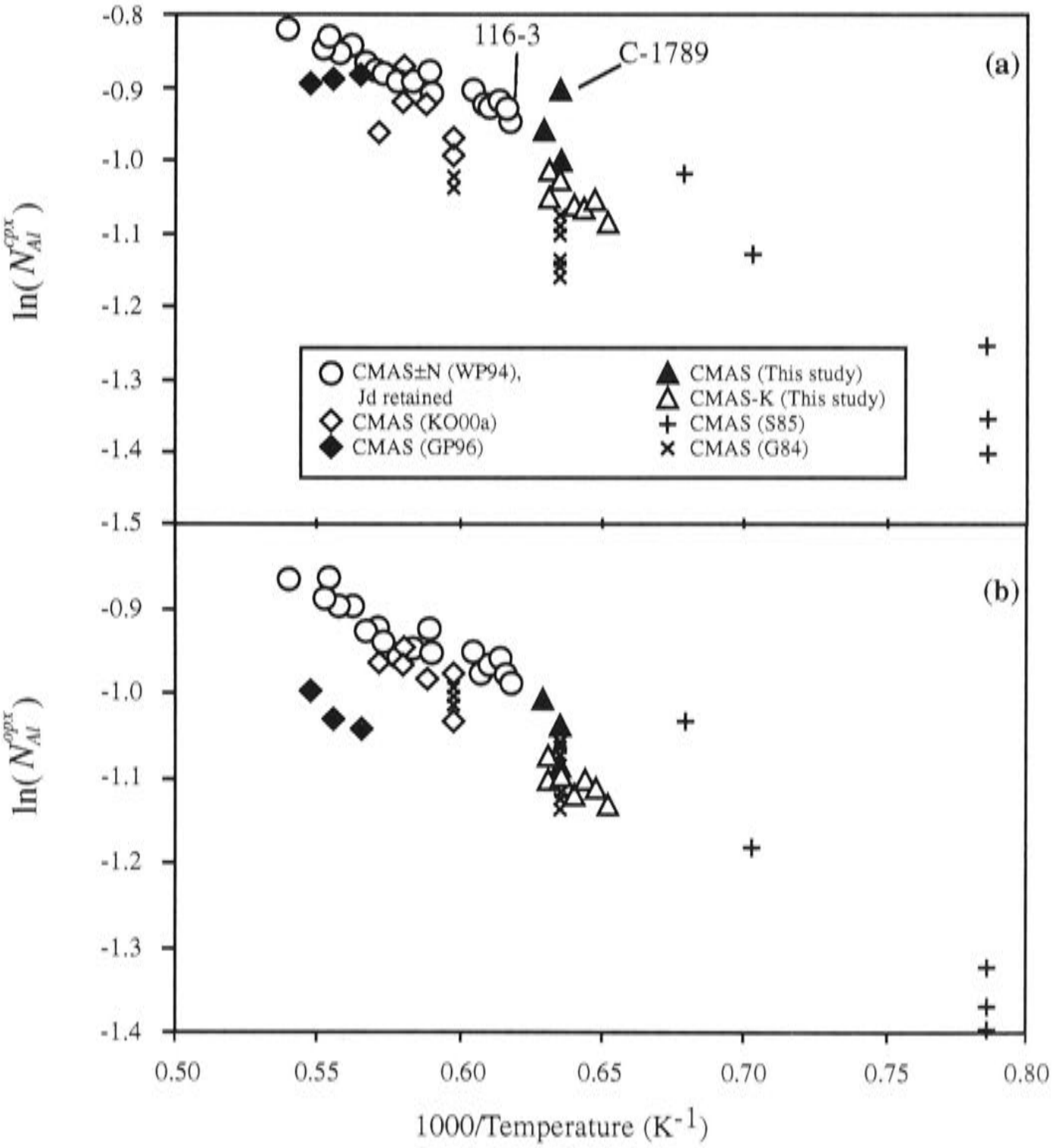

Fig. 9 The solubility of Al in Cpx (a) and Opx (b) for a Sp-lherzolite phase assemblage in system CMAS, CMAS-K_2O and CMAS-Na_2O. WP94, Walter & Presnall, 1994; KO00a, Klemme & O'Neill, 2000a; GP96, Gudfinnsson & Presnall, 1996; S85, Sen, 1985; G84, Gasparik, 1984.

Al_2O_3 in pyroxenes, particularly in Cpx, is always the most heterogenous component in my experiments and anomalous Al_2O_3 contents are a sign of disequilibrium. An example is the subsolidus reversal experiment C-1789, in which the

Al_2O_3 of the Cpx remains similar to that in the starting material, although the Opx in this run has changed its Al_2O_3 content to a lower value.

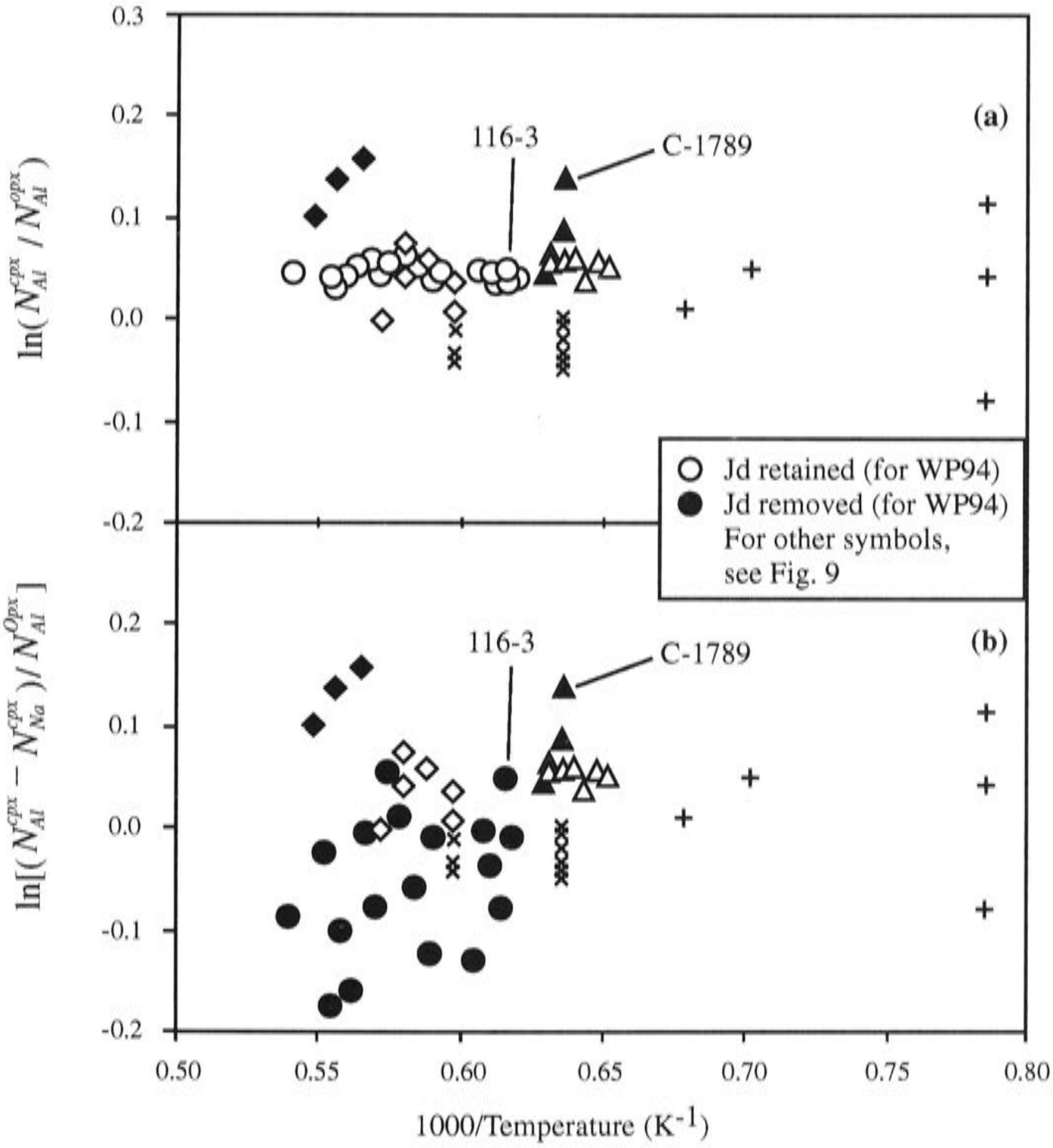

Fig. 10 Partitioning of Al between Cpx and Opx for a Sp-lherzolite phase assemblage in system CMAS, CMAS-K_2O and CMAS-Na_2O with Jd component ($NaAlSi_2O_6$) retained in Cpx (a) and with Jd removed from Cpx (b). For data sources, see Fig. 9.

Al_2O_3 in pyroxenes of other phase assemblages

Reactions (5) and (6) show that the absence of Fo would shift this equilibrium to the right-hand side so that the $MgAl_2SiO_6$ (MgTs) component in Opx and the $CaAl_2SiO_6$ (CaTs) component in Cpx increase. Therefore, the pyroxenes in the phase assemblage Sp+Opx+Cpx should have higher Al_2O_3 content than those in the phase assemblage Fo+Opx+Cpx+Sp, as observed in my experiments (Fig. 11).

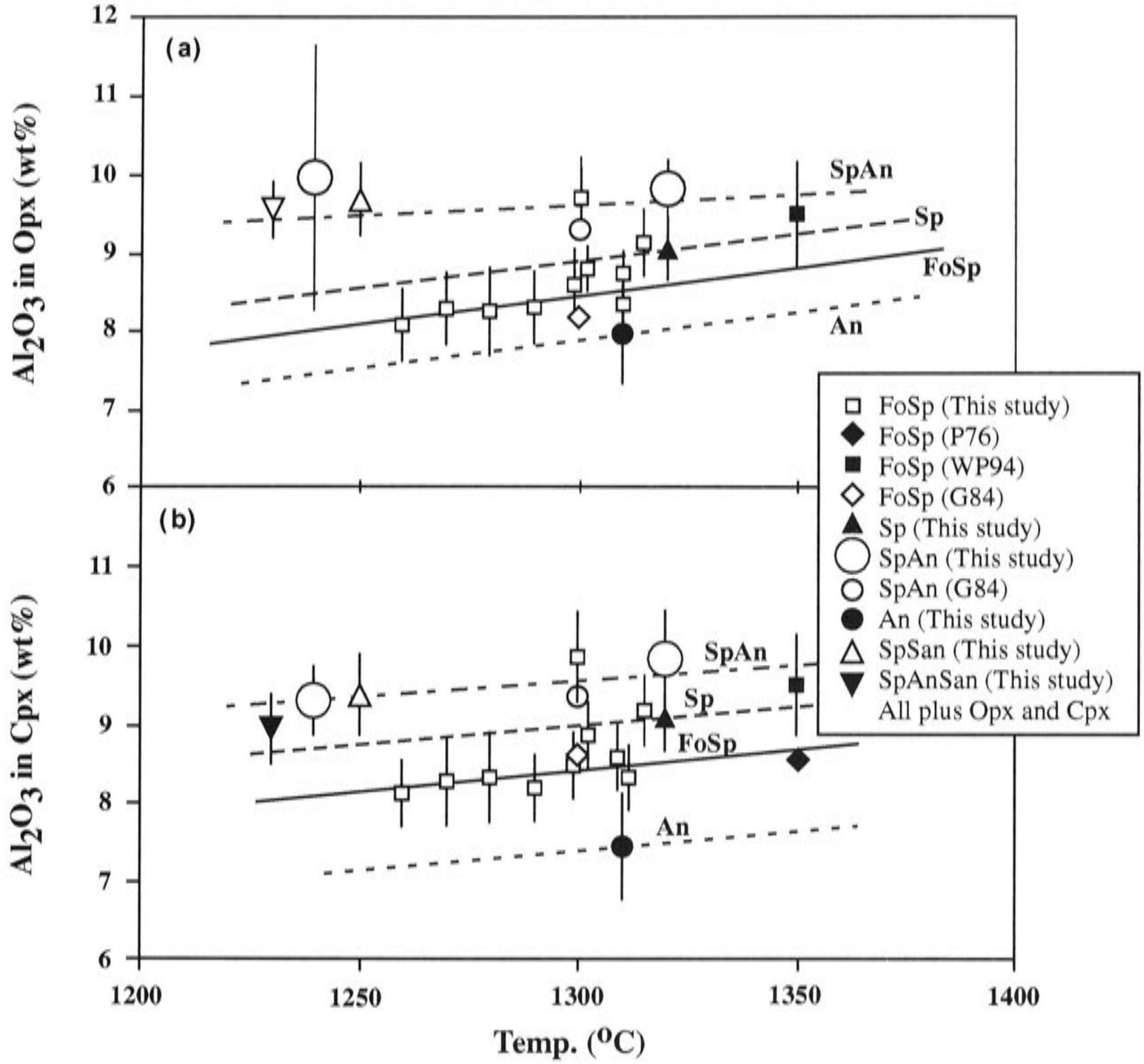

Fig. 11 Experimentally observed changing pattern of Al_2O_3 (wt%)-temperature (^oC) in Opx (a) and in Cpx (b) from phase assemblage to phase assemblage. Lines are fitted by eyes. Some data are slightly shifted horizontally.

A single governing reaction for the Al_2O_3 content in both pyroxenes coexisting with An+Sp can be written:

$$\underset{\text{Sp}}{MgAl_2O_4}+\underset{\text{An}}{CaAl_2Si_2O_8} = \underset{\text{Opx}}{MgAl_2SiO_6}+\underset{\text{Cpx}}{CaAl_2SiO_6} \qquad (7)$$

The absence of either Sp or An would shift this reaction to the left-hand side so that MgTs in Opx and CaTs in Cpx decrease. Again, this is observed in my experiments (Fig. 11).

Since the Al_2O_3 contents of pyroxenes depend on the identities of coexisting phases, the Al_2O_3 contents are useful indicators of equilibrium between the different

parts of sandwich experiments. While this kind of disequilibrium is clearly seen in a few experiments, in most runs the same Al_2O_3 contents in pyroxenes were indeed observed in the "filling" and the ends of the sandwich.

4.2 The effect of K_2O on melting relations of Sp-lherzolite in the system CMAS-K_2O

Effect of K_2O on melt compositions

Fig. 2 indicates that 1 wt% K_2O in the melt depresses the solidus temperature of the Sp-lherzolite phase assemblage at 11 kbar by about 5.8 degrees. Fig. 3 suggests that 1 wt% K_2O decreases MgO by 1.30% and CaO by 1.03%, but increases SiO_2 by 1.05% and Al_2O_3 by 0.28%.

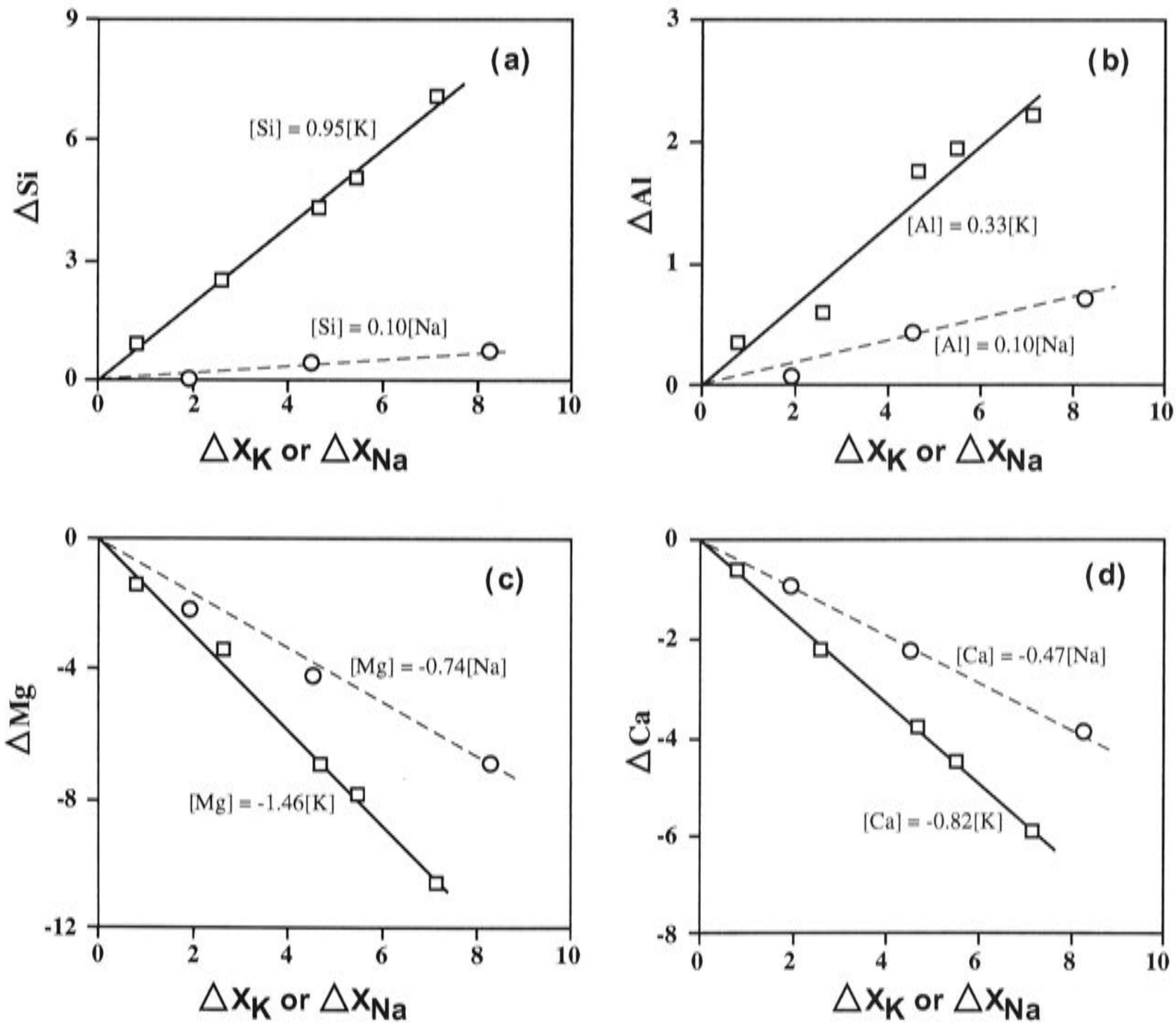

Fig. 12 Variation diagram showing cation trends (in mol%) for melts coexisting with a Sp-lherzolite in system CMAS-K_2O (this study) and system CMAS-Na_2O (Walter & Presnall, 1994). Thick solid line: system CMASK at 11 kbar; thin broken line, system CMAS-Na_2O at 20 kbar. Both K and Na increase the Si content and the Al content, and decrease the Mg content and the Ca content in melt. The K effect on melt composition, however, is much stronger than that of Na.

In order to compare the effect of K_2O on melt composition with that of Na_2O, I plot my experimental data in mole percent in Fig. 12, together with the data of Walter & Presnall (1994) in the system CMAS- Na_2O, at 20 kbar. (Walter and Presnall (1994) provided a global regression of their data to 35 kbar that shows that the difference in pressure between 11 and 20 kbar has a negligible effect in this context). For K, an increase of 1% molar increases Si by 0.95% and Al by 0.33%, and decreases Mg by 1.46% and Ca by 0.82%. For all cations, the effect of Na is similar in direction to that of K, but much weaker: a 1% molar increase in Na only increases Si by 0.1% and Al by 0.1%, and decreases Mg by 0.74% and Ca by 0.47%.

Hence, the effect of K_2O on modifying the composition of melts multiply saturated with FoOpxCpxSp in the system CMAS-K_2O is very different to that of Na_2O in the system CMAS-Na_2O. This is illustrated in Fig. 13, in which the composition of multiply saturated melts are plotted in the basalt tetrahedron projected from Ol (Fig. 13a) and Di (Fig 13b). The data for the system CMAS-Na_2O were taken from Walter and Presnall (1994) at 20 kb, the higher pressure being used because Na_2O stabilizes plagioclase at the expense of spinel at only ~ 2 wt% Na_2O at 11 kbars. The difference in the behaviours of K_2O and Na_2O can be summarized under three points: 1) The addition of K_2O drives the melt composition towards the Qz-normative field (defined by the join between AbAnOr-Hy in Fig. 13b), the melt becoming Qz-normative at ~ 2 wt% K_2O. The addition of Na_2O drives the melt composition towards the Ne-normative field (defined by the join AbAnOr-Ol in Fig. 13b), the melt becoming Ne-normative at ~ 2 wt% Na_2O; 2) K_2O decreases normative Di, whereas Na_2O has no effect on this normative component; 3) As a consequence, adding K_2O eventually produces a Corundum-normative melt at ~ 8 wt% K_2O. Na_2O-rich melts never become Corundum-normative.

Effect of K_2O on the partitioning of MgO between Olivine and Melt

The amount of MgO in a basaltic magma increases strongly with temperature. Several authors have attempted to quantify this effect, using the partition coefficient for MgO between Melt and Ol (Leeman, 1978; Ford et al., 1983; Gudfinnsson and Presnall, 2001). However, such single-element partition coefficients are generally expected to depend on other factors including the details of the melt chemistry (e.g., O'Neill and Eggins, 2002). Fig. 14 shows that adding K_2O to CMAS produces a quite different trend to that established by the systems CMAS, CMAS-Na_2O and CMAS-FeO (cf. Fig. 2 in Gudfinnsson & Presnall, 2001). This makes a useful warning that empirical

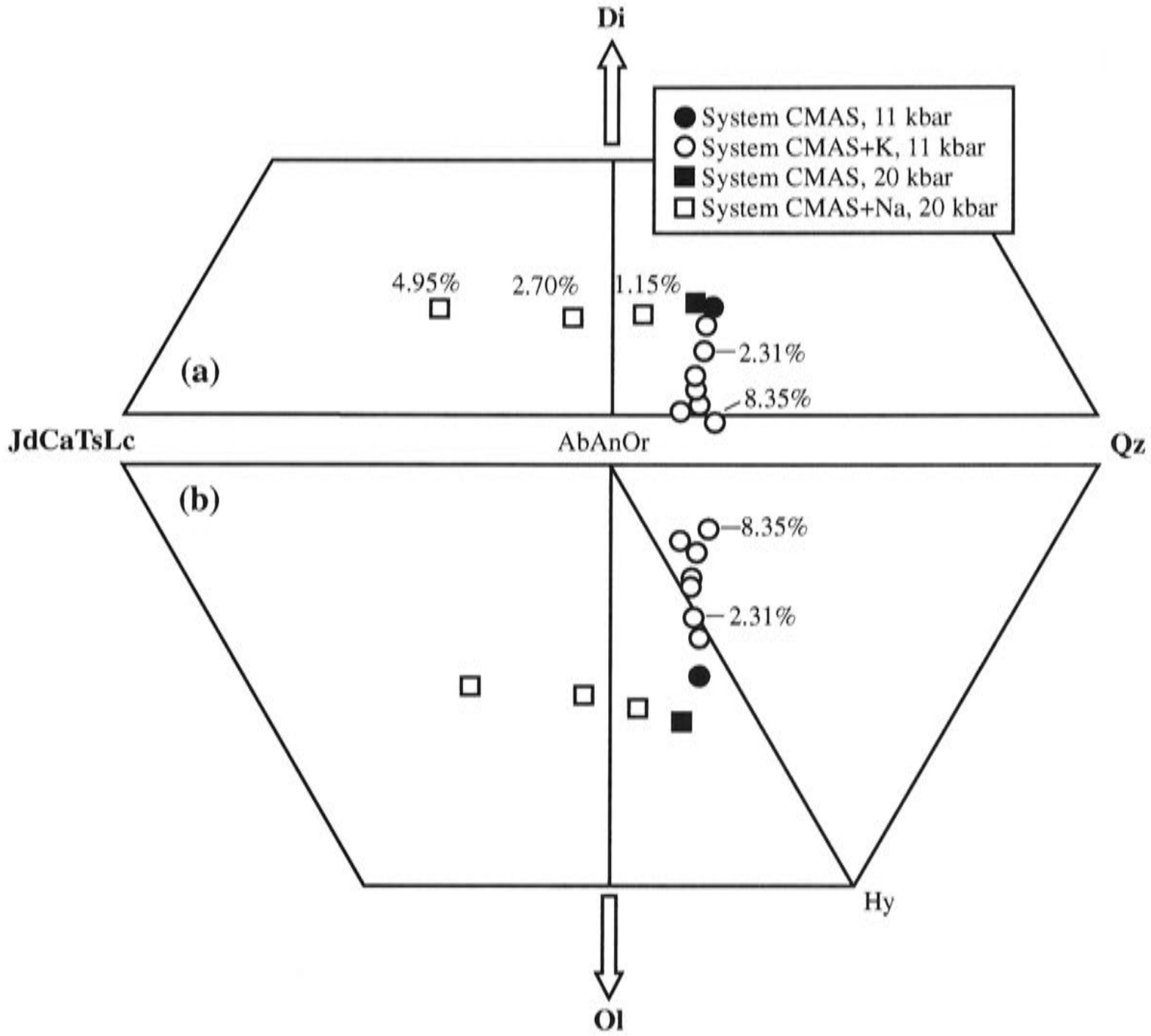

Fig. 13 A comparison of the effects of K_2O and Na_2O in modifying melt compositions: (a) projection of Di-JdCaTsLc-Qz from Ol (by mole); (b) projection of Ol-JdCaTsLc-Qz from Di (by mole). Plotting procedure is from Falloon & Green (1988). Data in the system CMAS at both 11 kbar and 20 kbar are from Walter & Presnall (1994). Data in the system CMAS-Na_2O (Na_2O) at 20 kbar are from Walter & Presnall (1994) as well. Data in the system CMAS-K_2O at 11 kbar are from this study.

geothermometers, with a less than rigorous thermodynamic basis, have limited reliability, and should never be applied to compositions outside those used in their formulation.

The MgO-partitioning "magmathermometer" due to Ford et al. (1983) has been used recently by Danyushevsky et al., (1996), Falloon & Danyushevsky (2000), Falloon et al., (1999), and Falloon et al., (2001). Falloon & Danyushevsky (2000) found that this formulation returns progressively larger errors in the calculated liquidus temperatures of basaltic melts as alkalis ($Na_2O + K_2O$) exceed 3 wt%. My data can be used to check this phenomenon further. The result is shown in Fig. 15. Apparently the Ford et al. (1983) geothermometer cannot reproduce the experimental temperatures accurately both in the system CMAS and in the system CMAS-K_2O (Fig. 15(a)). I also checked the effect of pressure on the geothermometer, with results shown in Fig. 15(b). Evidently pressure affects the calculated temperature as well.

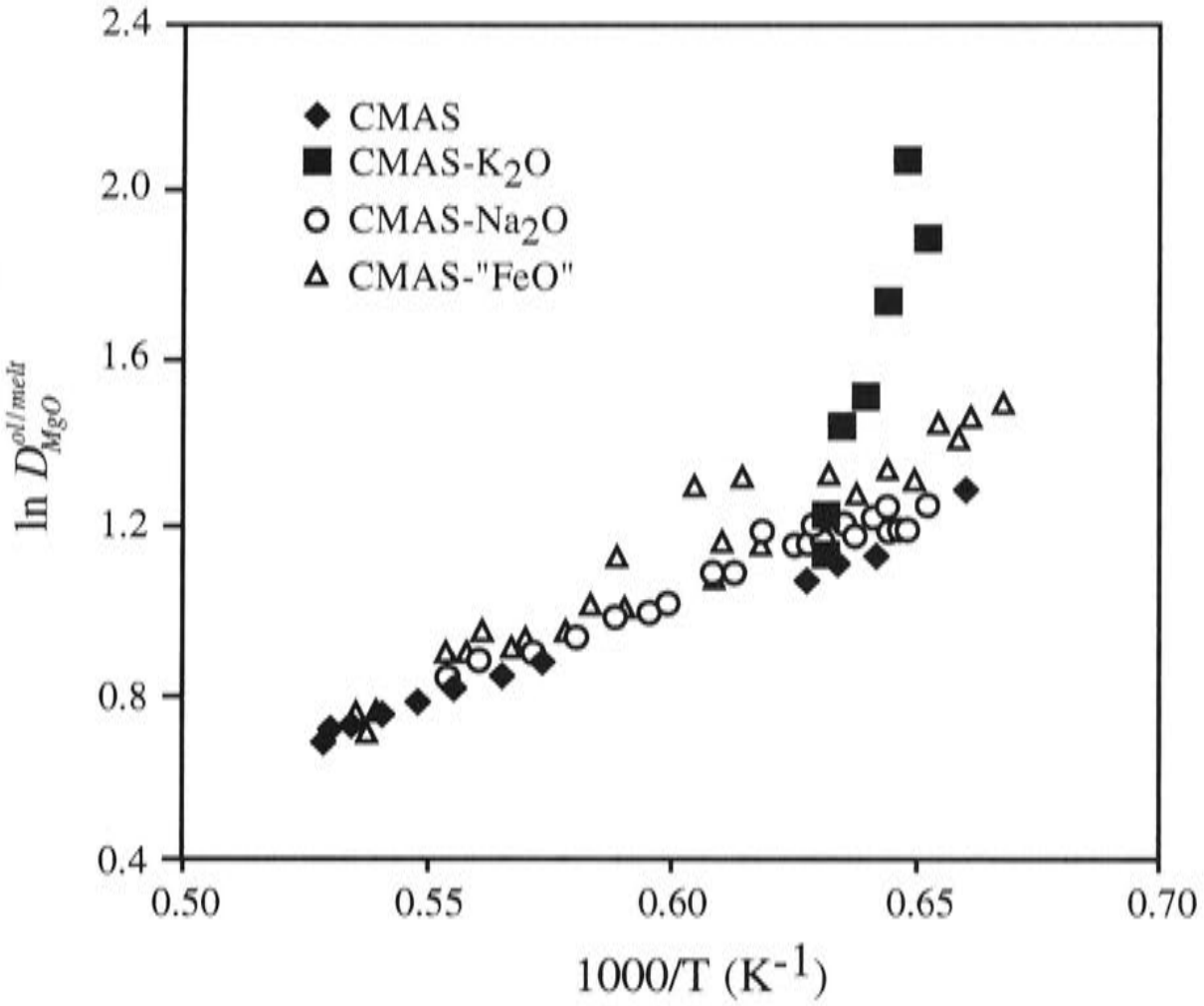

Fig. 14 K_2O's effect on the molar partition of MgO between forsterite and melt. Data from: CMAS, Walter & Presnall (1994), Gudfinnsson & Presnall (1996) and this study; CMAS-Na_2O, Walter & Presnall (1994); CMAS-FeO, Gudfinnsson & Presnall (2000); CMAS-K_2O, this study.

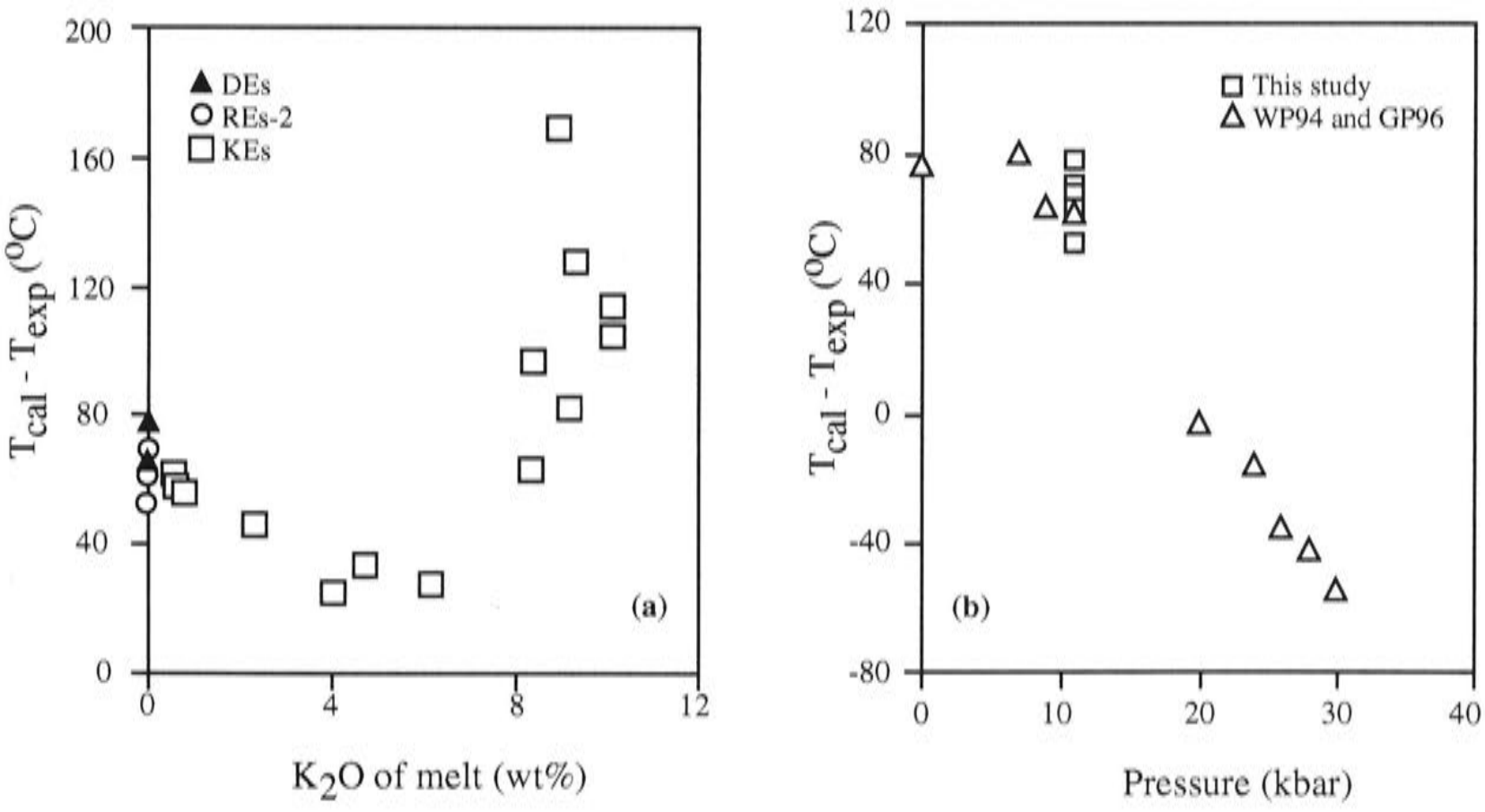

Fig. 15 Tests of the geothermometer of Ford et al. (1983) against K_2O content of melt (a) and pressure (b). In (a), data from this study in both system CMAS and system CMAS-K_2O are used while in (b) data from this study, WP94 (Walter & Presnall, 1994) and GP96 (Gudfinnsson & Presnall, 1996) in system CMAS are used. The possible pressure effect on the temperature measurement in those experiments using W/Re thermocouples (see Fig. 7 and Fig. 8) can not fully account for the pressure dependence of the temperature difference observed here so that the geothermometer of Ford et al. (1983) needs to be further corrected against pressure.

4.3 Melting reactions

Melt properties

The CIPW norms of the experimentally observed melt compositions are summarised in Table 6. Melts with K_2O contents below ~ 4.1 wt% K_2O are Ol-normative. The Melt becomes Qz-normative at higher K_2O. Melts with > 8 wt% K_2O are corundum-normative.

Phase relationships

Melt compositions observed in this study are plotted in Fig.16. In the system CMAS there are two isobaric invariant points of interest, A (Fo+Sp+Opx+Cpx+Melt) and A* (Sp+Opx+Cpx+An+Melt). Points B, C and D are isobaric invariant points in the system CMAS-K_2O, for the phase assemblages Fo+Sp+Opx+Cpx+San+Melt, Sp+Opx+Cpx+An+San+Melt and Sp+Opx+An+San+Sapph+Melt, respectively. All these invariant points are peritectic. From point A to point B the isobarically univariant phase assemblage is Fo+Sp+Opx+Cpx+Melt, while from point B to point C it is Sp+Opx+Cpx+San+Melt. At point C, the melt composition trend is joined by another melt composition trend emanating from point A*, with the isobarically univariant phase assemblage of Sp+Opx+Cpx+An+Melt. The isobarically univariant phase assemblage from point C to point D is Sp+Opx+San+An+Melt. Thermal maxima must be located between B and C, and between C and D. The temperature change is judged by my direct temperature observation or by the method of Presnall (1986). One interesting property of the system suggested by my experiments is that the univariant solidus curves have a relatively steep temperature decrease (1320-1240°C) from A to B or from A* to C, but the temperature interval between A and A* and the corresponding univariant solidus curves A-B and A*-C is very small.

Melting reactions

The compositions of Melt, Cpx and Opx in the experiments with the phase assemblage Fo+Sp+Opx+Cpx+Melt in the system CMAS-K_2O were fitted by regression to a second-degree polynomial of the form:

$$X_i^{\phi} = AT^2+BT+C$$

where X_i^{ϕ} is the concentration in weight percent of oxide i in phase ϕ and T is in °C.

Table 6: CIPW norms of melts in the CMAS and CMAS-K_2O systems

	CMAS				CMAS-K_2O											
	KEs	P79	WP94	C-1565	C-1422	C-1461	C-1448	C-1460	C-1447	C-1574	C-1585	C-1779	C-1701	C-1708	C-1580	C-1576
Temp.	1320	1350	1350	1320	1310	1310	1300	1290	1280	1270	1260	1250	1240	1230	1250	1230
Qz	0	0	0	0	0	0	0.51	0.84	2.88	6.09	1.86	1.56	4.94	3.44	13.72	20.83
Cor	0	0	0	0	0	0	0	0	0	0.35	0	1.35	0	0.25	2.32	2.58
Or	0	0	0	0	4.31	13.64	24.08	28.1	36.42	49.25	50.12	59.56	54.13	59.74	55.07	53.01
An	54.87	53.78	52.36	56.61	53.45	49.22	46.51	44.86	41.08	31.48	31.67	26.97	29.85	26.82	20.82	17.2
Di	16.49	17.88	16.78	15.82	14.77	11.38	7	5.35	2.49	0	1.63	0	0.71	0	0	0
Hy	23.43	22.61	23.99	26.81	24.36	23.98	21.8	20.75	17.03	12.7	14.62	10.47	10.56	9.67	8.01	6.32
Ol	5.14	5.68	7.01	0.66	3.03	1.69	0	0	0	0	0	0	0	0	0	0

KEs: regressed melt composition at K_2O=0; P79: Presnall et al (1979); WP94: Walter & Presnall (1994); for the initial data, see Table 5.
I believe local equilibrium for the middle parts of C-1580 and C-1576 was achieved (see discussion in text).
Qz, quartz; Cor, corundum; Or, orthoclase; An, anorthite; Di, diopside; Hy, hypersthene; Ol, olivine.

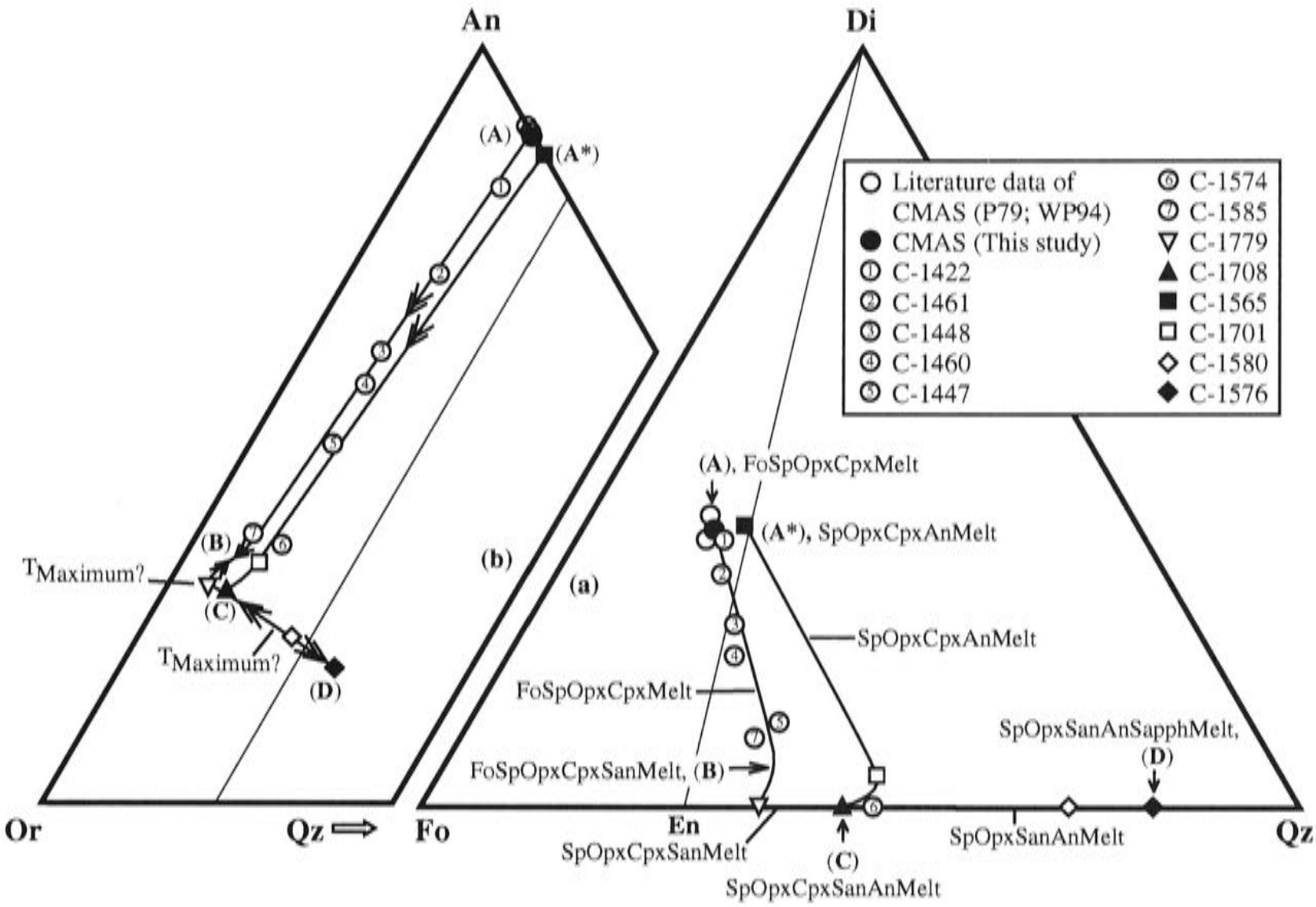

Fig. 16 Projections from An+Or (a) and from Fo+Di (b) showing the melt composition of the KEs (wt%). See Table 6 for the original data of CIPW norm. (a) is inappropriate for the melt with high K_2O content while (b) is inappropriate for the melt with 0 K_2O content. In the former case, melt is Ol-free and the missing An+Or has a very high proportion of the melt so that deflection ensues; in the latter case, melt is Or-free and the missing Fo+Di has a very high proportion of the melt so that deflection ensues as well. I combine these two diagrams to discuss the melt property. Point A and A* are the isobarically invariant point for FoSpOpxCpxMelt and SpOpxCpxAnMelt of system CMAS, respectively. Point B, point C and point D, displaying 6 coexisting phases (FoSpOpxCpxSanMelt, SpOpxCpxSanAnMelt or SpOpxSanAnSapphMelt), are isobarically invariant points of system CMAS-K_2O. Temperature decrease shown by arrows is based on direct experimental observation or on calculation using the phase composition data at the invariant point B, C or D with the method of Presnall (1986). Between point B and point C, and point C and point D, there are two liquidus maximums, from which temperature decreases towards both sides. Their accurate position has not been located. Partial melting reaction in this portion of system CMAS-K_2O is always peritectic. See Table 7 for related information.

To calculate the partial melting reaction along the univariant curve of Fo+Sp+Opx+Cpx+Melt, the method of Walter et al (1995) is used. The melting reaction is independent of the bulk composition as long as all phases present. The calculated reaction coefficients are plotted against temperature in Fig. 17. The partial melting reactions for some special temperatures are listed in Table 8.

Also listed in Table 8 are the partial melting reactions at the invariant points of system CMAS (Point A and A* in Fig. 16) and the invariant points of system CMAS-K_2O (Point B, C and D in Fig. 16) which are directly calculated from the experimentally observed phase compositions using the method of Korzhinskii (1959).

Partial melting is always peritectic along the univariant curve Fo+Sp+Opx+Cpx+Melt at 11 kbar in the system CMAS-K_2O (Fig. 17). At high

temperatures (from 1320°C down to 1265°C), Fo is in reaction relationship with melt. From 1276°C Sp becomes in reaction relationship.

Table 7: Regression coefficients for phases of variable compositions in experiments with Fo+Sp+Opx+Cpx+Melt

		CaO	MgO	Al_2O_3	SiO_2	K_2O
Melt	A	0.0016925	0.0019498	-0.0006571	-0.0015076	-0.0014776
	B	-4.206728	-4.848343	1.678342	3.718272	3.658458
	C	2620.00	3018.51	-1050.26	-2233.04	-2255.22
	D	0.64	0.70	0.34	0.82	0.54
Cpx	A	-0.0000256	-0.0001765	0.0008478	-0.0006457	-
	B	0.055271	0.460585	-2.177688	1.661832	-
	C	-10.17	-279.40	1406.49	-1016.92	-
	D	0.16	0.15	0.22	0.09	-
Opx	A	-0.0000508	-0.0002918	0.0005426	-0.0002001	-
	B	0.138646	0.742252	-1.392491	0.511593	-
	C	-92.14	-437.08	901.53	-272.31	-
	D	0.12	0.14	0.15	0.12	-

Regression equation: $X_i^{\phi} = AT^2 + BT + C$ where X_i^{ϕ} is the concentration in weight percent of oxide i in phase ϕ and T is in °C. D is the average difference between regressed and experimentally observed values.

Table 8: Comparison of melting reactions in the CMAS, CMAS-Na_2O and CMAS-K_2O systems at 11 kbar

System	Temp.	Method[1]	Reaction (wt.%)	Reference[2]
CMAS	1350	Korzhinskii	46.8 Opx + 71.4 Cpx + 11.7 Sp = 100.0 Melt + 29.9 Fo	GP96
CMAS	1320	Korzhinskii	40.7 Opx + 79.7 Cpx + 13.8 Sp = 100.0 Melt + 34.2 Fo	This study
CMAS	~1320	Korzhinskii	26.2 Opx + 26.2 Cpx + 50.1 An = 100.0 Melt + 2.5 Sp	This study
CMASN	-	Walter95	46 Opx + 75 Cpx + 13 Sp = 100 Melt + 34 Fo	Walter95
CMASK	1310	Walter95	41.5 Opx + 79.1 Cpx + 15.1 Sp = 100.0 Melt + 35.7 Fo	This study
CMASK	1280	Walter95	69.5 Opx + 58.9 Cpx + 9.4 Sp = 100.0 Melt + 37.8 Fo	This study
CMASK	1270	Walter95	94.8 Opx + 47.9 Cpx = 100.0 Melt + 17.4 Fo + 25.3 Sp	This study
CMASK	1260	Walter95	140.7 Opx + 33.0 Cpx + 36.4 Fo = 100.0 Melt + 110.1 Sp	This study
CMASK	1255	Walter95	181.5 Opx + 21.8 Cpx + 91.0 Fo = 100.0 Melt + 194.2 Sp	This study
CMASK	1252?	Korzhinskii	5.4 Sp + 20.7 Opx + 15.4 Cpx + 71.7 San = 100.0 Melt + 13.2 Fo	This study
CMASK	1230	Korzhinskii	23.4 An + 66.5 San + 12.7 Opx = 100.0 Melt + 1.7 Sp + 0.9 Cpx	This study
CMASK	1230	Korzhinskii	9.6 An + 63.0 San + 122.2 Sapph. = 100.0 Melt + 89.9 Sp + 4.8 Opx	This study

[1]Method: Korzhinskii, Korzhinskii (1959); Walter95, Walter et al (1995).

[2]References: GP96, Gudfinnsson & Presnall (1996); Walter95, Walter et al (1995).

In order to calculate the reaction for the isobaric invariant point Fo + Sp + Opx + Cpx + San + Melt at ~ 1252 °C, Fo was added to the phase assemblage observed in C-1779.

Average composition of Fo and Sp was used in the calculation.

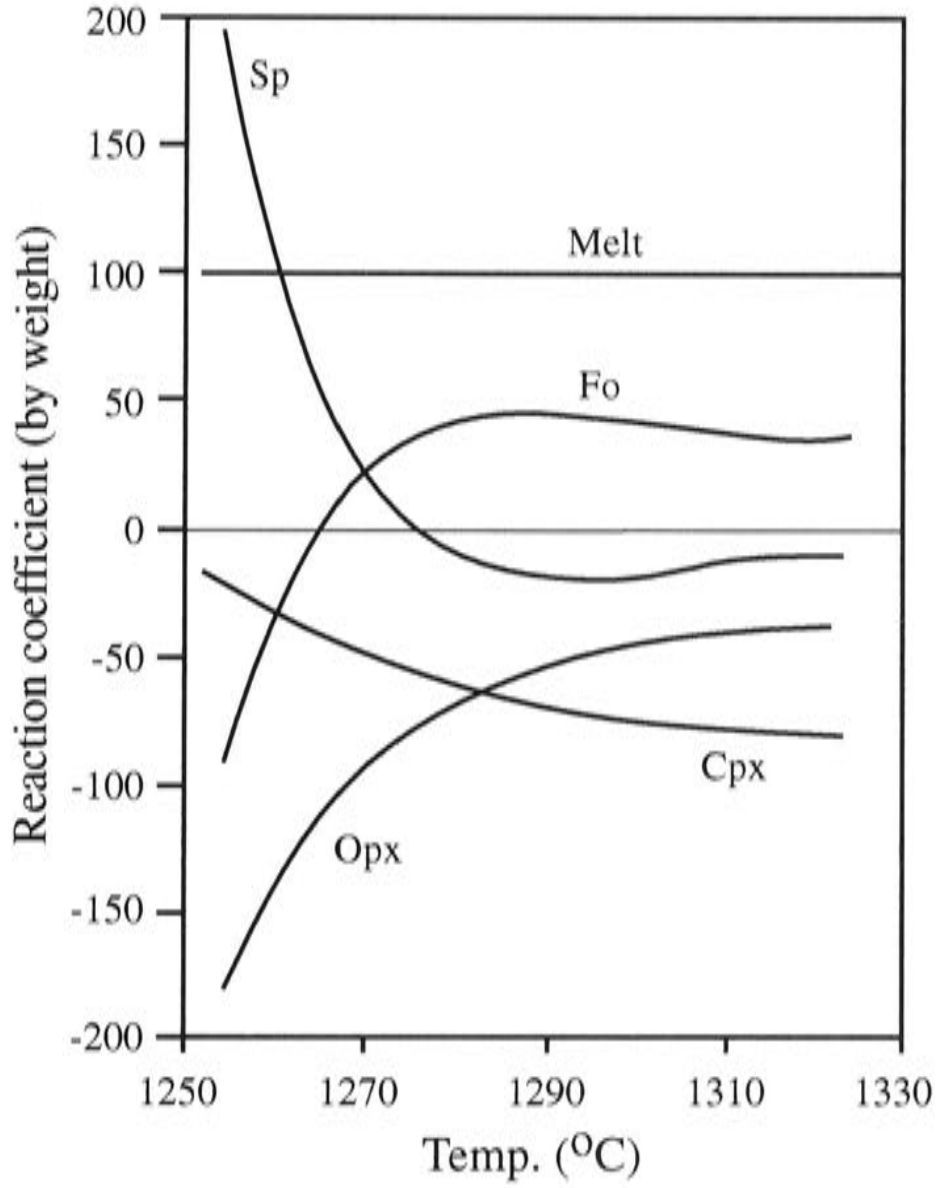

Fig. 17 Melting reaction along the univariant curve of Sp-lherzolite in system CMAS-K_2O (from point A to point B in Fig. 16. Increasing temperature corresponds to decreasing K_2O content of the melt. Calculating method for the coefficients of the melting reaction: Walter et al (1995). The melting reaction is independent to the bulk composition as long as all the phases coexist.

4.4 Experiment C-1768: an analogue of a diamond-aggregate melt extraction experiment

Run C-1768 is a crystallization experiment on the melt composition determined for the isobaric invariant point Fo+Sp+Opx+Cpx+Melt from the KEs, with additional Fo added in the sandwich geometry. Importantly, this particular run is at 1310°C, just below the solidus (1320°C). The experimental charge was prepared with layers of Fo sandwiching a layer of crushed glass of the anticipated solidus melt composition (synthesised at 1 atm). Initially, of course, both layers have considerable porosity. This porosity would not be expected to survive at 11 kbar and 1310°C even in a subsolidus run (for example, a pure Fo charge would be expected to recrystallize to near 100% density in a few minutes at these conditions), and indeed it does not. However, the interesting observation is that the Fo layers are thoroughly impregnated with material

that includes the components CaO and Al_2O_3 plus additional SiO_2, leading to the crystallization of Cpx, Opx and Sp among the original Fo. These components must come from the glass layer, through the action of a metastable melt present during the initial stages of the run. The metastable melt is inferred because the distances involved (~2 mm) are too large for solid state diffusion timescales. Whereas these layers ended up with the assemblage Fo+Sp+Opx+Cpx, the glass layer crystallized to An+Sp+Opx+Cpx and is hence not in equilibrium with the Fo layers. No quenched melt was observed in the final run products (either Fo or glass starting layers), indicating that the run was, as expected, thoroughly subsolidus. I believe that the scenario whereby material migrates into the Fo layers may be analogous to the processes occurring in diamond-aggregate melt-extraction experiments.

The diamond-aggregate technique was used to study the near solidus partial melting of mantle peridotite (Johnson and Kushiro, 1992; Hirose & Kushiro, 1993; Baker & Stolper, 1994; Baker et al., 1995; Kushiro, 1996). The results of one of these studies (Baker et al., 1995) was questioned by Falloon et al. (1996), who drew attention to possible pitfalls in the technique, particularly when applied to experiments with low degrees of partial melting (where it is potentially most useful). Falloon et al. (1997; 1999) then checked some of the melt compositions observed in these studies and concluded that the diamond aggregate technique compounds rather than solves the experimental problems. However, Kushiro (2001) has recently pointed out that "the analyses given by Baker et al. (1995) were too low in alkalies because of wrong correction procedures (Hirschmann et al., 1998)". Kushiro therefore concluded that the results of Baker et al. were "not inconsistent" with the tests of Falloon et al. (1997); but since Falloon et al. were evidently studying a different composition, consistency is difficult to judge. Although Kushiro (2001) inferred from this that "The diamond aggregate method can be a reliable technique for obtaining and analyzing low-degree partial melt", I suggest that more testing is needed.

Full evaluation of the diamond aggregate technique is beyond the scope of this study, but the observations obtained on C-1768 can be used to throw further doubt on the reliability of the diamond aggregate technique at low melt fractions. The existence of the CaO, Al_2O_3 and extra SiO_2 amidst the Fo supports the argument of Falloon et al. (1996) that the initial intra-pore pressure can lead to metastable melt production. As another possible example of this, Hirose and Kushiro (1993) found melt in every single experiment of their diamond-aggregate study, despite several runs being at temperatures

up to 50°C below the solidi of their two compositions as previously determined (Takahashi and Kushiro, 1983; Takahashi, 1986).

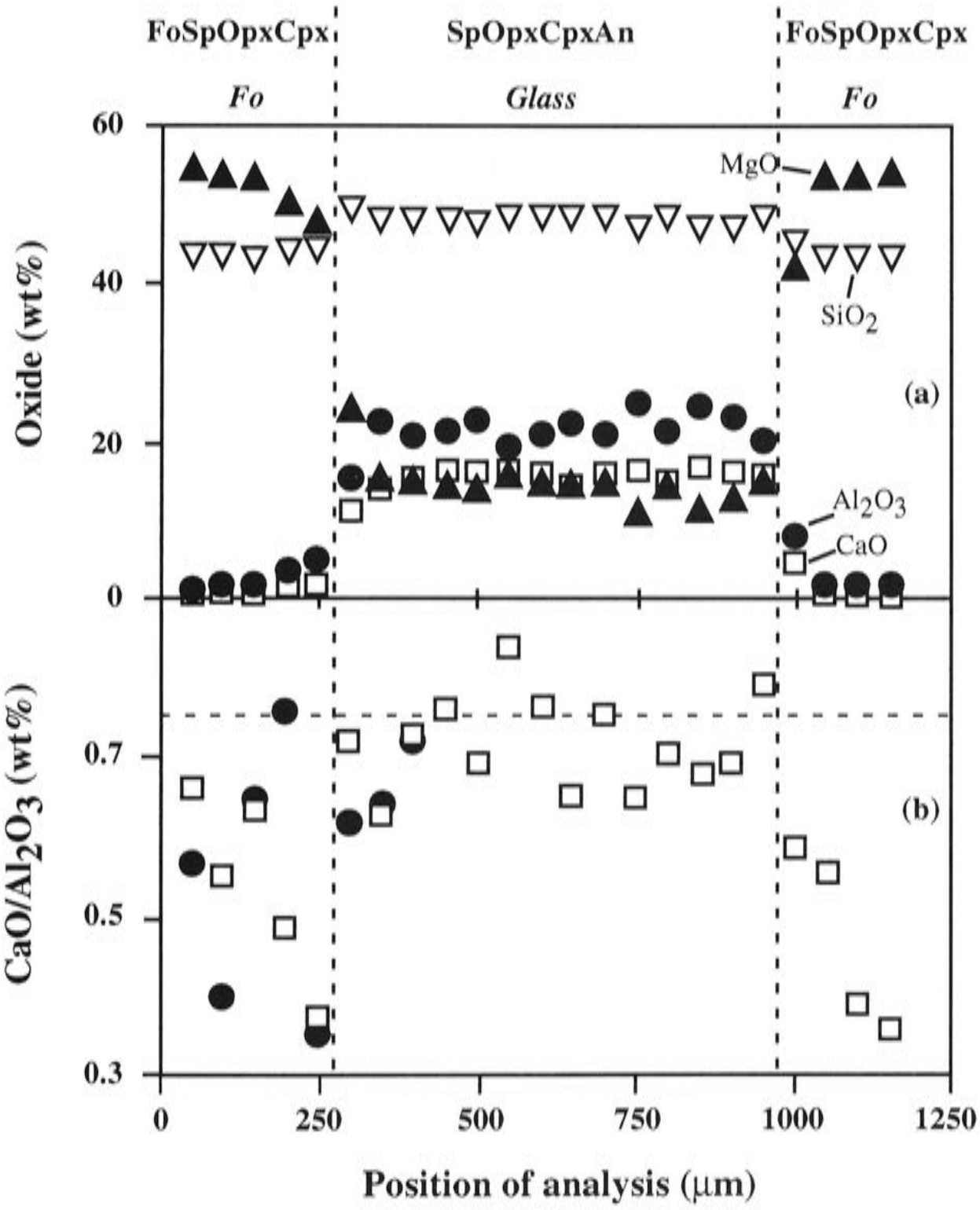

Fig. 18 Composition variation longitudinally along the experiment product of C-1768 detected using a defocused beam (~ 40 *50 μm^2). (a) shows a complete profile from one end of the capsule to the other while (b) shows not only the complete profile (empty squares) shown in (a) but also another incomplete profile (solid circles), which was not extended to the glass layer and to the other end of the capsule.

A defocussed beam of approximately 40x50 μm was used to analyse areas in C-1768 from one end of the capsule to the other. The results are shown in Fig. 18. Fig. 18(a) shows that the amount of material infiltrating the Fo layers (as monitored by CaO and Al_2O_3) decreases away from the interface with the glass layer, but some still reaches the edge of the capsule. What is strange is the decrease of the CaO/Al_2O_3 ratio (Fig. 18(b)) from that in the initial glass of 0.75, which suggests decoupling of CaO and Al_2O_3. The transient melt in the Fo layers appears to have a much lower ratio than equilibrium melt coexisting with either Fo+Sp+Opx+Cpx or Sp+Opx+Cpx+An. A low CaO/Al_2O_3 ratio is also observed in many of the diamond aggregate studies at low

degrees of partial melting, although a true comparison is obscured by the high Na_2O contents of these melts. It would be valuable to test the diamond-aggregate method directly in the system CMAS at 11 kbar at subsolidus and near solidus conditions.

4.5 The anorthite-sanidine solvus

Anorthite, albite (Ab) and sanidine are the three main components of natural feldspars. At high temperatures there is complete solid solution across the joins An-Ab (plagioclases) and Ab-San (alkali feldspars), but the solvus between An and San extends to their solidus. Despite the usefulness of the An-San solvus for constraining thermodynamic models of ternary feldspar solid solutions (Nekvasil, 1984), there are only two experimental studies on the binary An-San join at high temperaturres (Ai & Green, 1989; Nekvasil & Carroll, 1993), which disagree on the compositions of the coexisting feldspars as well as on the temperature of the solidus. Ai & Green (1989) located the eutectic in the An-San binary at 10 kbar at $An_{30}San_{70}$ and 1215±15 °C, and found the maximum mutual solubility of 18% San in An (by mole) and 7% An in San (Fig. 19). Nekvasil & Carroll (1993), however, found the eutectic at 11.3 kbar at $An_{19}San_{81}$ and 1280±10 °C, and the maximum mutual solubility is 11% San in An and 9% An in San (Fig. 19).

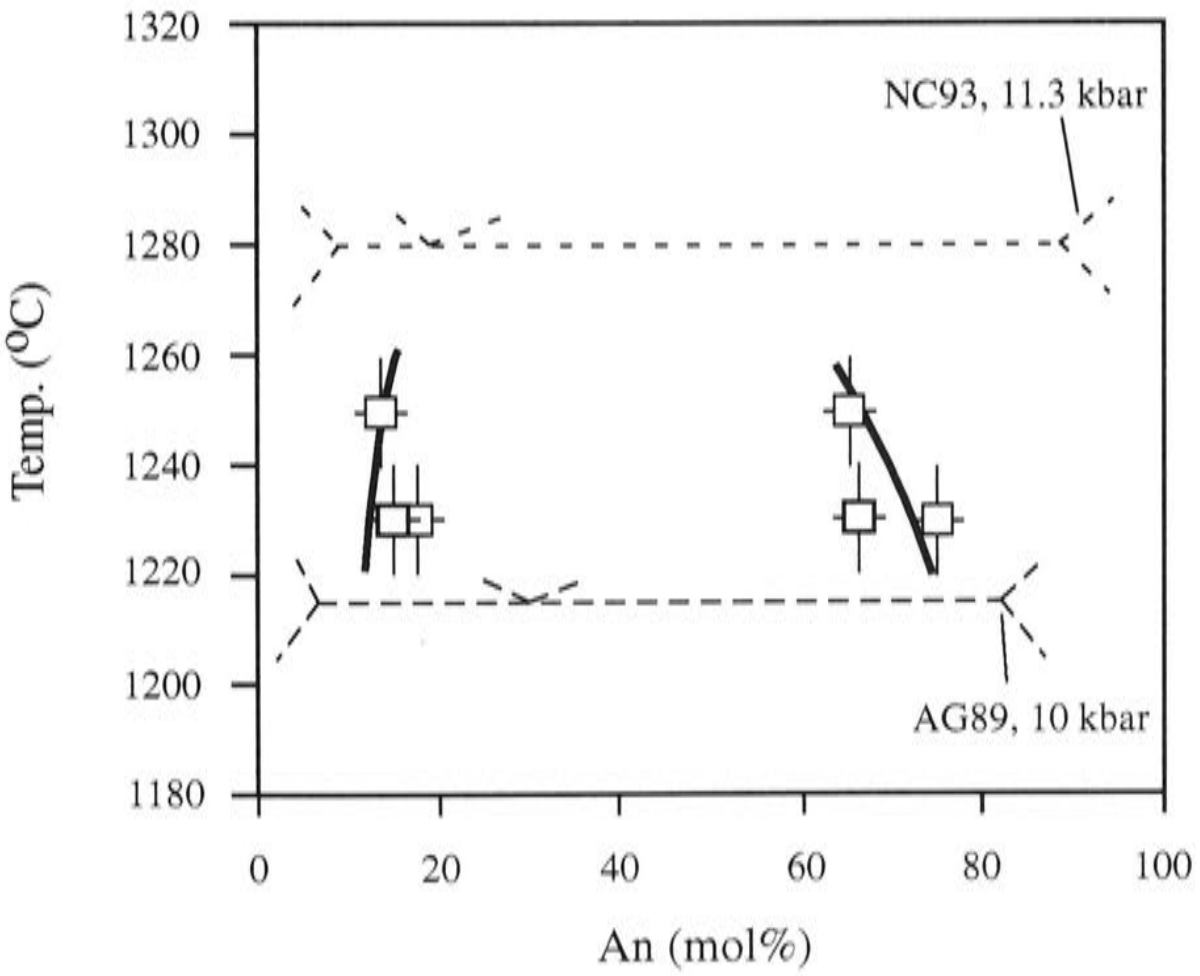

Fig. 19 The mutual solubility (mol%) of San and An at 11 kbar. AG89, Ai & Green, 1989; NC93, Nekvasil & Carroll, 1993). The small amount of MgO in An, up to ~ 0.6 wt%, is ignored.

Determining the phase relations around the An-San solvus and solidus is experimentally more difficult than it may seem at first sight. The kinetics of the mixing/unmixing process at the solvus are too sluggish for direct experimental investigation at subsolidus conditions. The assemblage An_{ss}+San_{ss}+Melt is isobarically invariant in the system $CaAl_2Si_2O_8$-$KAlSi_3O_8$, and thus observing this assemblage directly is not theoretically possible in the pure system (this is of course exactly the same problem I confront in this study). Indeed, the reported observations of both the Ai & Green (1989) and Nekvasil and Carroll (1993) on the solvus/solidus relations are inferences obtained by the bracketing technique.

In the same way that adding K_2O to the system CMAS enables me to constrain the phase relations around the Fo+Opx+Cpx+Sp+Melt invariant point, so the presence of MgO plus other minor CAS components in my experiments increases the variance of the system and enables me to observe An_{ss}+San_{ss}+Melt directly. I am thus able to report some useful points on the solvus, and also to put some constraints on the solidus of the $CaAl_2Si_2O_8$-$KAlSi_3O_8$ system at 11 kbar.

I have three runs that produced co-existing An_{ss} and San_{ss} (C-1580 at 1250°C and C-1708 and C-1576 at 1230°C), which are projected onto the $CaAl_2Si_2O_8$-$KAlSi_3O_8$ join in Fig. 19 as well. The maximum mutual solubility of An and San observed here is higher than that in Ai & Green (1989) and much higher than that in Nekvasil & Carroll (1993). These new data suggest that the feldspar model calibrated by Fuhrman & Lindsley (1988) has the best performance at higher temperatures. As shown by Nekvasil (1994), all other models calculate much lower mutual solubilities of An and San.

Since MgO concentrates in the melt relative to An_{ss} and San_{ss}, the eutectic in the MgO-free system $CaAl_2Si_2O_8$-$KAlSi_3O_8$ at 11 kbar must be higher than 1250 °C (run C-1580). Allowing for a representative slope dT/dP for silicate melting of about 10°C/kb, my results are not consistent with the solidus temperature of 1215±15 °C at 10 kbar found by Ai & Green (1989), but are consistent with the 1280±10 °C at 11.3 kbar suggested by Nekvasil & Carroll (1993). The molar Ca/(Ca+K) ratios in my three melts in equilibrium with An+San are 0.31, 0.27 and 0.25. On the grounds that some of the Ca in the melt is presumably associated with components other than An, but all the K can be assigned to a San component, I surmise that the composition of the solidus (eutectic) melt in the binary $CaAl_2Si_2O_8$-$KAlSi_3O_8$ would lie at lower molar Ca/(Ca+K), again consistent with the phase diagram of Nekvasil and Carroll (1993) (eutectic at $An_{19}San_{81}$), rather than that of Ai & Green (1989) ($An_{30}San_{70}$).

4.6 Sapphirine

In two of the sandwich experiments (C-1580 and C-1576), the middle melt-rich regions produced an assemblage containing sapphirine (Sapp); the phase assemblage consisted of An+San+Sapp+Melt at 1250°C (C-1580), which was joined by Opx and Sp at 1230°C to form the isobarically invariant assemblage An+San+Sapph+Sp+Opx+Melt. Neither assemblage is in equilibrium with the end regions, which consisted of the usual Fo+Opx+Cpx+Sp with no apparent melt, and with a texture showing minimal recrystallization, also indicative of no melt. However, the compositions of the pyroxenes in these regions are consistent with local equilibrium. Sapph is incompatible with Fo at 11 kbar and ~1250°C, reacting to form Opx+Sp (e.g., Liu and Presnall, 2000). A semi-schematic phase diagram showing the subsolidus phase relations in the system MgO-Al_2O_3-SiO_2 at ~1250°C and 11 kbar is shown in Fig. 20.

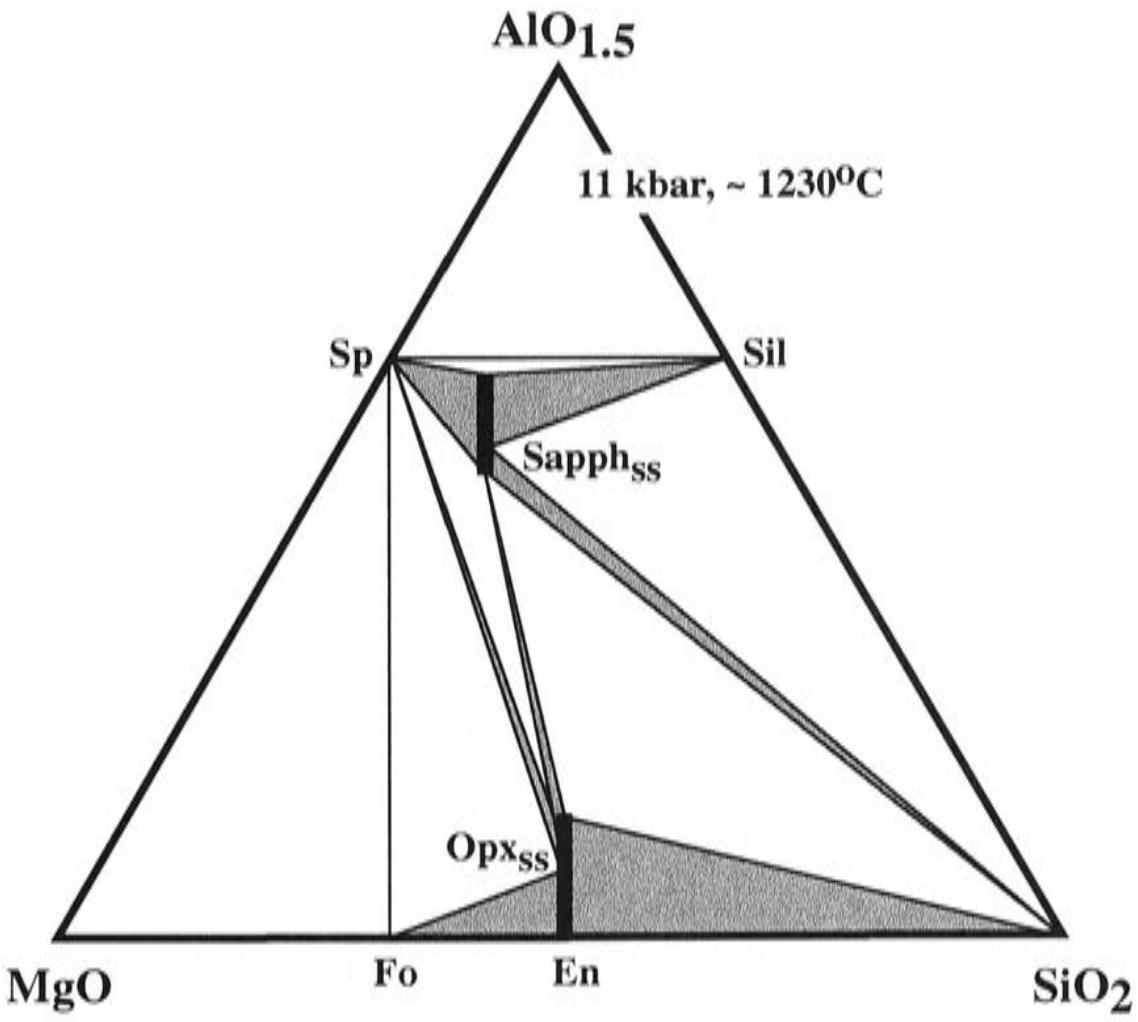

Fig. 20 Phase relationship of system MgO-$AlO_{1.5}$-SiO_2 at 11 kbar and ~ 1230°C. Small amount of CaO either in Opx or in Fo is ignored.

In C-1576, the Opx in the two regions was very different in composition; that in the subsolidus peridotitic assemblage had the usual 8.5 wt% Al_2O_3 (consistent with other experiments), while that in the sapphirine-bearing middle region had 14 wt%. The regions are separated by a thin band of orthopyroxene ~ 10 μm in width (Fig. 2a). Remarkably, the composition of the orthopyroxene changes across this narrow band,

from the 14 wt% of the An+San+Sapph+Sp+Opx+Melt assemblage on that side, to the 8.5 wt% on the other (see Fig. 2a).

The solubility of Al_2O_3 in Opx in equilibrium with Sapph+Qz (quartz) has recently been studied by Hollis and Harley (2002) at P-T conditions close to that of this study. The controlling reaction can be written:

$$4\ \underset{\text{Opx}}{MgAl_2SiO_6} = \underset{\text{Sapph}}{Mg_4Al_4Si_2O_{20}} + 2\ SiO_2 \qquad (8)$$

Thus lowering the activity of SiO_2 should move equilibrium (8) towards the right hand side, lowering Al_2O_3 in Opx (see also Fig. 20). However, the Al_2O_3 content of the Opx in equilibrium with Sapph+Sp in my experiment C-1576 is significantly higher than found by Hollis and Harley (2002) at similar temperatures and pressures (e.g., their experiments R50a,b at 1250°C and 12 kbar only has 9.5 to 10.5 wt% Al_2O_3 in Opx). My experiment, unlike those of Hollis and Harley (2002), is unreversed, so that it is possible that I am observing metastable Opx, rapidly crystallized from melt at the start of the experiment. However, the Opx and Sapph in this experiment are both homogenous and euhedral (Fig. 2a).

The compositional variation of sapphirine in the MgO-Al_2O_3-SiO_2 system can be considered by starting with the basic formula $Mg_4Al_4Si_2O_{20}$ (called 2:2:1 sapphirine). Most natural sapphirines are more aluminous than this, due to substitution of 2Al for Mg+Si (i.e., solid solution towards the 7:9:3 composition, $Mg_7Al_9Si_3O_{20}$; (e.g., Liu and Presnall, 2000; Hollis and Harley, 2002); here, by contrast, the reverse substitution of Mg+Si for 2Al occurs, to produce sapphirines with less alumina than in 2:2:1, as found by Liu and Presnall (2000). Thus if the formula is represented as $Mg_{4-x}Al_{4+2x}Si_{2-x}O_{20}$, x is usually in the range 0 to 0.5 (Hollis and Harley, 2002), but here x is approximately –0.15 in C-1580 and –0.3 in C-1576. Fig. 20 confirms that $Sapph_{ss}$ in equilibrium with Opx should contain the minimum Al_2O_3 at a given P and T.

5. Conclusions

In this study I made forward partial melting experiments to determine the phase relations at the solidus of the spinel-lherzolite assemblage in the system CMAS both with and without K_2O. I also made reversal crystallization experiments. The K_2O

method, thus, can be fully assessed both by internal consistency and by reference to the previous literature data (Presnall, 1976; Presnall et al., 1979; Walter & Presnall, 1994).

Compositions of all phases, including both pyroxene solid solutions and the melt compositions in the system CMAS derived from the KEs by extrapolating to zero K_2O all agree reasonably well with previous studies. The melt composition of Presnall et al (1979) is almost the same as my extrapolated result from the KEs.

Agreement on the solidus temperature for a Sp-lherzolite phase assemblage in the system CMAS at 11 kbar is consistent between the KEs and the REs and it is around 1320°C, with a probable uncertainty of less than ±10°C. The slightly higher temperature of 1350°C determined by Presnall (1976), later used in Presnall et al (1979), Walter & Presnall (1994) and Gudfinnsson & Presnall (1996, 2000 and 2001), may be due to the W/Re thermocouples used in that study, either from oxidation or from calibration errors. The oxidation problem of the W/Re thermocouples forced Walter & Presnall (1994) to use a nitrogen flow down the thermocouple insulator for their experiments at lower pressures. Recently, Falloon et al (2001) reported drift of W/Re thermocouples at 10 kbar to higher apparent temperature in the temperature range 1300-1400°C caused by oxidation. Commercially available W/Re thermocouples vary widely in their deviation from theoretical emf-temperature relations, requiring careful calibration of each batch (see Klemme & O'Neill 2000b).

The obvious agreement on the pyroxene composition, the melt composition and the solidus among the extrapolation result from the KEs, the result of the REs and the literature data argues that the K_2O method is generally successful. I will report on the application of this method to the determination of partial melting at the solidus in the system CMAS-Cr_2O_3 in Chapter 3 of this thesis.

Comparison with previous work on the system CMAS-Na_2O shows that the effect of K_2O on melting equilibria is much stronger than that of Na_2O, both as regards temperature and melt composition. Increasing K_2O causes the multiply-saturated solidus melt composition to trend towards silica enrichment, becoming quartz-normative above 4 wt% K_2O. By contrast, the effect of Na_2O at 11 kbar is for multiply-saturated melts to trend towards becoming more silica undersaturated; high Na_2O melts are nepheline normative. Note, however, that the activity of SiO_2 in both systems remains nearly the same, being buffered by Fo+Opx (reaction (3)).

6. References

Ai, Y. & Green, D. H. (1989). Phase relations in the system anorthite-potassium feldspar at 10 kbar with emphasis on their solid solutions. Mineralogical Magazine 53, 337-345.

Baker, M. B., Newman, s., Beckett, J. R. and Stolper, E. M. (1992). Separating liquid from crystals in high-pressure melting experiments using diamond aggregates. Geol. Soc. Am. Prog. 24, A256 (Abstracts).

Baker, M. B. & Stolper, E. M. (1994). Determining the composition of high-pressure mantle melts using diamond aggregates. Geochimica. et. Cosmochimica. Acta 58, 2811-2827.

Baker, M. B., Hirschmann, M. M., Ghiorso, M. S. & Stolper, E. M. (1995). Compositions of near-solidus peridotite melts from experiments and thermodynamics calculation. Nature 375, 308-311.

Baker, M. B., Hirschmann, M. M., Wasylenki, L. E. and Stolper, E. M. (1996). Quest for low-degree mantle melts: a reply. Nature 381, 285.

Bose, K. & Ganguly, J. (1995). Quartz-coesite transition revisited: Reversed experimental determination at 500-1200°C and retrieved thermochemical properties. Am Mineral 80, 231-238.

Boyd, F. R. & England, J. L. (1960). Apparatus for phase-equilibrium measurements at pressures up to 50 kbar and temperatures up to 1750°C. J. Geophy. Res. 65, 741-748.

Brey, G. P. & Kohler, T. (1990). Geothermobarometry in four-phase lherzolite II: new thermobarometers, and practical assessment of existing thermobarometers. J. Petrol. 31, 1353-1378.

Chen, C-H & Presnall, D. C. (1975). The system Mg_2SiO_4-SiO_2 at pressures up to 25 kilobars. Am. Mineral. 60, 398-406.

Danckwerth, P. A. & Newton, R. C. (1978). Experimental determination of the spinel peridotite to garnet peridotite reaction in the system MgO-Al_2O_3-SiO_2 in the range 900°-1100° C and Al_2O_3 isopleths of enstatite in the spinel field. Contrib. Mineral. Petrol. 66, 189-201.

Danyushevsky, L. V., Sololev, A. V. & Dmitriev, L. V. (1996). Estimation of the pressure of crystallisation and H_2O content of MORB and BABB glasses: calibration of an empirical technique. Mineral. Petrol. 57, 185-204.

Falloon, T. J. & Green, D. H. (1987). Anhydrous partial melting of MORB pyrolite and other peridotite compositions at 10 kbar: Implications for the origin of MORB glasses. Miner. Petrol. 37, 181-219.

Falloon, T. J. & Green, D. H. (1988). Anhydrous partial melting of peridotite from 8 to 35 kbars and the petrogenesis of MORB. J. Petrol. Special Issue 379-414.

Falloon, T. J., Green, D. H., Hatton, C. J. & Harris, K. L. (1988). Anhydrous partial melting of a fertile and depleted peridotite from 2 to 30 kbar and application to basalt petrogenesis. J. Petrol. 29, 1257-1282.

Falloon, T. J., Green, D. H., O'Neill, H. St. C. & Ballhaus, C. G. (1996). Quest for low-degree mantle melts. Nature 381, 285.

Falloon, T. J., Green, D. H., O'Neill, H.St.C. & Hibberson, W. O. (1997). Experimental tests of low degree peridotite partial melt compositions: implications for the nature of anhydrous near-solidus peridotite melts at 1 GPa. Earth Planet. Sci. Lett 152, 149-162.

Falloon, T. J., Green, D. H., Danyushevsky, L. V & Faul, U. H. (1999). Peridotite melting at 1.0 and 1.5 Gpa: an experimental evaluation of techniques using diamond aggregates and mineral mixes for determination of near-solidus melts. J. Petrol. 40, 1343-1375.

Falloon, T. J. & Danyushevsky L. V. (2000). Melting of refractory mantle at 1.5, 2 and 2.5 GPa under anhydrous and H_2O-undersaturated conditions: implications for the petrogenesis of high-Ca boninites and the influences of subduction components on mantle melting. J. Petrol. 41, 257-283.

Falloon, T. J., Danyushevsky, L. V. & Green, D. H. (2001). Peridotite melting at 1 GPa: reversal experiments on partial melt compositions produced by peridotite-basalt sandwich experiments. J. Petrol. 42, 2363-2390.

Ford, C. E., Russell, D. G., Graven, J. A. & Fisk, M. R. (1983). Olivine-liquid equilibria: temperature, pressure and composition dependence of the crystal/liquid cation partition coefficients for Mg, Fe^{2+}, Ca and Mn. J. Petrol. 24, 256-265.

Fuhrman, M. L. & Lindsley, D. H. (1988). Terneary-feldspar modelling and thermometry. Am. Mineral. 75, 544-559.

Fujii, T. (1977). Pyroxene equilibria in spinel lherzolite. Yb. Carnegie Instn. Wash. 76, 569-572.

Fujii, T. & Scarfe, C. M. (1985). Composition of liquids coexisting with spinel lherzolite at 10 kbar and the genesis of MORBs. Contrib. Mineral. Petrol. 131, 323-346.

Gasparik, T. (1984). Two-pyroxene thermobarometry with new experiment data in the system CaO-MgO-Al_2O_3-SiO_2. Contrib. Mineral. Petrol. 87, 87-97.

Green, T. H., Ringwood, A. E. & Major, A. (1966). Friction effects and pressure calibration in a piston-cylinder high pressure-temperature apparatus. J. Geophy. Res. 71, 3589-3594.

Gudfinnsson, G. H. & Presnall, D. C. (1996). Melting relations of model lherzolite in the system CaO-MgO-Al_2O_3-SiO_2 at 2.4-3.4 Gpa and the generation of komatiites. J. Geophy. R. 101, 27701-27709.

Gudfinnsson, G. H. & Presnall, D. C. (2000). Melting behaviour of model lherzolite in the system CaO-MgO-Al_2O_3-SiO_2-FeO at 0.7-2.8 Gpa. J. Petrol. 41, 1241-1269.

Gudfinnsson, G. H. & Presnall, D. C. (2001). A pressure-independent geothermometer for primitive mantle melts. J. Geophy. R. 106, 16205-16211.

Herzberg, C. (1978). Pyroxene geothermometry and geobarometry: experimental and thermodynamic evaluation of some subsolidus phase relations involving pyroxenes in the system CaO-MgO-Al_2O_3-SiO_2. Geochim. cosmochim. Acta 42, 945-957.

Herzberg, C. & Zhang, J. (1998). Melting experiments in the systems CaO-MgO-Al_2O_3-SiO_2 and MgO-SiO_2 at 3 to 15 Gpa. Am. Mineral. 83, 491-500.

Hirose, K. & Kushiro, I. (1993). Partial melting of dry peridotite at high pressures: determination of compositions of melts segregated from peridotite using aggregates of diamond. Earth Planet. Sci. Lett. 114, 477-489.

Hirose, K.& Kawamoto, T. (1995). Hydrous partial melting of lherzolite at 1 GPa: the effect of H_2O on the genesis of basaltic magmas. Earth Planet. Sci. Lett. 133, 463-473.

Hirose, K. (1997). Melting experiments on lherzolite KLB-1 under hydrous conditions and generation of high-magnesian andesitic melts. Geology 25, 42-44.

Hirschmann, M. M., Baker, M. B. & Stolper, E. M. (1998). The effect of alkalis on the silica content of mantle-derived magmas. Geochimi. Cosmochimi. Acta 62 (5), 883-902.

Hollis, J. A. & Harley, S. L. (2002). Alumina solubility in orthopyroxene coexisting with sapphirine and quartz. Contrib. Mineral. Petrol., DOI 10.1007/s00410-002-0412-3.

Jochum, K. P., Dingwell, D. B., Rocholl, A., Stoll, B., Hofmann, A. W., Becker, S., Besmehn, A., Bessette, D., Dietze, H.-J., Dulski, P., Erzinger, J., Hellebrand, E., Hoppe, P., Horn, P., Janssens, K., Jenner, G. A., Klein, M., McDonough, W. F., Maeetz, M., Mezger, K., Munker, C., Nikogosian, I. K., Pickhardt, C., Raczek, I., Rhede, D.,

Seufert, H. M., Simakin, S. G., Sobolev, A. V., Spettel, B., Straub, S., Vincze, L., Wallianos, A., Weckwerth, G., Weyer, S., Wolf, D. & Zimmer, M. (2000). The preparation and preliminary characterisation of eight geological MPI-DING reference glasses for in-situ microanalysis. J. Geostand. Geoanaly. 24, 87-133.

Johannes, W., Bell, P. M., Mao, H. K., Boettcher, A. L., Chipman, D. W., Hays, J. F., Newont, R. C., Seifert, F. (1971). An interlaboratory comparison of piston-cylinder pressure calibration using albite-breakdown reaction. Contrib. Mineral. Petrol. 32:24-38.

Johnson, K. T. M. & Kushiro, I. (1992). Segregation of high pressure partial melts from peridotite using aggregates of diamond: a new experimental approach. Geophys. Res. Lett. 19, 1703-1706.

Klemme, S. & O'Neill, H. St. C. (1997). The reaction $MgCr_2O_4 + SiO_2 = Cr_2O_3 + MgSiO_3$ and the free energy of formation of magnesiochromite ($MgCr_2O_4$). Contrib. Mineral. Petrol. 130, 59-65.

Klemme, S. & O'Neill, H. St. C. (2000a). The near-solidus transition from garnet lherzolite to spinel lherzolite. Contrib. Mineral. Petrol. 138, 237-248.

Klemme, S. & O'Neill, H. St. C. (2000b). The effect of Cr on the solubility of Al in orthopyroxene: experiments and thermodynamic modelling. Contrib. Mineral. Petrol. 140, 84-98.

Korzhinskii, D. S. (1959). Physicochemical basis of the analysis of the paragenesis of minerals. Consultants Bureau, New York.

Kushiro, I. (1972). Partial melting of synthetic and natural peridotites at high pressures. Yb. Carnegie Instn. Wash. 71, 357-362.

Kushiro, I. & Hirose, K. (1992). Experimental determination of composition of melt formed by equilibrium partial melting of peridotite at high pressures using aggregates of diamond grains. Proc. Jpn. Acad. Ser. B 68, 63-68.

Kushiro, I. (1996). Partial melting of a fertile mantle peridotite at high pressure: an experimental study using aggregates of diamond. In Earth processes: Reading the isotopic code, ed. Basu, A. & Hart, S. R. Geophysical monograph 95: 109-122. Am. Geophys. Union, Washington, D. C.

Kushiro, I. (2001). Partial melting experiments on peridotite and origin of mid-ocean ridge basalt. Annu. Rev. Earth Planet. Sci. 29, 71-107.

Lane, D. L. & Ganguly, J. (1980). Al_2O_3 solubility in orthopyroxene in the system MgO-Al_2O_3-SiO_2: a re-evaluaion, and mantle geotherm. J. Geophy. Res. 85, 6963-6972.

Leeman, W. P. (1978). Distribution of Mg2+ between olivine and silicate melt, and its implications regarding melt structure. Geochim. Cosmochim Acta 42, 789-800.

Liu, T. C. & Presnall, D. C. (1990). Liquidus phase relationships on the join anorthite-forsterite-quartz at 20 kbar with applications to basalt petrogenesis and igneous sapphirine. Contrib. Miner. Petrol. 104, 735-742.

Liu, T. C. & Presnall, D. C. (2000). Liquidus phase relations in the system CaO-MgO-Al_2O_3-SiO_2 at 2.0 GPa: applications to basalt fractionation, eclogites, and igneous sapphirine. J. Petrol. 41, 3-20.

Longhi, J. (1987). Liquidus equilibrium and solid solution in the system $CaAl_2Si_2O_8$-$CaSiO_3$-SiO_2 at low pressure. Am. J. Sci. 287, 265-331.

Miholland, C. S. & Presnall, D. C. (1998). Liquidus phase relations in the CaO-MgO-Al_2O_3-SiO_2 system at 3.0 Gpa; the aluminous pyroxene thermal divide and high-pressure fraction of picritic and komatiitic magmas. J. Petrol. 39, 3-27.

Nekvasil, H. & Carrol, W. (1993). Experimental constrains on the high-temperature termination of the anhydrous 2 feldspar + L curve in the feldspar system at 11.3 kbar. Am. Mineral. 78, 601-606.

Nekvasil, H. (1994). Ternary feldspar/melt equilibria: a review. In: Feldspars and their reactions, 195-219, ed. Parson, I.

Nickel, K. G., Brey, G. P. & Kogarto, L. (1985). Orthopyroxene-clinopyroxene equilibria in the system CaO-MgO-Al_2O_3-SiO_2. Contr. Miner. Petrol. 91: 44-53.

Obata, M. (1976). The solubility of Al_2O_3 in orthopyroxenes in spinel and plagioclase peridotites and spinel pyroxenite. Am. Mineral. 61, 804-816.

O'Hara, M. J. (1968). The bearing of phase equilibria studies in synthetic and natural systems on the orgin and evolution of basic and ultrabasic rocks. Earth Sci. Rev. 4, 69-133.

O'Neill, H. St. C. and Eggins, S. M. (2002).The effect of melt composition on trace element partitioning: an experimental investigation of the activity coefficients of FeO, NiO, CoO, MoO_2 and MoO_3 in silicate melts. Che. Geol 186, 151-181.

Presnall, D. C. (1976). Alumina content of enstatite as a geobarometer for plagioclase and Sp-lherzolites. Am. Mineral. 61, 582-588.

Presnall, D. C., Dixon, S. A., Dixon, J. R., O'Donnell, T. H., Brenner, N. L., Schrock, R. L. & Dycus, D. W. (1978). Liquidus phase relations on the joint diopside-forsterite-anorthite from 1 atm. to 20 kbar: their bearing on the generation and crystallization of basaltic magma. Contr. Miner. Petrol. 66, 203-220.

Presnall, D. C., Dixon, J. R., O'Donnell T. H. & Dixon, S. A. (1979). Generation of mid-ocean ridge tholeiites. J. Petrol. 20, 3-36.

Presnall, D. C. (1986). An algebraic method for determining equilibrium crystallization and fusion paths in multicomponent systems. Am. Mineral. 71, 1061-1070.

Presnall, D. C (1999). Effect of pressure on the fractional crystallisation of basaltic magma. In: Yingwei, Fei, Bertka, C. M. & Mysen, B. O. (ed.), "Mantle petrology: Field observations and high pressure experimentation: A tribute to Francis R. (Joe) Boyd". The Geochemical Society. Special publication 6.

Robinson, J. A. C., Wood, B. J. & Blundy, J. D. (1998). The beginning of melting of fertile and depleted peridotite at 1.5 Gpa. Earth Planet. Sci. Lett 155, 97-111.

Sen, G. & Presnall, D. C. (1984). Liquidus phase relationships on the join anorthite-forsterite-quartz at 10 bar with applications to basalt petrogenesis. Contr. Miner. Petrol. 85, 404-408.

Sen, G. (1985). Experimental determination of pyroxene compositions in the system CaO-MgO-Al_2O_3-SiO_2 at 900-1200°C and 10-15 kbar using PbO and H_2O fluxes. Am. Mineral. 70, 678-695.

Stolper, E. (1980). A phase diagram for mid-ocean ridge basalts: preliminary results and implications for petrogenesis. Contrib. Mineral. Petrol. 74, 13-27.

Takahashi, E. & Kushiro, I. (1983). Melting of a dry peridotite at high pressures and basalt magma genesis. Am. Mineral. 68, 859-879.

Takahashi, E. (1986). Melting of a dry peridotite KLB-1 up to 14 Gpa: Implications on the origin of peridotitic upper mantle. J. Geophys. Res. 91, 9367-9382.

Walter, M. J. & Presnall, D. C. (1994). Melting behaviour of simplified lherzolite in the system CaO-MgO-Al_2O_3-Na_2O from 7 to 35 kbar. J. Petrol. 35, 329-359.

Walter, M. J., Sisson, T. W. & Presnall, D. C. (1995). A mass proportion method for calculating melting reaction and application to melting of model upper mantle lherzolite. Earth Planet. Sci. Lett. 135, 77-90.

Ware, N. G. (1991). Combined energy-dispersive-wavelength-dispersive quantitative electron microprobe analysis. X-ray Spectrometry 20, 73-79.

Chapter 3

The effect of Cr_2O_3 on the partial melting of spinel lherzolite in the system $CaO-MgO-Al_2O_3-SiO_2-Cr_2O_3$ at 11 kbar

1. Introduction

Most if not all basaltic magmas are produced by the partial melting of mantle peridotite. From the chemical perspective, partial melting involves a reaction between melt and residual solid phases, but igneous petrologists have traditionally taken a magmacentric view of the process, because it is the magma that emerges at the Earth's surface for examination. This view has led to the assumption regarding basalt petrogenesis that all the necessary information about the partial melting process is contained in the magma composition. Such an assumption would not be valid if there were a component of the system that was completely absent from the magma, occurring only in the residue – i.e., a completely compatible component.

Chromium as Cr_2O_3 is a highly compatible component that is present in magmas only in minor to trace amounts. Thus its importance in determining the chemical composition of basaltic magmas may not be obvious from the chemistry of the magmas themselves. However, Cr_2O_3 substitutes for Al_2O_3 in the solid phases of the mantle, reducing the activity of Al_2O_3 in the system, hence in derived partial melts.

Chromium is the 7th most abundant element by weight in the Earth's primitive mantle, after O, Si, Mg, Fe, Al, and Ca (e.g., O'Neill & Palme, 1998). The Cr abundance in mantle peridotites is on average about 2600 ppm (O'Neill & Palme, 1998) and it occurs as Cr^{3+} (or Cr_2O_3 as an oxide component) in minerals in the terrestrial environment. This study aims to evaluate the effect of Cr on partial melting of mantle peridotite, by systematic additions of Cr_2O_3 to the model system $CaO-MgO-Al_2O_3-SiO_2$ (CMAS). The CMAS system is the simplest system in which four phases (olivine, orthopyroxene, clinopyroxene and an aluminous phase, plagioclase, spinel or garnet, depending on pressure), as typically developed in the upper mantle composition, are stable. It therefore provides an excellent starting point from which to understand mantle phase equilibria.

Partial melting of a four-phase assemblage in the system CMAS is isobarically invariant, and the chemical potentials of all four components (CaO, MgO, Al_2O_3 and SiO_2) of the melt are completely defined, as, for example, by the following reactions:

$$CaO + 1.5Mg_2Si_2O_6 = CaMgSi_2O_6 + Mg_2SiO_4 \quad (1)$$
Melt Opx Cpx Ol

$$MgO + 0.5Mg_2Si_2O_6 = Mg_2SiO_4 \quad (2)$$
Melt Opx Ol

$$SiO_2 + Mg_2SiO_4 = Mg_2Si_2O_6 \quad (3)$$
Melt Ol Opx

and in the spinel stability field,

$$AlO_{1.5} + 0.5Mg_2SiO_4 = 0.5MgAl_2O_4 + 0.25Mg_2Si_2O_6 \quad (4)$$
Melt Ol Sp Opx

Reaction (4) encapsulates the pivotal point of this study. As Cr_2O_3 substitutes for Al_2O_3 in Sp, the activity of Al_2O_3 in the melt is correspondingly reduced. Since molar Cr/(Cr+Al) in spinel can vary from 0.1 to 0.8 in mantle peridotites (e.g., with depletion by previous melt extraction; Dick & Bullen (1984) and Barnes & Roeder (2001)), the effect is very large. The other melt components (CaO, MgO and SiO_2) do not depend directly on the activities of aluminous components (reactions 1 to 3), hence their activities remain nearly constant as Cr_2O_3 is increased. It is important to note that the Cr effect does not depend on the presence of spinel, although it does depend on the pressure regime. For example, the reaction controlling Al_2O_3 in the melt could be written:

$$AlO_{1.5} + 0.25\ Mg_2Si_2O_6 = 0.5MgAl_2SiO_6 \quad (5)$$
Melt Opx Opx

Cr_2O_3 substituting in orthopyroxene in the pressure regime of the spinel-lherzolite facies diminishes the activity of the $MgAl_2SiO_6$ component (see Klemme and O'Neill, 2000), reducing the Al_2O_3 in the melt similarly. Reaction (5) becomes equivalent to reaction (4) at spinel saturation, the two reactions being linked by the reaction:

$$MgAl_2O_4 + Mg_2Si_2O_6 = MgAl_2SiO6 + Mg_2SiO_4 \quad (6)$$
Sp Opx Opx Ol.

Experimentally it is convenient to study the phenomenon at spinel saturation since the thermodynamic properties of the melt are most rigorously constrained when it is saturated in all four solid phases.

2. Previous work

Previous work on the effect of Cr_2O_3 on the phase relationships of system CMAS at supersolidus conditions is limited. Irvine (1977) showed that Sp can be stabilised in all melts in the join Fo-Di-An-Qz by adding a small amount of Cr_2O_3 into the CMAS system. Libourel (1991) found that the addition of Cr_2O_3 to the system CMAS stabilises spinel in equilibrium with plagioclase lherzolite at 1 bar, and the melt (containing only 0.15 wt% Cr_2O_3) coexisting with five solid phases at the isobaric invariant point (i.e., Ol, Opx, Cpx, Sp and Pl) is enriched in SiO_2 to 56.5 wt%, compared to 55.8 wt% SiO_2 for melt coexisting with Ol, Opx, Cpx and Pl in CMAS (Walter & Presnall, 1994). However, Libourel's study appears only as a conference abstract, and the effect of Cr_2O_3 on the content of other oxides of the melt was not specified. I am not aware of any studies at higher pressure.

The effect of Cr_2O_3 on subsolidus equilibria is better known. O'Neill (1981) and Nickel (1986) demonstrated the importance of Cr_2O_3 on the transition between garnet lherzolite and spinel lherzolite. Klemme & O'Neill (2000) studied the equilibrium between Opx and Sp coexisting with Fo in the system MAS-Cr_2O_3; these phase relations are the key to understanding the controls on the activity of Al_2O_3 (reactions 4 to 6). Li et al. (1995) studied the system MgO-SiO_2-Cr-O in equilibrium with metallic Cr, in which most of the Cr occurs as Cr^{2+}. They showed that Cr^{2+} readily substitutes for Mg in Ol and Opx solid solutions.

3. Experimental technique

3.1. Experimental strategy

Experimentally, the aim of this study is to determine how Cr_2O_3 affects the

compositions of the melt and the solid phases, as well as the partial melting temperature, for the spinel lherzolite phase assemblage in the system CMAS-Cr_2O_3 (CMASCr). A pressure of 11 kbar was chosen since the spinel lherzolite phase assemblage is stable at this pressure, and I could build on previous work in the system CMAS (Presnall et al., 1979, Walter and Presnall, 1994; Chapter 2 of this thesis). Moreover, this pressure has been identified as close to the average pressure for the production of MORB, both from experimental constraints (Presnall et al., 1979; Sen, 1982; Presnall & Hoover, 1984, 1987; Presnall et al., 2002) and seismic observations (Melt Seismic Team, 1998; Dunn & Forsyth, 2001).

There are five components in the system CMAS-Cr_2O_3; if the presence of five phases at the solidus is stipulated (Fo + Sp + Opx + Cpx + Melt), the system has one degree of freedom, and requires one additional variable to be completely specified. In this study, the parameter $Cr\#_{sp}$, defined as molar Cr/(Cr+Al) in spinel, is used as the necessary variable.

Since the system is isobarically univariant in the presence of four crystalline phases, it should be possible, at least theoretically, to observe the full spinel lherzolite phase assemblage coexisting with melt over a finite temperature interval above the solidus. However, preliminary experiments showed that in practice, for experimentally feasible bulk compositions that give reasonable amounts of all phases, this temperature interval was only ~ 10°C, which is close to the temperature resolution of the experiments (~ ± 5°C). I therefore adopted the strategy of deliberately introducing an extra component into the system, in order to increase the temperature interval over which Fo + Sp + Opx + Cpx + Melt could coexist. I chose K_2O, as this component only enters the melt. Previously I have found that adding K_2O expands the temperature interval over which Fo + Sp + Opx + Cpx + Melt is stable to ~ 60 degrees in the system CMAS-K_2O (Chapter 2 of this thesis). The composition of the melt in the K_2O-free system is then obtained by extrapolating the data empirically to zero K_2O. This procedure has been thoroughly tested for the system CMAS-K_2O (Chapter 2 of this thesis), and produces results in good agreement with previous work.

An experimental problem in many peridotite partial melting studies is crystallization from the melt during quenching. In the system CMAS-Cr_2O_3, the temperature of the solidus and the amount of MgO in the melt both increase with increasing $Cr\#_{sp}$, exacerbating the problem. In my first attempts at experiments at high-Cr_2O_3 compositions in the system CMAS-Cr_2O_3, quench forsterite (Fo) was ubiquitous, and melt compositions could not be confidently determined. This problem is also

ameliorated by the addition of K_2O, both by lowering the solidus temperature and by making the melt composition less picritic. The "K_2O method", in conjunction with the "sandwich method", can produce large pools of melt in run products, in which the effects of quench modification are effectively eliminated except at $Cr\#_{sp} = 1$, at which quench modification is so severe that I was unable to gain any useful results.

3.2 Starting materials

Table 1 summarises the starting materials used in this study.

Two types of starting materials were prepared. Crystalline mixtures SEM02-1, SEM05-1, SEM04-1, SEM01-1, SEM03-1 and SEM06-1 were made with a 5/8 inch piston-cylinder press by crystallising the decarbonated oxide mixes at 1300°C, 11 kbar and 48 hours in a 3.5mm diameter Pt capsule. Glasses SEM02-3, SEM02-4, SEM01-4-1, SEM01-4-2 and SEM01-5 were synthesised at 1400°C, one atm and 20 minutes, and then quenched to glass. High-purity oxides (SiO_2, Al_2O_3, Cr_2O_3 and MgO) and carbonates ($CaCO_3$ and K_2CO_3) were used. All mixtures were checked for compositions with electron microprobe (Ware, 1991).

In order to control experimental oxygen fugacity, RuO_2 was mixed into SEM05-1 and SEM01-4-1. All starting materials were stored in an oven at 150°C prior to use.

3.3 Capsule configuration and cell arrangement

All experiments were made in a conventional 1/2 inch piston-cylinder apparatus (Boyd & England, 1960), using sealed Pt capsules, and the so-called 'sandwich technique' (Stolper, 1980; Takahashi & Kushiro, 1983; Fujii & Scarfe, 1985; Falloon et al., 2001), in which a layer of the anticipated melt composition (powdered glass starting material) is placed between two layers of an appropriate crystalline assemblage of Fo+Opx+Cpx+Sp. The proportion of the melt part to the crystalline part was adjusted to keep the Cr/(Cr+Al) ratio of the bulk compositions in each set of experiments constant.

In order to keep the Cr as Cr^{3+} and prevent reduction to Cr^{2+}, it is critically important to eliminate any diffusion of H_2 into the capsule. Such a precaution also ensures that the experiments are not contaminated by water. Therefore, based on Hibberson (1978) and Robinson et al. (1998), a new cell arrangement shown in Fig. 1 was used in this study. The cell arrangement is composed of three concentric shells: a graphite heater, a pyrex glass tube and an outermost sleeve of NaCl, pressed to > 95% of the theoretical density. In the central part of the new assembly, Pt capsule is put into

Table 1 Compositions of starting materials used in this study

	Sandwiching part						Sandwiched Part				
	SEM02-1	SEM05-1	SEM04-1	SEM01-1	SEM03-1	SEM06-1	SEM02-3	SEM02-4	SEM01-4-1	SEM01-4-2	SEM01-5
SiO_2	36.95	37.02	37.86	37.90	38.77	38.81	48.71	49.37	52.39	52.39	51.34
Al_2O_3	22.63	17.49	12.76	9.73	5.90	3.61	18.97	20.20	14.66	14.66	14.37
Cr_2O_3	0.00	5.64	9.59	12.40	14.86	17.18	0.00	0.00	0.48	0.48	0.47
MgO	35.06	34.40	34.38	34.75	34.94	34.88	16.60	13.52	17.15	17.15	16.80
CaO	5.36	5.45	5.40	5.21	5.53	5.53	14.72	13.91	14.31	14.31	14.02
K_2O	0.00	0.00	0.00	0.00	0.00	0.00	1.00	3.00	1.00	1.00	3.00
Total	100.00	100.00	100.00	100.00	100.00	100.00	100.00	100.00	100.00	100.00	100.00
$Cr^{\#}$ (by mole)*	0.00	17.78	33.52	46.10	62.83	76.14	0.00	0.00	2.14	2.14	2.14
Internal buffer**	No	No	No	Yes	No	No	No	No	Yes	No	No

$Cr^{\#}$*, the ratio of Cr/(Cr+Al). Internal buffer**, buffer RuO_2 (11.3 wt% in SEM01-1 and 8.47 wt% in SEM01-4-1). The ratio of Fo, Sp, Opx and Cpx in SEM02-1, SEM05-1, SEM04-1, SEM03-1 and SEM06-1 approximates 1:1:1:1. The compositions of these solid phases came from Walter & Presnall (1994) or from my priliminary experiments.

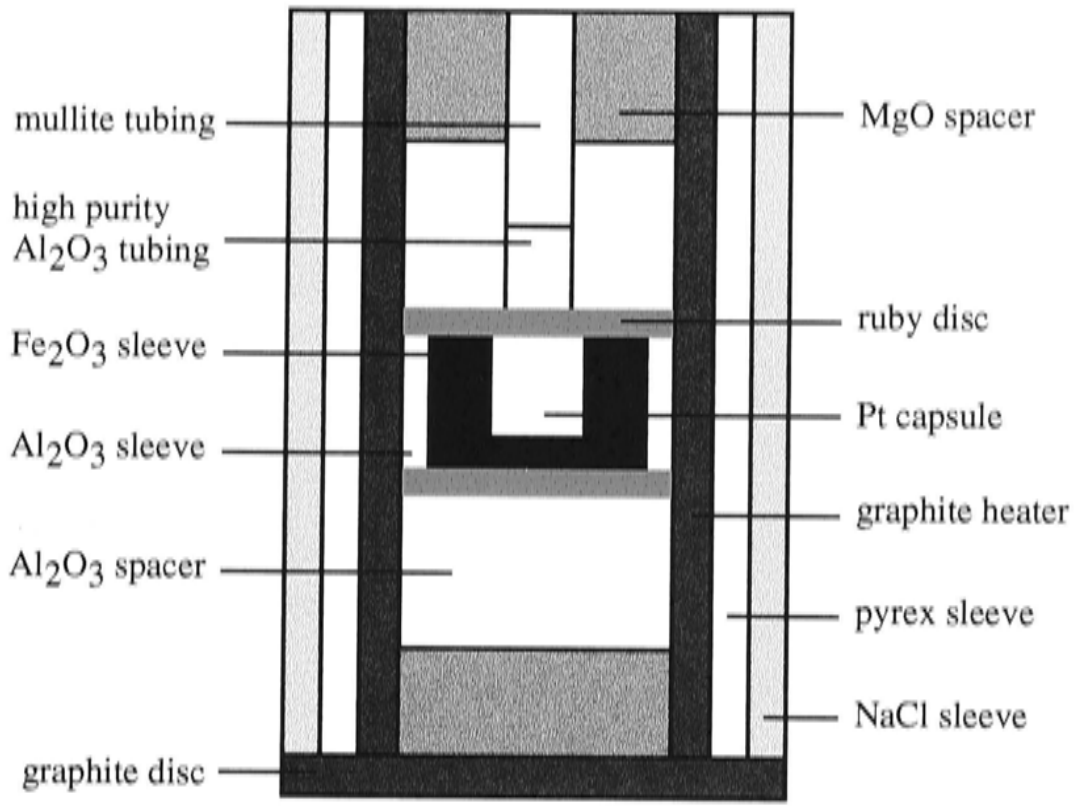

Fig. 1 Experimental assembly used in this study (not to scale).

an Fe_2O_3 sleeve, which is in turn surrounded by an alumina sleeve. At each end of the alumina sleeve, there is a ruby disc (0.5 mm thick) which completely separates the Fe_2O_3 sleeve from other parts of the assembly. This structure can successfully prevent reduction of the Fe_2O_3 sleeve by the graphite heater, or contamination of thermocouple. Alumina and then MgO spacers are positioned next to the ruby discs. This enhances the mechanic stability of the assembly. The Fe_2O_3 sleeve was made by cold pressing in a steel die using acetone as a binder; it was then sintered at 850°C, 1 atm for 3 hours.

Salt cells have low friction (e.g., Green et al., 1966), and any initial friction is expected to decay to a negligible level during the long run times at high temperatures used in this study (Bose & Ganguly, 1995). Consequently, no pressure correction is required.

3.4 Experimental procedure and P-T control

For each experiment, a total of 8-10 mg starting materials were loaded into a Pt capsule. The loaded Pt capsule was stored at 150°C for 6-8 hours and then held in a steel block which had been pre-heated to 750°C while it was welded (Robinson et al., 1998; Chapter 2 of this thesis).

All experiments were performed using the 'piston-out' method, i. e. the pressure was first raised to a few kilobars, then the temperature increased to ~ 450°C to soften the pyrex sleeve; the pressure was then increased up to ~ 0.5 kbar higher than the desired pressure, and the temperature to the nominal temperature of the run. Finally the pressure was lowered to the required pressure (Johannes et al., 1971).

The pressures were continuously monitored and adjusted, if necessary. The continual adjustment of pressure allowed each run to be controlled to within ± 0.2 kbar of the desired pressure of 11.0 kbar.

Temperature was measured and controlled to the nearest degree centigrade with a $Pt_{94}Rh_6$-$Pt_{70}Rh_{30}$ thermocouple (type B); other thermocouples made from the same spools of wire have been several times calibrated against the melting point of gold at 1 atm., and found to perform to within ± 1°C of the theoretical temperature at this temperature. Possible pressure effects on the emf of the thermocouple have been neglected. The thermocouple is protected by a combination of high-purity alumina tubing in the hot part of the assembly (~ 4 mm long), with mullite tubing above this. The tip of the thermocouple, the upper ruby disc and the whole Pt capsule containing experimental charge were all carefully placed in the approximately 5-mm-long hot spot of the experimental assemblage as previously determined in this laboratory (W. O. Hibberson, pers. comn.). In Chapter 2 of this thesis, I argued from the reproducibility of their results that the precision in temperature measurement is approximately ± 5°C.

Klemme & O'Neill (2000) found that type B thermocouples were very stable under similar experimental conditions, and argued that their performance under these conditions (< 1500°C) was likely to be superior to the more widely used W-Re thermocouples (e.g., type C: $W_{97}Re_3$-$W_{75}R_{25}$; type D: $W_{95}Re_5$-$W_{74}Re_{26}$). In order to compare directly the performance of type B thermocouple with type D, two experiments were carried out using both types simultaneously. These experiments used the type B as the controlling thermocouple, such that the type D thermocouple simply monitored the temperature. The experimental conditions are summarised in Table 2.

In experiment D-81, the emf of the type D thermocouple increased linearly with time while the power consumption (which reflects the performance of the controlling type B thermocouple) remained rather constant for most of the run duration, but increased sharply near the end of the experiment (Fig. 2a). The temperature difference between the temperature indicated by the type D thermocouple and the nominal experimental temperature measured by the type B thermocouple is shown as a function of time in Fig. 2b. If the type D thermocouple were recording the real temperature, the temperature at the end of D-81 would be ~ 1600°C, which is not reasonable given the observed run products (Table 2). The melt composition in D-81 (51.73 wt% SiO_2, 17.10 wt% Al_2O_3, 0.28 wt% Cr_2O_3, 15.47 wt% MgO, 13.60 wt% CaO and 1.82 wt% K_2O) gives a calculated temperature of 1412°C using the olivine/melt MgO-partitioning geothermometer of Ford et al. (1983). Since temperatures calculated from this

Table 2 Experimental conditions and results

Exp. Set	Run #	Starting material	Temp.	T(hrs)	T/C	Phase observed	K_2O-melt	T-1	T-2	T-3	T-4	Note
Experiment Set 5	C-1550	SEM05-1+SEM01-5	1360	51.5	B	Fo+Sp+Opx+Melt	1.61	-	-	-	-	
	C-1527	SEM05-1+SEM01-4-2	1350	53	B	Fo+Sp+Opx+Cpx+Melt	0.85	1308	1352	1315	1379	
	D-81**	SEM05-1+SEM01-5	1340	49	B, D	Fo+Sp+Melt	-	-	-	-	1412	
	D-82	SEM05-1+SEM01-5	1340	50	B, D	Fo+Sp+Opx+Cpx+Melt	2.62	1305	1347	1290	1331	
	C-1511	SEM05-1+SEM01-5	1330	92	B	Fo+Sp+Opx+Cpx+Melt	4.08	1306	1350	1286	1296	zoned Sp and Cpx*
Experiment Set 4	C-1499	SEM04-1+SEM01-5	1360	70	B	Fo+Sp+Opx+Cpx+Melt	1.80	1357	1388	1339	1424	
	C-1481	SEM04-1+SEM01-5	1350	71	B	Fo+Sp+Opx+Cpx+Melt	3.06	1405	1428	1347	1397	
	C-1478	SEM04-1+SEM01-5	1340	70	B	Fo+Sp+Opx+Cpx+Melt	5.76	1345	1381	1302	1375	zoned Sp and Cpx
	C-1480	SEM04-1+SEM01-5	1320	74	B	Fo+Sp+Opx+Cpx+Melt***	-	1340	1378	1307	-	zoned Sp and Cpx
Experiment Set 1	C-1459	SEM01-1+SEM01-5	1360	70	B	Fo+Sp+Opx+Melt	1.77	-	-	-	-	
With internal buffer	C-1414	SEM01-1+SEM01-4-1	1360	72	B	Fo+Sp+Opx+Cpx+Melt	0.87	1358	1395	1362	1430	
$Ru+RuO_2$	C-1472	SEM01-1+SEM01-5	1350	70	B	Fo+Sp+Opx+Cpx+Melt	2.54	1372	1400	1327	1410	
	C-1449	SEM01-1+SEM01-5	1340	72	B	Fo+Sp+Opx+Cpx+Melt	3.26	1352	1389	1319	1392	zoned Sp and Cpx
	C-1469	SEM01-1+SEM01-5	1330	72	B	Fo+Sp+Opx+Cpx+Melt	4.26	1351	1390	1311	1326	zoned Sp and Cpx
Experiment Set 3	C-1489	SEM03-1+SEM01-4-2	1360	74	B	Fo+Sp+Opx+Cpx+Melt	1.19	1454	1457	1377	1451	
	C-1463	SEM03-1+SEM01-5	1350	74	B	Fo+Sp+Opx+Cpx+Melt	2.97	1390	1419	1358	1426	zoned Sp
	C-1476	SEM03-1+SEM01-5	1330	72	B	Fo+Sp+Opx+Cpx+Melt	5.11	1372	1404	1358	1407	zoned Sp and Cpx
Experiment Set 6	C-1516	SEM06-1+SEM01-5	1380	52	B	Fo+Sp+Opx+Cpx+Melt	2.07	1561	1504	1396	1477	
	C-1512	SEM06-1+SEM01-5	1370	56	B	Fo+Sp+Opx+Cpx+Melt	3.02	1486	1480	1381	1456	zoned Sp
	C-1515	SEM06-1+SEM01-5	1360	68.5	B	Fo+Sp+Opx+Cpx+Melt	4.01	1448	1458	1362	1444	zoned Sp and Cpx

zoned Sp and Cpx*: only in the sandwiched layer of the experiments with low partial melting extent. Where crystals in sandwiched layer are zoned, the reported compositions (Table 3) refer to the compositions of the homogeneous crystals in the sandwiching layers.

D-81**: probable thermocouple contamination (see text) and no phase composition data except that for melt (see text) reported here.

Melt***: confirmed but cannot be properly analysed.

T-1, temperature calculated using the geothermometer of Nickel et al. (1985); T-2, temperature calculated using the Opx-Cpx geothermometer of Brey & Kohler (1990; equation 9); T-3, temperature calculated using the Ca-in-Opx geothermometer of Brey & Kohler (1990; equation 10); T-4, temperature calculated using the geothermometer of Ford et al. (1983).

The sandwich technique was used in all experiments.

geothermometer are always 30 to 80 °C higher than the nominal temperature in my experiments (see later discussion), the real final temperature of D-81 is possibly 1370 ± 30 °C.

The thermocouples of D-81 were carefully recovered, mounted in epoxy, polished and optically examined in reflected light. Two brownish rust-like haloes surrounding the legs of the type D thermocouple were observed (Fig. 3), indicating oxidation. This probably occurs because the high-purity alumina insulating ceramic is sufficiently strong to resist complete collapse at 11 kbar, allowing air to percolate down to the hot end of the wires. Recently, similar observations for type C thermocouples were reported by Falloon et al, (2001). Although I do not see any direct contact between the brownish halo and the type B thermocouple in this section, I believe that in this particular experiment the oxidation of the type D thermocouple eventually poisoned the type B thermocouple, thus explaining the abrupt power increase near the end of the run.

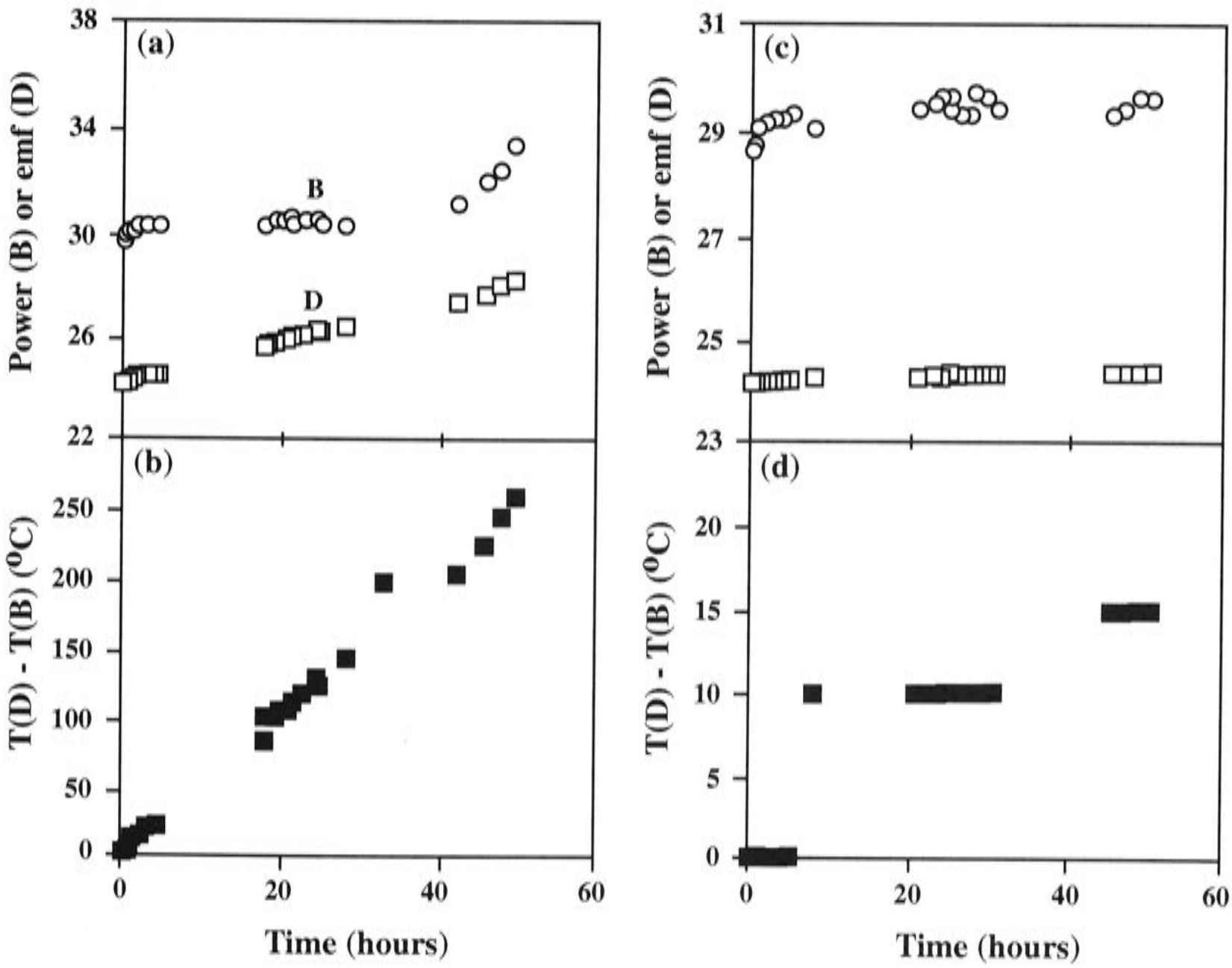

Fig. 2 A comparison of thermocouples (type B vs. type D) made in D-81 (a and b) and in D-82 (c and d). Experiments were controlled by the type B thermocouple but monitored by the type D thermocouple. See Table 2 for experimental details.

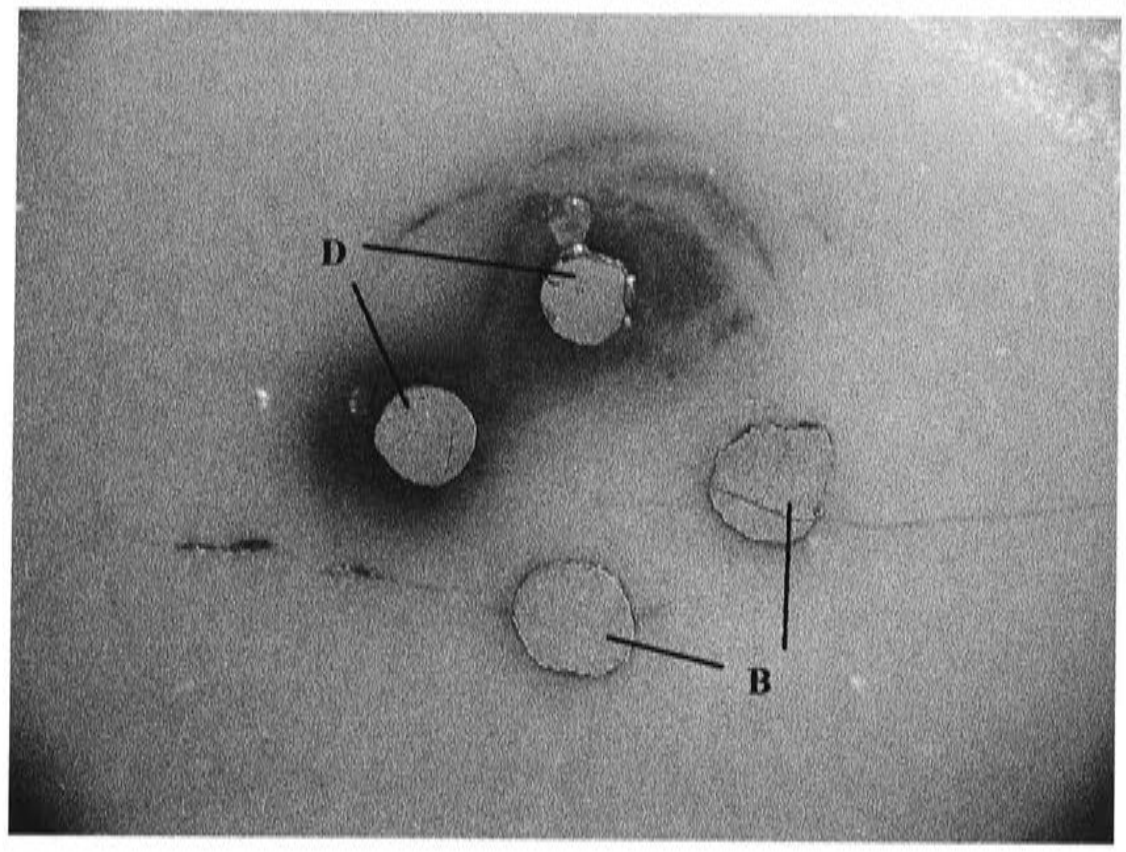

Fig. 3 Photograph of the thermocouples recovered from D-81 (under reflected light).

D-82 is a repeat experiment under identical conditions, except that some super glue was placed on the top of both thermocouples to stop the air flowing down into the assembly. This seems to have prevented the oxidation seen in D-81, and the performances of type B and type D thermocouples generally agree with each other (Fig. 2c, 2d). Nevertheless, in detail the temperature difference between the type D thermocouple and the type B thermocouple increased from zero at the beginning to ~15 °C at the end of the experiment.

3.5 Analysis of run products

At the end of a run, the sample was sectioned longitudinally, mounted in epoxy and polished using a series of diamond pastes. Run products were carbon-coated and analysed on a JEOL 6400 scanning electron microprobe in energy dispersive mode (EDS) at the Electron Microprobe Unit (EMU) at ANU. Phases in run products were identified by back-scattered electron imaging and secondary electron imaging. Beam current was 1 nA, accelerating voltage was 15 keV and the ZAF correction procedure was applied to all analyses (Ware, 1991). A beam spot size of 1 μm was used for all crystalline phases while both 1 μm and 10 μm beam spot sizes were used for glass analyses. The accumulation time was 100 seconds. As reported in Chapter 2 of this thesis, analytical precision was estimated by replicate measurements of three internationally-recognised glass standards, GOR132G, T1G and KL2G (Jochum et al., 2000).

Besides the oxides CaO, MgO, Cr_2O_3, Al_2O_3, SiO_2 and K_2O, FeO and Na_2O were analysed for all the phases present in the experiments. FeO contamination is a potential possibility from the Fe_2O_3 sleeve (see also Chapter 2 of this thesis). Na_2O is a good indicator of the quality of starting materials used. It concentrates in the melt with a content of 0.1-0.5 wt%, depending on the proportion of melt to solids in the experiment; such minor amounts are close to the limit of detection (~ 0.1 wt%), and since they also have almost negligible effect (Walter & Presnall, 1994; Chapter 4 of this thesis) they have been ignored. Analyses were renormalised to 100 percent in order to facilitate data interpretation and comparison.

Lithium and boron have potentially been cryptic contaminants of previous piston-cylinder studies, as these elements have not been amenable to microbeam analysis until recently. Li salts are sometimes used in noble-metal fabrication processes, and B could come from the pyrex glass (it apparently diffuses readily through Pt). To check for any such contamination, Li and B were measured in the glasses in runs C-1472, C-1516 (see Table 2 for experimental conditions) by LA-ICP-MS at RSES, ANU. The Li contents were 2.7±0.3 ppm and 1.8±0.1 ppm, respectively. The B contents were slightly higher at 65±4 and 60±1 ppm. These levels are very similar to that found previously in experiments in the system CMAS-K_2O (Chapter of this thesis), and should have a negligible effect on phase relations.

The Pt capsules from two runs, C-1469 and C-1476 (See Table 2 for experimental conditions) were checked for Fe, Cr and Ru (from RuO_2 used as an internal oxygen buffer in the fomer run) on a Cameca electron microprobe in WDS mode at RSES, ANU; the results are shown in Fig. 4. Clearly, some Fe had diffused into the Pt capsules from their Fe_2O_3 sleeves, but only to approximately the middle of the capsule. The presence of reduced Fe in the Pt establishes that some reduction of the Fe_2O_3 sleeves has taken place, confirming that there really was a need for them. The diffusion profile shows that there is a limit to the run duration possible with my experimental assembly, since eventually Fe would diffuse right through the capsule into the charge (I checked for this possibility in every experiment by including Fe in the electron microprobe analytical routine). The presence of Ru is also confirmed by the electron microprobe analyses, indicating some reduction in the experiment. The quantity of metal Cr in the Pt capsules, however, is essentially negligible. This was not the case in some preliminary experiments run without the Fe_2O_3 sleeves, in which the presence of Cr in the Pt provided clear evidence for the reduction of Cr_2O_3.

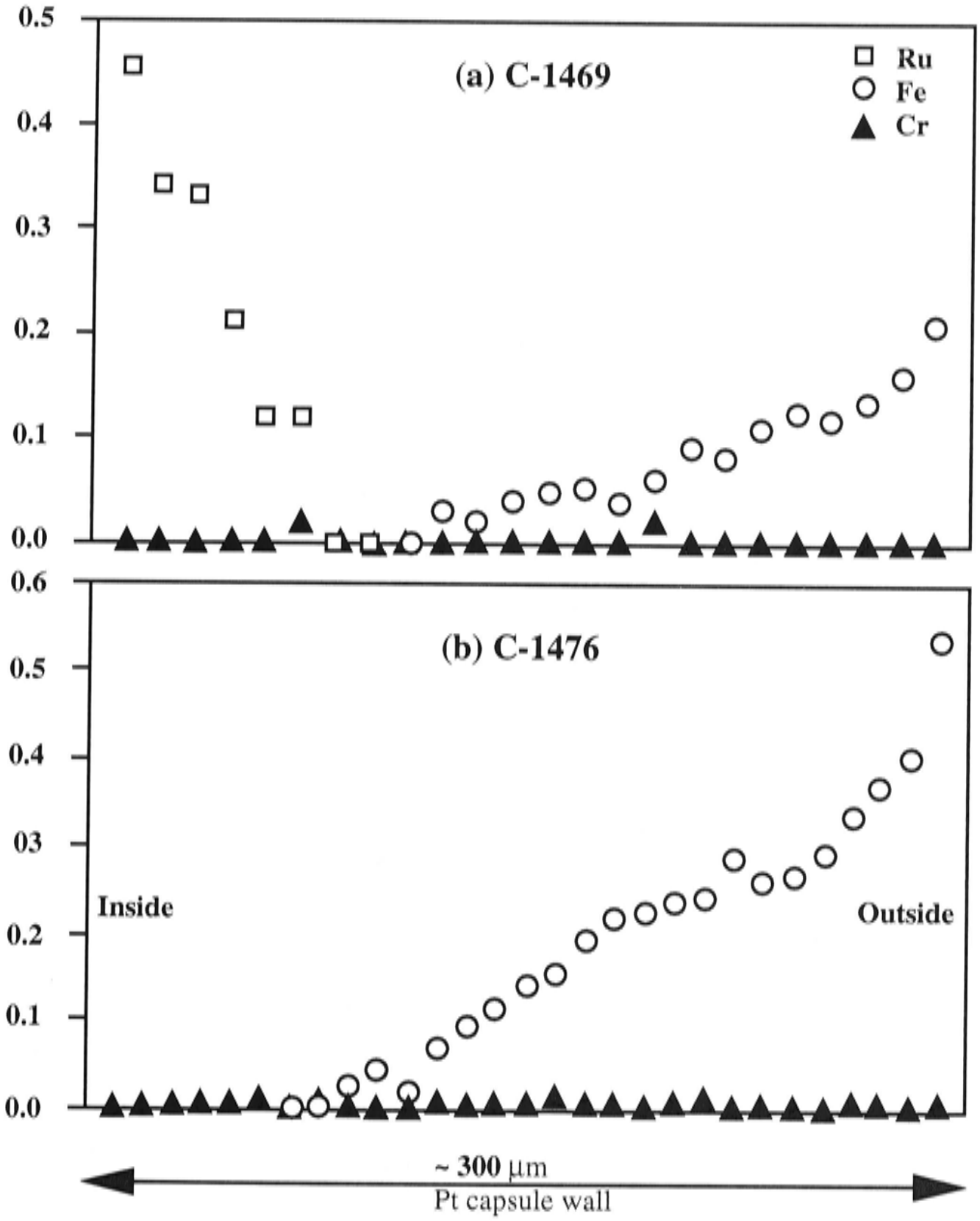

Fig. 4 Electron microprobe analyses across two Pt capsules: (a) C-1469 with Ru+RuO_2 buffer and (b) C-1476 without Ru+RuO_2 buffer. See Table 2 for experimental details.

3.6 Oxidation state of chromium

This study is specifically concerned with Cr as Cr^{3+}. However, during the course of a typical piston-cylinder experiment, a trace of water could be released from incompletely dry material in the pressure assembly and react with the graphite heater to produce hydrogen, which then diffuses through the Pt capsule and reduces the charge, also producing water inside the capsule. The suspected presence of detectable water in many previous "anhydrous" melting experiments argues for the probability of this scenario, unless extreme care is taken (e.g., as here and in the experiments of Robinson et al., 1998; see Chapter 4 of this thesis). Any ingress of H_2 would result in reduction of Cr^{3+} to Cr^{2+}. The latter has quite different chemical properties (e.g., Li et al., 1995; Hanson & Jones,1998); broadly speaking, whereas Cr^{3+} substitutes for Al and is highly

compatible, Cr^{2+} substitutes for Mg and is probably mildly incompatible). Since Cr^{2+} cannot be distinguished from Cr^{3+} by the analytical methods employed in this study (electron microprobe), its presence as a significant proportion of total Cr would fatally scramble the message from the experimental results. Thus a relatively high oxygen fugacity is a prerequisite to success in these experiments. Consequently I attempted to prevent H_2 from entering the capsule by means of enclosing it in the Fe_2O_3 sleeve (Fig. 1). The effectiveness of this method in keeping H_2 from entering the capsule is discussed more fully in Chapter 2 of this thesis.

Initially I also buffered oxygen fugacity internally by adding RuO_2 to the starting compositions (Table 1). During the course of the experiment, a small fraction of the RuO_2 reduces to Ru metal. The oxygen fugacity of the Ru+RuO_2 buffer is close to Fe_3O_4-Fe_2O_3 at the temperatures of this study (O'Neill and Nell, 1997). Unfortunately, the presence of RuO_2 plus Ru in the experiment adds to the difficulty of finding melt pools with pristine glass (i.e., not quench modified), and in subsequent experiments I relied only on the external Fe_2O_3 sleeve to prevent reduction. The amounts of Cr in all phases, including Fo and Melt, in these experiments are consistent with the amounts in the internally buffered experiments. Moreover, there is no significant difference between the stoichiometries of crystalline phases in the Cr-bearing and Cr-free experiments, when these are calculated assuming all chromium in the former is Cr^{3+} (Figs. 5). The slightly but consistently lower cation totals in Cpx (Fig. 5d) are possibly related to the presence of a small amount of Na_2O, not reported in the analyses.

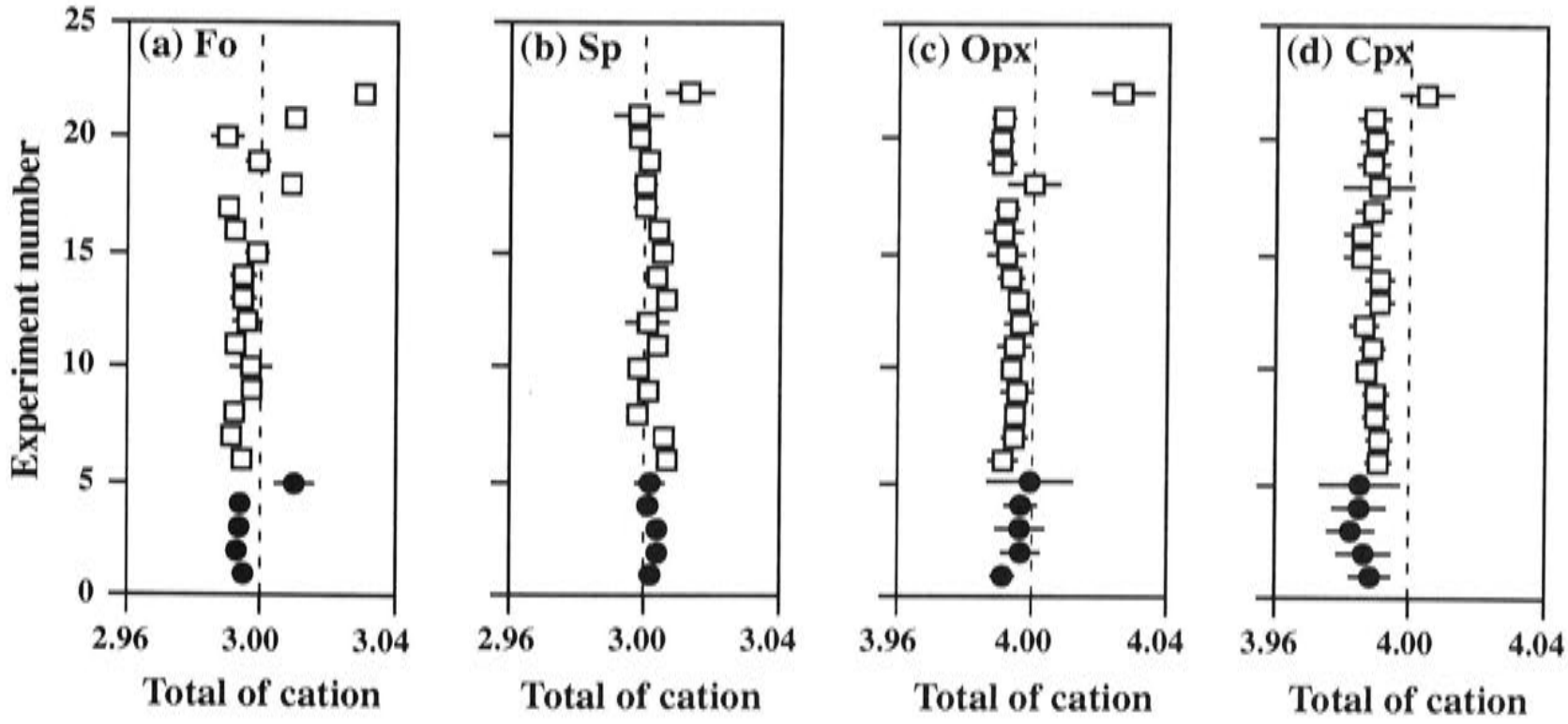

Fig. 5 Stoichiometric calculation for Fo (a), Sp (b), Opx (c) and Cpx (d) by assuming all chromium as Cr^{3+}, on the basis of four oxygens per formula unit for Fo and Sp while 6 oxygens per formula unit for Opx and Cpx. Only experiments (22 runs) displaying melt coexisting with a full Sp lherzolite phase assemblage shown here (See Table 2 for experiment details). These experiments, from the top to the bottom of Table 2, are re-numbered from 1 to 22 in Fig. 5.

3.7 Attainment of equilibrium

My previously reported results in the Cr-free system (CMAS-K_2O) show that the experimental technique used in this study (i.e., the sandwich method with pre-crystallised solid phases) is capable of attaining well equilibrated phase assemblages; exceptions were for melt compositions with relatively high SiO_2 that were not in equilibrium with Fo, and experiments with very low melt fractions. The evidence for disequilibrium is obvious (see discussion in Chapter 2 of this thesis), and for the majority of the experiments, the only sign of disequilibrium was some minor zoning of Al_2O_3 in the cores of larger pyroxene crystals grown in the melt layer of the sandwich.

However, Cr-containing systems are notoriously difficult to equilibrate (O'Neill, 1981; Nickel, 1986; Klemme and O'Neill, 2000), and a more troublesome equilibration problem occurs in some of the present experiments. Particularly in those experiments where the extent of partial melting is relatively low, Cpx, Opx ± Sp crystallise in the sandwiched glass layer. Analyses show that the Cpx and Sp crystals generally have low and variable Cr/(Cr+Al), being lowest in the cores of larger crystals. This is entirely expected, since the glass starting compositions have zero or low Cr_2O_3, hence any crystals forming from such compositions must similarly have low Cr_2O_3. Having once crystallised, interdiffusion of Cr and Al is then too sluggish to permit complete re-equilibration. However, smaller crystals and the rims of the larger crystals both tend to approach the compositions of the phases in the crystalline layers of the sandwich, which are generally very homogenous. I therefore make the major assumption in interpreting these experiments, that the outermost rims of the crystals in the melt layer that are zoned in Cr/(Cr+Al) would be similar to the homogenous crystals in the crystalline layers, and it are these compositions that are in equilibrium with the melt.

Examples of this behaviour are shown in Fig 6 for Cpx in experiments C-1476 and C-1480 and for Sp in C-1463. Note that the Mg/(Ca+Mg) ratio of the Cpx closely follows the Cr/(Cr+Al) ratio. The significance of this will be discussed below.

The experiments with high melting extent (generally also at higher temperatures) do not have this problem and the equilibrium compositions of the solid phases are easily obtained. This is important, as the good internal consistency between these experiments and the ones with zoned crystals at low partial melting extents is an indicator that my assumption regarding the latter is appropriate.

The crystalline phases in all experiments are always euhedral (Fig. 7), and have good stoichiometry from the electron microprobe analyses (Fig. 5).

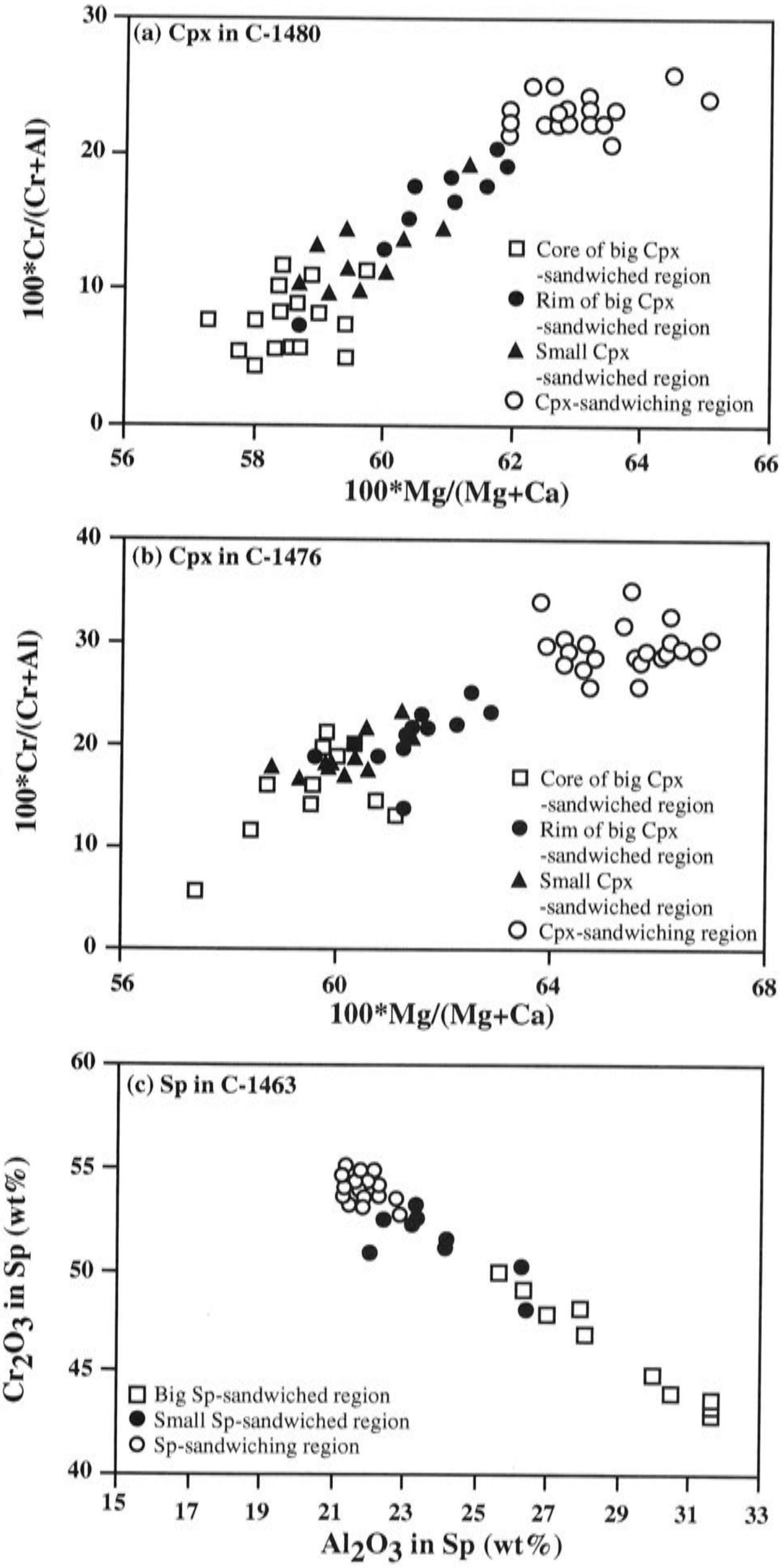

Fig. 6 Covariation of 100*Mg/(Mg+Ca) and 100*Cr/(Cr+Al) in clinopyroxene (a, b), and covariation of Al_2O_3 and Cr_2O_3 in Sp (c).

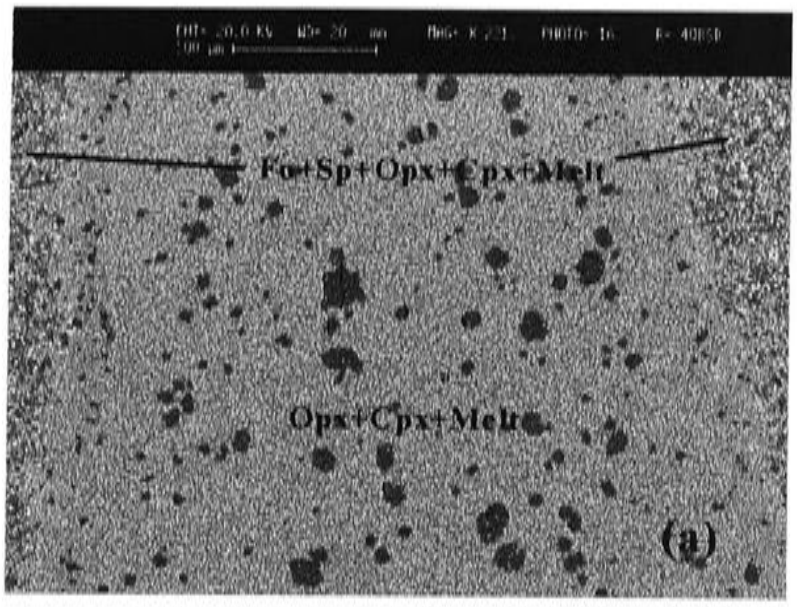

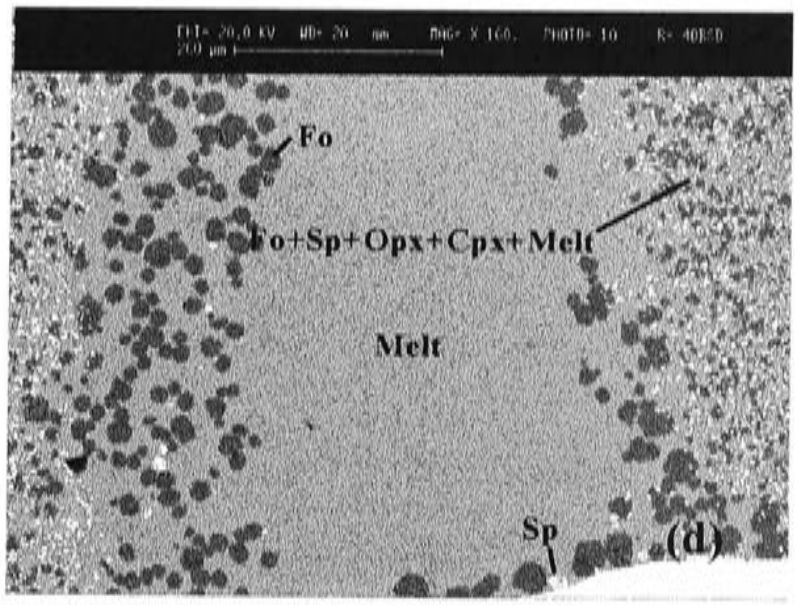

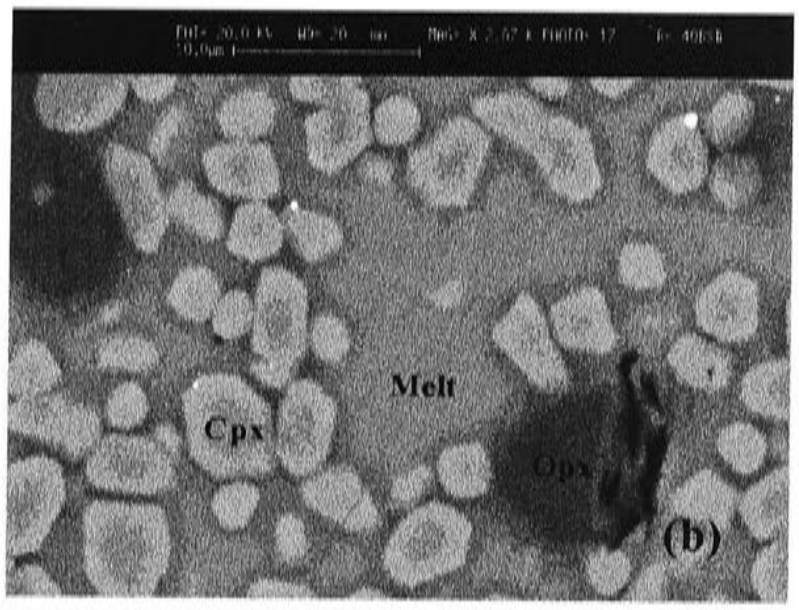

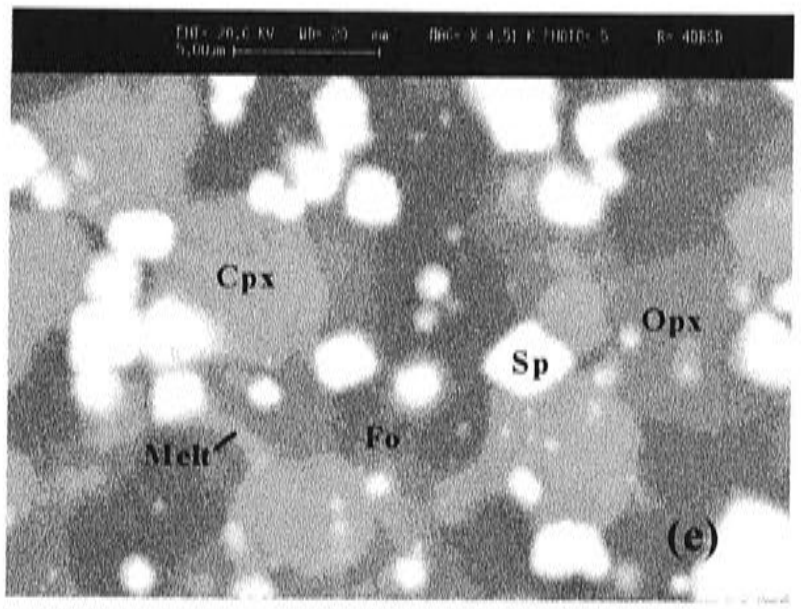

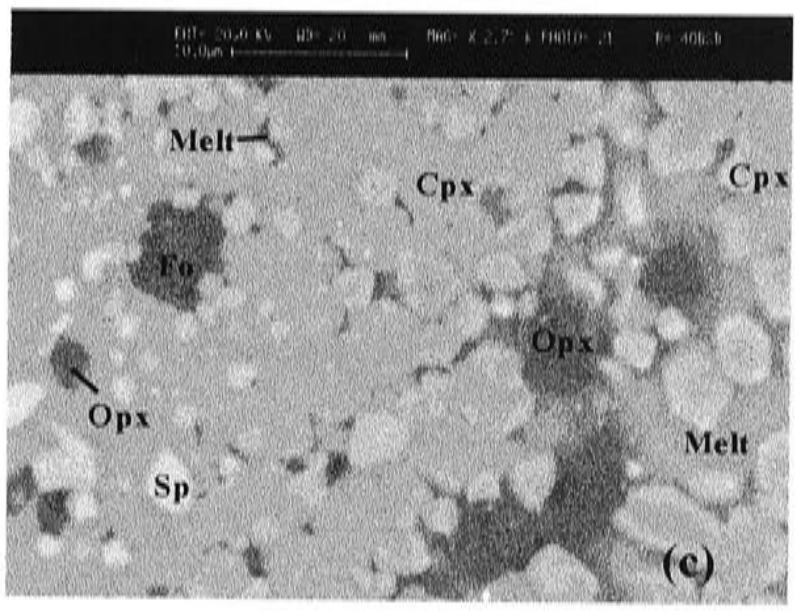

Fig. 7 Back-scatter images for C-1480 (a, b, c) and C-1463 (d, e). C-1480 has a very low melting extent while C-1463 has a high melting extent of ~ 30%. (a) shows the sandwiched zone (Cpx+Opx+trace melt only) and the sandwiching zone (Fo+Sp+Opx+Cpx+trace melt). (b) shows the sandwiched zone. Cpx is slightly compositionally zoned while Opx is relatively homogenous. (c) shows the boundary between the sandwiched zone (right side) and the sandwiching zone (left side). The solid phases in both zones are euhedral. (d) shows the sandwiched zone (Fo+Sp+clean melt only) and the sandwiching zone (Fo+Sp+Opx+Cpx+trace melt). (e) shows the texture in the sandwiching zone which consists of euhedral solid phases and trace melt.

4. Experiment results

Table 2 summarises the starting materials, the experimental techniques, the run conditions and the results of the experiments. The K_2O content of the melts and the calculated temperature by using different geothermometers in the literature are shown in Table 2 as well. The experimental temperature range was 1280-1380 °C and the running time varied from 49 to 92 hours, much longer than 48 hours in most cases. 22 experiments, among 26, display melt coexisting with a Sp-lherzolite phase assemblage while the remaining 4 experiments display melt coexisting with a phase assemblage of

Fo + Sp ± Opx. The amount of melt in one experiment with the full Sp-lherzolite phase assemblage (C-1480) is too low to be properly analysed.

The phase composition data are compiled in Table 3.

4.1 Melt composition

The phase assemblage Fo + Sp + Opx + Cpx + Melt has two degrees of freedom in the system CMAS-Cr_2O_3 - K_2O at a specified pressure, which I have chosen to describe using the two variables of K_2O in the melt (here labelled [K_2O]) and $Cr\#_{sp}$; consequently, the solidus temperature and the composition of the melt can all be described using these two variables. By fitting the data to empirical equations in [K_2O] and $Cr\#_{sp}$, I can then extrapolate the data to zero [K_2O] to find the main object of this study, the composition of melt along the spinel-lherzolite solidus as a function of $Cr\#_{sp}$.

The solidus temperature is given by:

$$T_{solidus} = 1318 - 5.62\,[K_2O] + 3.25\,Cr\#_{sp} - 0.08\,(Cr\#_{sp})^2 + 6.72*10^{-4}\,(Cr\#_{sp})^3 \qquad (7)$$

This was obtained from a fit to data in both the system CMAS-K_2O (Chapter 2 of this thesis) with [K_2O] < 7 wt% and the system CMAS-Cr_2O_3-K_2O (Fig. 8). Using Equation 7, I recalculated the temperature in my experiments, and the average difference between the calculated temperature and the nominal experimental temperature is just 18 degrees. It is obvious in Fig. 8 that Cr^{3+} strongly increases the partial melting temperature. The increase is not linear, being strong at low $Cr\#_{sp}$, weak at mediate $Cr\#_{sp}$ and strong again at high $Cr\#_{sp}$.

For describing the melt compositions at the solidus, it is apparent from the raw data that the effect of K_2O is rather different in the system CMAS-Cr_2O_3-K_2O from the system CMAS-K_2O (Fig. 9). This may be due to interactions between K_2O and Al_2O_3 in the melt. In any case, in order to obtain a good fit to the data, I fitted the Cr-containing and Cr-free experiments separately. I also found that one experiment, C-1469, has an anomalous melt composition, and this experiment was removed from the regression. For the remaining 15 data in CMAS-Cr_2O_3-K_2O I obtained (for $Cr\#_{sp} \geq 20$):

$$[SiO_2] = 49.8 + 0.53\,[K_2O] + 0.051\,Cr\#_{sp} \qquad (8)$$

Table 3 Experimentally observed phase compositions. Fo, forsterite; Sp, spinel; Opx, orthopyroxene; Cpx, clinopyroxene. Composition data in weight percent normalised to 100%. Fo(12) is phase name followed by the number of analyses. 42.72(0.12) is an average followed by one standard deviation and should be read as 42.72 ± 0.12. Cations are calculated by charge-balance technique, on the basis of 4 oxygens for Fo and Sp and 6 oxygens for Cpx and Opx. *, 16 analyses conducted but only the one in agreement with other experiments in the same experiment set reported here; **, phase confirmed but data with high quality unavailable. Six Cr-free experiments from chapter 2 of this thesis are re-reported here with cation data.

C-1423, 1320°C	**Fo(12)**	**Sp(17)**			**Melt(22)**
SiO_2	42.72(0.12)	0.00(0.00)			49.43(0.11)
Al_2O_3	0.00(0.00)	71.51(0.11)			20.40(0.08)
MgO	56.96(0.11)	28.42(0.11)			14.91(0.07)
CaO	0.33(0.04)	0.08(0.04)			14.64(0.07)
K_2O	-	-			0.63(0.02)
Si	1.001(0.002)	0.000(0.000)			
Al	0.000(0.000)	1.996(0.003)			
Mg	1.990(0.004)	1.003(0.004)			
Ca	0.008(0.001)	0.002(0.001)			
Total	2.999(0.002)	3.002(0.001)			
C-1422, 1310°C	**Fo(18)**	**Sp(13)**	**Opx(19)**	**Cpx(19)**	**Melt(19)**
SiO_2	42.91(0.11)	0.00 (0.00)	54.57(0.27)	51.96(0.30)	49.98(0.11)
Al_2O_3	0.00(0.00)	71.52(0.10)	8.60(0.34)	8.67(0.42)	20.39(0.10)
MgO	56.78(0.11)	28.35(0.09)	34.36(0.32)	21.15(0.26)	14.30(0.07)
CaO	0.31(0.03)	0.13(0.08)	2.47(0.41)	18.22(0.40)	14.60(0.07)
K_2O	-	-	-	-	0.73(0.03)
Si	1.005(0.002)	0.000(0.000)	1.837(0.008)	1.831(0.010)	
Al	0.000(0.000)	1.997(0.002)	0.341(0.013)	0.360(0.017)	
Mg	1.982(0.004)	1.001(0.003)	1.725(0.014)	1.111(0.013)	
Ca	0.008(0.001)	0.003(0.002)	0.089(0.015)	0.688(0.016)	
Total	2.995(0.002)	3.001(0.001)	3.992(0.003)	3.989(0.006)	
C-1461, 1310°C	**Fo(8)**	**Sp(8)**	**Opx(21)**	**Cpx(21)**	**Melt(15)**
SiO_2	42.99(0.06)	0.08(0.04)	54.59(0.33)	52.17(0.26)	51.52(0.13)
Al_2O_3	0.00(0.00)	71.28(0.10)	8.34(0.42)	8.39(0.34)	20.55(0.16)
MgO	56.72(0.04)	28.56(0.12)	34.84(0.30)	21.00(0.40)	12.75(0.13)
CaO	0.29(0.03)	0.08(0.04)	2.23(0.17)	18.44(0.35)	12.87(0.14)
K_2O	-	-	- -	-	2.31(0.07)
Si	1.007(0.001)	0.002(0.001)	1.837(0.011)	1.839(0.018)	
Al	0.000(0.000)	1.990(0.003)	0.331(0.017)	0.348(0.014)	
Mg	1.980(0.002)	1.009(0.005)	1.748(0.016)	1.103(0.021)	
Ca	0.007(0.001)	0.002(0.001)	0.080(0.006)	0.697(0.014)	
Total	2.993(0.001)	3.003(0.002)	3.997(0.006)	3.987(0.008)	
C-1448, 1300°C	**Fo(9)**	**Sp(8)**	**Opx(19)**	**Cpx(19)**	**Melt(20)**
SiO_2	42.89(0.15)	0.10(0.09)	54.51(0.37)	52.22(0.35)	53.17(0.15)
Al_2O_3	0.09(0.13)	71.25(0.16)	8.50(0.40)	8.58(0.43)	21.47(0.12)
MgO	56.71(0.19)	28.51(0.07)	34.80(0.36)	20.90(0.42)	10.09(0.11)
CaO	0.30(0.05)	0.14(0.06)	2.19(0.30)	18.30(0.47)	11.19(0.13)
K_2O	-	-	-	-	4.08(0.09)
Si	1.004(0.003)	0.002(0.002)	1.835(0.012)	1.839(0.011)	
Al	0.003(0.004)	1.990(0.004)	0.337(0.016)	0.356(0.018)	
Mg	1.980(0.007)	1.007(0.003)	1.746(0.018)	1.097(0.022)	
Ca	0.008(0.001)	0.004(0.001)	0.079(0.011)	0.691(0.019)	
Total	2.994(0.003)	3.003(0.001)	3.997(0.007)	3.983(0.007)	
C-1460, 1290°C	**Fo(7)**	**Sp(13)**	**Opx(20)**	**Cpx(23)**	**Melt(14)**
SiO_2	42.96(0.09)	0.30(0.19)	54.72(0.24)	52.24(0.39)	53.85(0.17)
Al_2O_3	0.03(0.06)	71.15(0.24)	8.19(0.39)	8.28(0.45)	21.60(0.21)
MgO	56.71(0.09)	28.45(0.12)	34.99(0.32)	20.76(0.45)	9.36(0.23)
CaO	0.30(0.03)	0.11(0.07)	2.10(0.26)	18.71(0.38)	10.43(0.11)
K_2O	-	-	-	-	4.76(0.15)
Si	1.006(0.002)	0.007(0.004)	1.841(0.018)	1.842(0.013)	
Al	0.001(0.002)	1.986(0.007)	0.325(0.016)	0.344(0.019)	
Mg	1.980(0.004)	1.004(0.004)	1.755(0.016)	1.092(0.023)	
Ca	0.007(0.001)	0.003(0.002)	0.076(0.009)	0.707(0.015)	
Total	2.994(0.002)	3.000(0.002)	3.997(0.005)	3.985(0.008)	

Table 3 continued

C-1447, 1280°C	**Fo(6)**	**Sp(6)**	**Opx(15)**	**Cpx(15)**	**Melt(11)**
SiO_2	42.73(0.21)	0.13(0.11)	54.64(0.38)	52.29(0.38)	55.83(0.28)
Al_2O_3	0.00(0.00)	71.32(0.21)	8.33(0.58)	8.27(0.56)	21.74(0.35)
MgO	57.00(0.18)	28.47(0.13)	34.83(0.54)	21.17(0.62)	7.33(0.143)
CaO	0.28(0.05)	0.08(0.04)	2.19(0.30)	18.28(0.45)	8.93(0.17)
K_2O	-	-	-	-	6.17(0.11)
Si	1.003(0.005)	0.002)(0.004)	1.841(0.011)	1.840(0.013)	
Al	0.000(0.000)	1.995(0.008)	0.331(0.024)	0.343(0.024)	
Mg	1.997(0.005)	1.005(0.005)	1.749(0.027)	1.111(0.033)	
Ca	0.010(0.000)	0.000(0.000)	0.079(0.012)	0.691(0.018)	
Total	3.010(0.006)	3.002(0.004)	4.000(0.012)	3.985(0.012)	

C-1550, 1360°C	**Fo(10)**	**Sp(10)**	**Opx(10)**	**Melt(10)**
SiO_2	42.70(0.10)	0.46(0.08)	55.26(0.15)	51.82(0.11)
Al_2O_3	0.12(0.08)	46.42(0.58)	5.67(0.15)	16.97(0.06)
Cr_2O_3	0.15(0.07)	26.85(0.74)	1.49(0.13)	0.22(0.07)
MgO	56.67(0.11)	26.02(0.10)	35.06(0.20)	15.70(0.11)
CaO	0.35(0.03)	0.26(0.05)	2.52(0.13)	13.68(0.07)
K2O	-	-	-	1.61(0.03)
Si	1.000(0.000)	0.010(0.000)	1.869(0.006)	
Al	0.002(0.004)	1.420(0.015)	0.226(0.007)	
Cr	0.000(0.000)	0.552(0.016)	0.040(0.005)	
Mg	1.978(0.006)	1.009(0.003)	1.767(0.008)	
Ca	0.010(0.000)	0.009(0.003)	0.090(0.007)	
Total	2.990(0.007)	3.000(0.007)	3.992(0.009)	

C-1527, 1350°C	**Fo(10)**	**Sp(14)**	**Opx(22)**	**Cpx(21)**	**Melt***
SiO_2	42.72(0.14)	0.31(0.09)	55.05(0.29)	52.27(0.23)	51.61
Al_2O_3	0.24(0.08)	52.90(0.40)	6.44(0.29)	6.36(0.23)	18.32
Cr_2O_3	0.19(0.09)	19.59(0.41)	1.31(0.11)	1.51(0.12)	0.16
MgO	56.47(0.09)	26.98(0.10)	34.65(0.30)	21.03(0.45)	14.67
CaO	0.39(0.05)	0.21(0.08)	2.54(0.20)	18.83(0.52)	14.37
K_2O	-	-	-	-	0.85
Si	1.001(0.003)	0.008(0.002)	1.862(0.009)	1.855(0.008)	
Al	0.007(0.002)	1.580(0.010)	0.257(0.012)	0.266(0.009)	
Cr	0.003(0.002)	0.393(0.009)	0.035(0.003)	0.042(0.003)	
Mg	1.973(0.004)	1.019(0.004)	1.749(0.015)	1.112(0.023)	
Ca	0.010(0.001)	0.006(0.002)	0.092(0.007)	0.716(0.021)	
Total	2.994(0.002)	3.006(0.001)	3.992(0.004)	3.991(0.004)	

D-82, 1340°C	**Fo(14)**	**Sp(18)**	**Opx(20)**	**Cpx(17)**	**Melt(13)**
SiO_2	42.91(0.21)	0.37(0.15)	55.21(0.21)	52.25(0.27)	52.38(0.20)
Al_2O_3	0.19(0.07)	51.16(0.37)	6.07(0.34)	6.39(0.37)	19.90(0.35)
Cr_2O_3	0.10(0.08)	21.47(0.40)	1.31(0.11)	1.52(0.14)	0.10(0.06)
MgO	56.41(0.26)	26.84(0.12)	35.04(0.28)	20.90(0.38)	11.58(0.31)
CaO	0.39(0.09)	0.16(0.06)	2.38(0.15)	18.94(0.51)	13.41(0.30)
K_2O	-	-	-	-	2.62(0.13)
Si	1.005(0.004)	0.009(0.004)	1.866(0.007)	1.855(0.009)	
Al	0.005(0.002)	1.538(0.009)	0.242(0.013)	0.267(0.015)	
Cr	0.002(0.001)	0.433(0.009)	0.035(0.003)	0.043(0.004)	
Mg	1.969(0.010)	1.021(0.005)	1.766(0.014)	1.106(0.019)	
Ca	0.010(0.002)	0.004(0.002)	0.086(0.005)	0.720(0.020)	
Total	2.991(0.004)	3.005(0.002)	3.995(0.004)	3.991(0.004)	

C-1511, 1330°C	**Fo(8)**	**Sp(16)**	**Opx(16)**	**Cpx(16)**	**Melt(12)**
SiO_2	42.99(0.19)	0.33(0.10)	55.13(0.29)	52.48(0.32)	52.93(0.16)
Al_2O_3	0.00(0.00)	52.88(0.33)	6.19(0.30)	6.07(0.42)	22.00(0.40)
Cr_2O_3	0.12(0.05)	20.20(0.36)	1.33(0.12)	1.52(0.13)	0.07(0.06)
MgO	56.53(0.21)	26.42(0.13)	35.02(0.19)	21.10(0.38)	9.22(0.36)
CaO	0.36(0.03)	0.16(0.06)	2.34(0.10)	18.83(0.48)	11.71(0.19)
K_2O	-	-	-	-	4.08(0.16)
Si	1.007(0.004)	0.509(0.514)	1.864(0.009)	1.862(0.011)	
Al	0.000(0.000)	1.631(0.652)	0.247(0.012)	0.254(0.017)	
Cr	0.002(0.001)	0.357(0.367)	0.035(0.003)	0.043(0.004)	
Mg	1.974(0.008)	1.491(0.499)	1.765(0.009)	1.116(0.019)	
Ca	0.009(0.001)	0.008(0.002)	0.085(0.004)	0.71(0.019)	
Total	2.992(0.004)	2.996(0.006)	3.995(0.003)	3.990(0.004)	

Table 3 continued

C-1499, 1360°C	**Fo(7)**	**Sp(17)**	**Opx(20)**	**Cpx(17)**	**Melt(13)**
SiO_2	42.74(0.14)	0.52(0.11)	55.86(0.36)	53.04(0.38)	52.75(0.23)
Al_2O_3	0.00(0.00)	35.03(0.38)	4.38(0.32)	4.83(0.27)	15.40(0.14)
Cr_2O_3	0.14(0.09)	39.34(0.39)	1.79(0.17)	2.12(0.21)	0.27(0.07)
MgO	56.75(0.22)	24.86(0.14)	35.28(0.28)	22.28(0.31)	15.98(0.17)
CaO	0.37(0.04)	0.25(0.06)	2.70(0.36)	17.73(0.35)	13.79(0.12)
K_2O	-	-	-	-	1.80(0.05)
Si	1.002(0.003)	0.014(0.003)	1.893(0.011)	1.879(0.011)	
Al	0.000(0.000)	1.124(0.011)	0.175(0.013)	0.202(0.012)	
Cr	0.003(0.002)	0.847(0.010)	0.048(0.005)	0.059(0.006)	
Mg	1.983(0.008)	1.008(0.006)	1.782(0.013)	1.177(0.015)	
Ca	0.009(0.001)	0.007(0.002)	0.098(0.013)	0.673(0.014)	
Total	2.997(0.003)	3.000(0.002)	3.996(0.005)	3.990(0.004)	
C-1481, 1350°C	**Fo(8)**	**Sp(24)**	**Opx(21)**	**Cpx(21)**	**Melt (20)**
SiO_2	42.68(0.17)	0.34(0.09)	55.50(0.34)	53.28(0.30)	53.21(0.17)
Al_2O_3	0.00(0.00)	37.72(0.34)	5.01(0.38)	5.21(0.33)	17.04(0.11)
Cr_2O_3	0.22(0.08)	36.91(0.33)	1.84(0.18)	1.99(0.16)	0.22(0.12)
MgO	56.76(0.15)	24.79(0.11)	34.92(0.24)	23.43(0.34)	13.85(0.18)
CaO	0.33(0.03)	0.25(0.06)	2.74(0.25)	16.08(0.37)	12.61(0.18)
K_2O	-	-	-	-	3.06(0.08)
Si	1.001(0.003)	0.009(0.002)	1.881(0.011)	1.877(0.009)	
Al	0.000(0.000)	1.199(0.009)	0.200(0.015)	0.216(0.014)	
Cr	0.004(0.001)	0.787(0.008)	0.049(0.005)	0.055(0.004)	
Mg	1.984(0.006)	0.996(0.005)	1.764(0.011)	1.231(0.017)	
Ca	0.008(0.001)	0.007(0.002)	0.100(0.009)	0.607(0.015)	
Total	2.997(0.003)	2.998(0.002)	3.994(0.003)	3.987(0.003)	
C-1478, 1340°C	**Fo(12)**	**Sp(15)**	**Opx(19)**	**Cpx(21)**	**Melt (21)**
SiO_2	42.89(0.10)	0.45(0.20)	55.66(0.33)	52.96(0.16)	54.63(0.13)
Al_2O_3	0.17(0.06)	39.47(0.55)	4.88(0.27)	5.10(0.15)	18.81(0.16)
Cr_2O_3	0.12(0.10)	34.38(0.52)	1.71(0.20)	2.05(0.15)	0.13(0.07)
MgO	56.48(0.15)	25.46(0.11)	35.29(0.18)	22.03(0.47)	10.57(0.13)
CaO	0.34(0.06)	0.24(0.08)	2.45(0.11)	17.87(0.49)	10.10(0.21)
K_2O	-	-	-	-	5.76(0.16)
Si	1.004(0.002)	0.012(0.005)	1.885(0.009)	1.876(0.005)	
Al	0.005(0.002)	1.243(0.015)	0.195(0.011)	0.213(0.006)	
Cr	0.002(0.002)	0.727(0.012)	0.046(0.005)	0.057(0.004)	
Mg	1.972(0.005)	1.014(0.004)	1.781(0.009)	1.163(0.023)	
Ca	0.009(0.002)	0.007(0.002)	0.089(0.004)	0.679(0.019)	
Total	2.992(0.002)	3.003(0.002)	3.995(0.005)	3.989(0.004)	
C-1480, 1320°C	**Fo(8)**	**Sp(16)**	**Opx(17)**	**Cpx(16)**	**Melt****
SiO_2	42.81(0.13)	0.62(0.27)	55.59(0.42)	52.834(0.26)	
Al_2O_3	0.00(0.00)	39.83(0.57)	4.77(0.38)	5.19(0.20)	
Cr_2O_3	0.06(0.04)	34.21(0.49)	1.85(0.27)	2.23(0.18)	
MgO	56.76(0.13)	25.11(0.16)	35.30(0.36)	21.74(0.24)	
CaO	0.37(0.05)	0.23(0.07)	2.49(0.28)	18.00(0.32)	
K_2O	-	-	-	-	
Si	1.003(0.003)	0.016(0.007)	1.883(0.012)	1.874(0.008)	
Al	0.000(0.000)	1.255(0.018)	0.190(0.015)	0.217(0.008)	
Cr	0.001(0.001)	0.724(0.012)	0.050(0.007)	0.063(0.005)	
Mg	1.983(0.005)	1.002(0.008)	1.783(0.017)	1.149(0.012)	
Ca	0.009(0.001)	0.009(0.003)	0.090(0.010)	0.684(0.013)	
Total	2.996(0.002)	3.001(0.006)	3.997(0.005)	3.987(0.004)	
C-1459, 1360°C	**Fo(6)**	**Sp(8)**	**Opx(15)**		**Melt(8)**
SiO_2	43.11(0.14)	0.27(0.13)	57.13(0.38)		53.53(0.13)
Al_2O_3	0.00(0.00)	24.73(0.48)	2.83(0.25)		13.38(0.06)
Cr_2O_3	0.14(0.06)	50.94(0.51)	1.63(0.22)		0.58(0.10)
MgO	56.43(0.12)	23.82(0.14)	35.72(0.41)		16.99(0.11)
CaO	0.32(0.07)	0.25(0.08)	2.68(0.25)		13.76(0.06)
K_2O	-	-	-		1.77(0.09)
Si	1.009(0.003)	0.008(0.003)	1.933(0.015)		
Al	0.000(0.000)	0.830(0.016)	0.113(0.011)		
Cr	0.003(0.002)	1.147(0.017)	0.044(0.005)		
Mg	1.969(0.005)	1.011(0.010)	1.802(0.015)		
Ca	0.008(0.001)	0.008(0.003)	0.097(0.008)		
Total	2.989(0.003)	3.004(0.005)	3.992(0.004)		

Table 3 continued

C-1414, 1360°C	**Fo(18)**	**Sp(20)**	**Opx(19)**	**Cpx(20)**	**Melt(15)**
SiO_2	42.70(0.14)	0.33(0.08)	56.56(0.21)	53.19(0.14)	52.83(0.19)
Al_2O_3	0.00(0.00)	29.05(0.36)	3.43(0.15)	4.67(0.28)	14.40(0.14)
Cr_2O_3	0.37(0.11)	45.87(0.46)	1.52(0.12)	2.03(0.05)	0.47(0.11)
MgO	56.57(0.12)	24.53(0.23)	35.62(0.17)	22.56(0.26)	16.83(0.16)
CaO	0.35(0.02)	0.23(0.05)	2.86(0.18)	17.55(0.47)	14.59(0.12)
K_2O	-	-	-	-	0.87(0.06)
Si	1.001(0.003)	0.009(0.002)	1.916(0.006)	1.883(0.004)	
Al	0.000(0.000)	0.956(0.010)	0.137(0.006)	0.195(0.011)	
Cr	0.007(0.002)	1.013(0.012)	0.041(0.003)	0.057(0.001)	
Mg	1.978(0.005)	1.021(0.009)	1.798(0.008)	1.191(0.012)	
Ca	0.009(0.001)	0.007(0.001)	0.104(0.007)	0.666(0.019)	
Total	2.995(0.002)	3.006(0.003)	3.996(0.003)	3.991(0.004)	
C-1472, 1350°C	**Fo(8)**	**Sp(17)**	**Opx(15)**	**Cpx(17)**	**Melt(9)**
SiO_2	42.80(0.14)	0.35(0.09)	56.44(0.22)	53.50(0.26)	53.74(0.13)
Al_2O_3	0.00(0.00)	29.95(0.39)	3.53(0.18)	4.12(0.24)	15.39(0.09)
Cr_2O_3	0.17(0.05)	45.06(0.30)	1.78(0.21)	2.17(0.26)	0.44(0.05)
MgO	56.68(0.17)	24.36(0.18)	35.63(0.24)	22.95(0.24)	14.75(0.04)
CaO	0.35(0.06)	0.27(0.05)	2.62(0.10)	17.25(0.14)	13.14(0.10)
K_2O	-	-	-	-	2.54(0.08)
Si	1.003(0.003)	0.010(0.002)	1.912(0.006)	1.893(0.008)	
Al	0.000(0.000)	0.983(0.012)	0.141(0.007)	0.172(0.010)	
Cr	0.003(0.001)	0.992(0.008)	0.048(0.006)	0.061(0.007)	
Mg	1.980(0.006)	1.011(0.008)	1.799(0.012)	1.211(0.012)	
Ca	0.009(0.002)	0.008(0.001)	0.095(0.004)	0.654(0.005)	
Total	2.995(0.003)	3.003(0.003)	3.994(0.004)	3.991(0.004)	
C-1449, 1340°C	**Fo(8)**	**Sp(16)**	**Opx(17)**	**Cpx(22)**	**Melt(13)**
SiO_2	42.64(0.23)	0.39(0.11)	56.49(0.20)	53.61(0.24)	53.13(0.16)
Al_2O_3	0.00(0.00)	31.49(0.35)	3.59(0.22)	4.05(0.22)	16.30(0.18)
Cr_2O_3	0.12(0.06)	43.24(0.45)	1.73(0.16)	2.22(0.18)	0.34(0.07)
MgO	56.90(0.28)	24.66(0.15)	35.62(0.30)	22.47(0.34)	13.42(0.28)
CaO	0.34(0.05)	0.22(0.06)	2.57(0.13)	17.66(0.33)	12.55(0.12)
K_2O	-	-	-	-	3.26(0.06)
Si	1.000(0.005)	0.011(0.003)	1.912(0.006)	1.899(0.008)	
Al	0.000(0.000)	1.026(0.010)	0.143(0.009)	0.169(0.009)	
Cr	0.002(0.001)	0.945(0.011)	0.046(0.004)	0.062(0.005)	
Mg	1.989(0.011)	1.016(0.006)	1.797(0.015)	1.186(0.017)	
Ca	0.009(0.001)	0.007(0.002)	0.093(0.005)	0.670(0.013)	
Total	2.999(0.005)	3.004(0.002)	3.993(0.005)	3.986(0.005)	
C-1469, 1330°C	**Fo(8)**	**Sp(13)**	**Opx(17)**	**Cpx(23)**	**Melt(6)**
SiO_2	42.94(0.12)	0.37(0.15)	56.56(0.29)	53.48(0.32)	55.22(0.10)
Al_2O_3	0.17(0.12)	33.24(0.37)	3.48(0.23)	4.33(0.36)	18.45(0.16)
Cr_2O_3	0.01(0.02)	41.38(0.44)	1.77(0.17)	2.19(0.22)	0.33(0.11)
MgO	56.55(0.14)	24.80(0.22)	35.68(0.19)	22.41(0.34)	10.01(0.17)
CaO	0.34(0.07)	0.21(0.09)	2.52(0.18)	17.60(0.40)	11.72(0.28)
K_2O	-	-	-	-	4.26(0.11)
Si	1.005(0.003)	0.010(0.004)	1.915(0.009)	1.893(0.010)	
Al	0.005(0.003)	1.075(0.011)	0.139(0.009)	0.181(0.015)	
Cr	0.000(0.000)	0.898(0.011)	0.047(0.004)	0.061(0.006)	
Mg	1.974(0.005)	1.014(0.008)	1.800(0.010)	1.183(0.017)	
Ca	0.008(0.002)	0.006(0.003)	0.091(0.006)	0.668(0.016)	
Total	2.992(0.002)	3.003(0.003)	3.992(0.005)	3.986(0.005)	
C-1489, 1360°C	**Fo(8)**	**Sp(20)**	**Opx(17)**	**Cpx(19)**	**Melt(15)**
SiO_2	42.83(0.11)	0.44(0.09)	56.92(0.23)	54.54(0.28)	53.20(0.13)
Al_2O_3	0.16(0.07)	23.71(0.31)	2.75(0.24)	3.34(0.20)	13.21(0.12)
Cr_2O_3	0.40(0.05)	51.97(0.42)	1.74(0.14)	2.09(0.16)	0.44(0.07)
MgO	56.26(0.16)	23.54(0.22)	35.61(0.15)	25.53(0.53)	17.61(0.26)
CaO	0.35(0.03)	0.34(0.05)	2.99(0.07)	14.49(0.53)	14.36(0.26)
K_2O	-	-	-	-	1.19(0.05)
Si	1.004(0.002)	0.013(0.002)	1.929(0.007)	1.913(0.007)	
Al	0.004(0.002)	0.799(0.009)	0.110(0.010)	0.138(0.008)	
Cr	0.007(0.001)	1.175(0.011)	0.047(0.004)	0.058(0.005)	
Mg	1.966(0.006)	1.004(0.009)	1.799(0.008)	1.335(0.026)	
Ca	0.009(0.001)	0.011(0.001)	0.108(0.003)	0.545(0.021)	
Total	2.990(0.003)	3.000(0.003)	3.993(0.003)	3.989(0.005)	

Table 3 continued

C-1463, 1350°C	**Fo(6)**	**Sp(14)**	**Opx(19)**	**Cpx(25)**	**Melt(20)**
SiO_2	42.79(0.12)	0.46(0.15)	57.10(0.38)	54.57(0.35)	54.92(0.15)
Al_2O_3	0.00(0.00)	21.96(0.41)	2.29(0.23)	2.75(0.29)	13.79(0.13)
Cr_2O_3	0.25(0.17)	53.87(0.40)	1.82(0.30)	2.20(0.32)	0.30(0.07)
MgO	56.61(0.14)	23.35(0.20)	35.95(0.24)	23.92(0.33)	15.16(0.12)
CaO	0.35(0.04)	0.37(0.06)	2.85(0.14)	16.56(0.39)	12.85(0.10)
K_2O	-	-	-	-	2.97(0.09)
Si	1.008(0.004)	0.013(0.004)	1.938(0.010)	1.928(0.010)	
Al	0.000(0.000)	0.746(0.013)	0.092(0.010)	0.115(0.012)	
Cr	0.003(0.005)	1.227(0.011)	0.049(0.008)	0.062(0.008)	
Mg	1.987(0.005)	1.003(0.008)	1.817(0.012)	1.259(0.017)	
Ca	0.010(0.000)	0.011(0.002)	0.103(0.005)	0.627(0.015)	
Total	3.008(0.004)	3.000(0.003)	4.001(0.008)	3.991(0.010)	
C-1476, 1330°C	**Fo(7)**	**Sp(13)**	**Opx(16)**	**Cpx(22)**	**Melt(11)**
SiO_2	42.92(0.20)	0.51(0.18)	57.16(0.35)	54.05(0.47)	55.20(0.20)
Al_2O_3	0.00(0.00)	27.29(0.50)	2.68(0.33)	3.38(0.51)	16.06(0.20)
Cr_2O_3	0.17(0.06)	47.93(0.55)	1.52(0.19)	2.09(0.22)	0.18(0.07)
MgO	56.55(0.15)	23.93(0.15)	35.80(0.28)	23.29(0.39)	12.53(0.15)
CaO	0.36(0.03)	0.34(0.10)	2.84(0.28)	17.19(0.47)	10.92(0.17)
K_2O	-	-	-	-	5.11(0.09)
Si	1.009(0.007)	0.014(0.005)	1.935(0.010)	1.911(0.015)	
Al	0.000(0.000)	0.905(0.015)	0.107(0.013)	0.141(0.021)	
Cr	0.000(0.000)	1.066(0.014)	0.041(0.005)	0.059(0.006)	
Mg	1.980(0.008)	1.004(0.005)	1.806(0.013)	1.228(0.019)	
Ca	0.010(0.000)	0.010(0.003)	0.103(0.010)	0.651(0.019)	
Total	2.999(0.004)	3.000(0.002)	3.991(0.004)	3.989(0.005)	
C-1516, 1380°C	**Fo(12)**	**Sp(18)**	**Opx(16)**	**Cpx(16)**	**Melt(15)**
SiO_2	42.83(0.12)	0.44(0.12)	57.94(0.28)	56.62(0.16)	54.80(0.18)
Al_2O_3	0.16(0.05)	13.74(0.22)	1.56(0.25)	1.73(0.10)	10.23(0.17)
Cr_2O_3	0.40(0.08)	63.14(0.29)	1.27(0.19)	1.61(0.10)	0.59(0.09)
MgO	56.23(0.16)	22.31(0.15)	36.10(0.22)	30.73(0.39)	18.15(0.25)
CaO	0.39(0.04)	0.37(0.07)	3.12(0.10)	9.31(0.32)	14.15(0.16)
K_2O	-	-	-	-	2.08(0.04)
Si	1.004(0.003)	0.013(0.004)	1.961(0.018)	1.953(0.004)	
Al	0.004(0.001)	0.484(0.007)	0.062(0.010)	0.070(0.004)	
Cr	0.007(0.001)	1.494(0.008)	0.034(0.005)	0.044(0.003)	
Mg	1.965(0.006)	0.995(0.006)	1.821(0.011)	1.580(0.019)	
Ca	0.010(0.001)	0.012(0.002)	0.113(0.004)	0.344(0.012)	
Total	2.990(0.003)	2.998(0.002)	3.991(0.003)	3.990(0.005)	
C-1512, 1370°C	**Fo(8)**	**Sp(20)**	**Opx(19)**	**Cpx(14)**	**Melt(14)**
SiO_2	42.77(0.11)	0.44(0.12)	57.75(0.24)	55.74(0.24)	54.99(0.10)
Al_2O_3	0.00(0.00)	16.58(0.24)	1.77(0.19)	2.15(0.24)	11.74(0.17)
Cr_2O_3	0.34(0.10)	60.38(0.26)	1.37(0.15)	1.80(0.17)	0.41(0.11)
MgO	56.50(0.18)	22.25(0.14)	36.11(0.16)	27.68(0.38)	16.49(0.12)
CaO	0.39(0.06)	0.35(0.08)	3.00(0.07)	12.63(0.38)	13.34(0.21)
K_2O	-	-	-	-	3.02(0.05)
Si	1.009(0.004)	0.013(0.004)	1.954(0.007)	1.942(0.007)	
Al	0.000(0.000)	0.579(0.007)	0.071(0.008)	0.088(0.010)	
Cr	0.008(0.005)	1.414(0.008)	0.037(0.004)	0.050(0.005)	
Mg	1.983(0.007)	0.982(0.006)	1.822(0.008)	1.438(0.019)	
Ca	0.010(0.000)	0.011(0.002)	0.109(0.002)	0.471(0.015)	
Total	3.009(0.008)	2.998(0.007)	3.992(0.003)	3.989(0.005)	
C-1515, 1360°C	**Fo(8)**	**Sp(17)**	**Opx(16)**	**Cpx(12)**	**Melt(15)**
SiO_2	41.69(0.16)	0.71(0.19)	56.96(0.32)	54.88(0.32)	55.34(0.14)
Al_2O_3	0.00(0.00)	19.79(0.59)	1.30(0.30)	2.31(0.36)	12.93(0.12)
Cr_2O_3	0.44(0.06)	55.32(0.59)	1.45(0.23)	1.98(0.31)	0.32(0.08)
MgO	57.52(0.16)	23.82(0.17)	37.43(0.34)	26.48(0.27)	15.18(0.10)
CaO	0.35(0.06)	0.37(0.07)	2.86(0.35)	14.36(0.40)	12.23(0.11)
K_2O	-	-	-	-	4.01(0.06)
Si	0.985(0.005)	0.020(0.006)	1.935(0.012)	1.928(0.011)	
Al	0.000(0.000)	0.678(0.020)	0.051(0.012)	0.096(0.015)	
Cr	0.010(0.000)	1.272(0.016)	0.039(0.008)	0.055(0.009)	
Mg	2.025(0.008)	1.033(0.008)	1.896(0.015)	1.387(0.012)	
Ca	0.010(0.000)	0.011(0.002)	0.104(0.014)	0.540(0.015)	
Total	3.030(0.008)	3.013(0.007)	4.026(0.009)	4.005(0.008)	

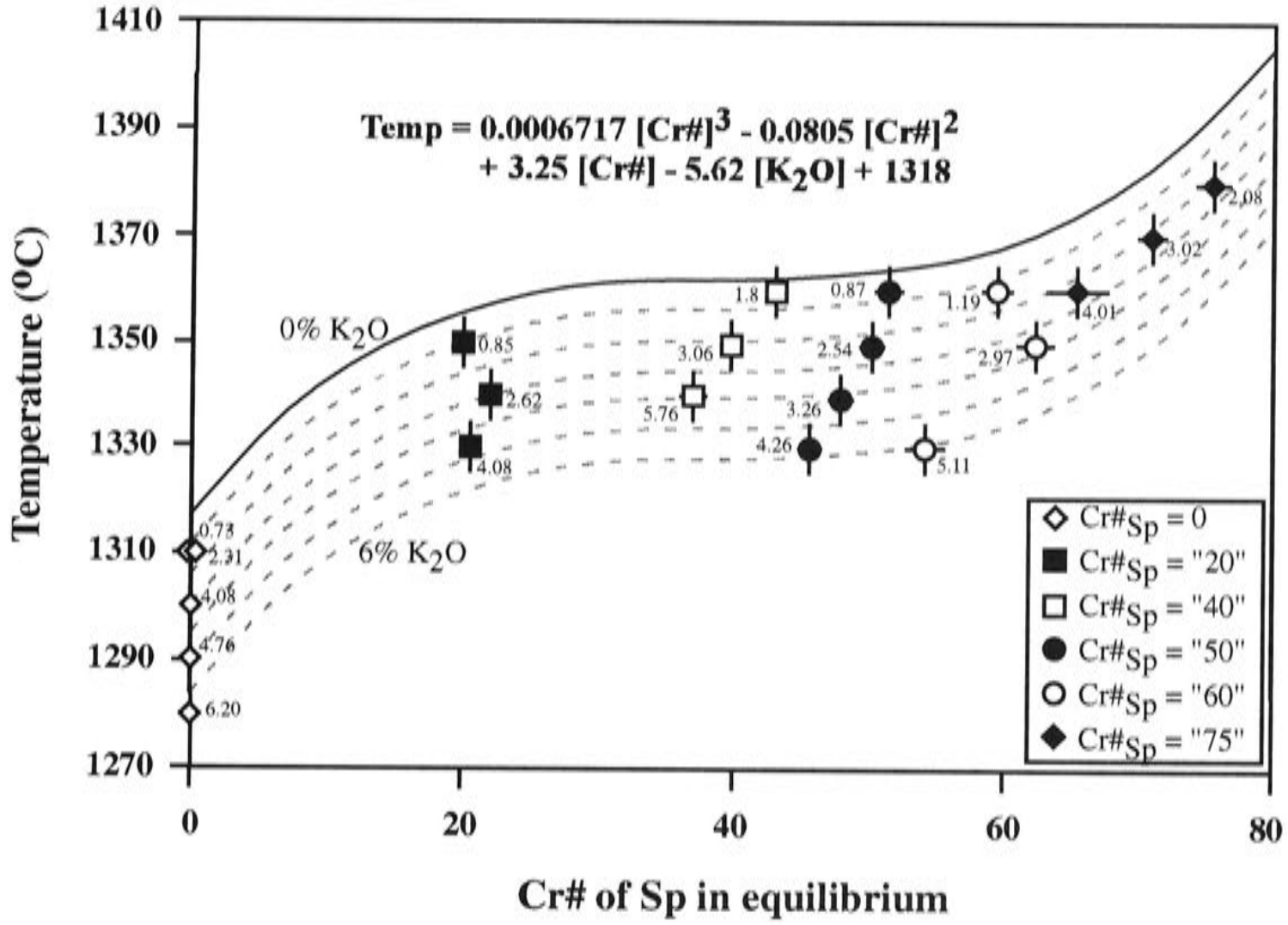

Fig. 8 The Cr_2O_3 effect on partial melting temperature. Numbers in the figure are the K_2O content in the experimentally observed melts. Curves indicated by the K_2O content are from the regression (Equ. 7). An uncertainty of five degrees (one standard deviation) for the experimental temperature measurement is used in the regression.

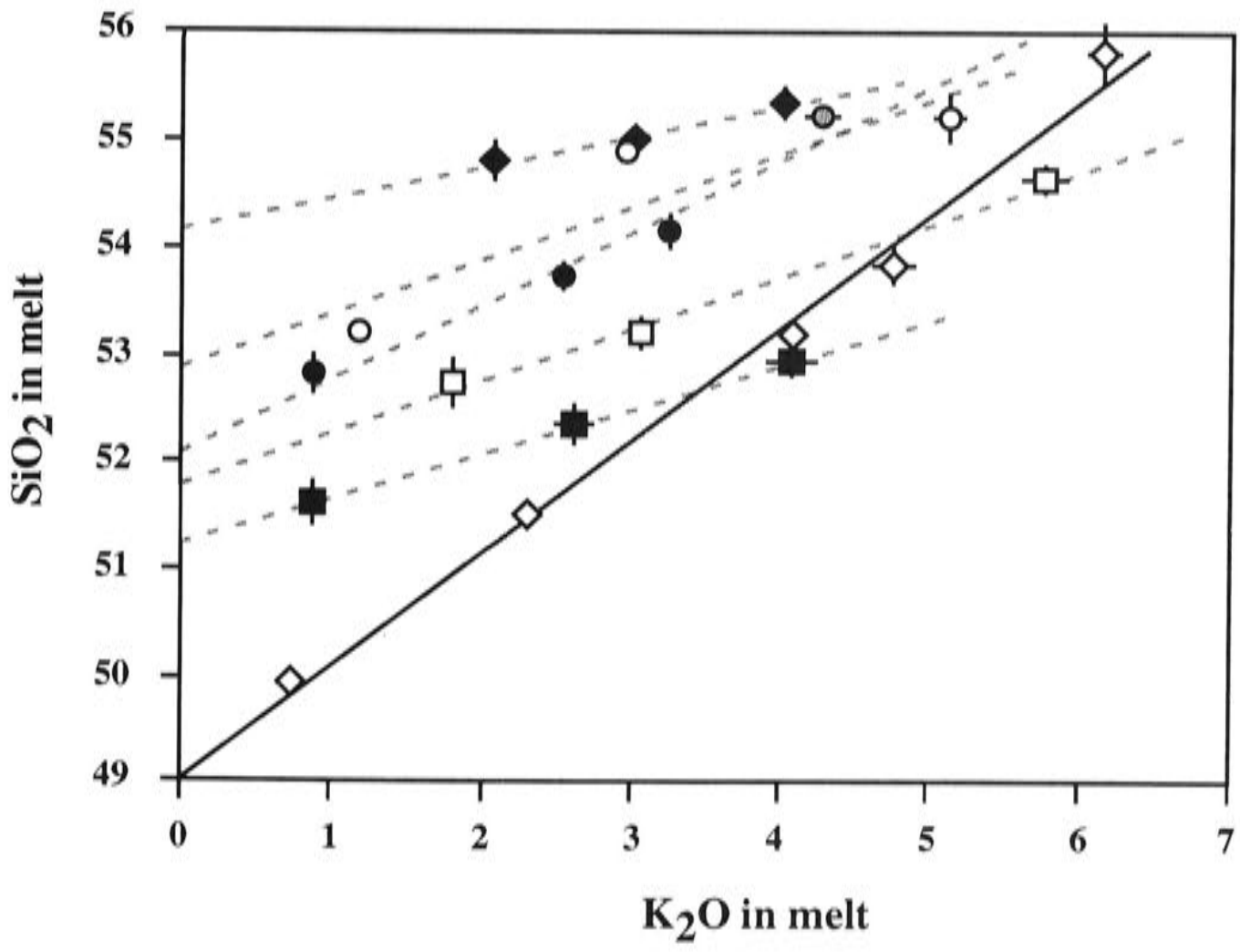

Fig. 9 Correlation of SiO_2 and K_2O of melts both in the system CMAS+K_2O (thick solid line) and in the system CMASCr+K_2O (thin broken lines). Raw experimental data are used. Lines are drawn by least-squares regression. Symbols are the same as those in Fig. 8, with the exception that Run C-1469 with a K_2O content of 4.26% is shown in grey.

$$[Al_2O_3] = 25.9 + 0.62\,[K_2O] - 0.535\,Cr\#_{sp} - 9.41x10^{-3}\,(Cr\#_{sp})^2 + 7.09x10^{-5}\,(Cr\#_{sp})^3 \quad (9)$$

$$[MgO] = 6.8 - 1.84\,[K_2O] + 0.685\,Cr\#_{sp} - 1.42x10^{-2}\,(Cr\#_{sp})^2 + 9.84x10^{-5}\,(Cr\#_{sp})^3 + 1.39x10^{-2}\,[K_2O]Cr\#_{sp} \quad (10)$$

and

$$[CaO] = 14.8 - 0.86\,[K_2O] + 0.012\,Cr\#_{sp} \quad (11)$$

These entirely empirical equations then allow the melt composition in CMAS-Cr_2O_3 to be calculated as a function of $Cr\#_{sp}$. The average difference between the calculated melt composition using these equations and the experimentally observed melt composition is 0.23 wt% for SiO_2, 0.31 wt% for Al_2O_3, 0.32 wt% for MgO and 0.13 wt% for CaO.

The regressed melt compositions are shown in Figs. 10a to 10d. With Cr_2O_3 addition into the system CMAS, the SiO_2 content of melt increases from 49.1 wt% ($Cr\#_{Sp}$ = 0) to 54.7 wt% ($Cr\#_{Sp}$ = 80), the MgO content from 15.45 wt% to 21.4 wt% and the CaO content from 15.33 wt% to 16.0 wt% while the Al_2O_3 content decreases from 20.12 wt% to 7.1 wt%.

Melt compositions in the system CMAS-Cr_2O_3 derived from the experiments in the system CMAS-Cr_2O_3-K_2O by equations 8 to 11 are projected from Ol onto the plane Di-JdCaTsLc-Qz (Fig. 11a) and from Di onto the plane Ol-JdCaTsLc-Qz (Fig. 11b). To handle Cr in these plots, the Cr_2O_3 contents of the melts were subtracted and other oxides were renormalised to 100 wt% (An alternative procedure would be to subtract a $Mg_2Cr_2O_4$ component as this would be an early crystallizing phase. Doing this would make the melts slightly more Qz normative, from 0.17 mol% at $Cr\#_{sp}$=20 to 0.96 mol% at $Cr\#_{sp}$=80).

The most striking features about the melt in the system CMASCr are the increasing Di component (Fig.11a), the increasing Hy component and the generally quartz-normative nature (Fig. 11b) at 11 kbar.

The isobarically invariant melt produced by the Sp-lherzolite assemblage in the system CMAS is an olivine-normative tholeiite (Presnall et al., 1979; Walter & Presnall,

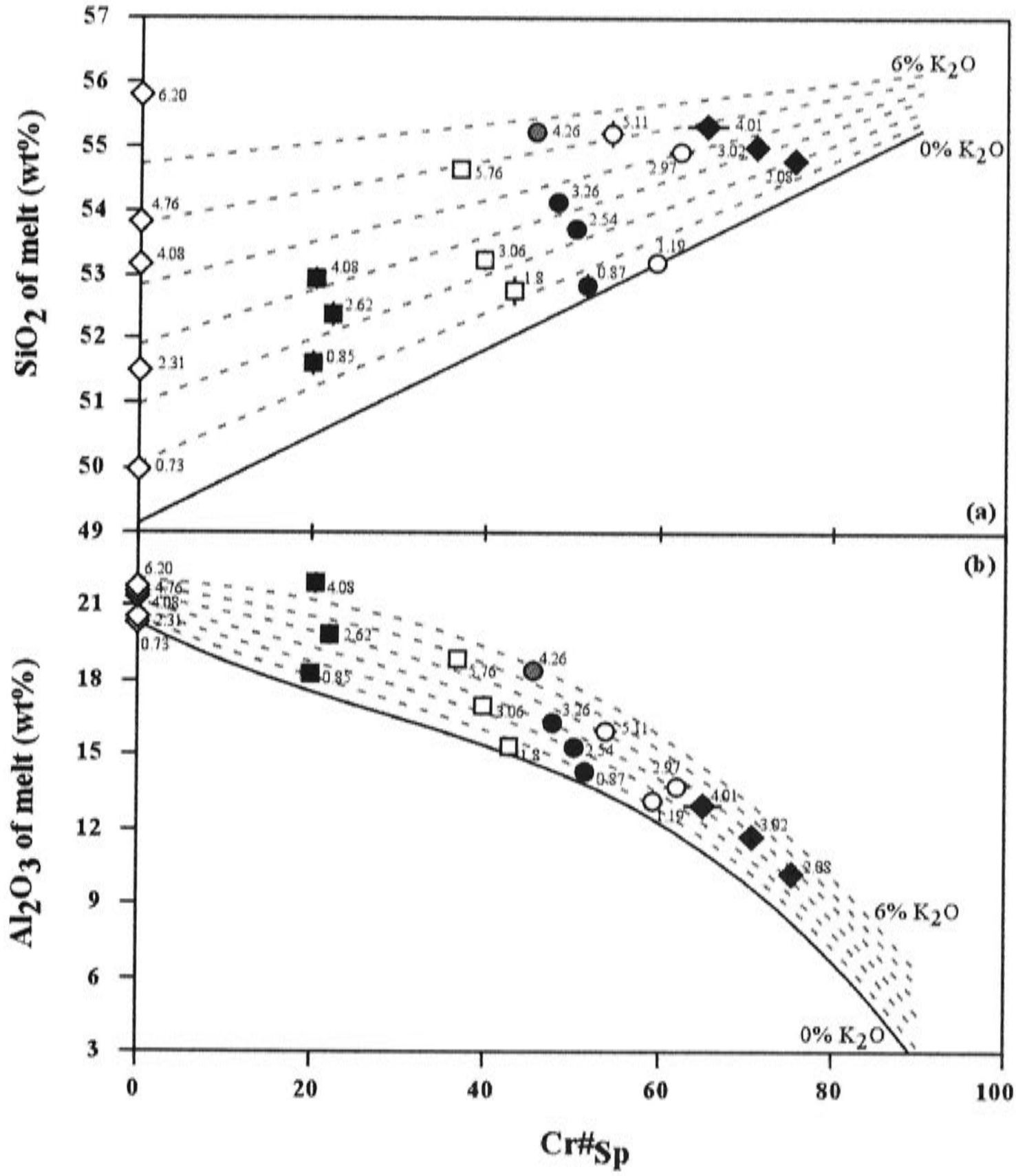

Fig. 10 The Cr_2O_3 effect on melt composition: (a) SiO_2, (b) Al_2O_3, (c) MgO and (d) CaO. Symbols are the same as those in Fig. 9. Run C-1469 with a K_2O content of 4.26%, which does not fit in the regression (see text), is shown in grey. Curves are drawn according to the following procedure: 1. Calculate melt compositions with certain K_2O content (from 0% to 6%) at $Cr\#_{sp} \geq 20$ using Equation 8 to Equation 11 in the text; 2. Calculate melt compositions with certain K_2O content (from 0% to 6%) at $Cr\#_{sp} = 0$ using the regression result in the system CMAS+K_2O from Chapter 2 of this thesis; 3. Regress these calculated melt compositions to draw the curves.

1994; Chapter 2 of this thesis). However, the melt composition reaches the join An-Hy and becomes Qz-normative at $Cr\#_{sp} = 20$. As Cr_2O_3 is added to the system, the Al_2O_3 content of melt drops sharply, so that the An component of the melt decreases. The effect of less An component, coupled with the almost negligible effect of Cr_2O_3 on the CaO content of the melt (Equation 11), means that more CaO is available to form Di.

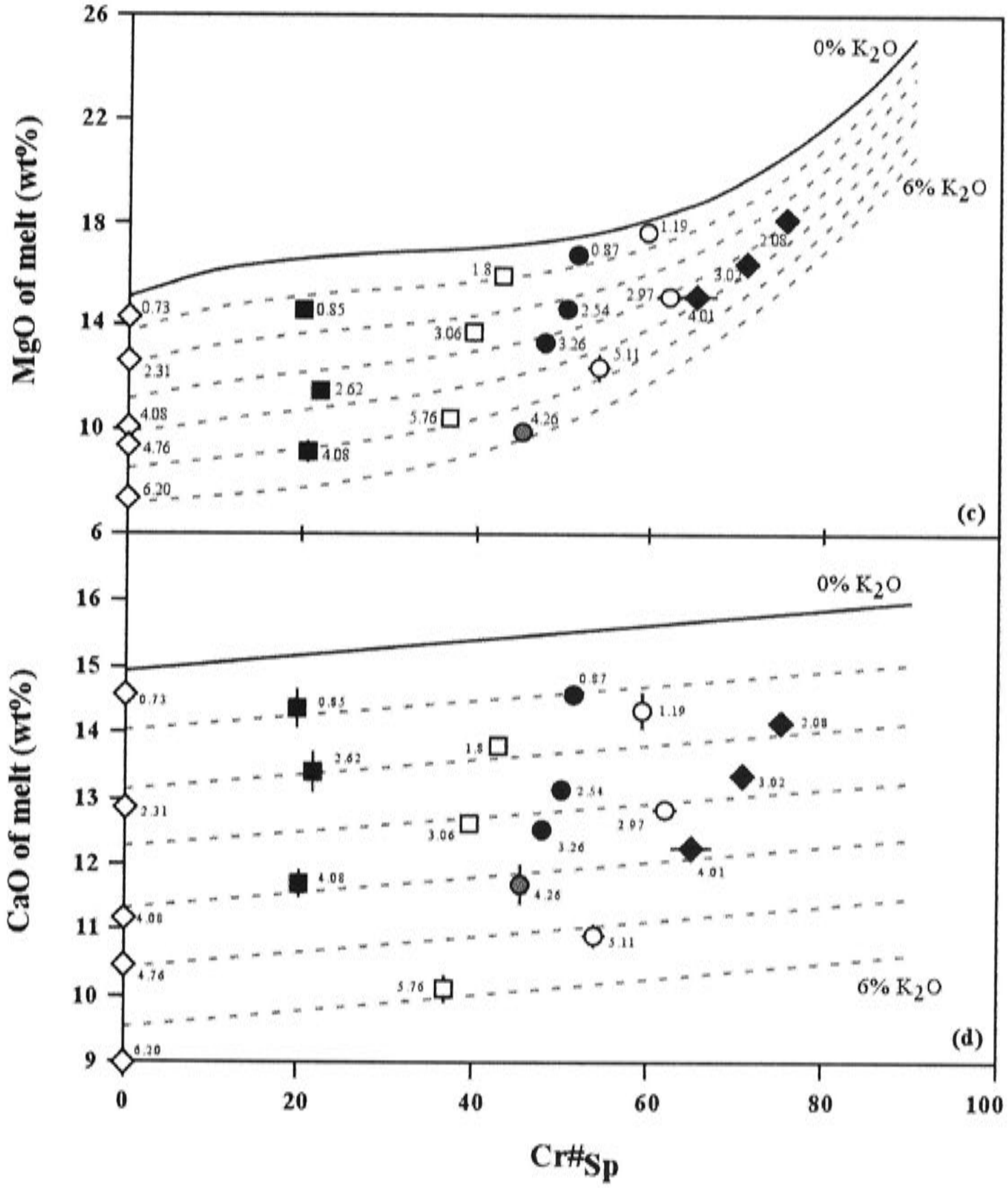

Fig. 10 continued.

An increase in Di component in turn requires more MgO, but this is more than compensated for by the effect that Cr_2O_3 has on increasing MgO (Equation 10). The net result is an increase in the Hy + Ol or Qz components of the melt. An interesting point is that for $Cr\#_{sp} \geq 20$, the extra MgO and SiO_2 is approximately in the proportion of 1:1, so that the melt composition changes along a line virtually co-incident with the An-Hy join.

4.2 Fo compositions

Forsterite has near-endmember composition. The amount of Cr_2O_3 increases with $Cr\#_{sp}$, reaching 0.4 wt% at $Cr\#_{sp}$=60 (Fig. 12a). The CaO, however, is very constant, with a content of 0.35 ± 0.05 (Fig. 12b). Note that Fo in my preliminary

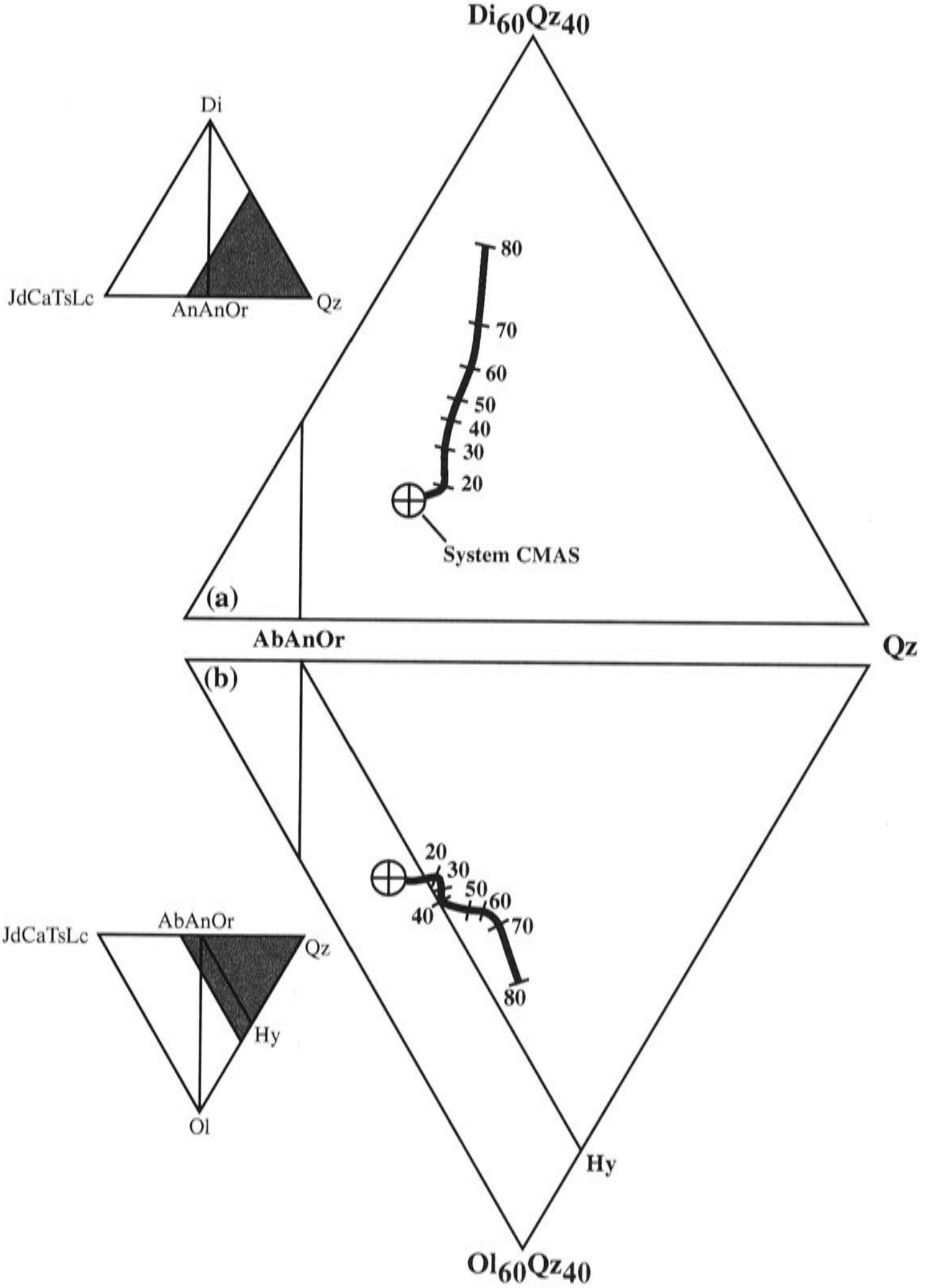

Fig. 11 Multiply-saturated melt compositions (Fo+Sp+Opx+Cpx+Melt) in the CMAS-Cr_2O_3 system projected from Ol onto the plane Di-JdCaTsLc-Qz (a) and from Di onto the plane JdCaTsLc-Qz-Ol (b). The projecting procedure of Falloon & Green (1988) is followed in this study. The melt composition in the system CMAS is from Chapter 2 of this thesis. Regressed melt compositions calculated using Equation 8 to Equation 11 are used. The Cr_2O_3 content is simply removed as Cr_2O_3 and melt composition is renormalised to 100%. Numbers in the diagram refer to $Cr\#_{sp}$ in equilibrium.

unbuffered experiments without Fe_2O_3 sleeves generally had higher Cr contents (up to ~ 0.8 wt% Cr_2O_3 at $Cr\#_{sp}$=60), indicative of Cr^{2+}.

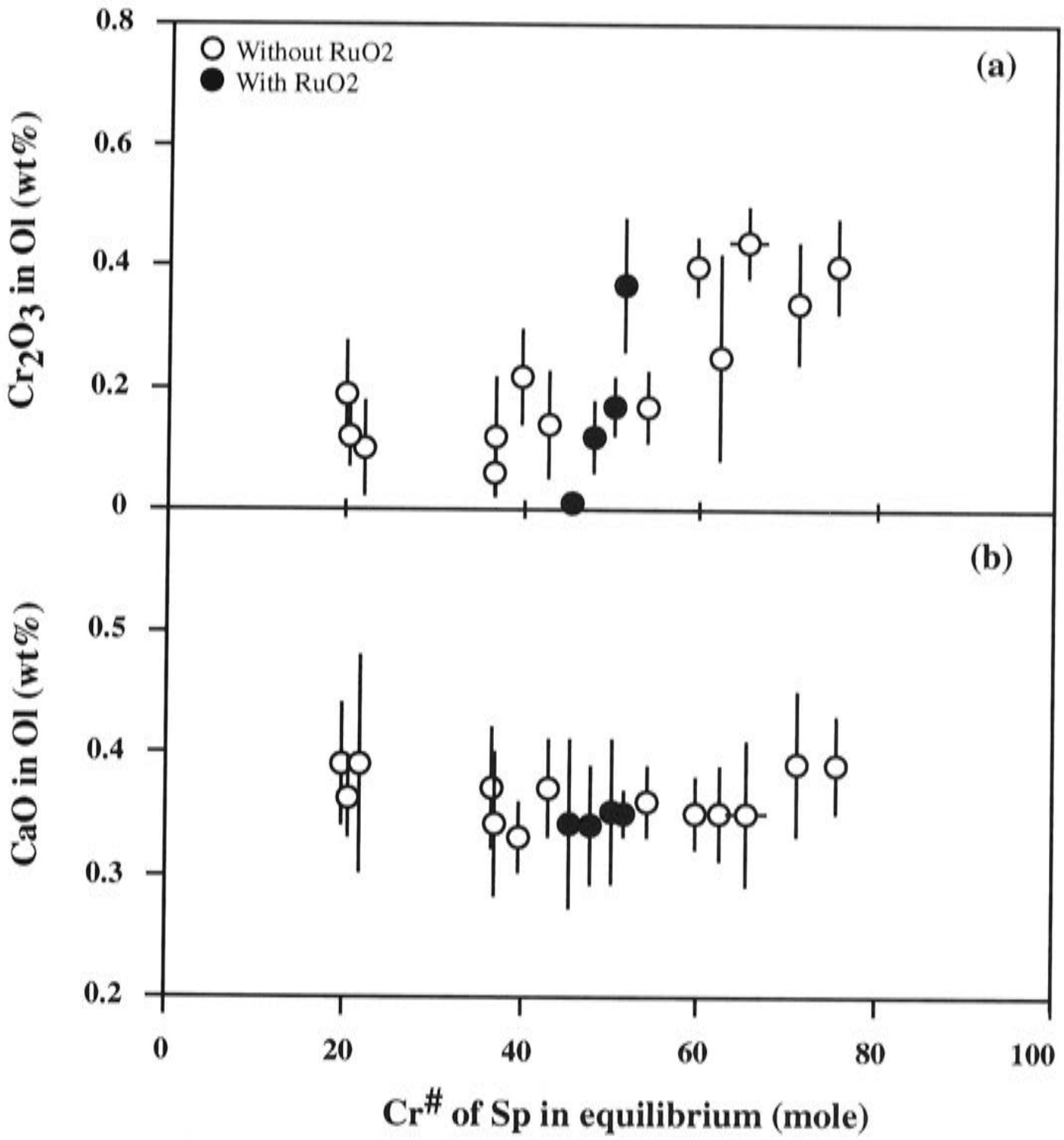

Fig. 12 The Cr_2O_3 content and the CaO content in the olivine.

4.3 Sp composition

The spinel in the system CMASCr (± K_2O) is a simple binary solid solution between $MgAl_2O_4$ and $MgCr_2O_4$. The electron probe analyses return small and variable amounts of SiO_2 and CaO, which may be spurious, caused by the generally small size of spinel crystals (typically 3-15 μm in diameter).

4.4 Pyroxene compositions

Al_2O_3 and Cr_2O_3

The relationship of Cr and Al in orthopyroxene observed in this study is shown in Fig. 14. For comparison, the data in system MASCr at subsolidus conditions from Klemme & O'Neill (2000) are shown as well.

The relationship between Cr and Al in Opx is not a mere substitution of one by the other. When Cr is added to the system, the Al content in Opx first decreases with

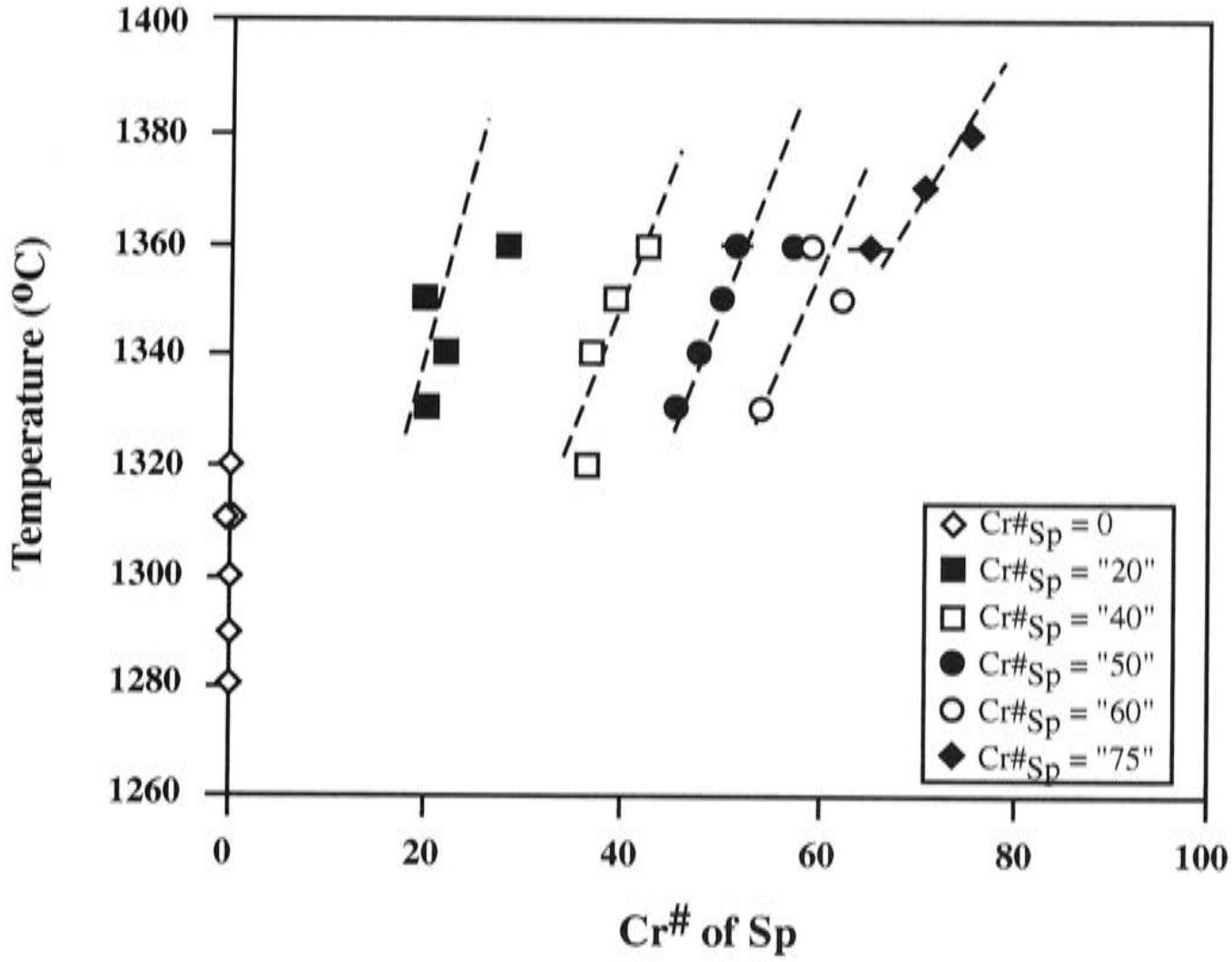

Fig. 13 Relationship between the temperature and the $Cr^{\#}$ (100*Cr/(Cr+Al)) of Sp. All experiments but D-81 are shown.

increasing Cr but then decreases. This behaviour was previously observed by Nagata et al. (1983) and Witt-Eickschen & Seck (1991) in natural peridotites.

The data of Klemme & O'Neill (2000) agrees with my data very well and defines a similar relationship for Cr and Al in Opx. Furthermore, both studies suggest that molar Al in Opx is higher than Cr, except, according to Klemme & O'Neill (2000), at very high $Cr\#_{sp}$. The relationship between Al and Cr in Cpx shown in Fig. 15 is similar.

It follows that the partitioning of Al^{3+} and Cr^{3+} between Opx and Cpx should also be similar. This is demonstrated in Fig. 16a, where all experimental data plot close to the 1:1 line.

Most experimental data from the literature at near-solidus temperatures (which are all in complex multicomponent systems) plot close to the 1:1 line, albeit with more scatter (Fig. 16b). The experiments in Falloon & Green (1987) at 10 kbar, however, define an almost horizontal line, suggesting that the Cr/Al ratio in Cpx does not change with that ratio in Opx. Possibly this difference is due to the short experimental duration (< 24 hours in most cases) which may be long enough to make some compositional change in the Opx, but too short to make any composition change in the Cpx. This would be quite similar to the observation in this study, in which Cpx in the sandwiched

layer in many of the low partial melting experiments is zoned in Cr/Al, whereas Opx is homogenous.

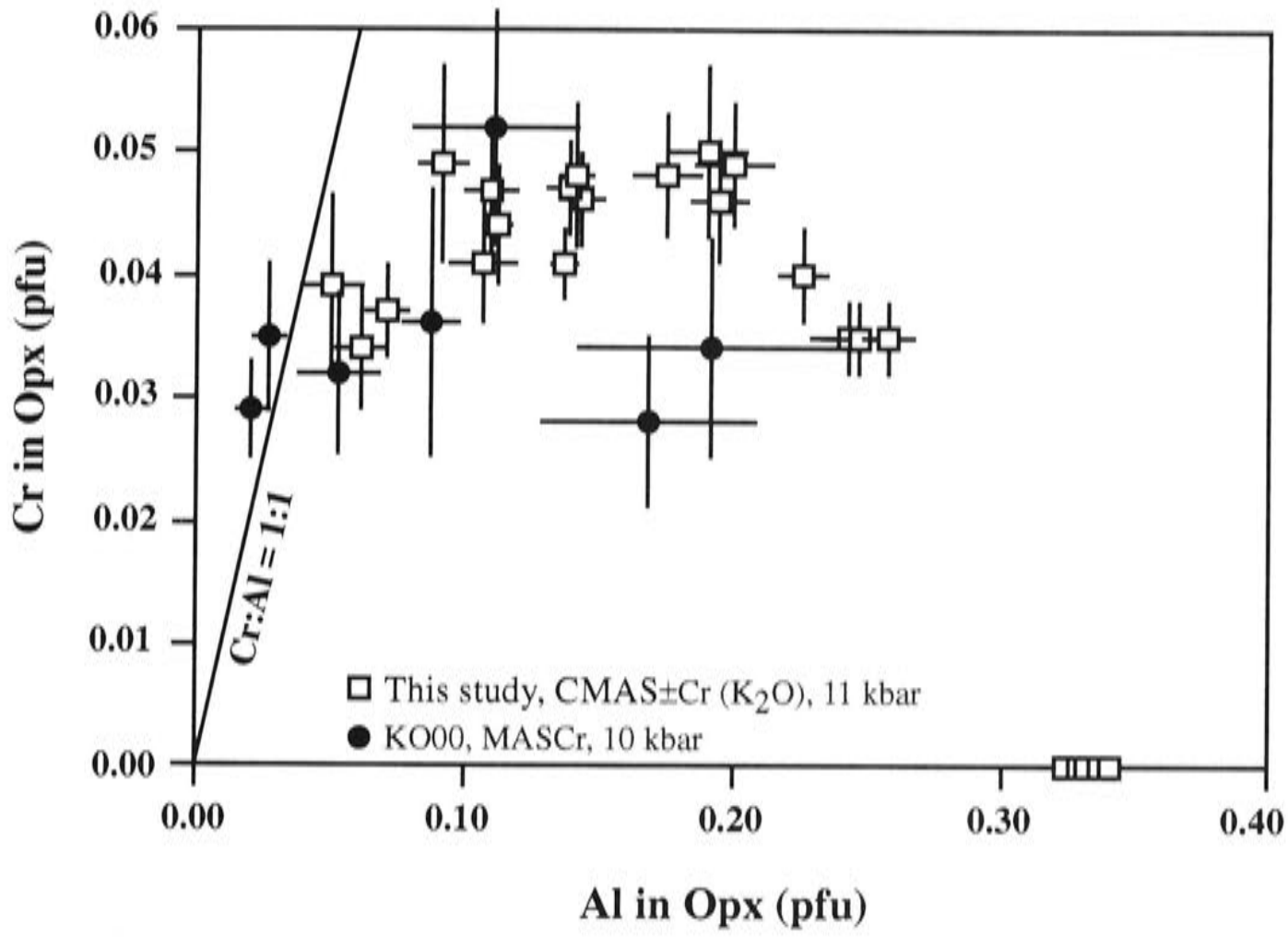

Fig. 14 Covariation of Cr and Al in Opx. KO00, Klemme & O'Neill (2000); pfu, per formula unit of six oxygens. All chromium has been assumed to be Cr^{3+}.

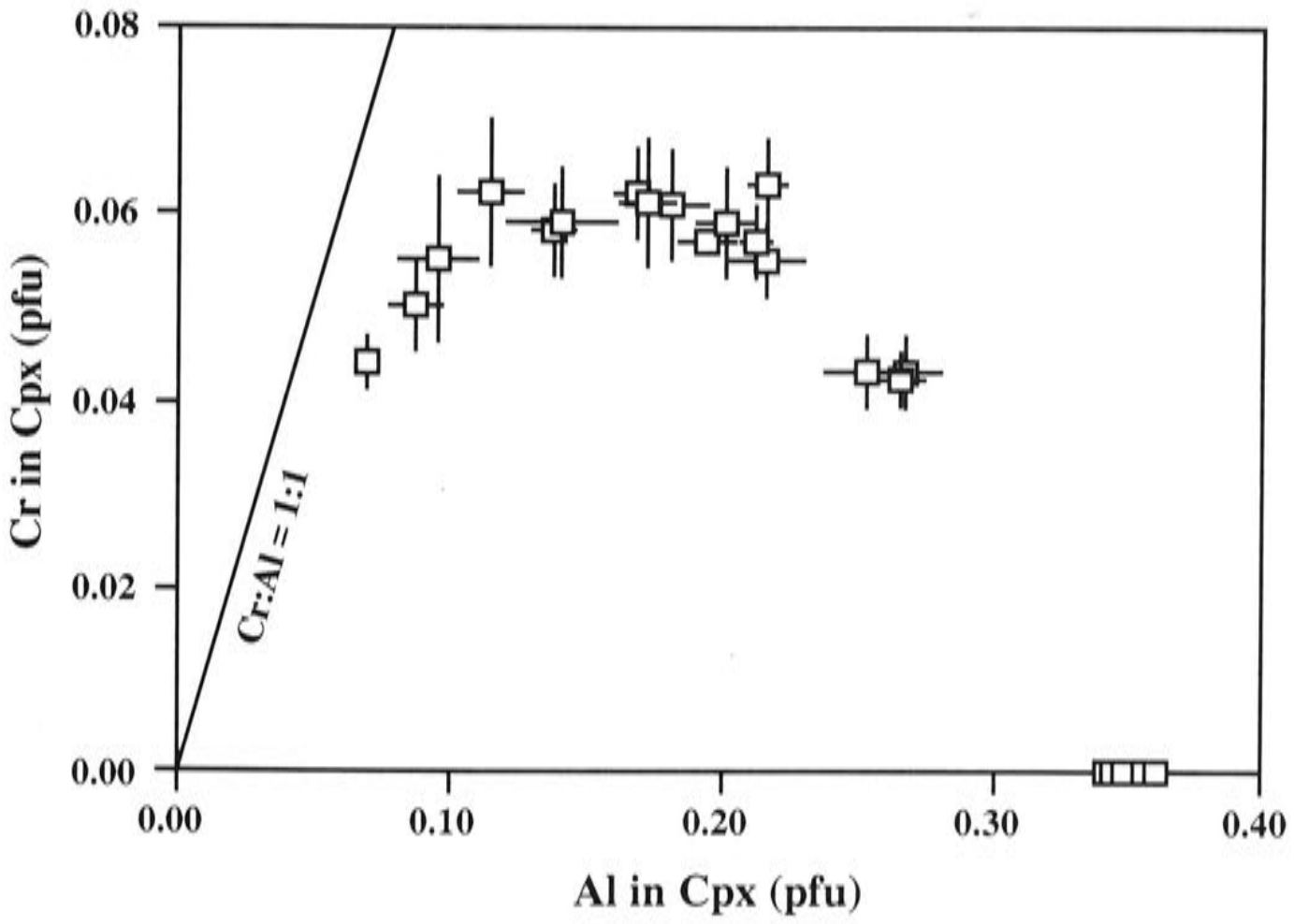

Fig. 15 Covariation of Cr and Al in Cpx. pfu, per formula unit of six oxygens. All chromium has been assumed to be Cr^{3+}.

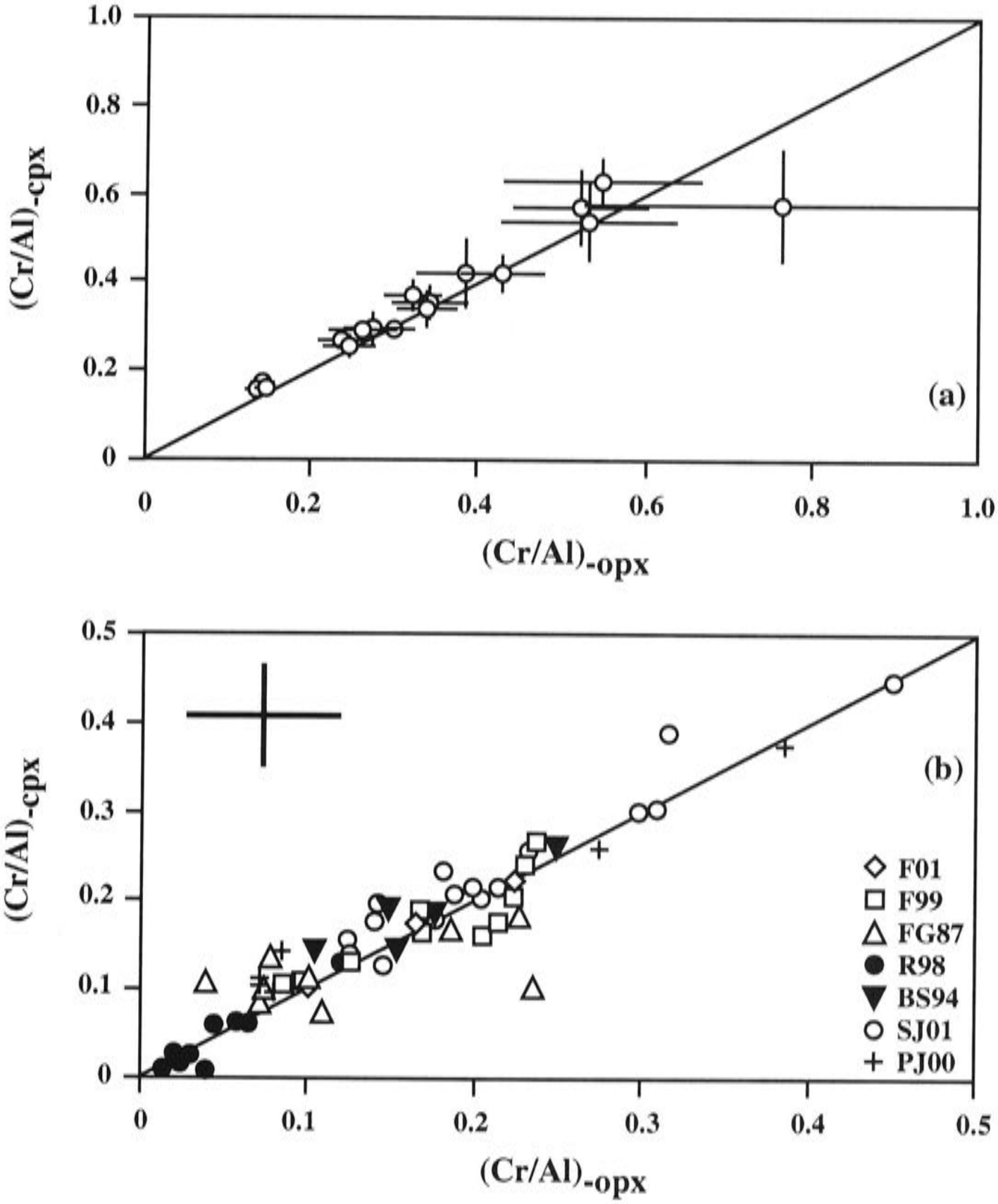

Fig. 16 Cr^{3+} and Al partitioning between Opx and Cpx observed in this study (a) and in literature studies (b; complex compositions used). The average of the one standard deviations (a) observed in our study is plotted in (b) to facilitate the data comparison. F01, Falloon et al., 2001; F99, Falloon et al., 1999; FG87, Falloon & Green, 1987 (we use the revised data by Falloon et al., 2001); R98, Robinson et al., 1998; BS94, Baker & Stolper, 1994; SJ01, Schwab & Johnston, 2001; PJ00, Pichering & Johnston, 2000. The pressure in all studies except Robinson et al. (1998; 15 kbar) and this study (11 kbar) is 10 kbar. Only experiments displaying melt plus a Sp-lherzolite phase assemblage are shown.

CaO and MgO

The exchange of Ca and Mg between Opx and Cpx is the basis of the two-pyroxene geothermometer, the main means of estimating temperatures of equilibration in lherzolitic assemblages. Previous experimental studies have mostly been at relatively low temperatures (Gasparik, 1984; Sen, 1985; Nickel et al., 1985; Brey et al, 1990) or in very simple chemical systems (Mori & Green, 1976; Lindsley & Dixon, 1976; Nickel & Brey, 1984). The experimental observations here offer an opportunity to evaluate the

CaO equilibrium at relatively high temperatures and in a chemical system of intermediate complexity.

Pyroxene phase relationships in the system CMS and CMAS at 11 to 15 kbar are shown in Fig. 17a. Data in the system CMAS are from assemblages saturated in Fo+Sp, and therefore have the maximum amount of dissolved alumina. The Ca/(Ca+Mg) ratio of Opx is almost independent of pressure and alumina content, but strongly dependent on temperature. The Ca/(Ca+Mg) ratio of Cpx is also almost independent of pressure, as illustrated by the data of Gasparik (1984); it, however, depends on both temperature and alumina. The presence of Al_2O_3 increases Ca/(Ca+Mg) in Cpx.

The geometry of the phase relations between Opx and Cpx is greatly influenced by the solvus that exists (mostly metastably) between low Ca Cpx and high Ca Cpx. The solidus of the Fo+Opx+Cpx+Sp assemblage in the system CMAS at 11 kbar is ~ 1320°C (Chapter 2 of this thesis), which is much lower than the crest of the solvus in CMS (~ 1450°C, from Fig. 5 of Nickel & Brey, 1984), and also lower than the temperature at which low Ca Cpx becomes stable (~ 1360°C). Thus in CMAS saturated with Fo+Sp only Opx and high Ca Cpx exist stably. There are no experimental data in the literature that can be used to define phase relationships at 11 kbar at temperatures >1320°C, except those in the pure CMS system. However, adding Cr_2O_3 to CMAS raises the solidus, permitting access to this temperature region, albeit at lower Al_2O_3 contents.

Our experimental data are plotted in Fig. 17b. It appears that the addition of Al_2O_3 and Cr_2O_3 into the system CMS must lower the crest of the Cpx solvus, such that the Cpx compositions in the highest temperature experiments are decidedly subcalcic. The phase relationship is hence drawn as shown in Fig. 17b.

This geometry is similar to the phase relationship observed at higher pressures (> ~18 kbar) in the system CMS (Mori & Green, 1976; Nickel & Brey, 1984; Longhi & Bertka, 1996). Partial melting studies using natural lherzolite compositions (Takahashi & Kushiro, 1983; Falloon & Green, 1988 and unpublished data) suggested that this solvus becomes metastable at a pressure between 15 and 18 kbar.

Experiments with variable Cpx compositions display a remarkably tight correlation between Ca/(Ca+Mg) and Cr/(Cr+Al) (Fig. 6). The increase of Ca with Al in Cpx is similar to the difference observed in Cpx compositions in equilibrium with Opx between the systems CMS and CMAS, as shown in Fig. 17a. I therefore interpret these correlations to be due to initial differences in Cr/(Cr+Al) in Cpx being preserved due to

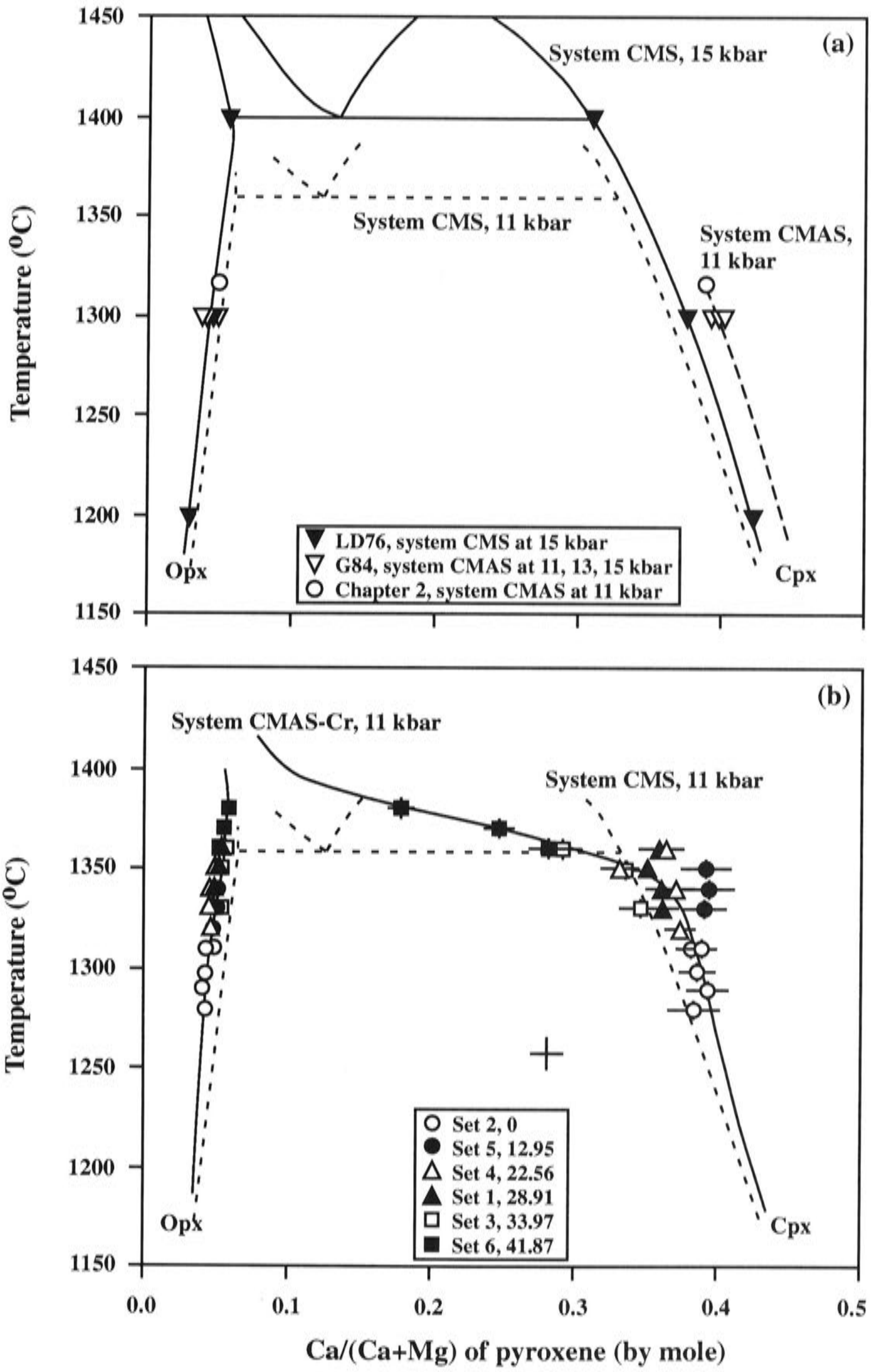

Fig. 17 Calcium partitioning between Opx and Cpx: (a) sketchy phase relationship of system CMS and system CMAS, and (b) sketchy phase relationship of system CMASCr. For clearance, the line for the CaO content in Opx in the system CMAS at 11 kbar is omitted in (a). Big cross in (b) approximates the ratio of Cpx component and Opx component in the bulk compositions used in this study. The initial ratio of Cpx to Opx in the starting materials SEM02-1, SEM05-1, SEM04-1, SEM01-1, SEM03-1 and SEM06-1 is 1:1 (see Table 1). With the addition of melt which should contain more Cpx component than Opx component, the ratio of Cpx to Opx in our experiments should be larger than 1:1. LD76, Lindsley & Dixon (1976); G84, Gasparik (1984). The 100*Cr/(Cr+Al) of the bulk compositions for every experiment set follows the name of the experiment set.

sluggish diffusion rates for Cr and Al, with Ca and Mg adjusting to the local Cr/(Cr+Al) ratio to maintain metastable equilibrium with Opx.

4.5 Geothermometry

Ca ± Mg-in-pyroxene geothermometer

The geothermometer of Nickel et al. (1985) was constructed from data at relatively low temperatures in the system CMAS and it returns temperatures in good agreement with experimental temperatures for the lower temperature experiments (< 1350°C) (Fig. 18a). As might be expected, it does not give such good agreement with the high temperature experiments (i.e. high Cr_2O_3 content), in which the Cpx becomes subcalcic.

The Opx-Cpx geothermometer (Equation 9 of Brey & Kohler, 1990) and the Ca-in-Opx geothermometer (Equation 10 of Brey & Kohler, 1990) were constructed mostly from data obtained at relatively low temperatures, including data from natural lherzolite compositions. The Opx-Cpx geothermometer generally returns higher calculated temperatures while the Ca-in-Opx geothermometer generally returns lower temperatures (Fig. 18b, 18c).

In order to see if the performance of these geothermometers depends systematically on composition, I plot the difference between the calculated temperature and the nominal temperature against the Cr# of the Sp in Figs. 18d to 18f. It is apparent from these diagrams that there is indeed a systematic effect, suggesting that further fine-tuning of these geothermometers would be profitable.

Al_2O_3-in-Opx geothermometer

The solubility of Al_2O_3 in Opx in equilibrium with Fo+Sp is another temperature-sensitive equilibrium that has been used as a geothermometer. The latest version was calibrated against the Ca-in-Opx geothermometer of Brey & Kohler (1990) by Witt-Eickschen & Seck (1991). My experimental data in the system CMASCr (± K_2O) plus some data from Klemme & O'Neill (2000) are plotted in Fig. 19.

The calculated temperature by the geothermometer of Witt-Eickschen & Seck is based on one of the following cation distribution models: 1) all Cr on M_1 site of Opx and 2) half Cr on M_1 site of Opx (Klemme & O'Neill, 2000). The average differences between the calculated temperature using this geothermometer and the experimental temperature are ~ 144 degrees for the former cation distribution model and

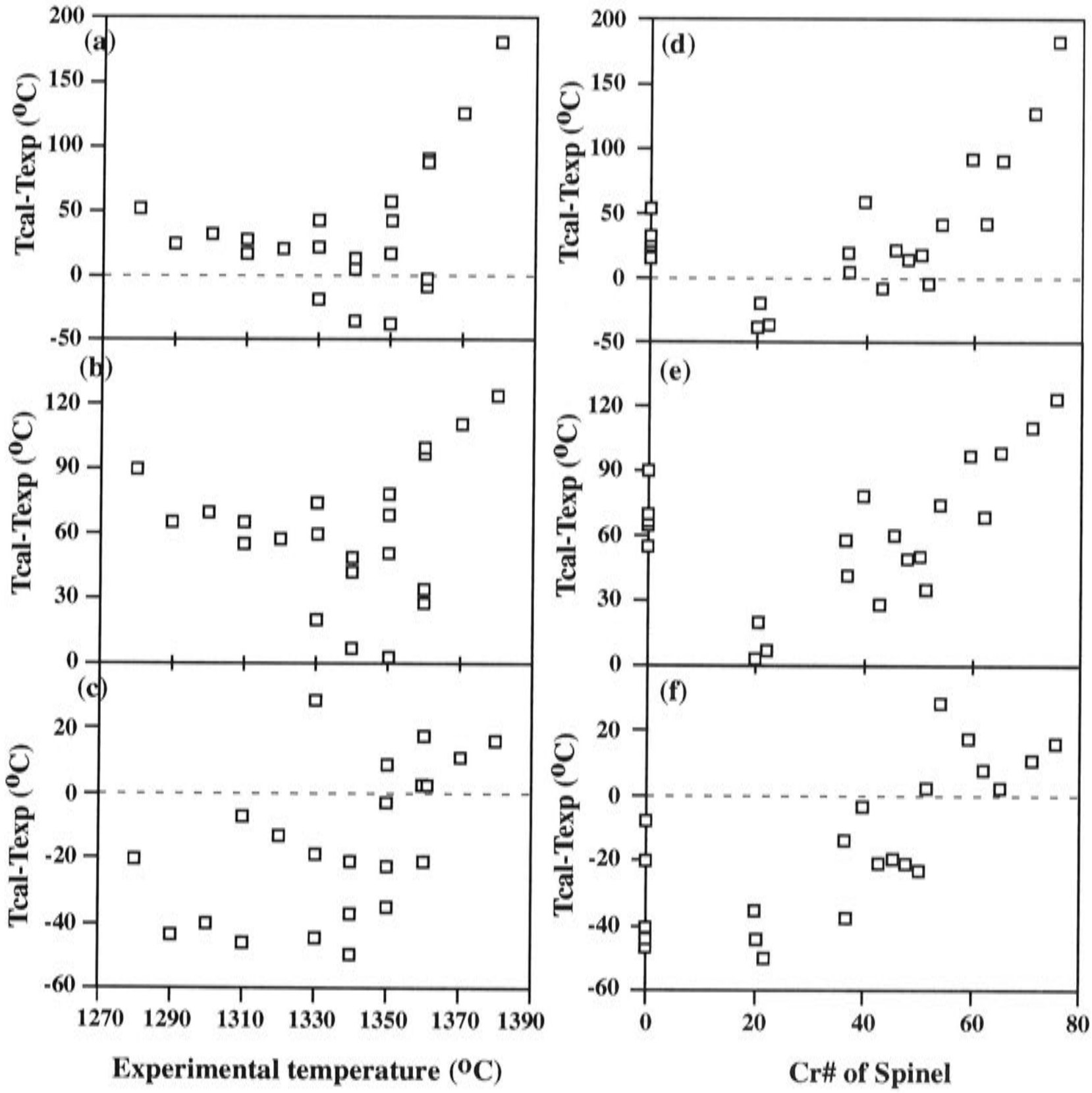

Fig. 18 Geothermometer-checking using the experimental data reported in this study: (a) and (d), for the geothermometer of Nickel et al. (1985); (b) and (e) for the Opx-Cpx geothermometer of Brey & Kohler (1990; equation 9); (c) and (f) for the Ca-in-Opx geothermometer of Brey & Kohler (1990; equation 10). The average difference for these three geothermometers is ~ 44 degrees, ~ 61 degrees, and ~ 23 degrees, respectively.

~ 289 degrees for the latter cation distribution model (Fig. 19a, 19b, respectively). When I plot the data against the Cr# of Sp in equilibrium, a compositional dependence emerges (Fig. 19c, 19d). The empirical correction made by Witt-Eickschen & Seck (1991) is thus not entirely successful and this geothermometer should be used with caution.

"Magmathermometer" of Ford et al. (1983)

The Ford et al. (1983) geothermometer is based on the olivine/melt cation partitioning for Mg and others and has recently been used widely (Danyushevsky et al.,

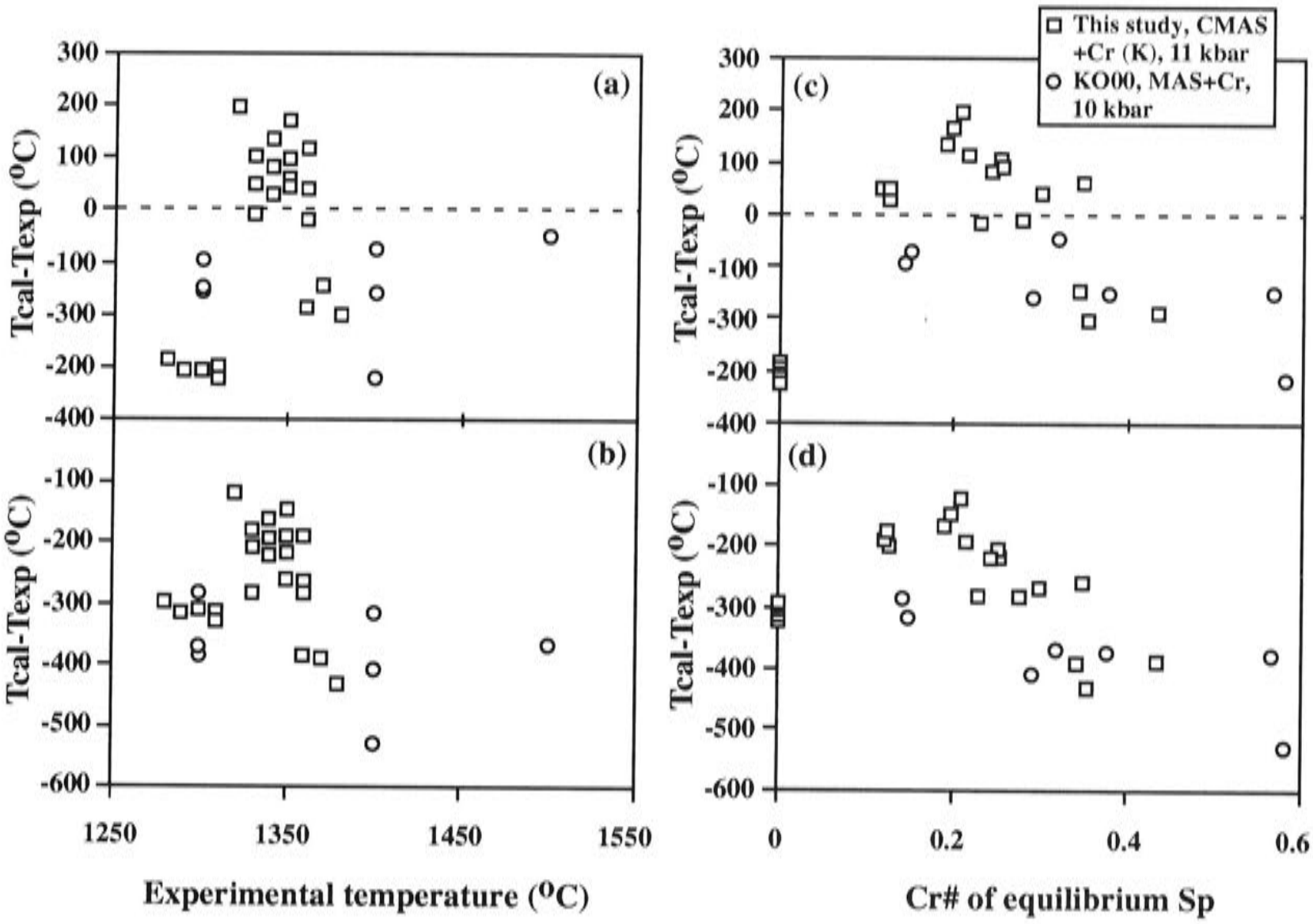

Fig. 19 Effect of chromium and cation distribution model on the performance of the Witt-Eickschen & Seck (1991) geothermometer: (a) and (c) assuming all Cr^{3+} on site M_1 in Opx while (b) and (d) assuming only half Cr^{3+} on site M_1. KO00, Klemme & O'Neill (2000). The average difference shown in (a) and (c) is ~ 144 degrees while it is ~ 289 degrees in (b) and (d).

1996; Falloon et al., 1999; Falloon & Danyushevsky, 2000; Green et al., 2000; Falloon et al., 2001). In Chapter 2 of this thesis, I discussed a possible K_2O-dependent problem and a possible pressure-dependent problem of this geothermometer while in Chapter 4 of this thesis, I examine the effect of H_2O. Since the Ford et al. (1983) geothermometer was not calibrated for the Cr_2O_3 content in the melt, it is instructive to use my experimental data to evaluate the effect of Cr_2O_3 on its performance.

In Fig. 20 I plot the temperature difference between the nominal temperature of the experiments and the temperature calculated from this geothermometer against the K_2O content in melt (Fig. 20a) and against the $Cr^{\#}$ of Sp in equilibrium (Fig. 20b). The addition of chromium into the system CMAS (+ K_2O) blurs the K_2O-dependence of this geothermometer observed in Chapter 2 of this thesis. The average difference between the calculated temperature and the nominal temperature of my experiments is ~ 53 degrees. In Fig. 20b, a Cr_2O_3-dependence of this geothermometer is suggested. This

illustrates well the importance of taking into account the effect of Cr_2O_3 on melt composition when using the Ford et al. (1983) geothermometer.

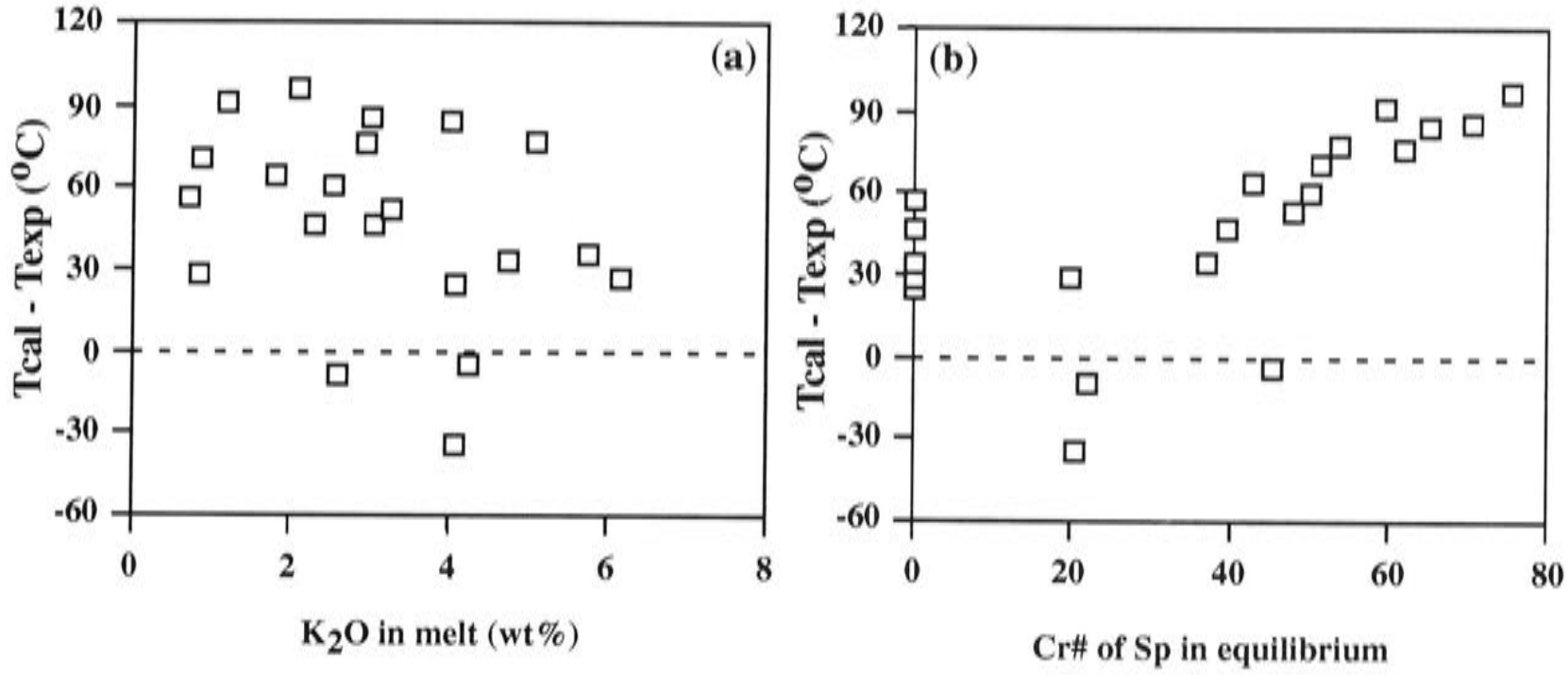

Fig. 20 Effect of K_2O (a) and Cr_2O_3 (b) on the performance of the Ford et al. (1983) geothermometer. The average difference between the calculated temperature and the nominal temperature is ~ 53 degrees. The partitioning of Mg between melt and olivine is used to calculate the temperature. Only those experiments with melt coexisting with a Sp-lherzolite phase assemblage are used here.

5. Discussions

5.1 Al_2O_3 content of melt

The dramatic decrease in Al_2O_3 with $Cr\#_{sp}$ for multiply-saturated melts in the system CMAS-Cr_2O_3 is entirely expected from Equation 4. To illustrate this more quantitatively, consider the equilibrium constant for this reaction:

$$K = \frac{a^{melt}_{AlO_{1.5}} (a^{ol}_{Mg_2SiO_4})^{1/2}}{(a^{sp}_{MgAl_2O_4})^{1/2} (a^{opx}_{Mg_2Si_2O_6})^{1/4}} \qquad (12)$$

In Fig. 21, I plot $\ln X^{melt}_{AlO_{1.5}}$ versus $1/2 \ln a^{sp}_{MgAl_2O_4} + 1/4 \ln a^{opx}_{Mg_2Si_2O_6}$ for all data from this study and those in Chapter 2 of this thesis, for melts multiply saturated in Fo + Sp + Opx + Cpx. I used the Opx and Sp models of Klemme and O'Neill (2000) to calculate $a^{sp}_{MgAl_2O_4}$ and $a^{opx}_{Mg_2Si_2O_6}$, and assumed $a^{ol}_{Mg_2SiO_4} = 1$. The stoichiometry of Equation 4 dictates that the data should plot on a line with a slope of -1 if they were isothermal, and if the activity coefficient of $AlO_{1.5}$ in the melt were constant. The line obtained by

extrapolation of the melt compositions to $[K_2O] = 0$ is a fairly good approximation to that expected.

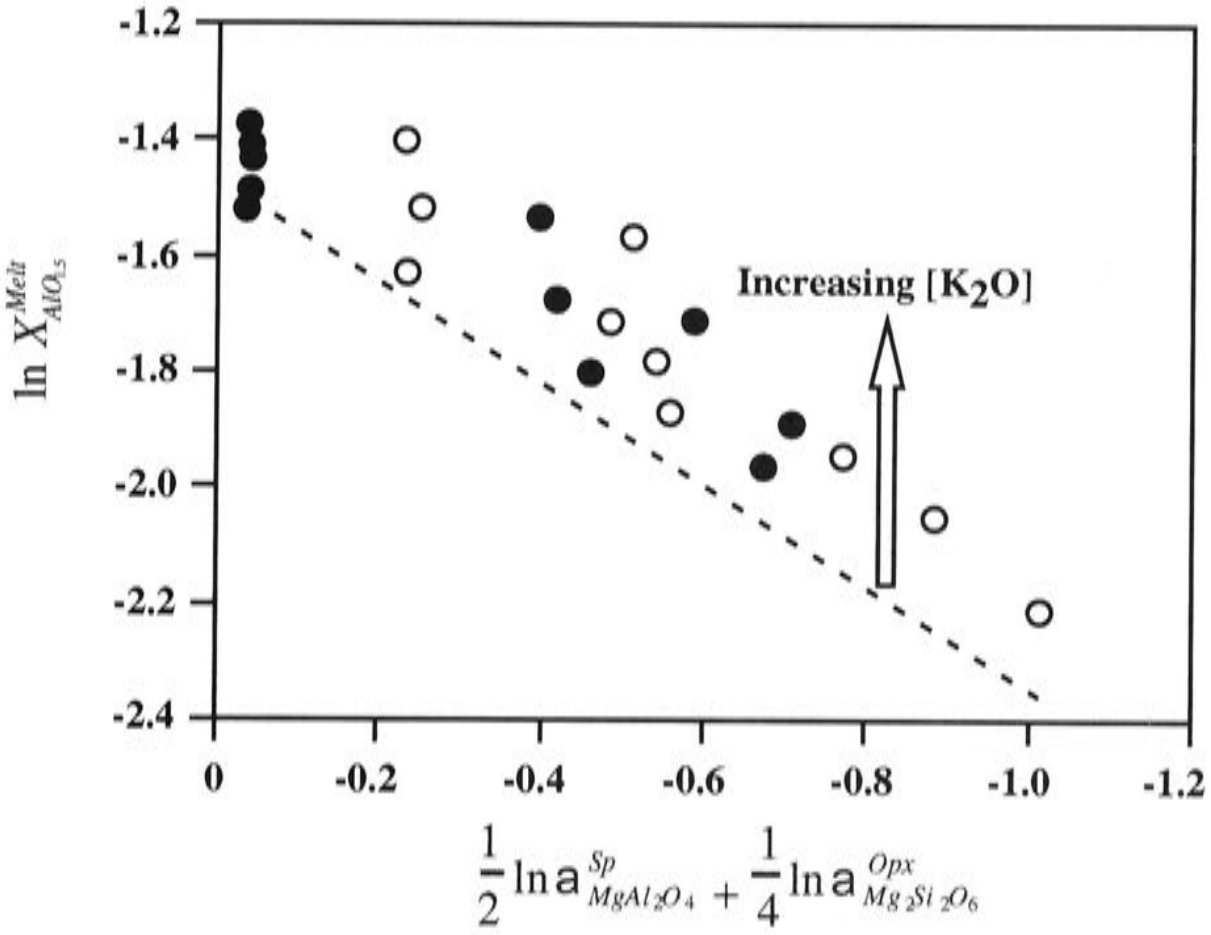

Fig. 21 Effect of Sp and Opx on the Al_2O_3 content in melts. The broken line (K_2O-free) is approximately calculated by the following procedure: 1. Estimate the $Cr\#_{sp}$ at $K_2O = 0$ for every set of experiments (Fig. 13); 2. Calculate the melt composition using the regression equations (Equation 8, 9, 10, 11 and 13; see later discussion); 3. Finalise the calculation (Equation 12) with Opx compositions from the experiment containing the lowest K_2O (in melt). Thermodynamic models for Sp and Opx are from Klemme & O'Neill (2000). The small amount of CaO in Opx is ignored. This gives the equation: $\ln X_{AlO_{1.5}}^{Melt} = 0.87(\frac{1}{2}\ln a_{MgAl_2O_4}^{Sp} + \frac{1}{4}\ln a_{Mg_2Si_2O_6}^{Opx}) - 1.48$. The effect of increasing $[K_2O]$ is to increase the $AlO_{1.5}$ in melt.

5.2 Cr_2O_3 in melt

The amount of Cr in the melt (as Cr_2O_3) is given by the regression as:

$$[\text{“}Cr_2O_3\text{”}] = 0.931\ Cr\#_{sp} - 0.10\ [K_2O]\ Cr\#_{sp} \qquad (13)$$

This includes experiments buffered by $Ru + RuO_2$ and unbuffered. That both types of experiments can be fit by the same equation implies that the Cr in the unbuffered experiments is in a similar oxidation state to the buffered experiments, i.e., mostly as Cr^{3+}. As might be expected, the primary control on Cr in the melt is $Cr\#_{sp}$, provided conditions are sufficiently oxidizing that Cr^{2+} is negligible. The average difference

between the calculated "Cr_2O_3" content by Equation 13 and the experimentally observed "Cr_2O_3" content is 0.04%.

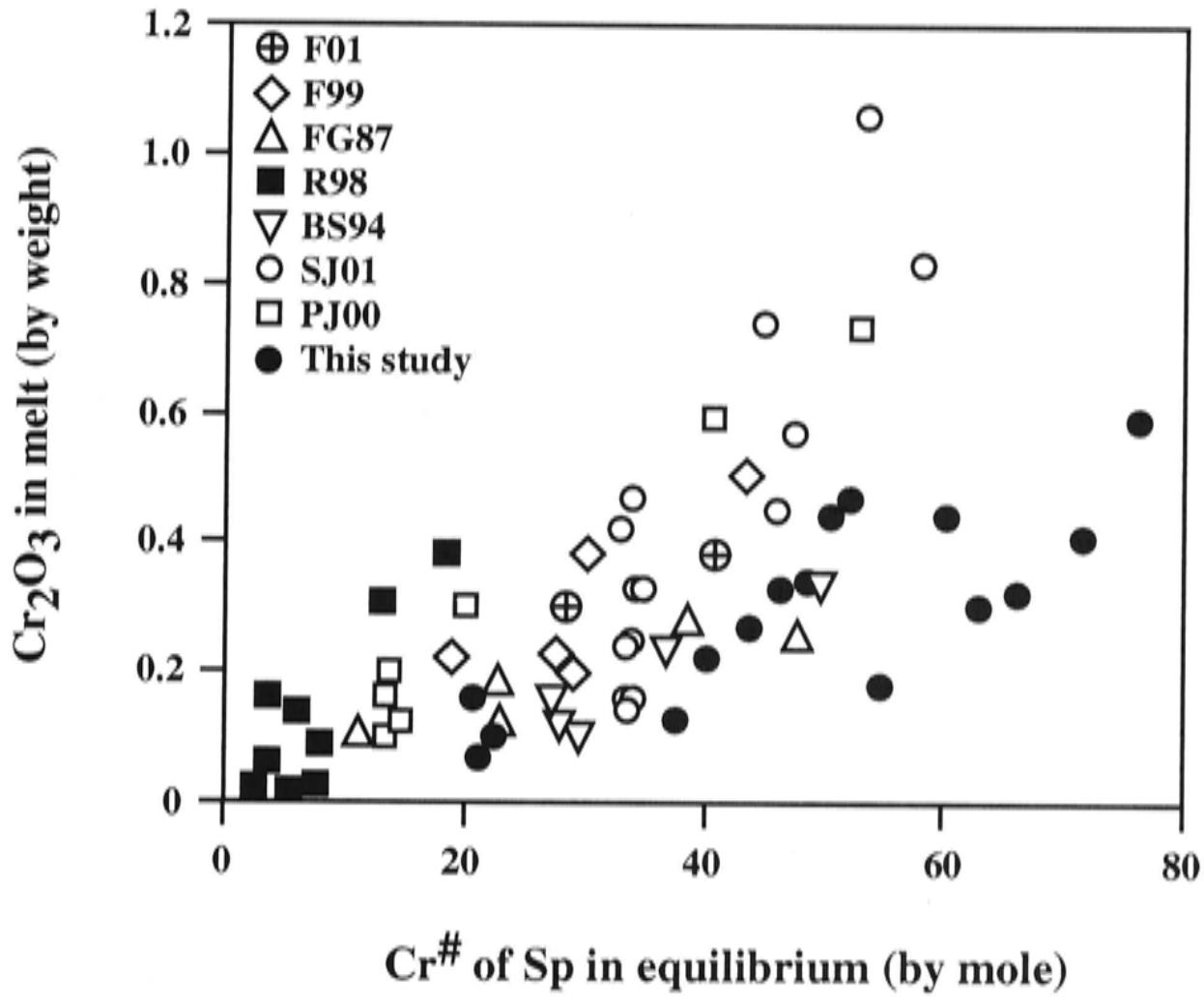

Fig. 22 The Cr_2O_3 content in melt from experiments in the system CMASCr (+K_2O) and the natural composition system. F01, Falloon et al., 2001; F99, Falloon et al., 1999; FG87, Falloon & Green, 1987 (we use the revised data by Falloon et al., 2001); R98, Robinson et al., 1998; BS94, Baker & Stolper, 1994; SJ01, Schwab & Johnston, 2001; PJ00, Pichering & Johnston, 2000. The pressure in all studies except Robinson et al. (1998; 15 kbar) and this study (11 kbar) is 10 kbar. Only experiments displaying melt plus a Sp-lherzolite phase assemblage are shown.

The experimentally observed "Cr_2O_3" contents in the melts in the current study are plotted in Fig. 22 versus $Cr\#_{sp}$, along with data from several partial melting studies on natural compositions in the literature. All these literature studies used an inner graphite capsule inside a sealed Pt capsule. This arrangement does not buffer oxygen fugacity, since this is given by $C_{(graphite)} + O_2 = CO_2$ and pCO_2 is generally not known. The maximum fO_2 occurs when $pCO_2 = P_{total}$. Thus fO_2 in such experiments could be relatively oxidizing when pCO_2 is near saturation, but proportionally lower if pCO_2 is low. Since fO_2 in experiments on natural systems affects the behaviour of Fe, and near-saturation levels of CO_2 also has an effect on phase relations (small but not entirely negligible at ~10 kbar; see Chapter 4 of this thesis), it is instructive to use the partitioning of Cr between spinel and melt (buffered by olivine + orthopyroxene, see Equation 4), to infer something about fO_2 and pCO_2 in these experiments. Differences in fO_2/pCO_2 might account for some of the differences in results.

Fig 22 shows that Cr partitioning is variable in many studies, suggesting a lack of consistency in fO_2/pCO_2 even within one study.

5.3 Cr partitioning

The partition coefficients of "Cr_2O_3" (i.e., total Cr as Cr_2O_3) between the various solid phases and melt ($D_{Cr}^{ol/melt}$ etc.) are shown as a function of $Cr\#_{sp}$ in Figs. 23a-23d. Partition coefficients are approximately constant over the range of conditions of this study. For a typical mantle peridotite, the bulk distribution coefficient ($D_{Cr}^{residue/melt}$) is about 5-10 (depending on the exact proportion of spinel at the solidus), confirming the compatible nature of Cr in its oxidized state.

Liang and Elthon (1990) pointed out that, empirically, the Cr content of mantle peridotites does not change as a function of MgO content, where the latter is a proxy for melt extracted. This implies that is $D_{Cr}^{residue/melt} \sim 1$. Liang and Elthon (1990) explained this by postulating that the melt extracted from the mantle peridotites was picritic to komatiitic (with ≥ 15 wt% MgO). It is true that if Sp ± Cpx were melted out, the value of $D_{Cr}^{residue/melt}$ must drop to a value intermediate between $D_{Cr}^{ol/melt}$ and $D_{Cr}^{opx/melt}$ for a harzburgite residue, but this is still likely to be > 1, at least in the pressure regime of the spinel lherzolite facies. Moreover, this does not explain the flat trend of Cr vs. MgO seen in the mantle peridotites. The discrepancy is likely to be due to Cr^{2+} in the melt during partial melting of the mantle, assuming that Cr^{2+} behaves moderately incompatibly.

5.4 CaO/Al_2O_3 ratio of MORBs

The CaO/Al_2O_3 ratio of the Earth's mantle is the chondritic ratio of 0.79 (e.g., O'Neill and Palme, 1998). The commonest basaltic magmas coincidentally have a very similar ratio, e.g., primitive MORB has $CaO/Al_2O_3 = 0.77 \pm 0.05$ (mean and standard deviation of 42 glass analyses compiled by Presnall and Hoover, 1987; see also Hess, 1992). The mantle ratio is the solar system ratio, whereas the basaltic ratio is controlled by phase equilibrium considerations (Equations 1 and 4). However, Cr_2O_3 must have an effect on this latter ratio through Equation 4. Clearly, increasing the Cr_2O_3/Al_2O_3 ratio in the system must result in a decrease in Al_2O_3 in the melt, hence elevation of CaO/Al_2O_3.

From a database of about 1700 analyses of abyssal basalt (MORB) glasses, Presnall & Hoover (1987) identified 42 primitive-looking compositions that they suggested were close to primary magma from the upper mantle. These primitive MORB

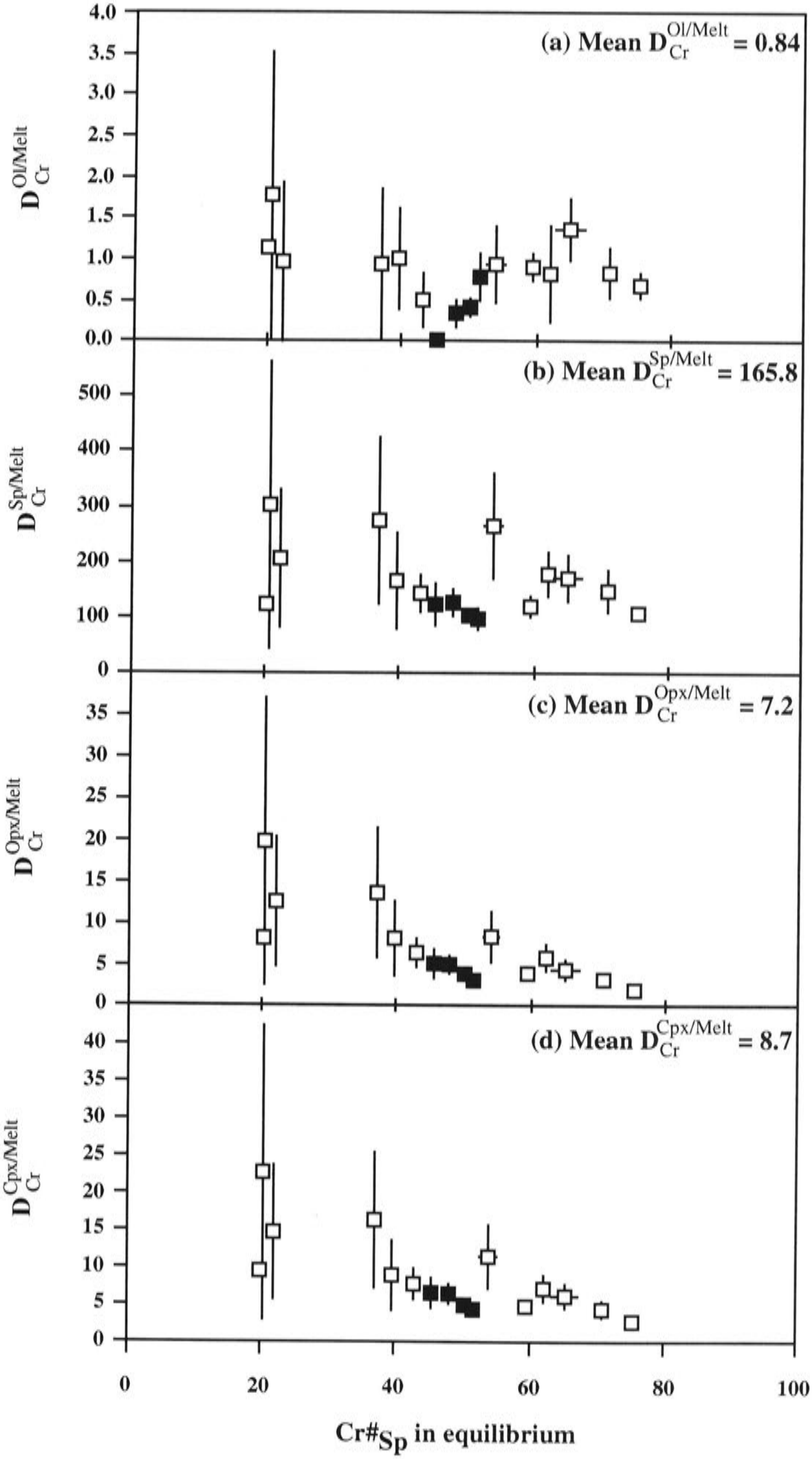

Fig. 23 Cr_2O_3 distribution between Ol and melt (a), between Sp and melt (b), between Opx and melt (c), and between Cpx and melt (d). Numbers are the average values. The experiments using $Ru+RuO_2$ buffer are shown as filled squares.

glasses are shown in Fig. 24. They plot close to the melt composition produced at the multiply saturated spinel-lherzolite solidus in the system CMAS at 11 kbar, but in detail are dispersed along vectors appropriate to the effect of small amounts of Na_2O (<3 wt%), and Cr#sp of between 20 and 30. The inferred range of Na_2O contents is consistent with that observed in the glasses (1.6 to 2.4 wt%). Considering that the effect of FeO as quantified recently by Gudfinsson and Presnall (2000) on diagrams of this type is small, and that the other components in the primitive MORB glasses are negligible or almost so, the general conclusion is that the primitive MORB glasses of Presnall and Hoover (1987) are indeed compatible with multiply-saturated melting of a peridotite source at an average pressure near 11 kbar.

Falloon et al. (1988) argued against the primitiveness of the MORB glasses assembled by Presnall & Hoover (1987) on the grounds of their high normative Di, compared to the experimentally produced melt in equilibrium with a Sp-lherzolite (Fig. 25). This is because the experimental database available to Falloon et al. (1988) was biased towards systems with high Al_2O_3/Cr_2O_3. In part, this may be because the use of graphite capsules reduces much of the Cr^{3+} to Cr^{2+} in the melt (cf. The high "Cr_2O_3" reported in melt compositions of Falloon et al., 1988).

5.5 Melt inclusions with high CaO/Al_2O_3 ratios

Recent studies of melt inclusions in phenocrysts from mid-ocean ridge (Kamenetsky, 1996; Kamenetsky & Crawford, 1998; Kamenetsky et al., 1998; Sours-Page et al., 1999), volcanic arc (Schiano et al., 2000), back-arc basin (Kamenetsky et al., 1997) and oceanic island (Sigurdsson et al., 2000; Slater et al., 2001) have documented glasses with unusually high CaO/Al_2O_3 ratios (up to 1.77; Kogiso & Hirschmann, 2001). High CaO/Al_2O_3 compositions have also been found in volcanic arcs (Barsdell, 1988; Barsdell & Berry, 1990). Generally the high CaO/Al_2O_3 silicate melts can be subdivided into two groups: SiO_2-poor nepheline-normative compositions from volcanic arcs and SiO_2-rich Hy-normative compositions from all other localities (Fig. 26).

The origin of these high CaO/Al_2O_3 silicate melts has not been satisfactorily explained to date. The modelling carried out by Barsdell & Berry (1990) using the program SILMIN of Ghiorso & Carmichael (1985) suggested that partial melting of typical upper mantle lherzolite cannot produce melt compositions found in volcanic arcs, but partial melting of a wehrlite source with < 10% normative (mole) Opx can. Although this argument was supported by Schiano et al. (2000), it has recently been

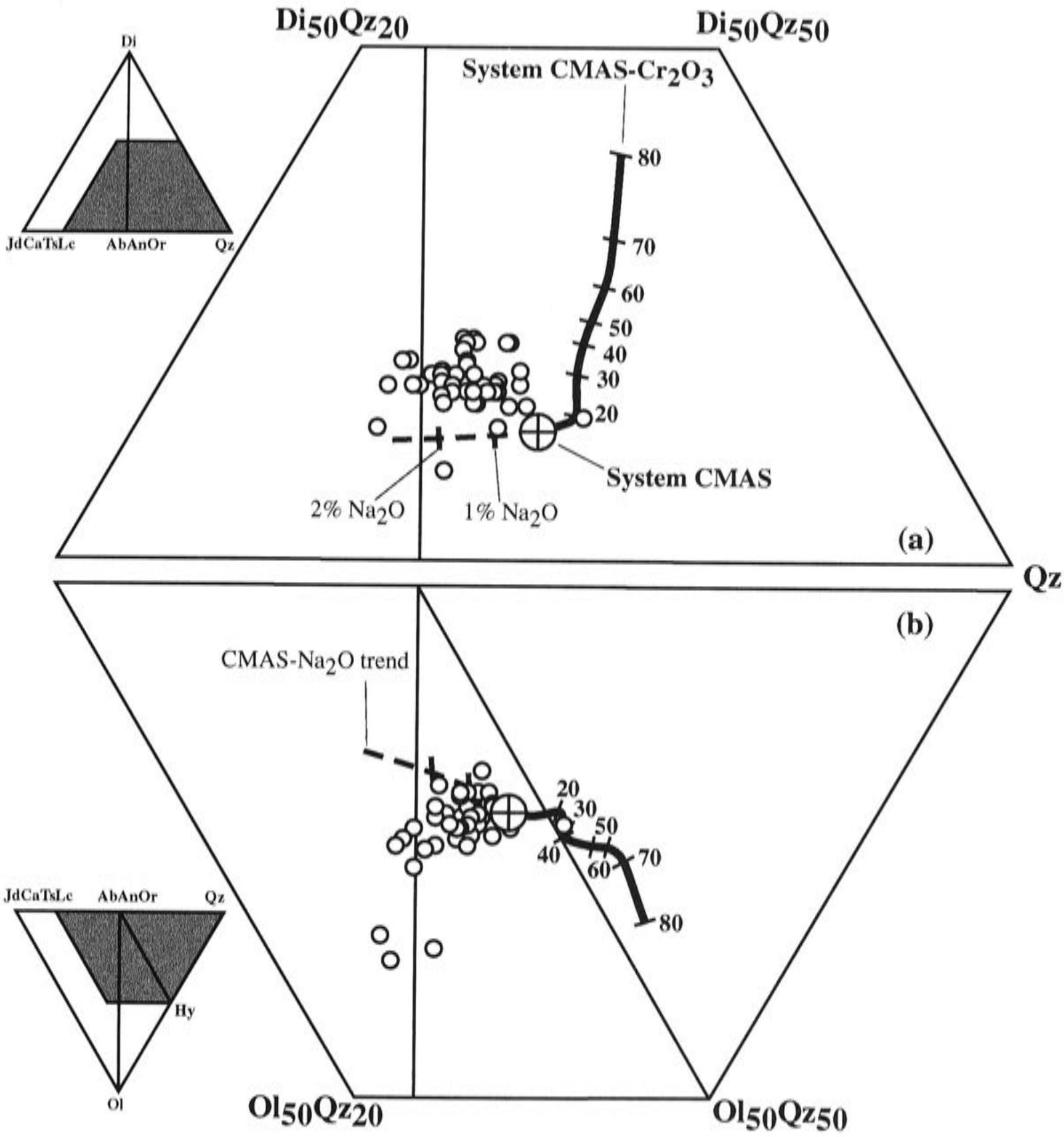

Fig. 24 Comparison of primitive MORB glass (Presnall & Hoover, 1987), multiply-saturated melt in the system CMAS (11 kbar; the 2nd chapter of this thesis), multiply-saturated melt in the system CMAS+Na_2O (11 kbar; the 4th chapter of this thesis) and melt in the system CMASCr (11 kbar; this chapter).

refuted by Kogiso & Hirschmann (2001) from a direct experimental study of the partial melting of a wehrlite. The experiments of Kogiso & Hirschman (2001) clearly demonstrated that the SiO_2-poor signature in those melt inclusions could not be produced by a CaO-rich pyroxenite. They suggested that partial melting of a depleted harzburgite may be important in the genesis of these unusual melts in these latter tectonic environments.

The strong Al_2O_3 decrease caused by the addition of Cr_2O_3 into the system CMAS (Fig. 10b) causes the CaO/Al_2O_3 of the melt to increase from ~ 0.7 at $Cr\#_{sp} = 0$

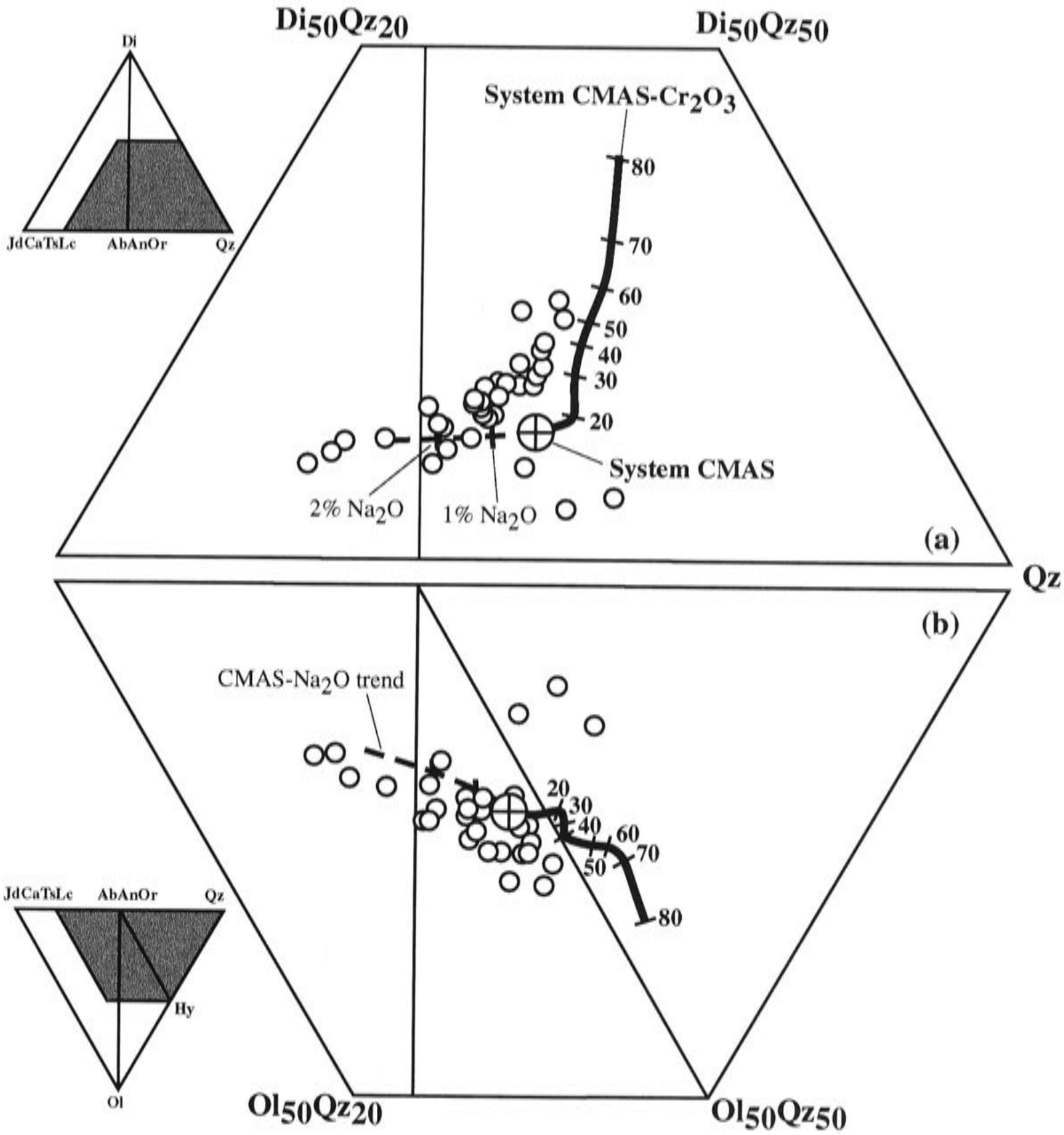

Fig. 25 Comparison of multiply-saturated (Ol+Sp+Opx+Cpx) melts from experiments in natural, complex upper mantle compositions with multiply-saturated melts in the system CMAS (11 kbar; the 2nd chapter of this thesis), multiply-saturated melts in the system CMAS+Na_2O (11 kbar; the 4th chapter of this thesis) and melts in the system CMASCr (11 kbar; this chapter). Experimental melt composition data for the complex upper upper mantle compositions are from Falloon et al. (1999), Baker & Stolper (1994), Pickering-Witter & Johnston (2000), Falloon et al. (2001) and Schwab & Johnston (2001). The experimental pressure in all these studies is 10 kbar.

to ~ 1.7 at $Cr\#_{sp}$ = 75 (Fig. 27). As discussed previously, the SiO_2 content and the Hy component of the melt also increase with $Cr\#_{sp}$. It follows that the SiO_2-rich, Hy normative and high CaO/Al_2O_3 melt inclusions found in nature can be explained by a decreasing Al/Cr ratio, which is an obvious consequence of depletion of the source peridotite by previous melt extraction, given that Al is incompatible while Cr is compatible. In a broad sense, this explanation agrees with the suggestion of Kogiso & Hirschmann (2001) that partial melting of a depleted source rock may be important in the genesis of these melts. I will examine this explanation further.

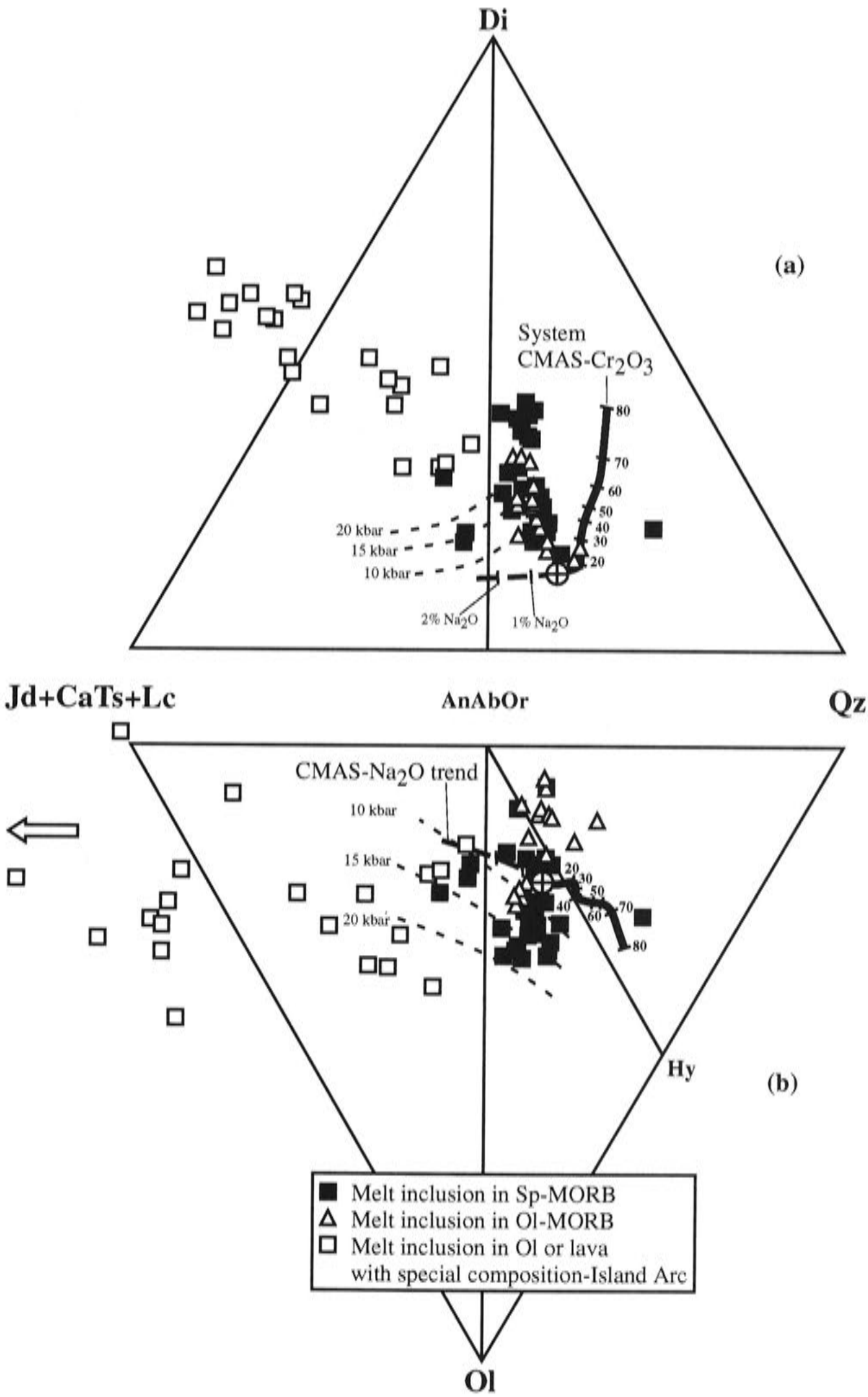

Fig. 26 Comparison of melt inclusion observed in nature, near solidus melt in the system CMAS (11 kbar; the 2nd chapter of this thesis), near solidus melt in the system CMAS+Na_2O (11 kbar; the 4th chapter of this thesis) and melt in the system CMAS-Cr_2O_3 (11 kbar; this chapter). Melt inclusions in Sp are from Donaldson & Brown (1977), Kamenetsky (1996), Kamenetsky & Crawford (1998), Kamenetsky et al. (1998), Sigurdsson et al. (2000), Kamenetsky et al. (2001). The tectonic environment for the melt inclusions in Sp is either mid-ocean ridge or oceanic island. The melt inclusions in Ol in the mid-ocean ridge region are from Danyushevsky et al. (1987), Kamenetsky & Crawford (1998) and Kamenetsky et al. (1998). The Fo component of the host Ol is ≥ 89. The melt inclusions in Ol (plus some special lavas with unusual high CaO/Al_2O_3) in island-arc region are from Schiano et al. (2000; Table 1 and Table 2) and the Fo component of the host Ol is ≥ 89. Some melt compositions from the island-arc region are plotted out of (b), as indicted by the arrow. It should be noted that the trapping pressures of these melt inclusions are unknown. The cotectics of OlSpOpxCpxMelt at different pressures shown as thin broken curves are for pyrolite (Green & Falloon, 1998).

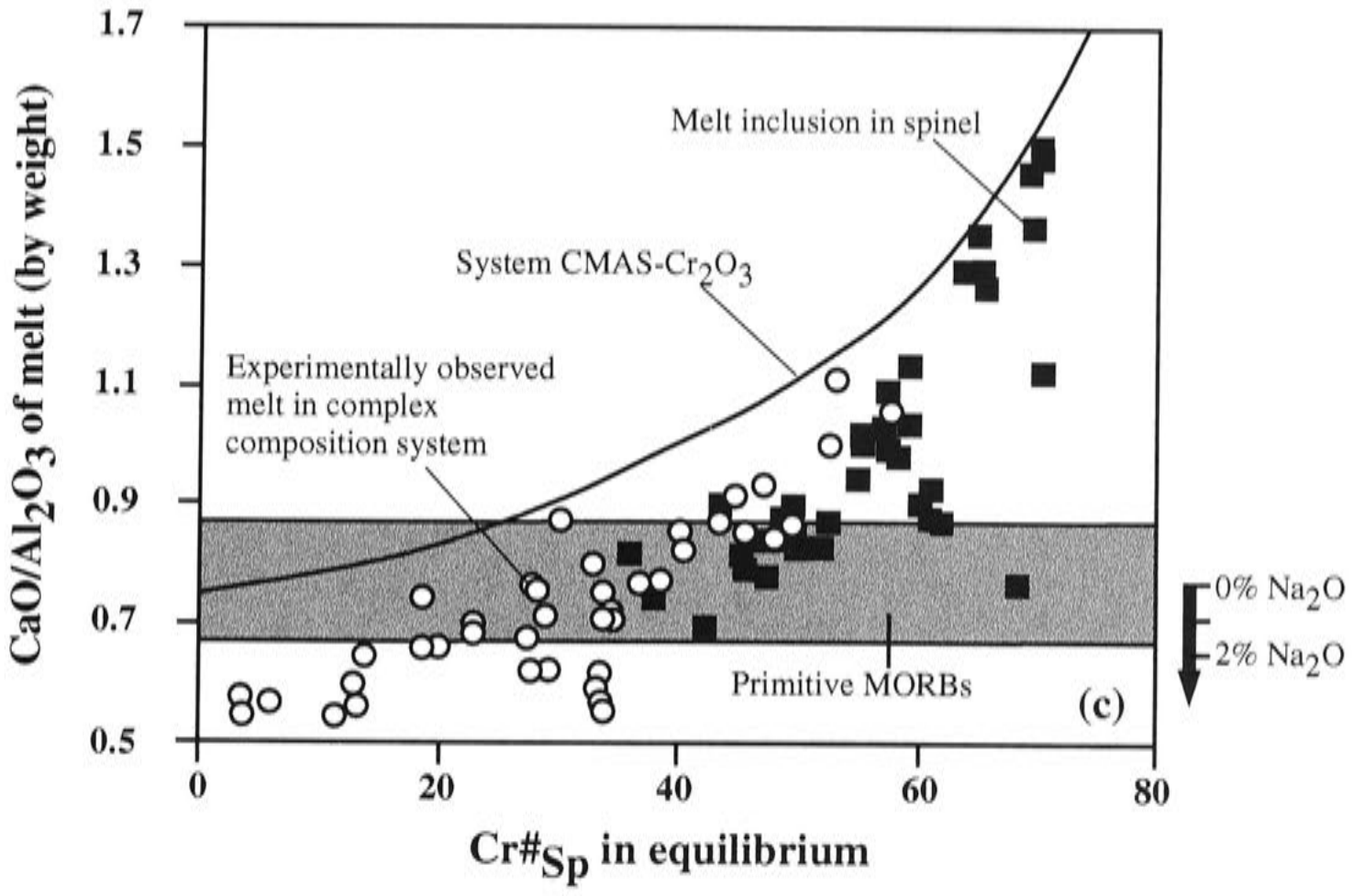

Fig. 27 The relationship of CaO/Al_2O_3 ratio of melt to $Cr\#_{Sp}$ in equilibrium. Experimental data in natural composition systems are from Falloon et al. (2001), Falloon et al. (1999), Robinson et al. (1998), Baker & Stolper (1994), Schwab & Johnston (2001) and Pichering & Johnston (2000). The pressure in all these experimental studies except Robinson et al. (1998; 15 kbar) is 10 kbar. Only experiments displaying melt with a full Sp-lherzolite phase assemblage are used here. The tectonic environment for the melt inclusions in Sp is either mid-ocean ridge or oceanic island. For the data source of these melt inclusions, see Fig. 26. The data for primitive MORBs is from Presnall & Hoover (1987).

In Fig. 27 I also plot the CaO/Al_2O_3 ratio of experimental multiply saturated melts in systems with natural lherzolitic compositions. Due to the presence of Na_2O, the CaO/Al_2O_3 ratio of the melt produced by the natural systems at low degrees of melting (i.e., multiply saturated by Ol+Opx+Cpx±Sp) is always lower than that in the system CMAS-Cr_2O_3.

The SiO_2-rich, Hy-normative and high CaO/Al_2O_3 melt inclusions hosted in spinel are shown in Fig. 27 as well. Remarkably, the CaO/Al_2O_3 of the melt inclusions are very similar to the experimental melts from the natural peridotitic compositions at similar Cr_2O_3 activity (which is indicated by $Cr\#_{sp}$). The implication is that these melt inclusions are produced from previously depleted sources.

5.6 The effect of pressure on the behaviour of Cr_2O_3

The behaviour of Cr_2O_3 in peridotites depends on the pressure. In the spinel lherzolite facies, Cr_2O_3 substitutes for Al_2O_3 in spinel and pyroxenes, and thus has a great effect on the activity of Al_2O_3 in the system. It behaves as a major element. But at

lower pressures plagioclase becomes stable, and the activity of Al_2O_3 in the system is given by:

$$\underset{\text{Melt}}{Al_2O_3} + \underset{\text{Cpx}}{CaMgSi_2O_6} = \underset{\text{Plag}}{CaAl_2Si_2O_8} + 0.5\underset{\text{Opx}}{Mg_2Si_2O_6} \qquad (14)$$

Since Cr^{3+} does not substitute significantly for the tetrahedrally coordinated Al in plagioclase, this reaction is nearly completely independent of the amount of Cr_2O_3 in the system. Hence at very low pressures, Cr_2O_3 does not behave so much like a major element component, but a minor element that forms its own accessory phase (that is, chromite), a bit like Zr forming zircon or S forming sulfide. At higher pressures, garnet becomes stable, and the activity of Al_2O_3 is given by:

$$\underset{\text{Melt}}{Al_2O_3} + 1.5\ \underset{\text{Opx}}{Mg_2Si_2O_6} = \underset{\text{Gt}}{Mg_3Al_2Si_3O_{12}} \qquad (15)$$

The amount of Cr^{3+} substituting into garnet is much less than in spinel, both because of the relative instability of Cr^{3+}-containing garnet components like $Mg_3Cr_2Si_3O_{12}$, but also because a larger fraction of the total Al_2O_3 in the peridotite composition is partitioned into garnet relative to pyroxenes, as compared to spinel relative to pyroxenes (because the solubility of Al_2O_3 in pyroxenes decreases with increasing pressure in the garnet stability field). Hence at higher pressures the effect of Cr_2O_3 on the activity of Al_2O_3, although not negligible, tends to become less significant, and the behaviour of Cr is more like a trace element. There is nothing anomalous in all this: the transitions in these contrasting styles of behaviour are smoothed out by the effect that Cr_2O_3 has on the phase boundaries between both plagioclase-lherzolite and spinel-lherzolite, and spinel-lherzolite and garnet-lherzolite (e.g., O'Neill, 1981). But the important point is that the Cr effect as described in this study has its maximum influence in the pressure regime where spinel lherzolite is stable; this is also the pressure regime at which partial melting in the mantle is most frequent.

5.7 Implications for the "Inverse Approach" in experimental petrology

In experimental petrology, the investigation of the origins of basalts has historically used two approaches, "Forward" and "Inverse". In the "Forward Approach", an assumed bulk composition is melted, and the phase relations studied. This is the

approach used in this study. One perceived problem with this approach is that the bulk composition of the system must be assumed, whereas in many situations it is only the composition of the derived partial melt (i.e., the basalt) that is known, or, more truthfully, thought to be known – this raises the issue of whether "primary magmas", which are defined as magmas sampled at the Earth's surface having undergone minimal low pressure crystal fractionation, really exist. This is controversial (e.g., Herzberg and O'Hara, 1998). Nevertheless, a theoretical "primary magma" composition might in principle be reconstructed.

The "Inverse Approach" takes the existence of a suitable primary magma composition as a given, and then seeks to ascertain the conditions under which it was produced by examining its crystallization behaviour as a function of pressure, temperature and other pertinent variables such as volatile content and redox state. There appears to be some misconceptions as regards this approach. For example, in one textbook, it is stated that "A basic tenet of experimental petrology is that primary magmas, produced by partial fusion of lherzolite, should be saturated with the residual mantle phases at temperatures and pressures corresponding to the depth of segregation……Thus all primary basalts derived from an olivine-rich mantle should have olivine, together with the other appropriate phases, on their liquidi at pressures corresponding to their depth of segregation" (Wilson, 1994, pp. 67-68). This is certainly not the case, since low-degree partial melts are produced from lherzolite in reaction relationship with olivine to pressures of approximately 30 kbar, that is, melting is peritectic-like and not eutectic-like to this pressure (e.g., Kushiro, 1979; Gudfinsson and Presnall, 1996; for a direct experimental demonstration of this behaviour, see Chapter 2 of this thesis). Thus olivine is not precipitated on the liquidi of such melts at the pressure of their generation, although it is in equilibrium with the melts.

These and some other problems with the "Inverse Approach" are discussed by Hess (1989; pp. 109-113) and more recently by Falloon et al. (1999). Here I add a more fundamental item to these critiques, deriving from the behaviour of Cr_2O_3 during partial melting.

The basic assumption underlying the "Inverse Approach" is that all the information needed to reconstruct the partial melting equilibrium is held in the melt composition. Heuristically, this would not be true were there a component of the system that was perfectly compatible, such that it entered only the solid phases of the partial melting equilibrium and not the melt. The concentration of such a component in the system could not be determined from the melt, but its presence in the solid phases

would affect the chemical potentials of other components in the system, and hence their concentrations in the melt. Although Cr_2O_3 is not quite perfectly compatible, its behaviour is as near to this as makes no practical difference. Although Cr_2O_3 does enter the melt, the amount is so small that it is commonly overlooked, and the role of Cr_2O_3 as a major element component during basalt generation has tended to go unrecognised. Secondly, Cr_2O_3-rich spinel is commonly the first phase to fractionate from a magma at low pressures, thus the original Cr_2O_3 abundances in near-primary magmas are very easily obscured. Thirdly, the compatible behaviour of interest here is specifically a property of Cr^{3+} and not Cr^{2+}, hence the proportion of total Cr as Cr^{3+} in the melt is what matters. This depends on the redox state of the system, i.e., the Fe^{3+}/Fe^{2+} ratio of the melt, T and P. Original Cr^{3+}/Cr^{2+} ratios are modified in natural Fe-rich magmas by the electronic exchange reaction: $Cr^{2+} + Fe^{3+} = Cr^{3+} + Fe^{2+}$; this reaction proceeds to the right hand side with cooling or crystallization (e.g., Berry et al., 2001), such that all Cr^{2+} is consumed by reaction with Fe^{3+} in terrestrial magmas.

It seems extremely doubtful that even a composition identified as "primary" (for example, on the usual grounds of high MgO and the appropriate Mg/Fe^{2+} ratio to be in equilibrium with olivine of Fo_{89} to Fo_{92}) would retain exactly the right Cr^{3+} content to reproduce the partial melting equilibrium; accordingly, the fundamental assumption of the "Inverse Approach", that all the necessary information is held in the melt composition, is not valid. Inferences from the "Inverse Approach" regarding the depth (etc.) of origin of primary magmas are therefore unsustainable.

The large amount of effort expended by experimental petrologists on the "Inverse Approach" should not be seen as wasted, however. "Inverse" experiments are a good means of obtaining the phase equilibrium data needed to formulate models for calculating melting phenomena under physically plausible conditions. In many ways, the simplistic answers sought originally from the "Inverse Approach", like the depth of melting, have become irrelevant as the physical context of partial melting has become better understood. Basaltic magmas are now recognized as being mostly, perhaps exclusively, produced by convective upwelling in the mantle, with partial melting occurring under nearly adiabatic conditions, and over an interval of pressure (e.g., McKenzie and Bickle, 1988). Melts are extracted more-or-less fractionally, resulting in changing bulk compositions during the melting process. The mantle may also act as an open system (e.g., to volatile components). These complex natural processes cannot be mimicked in the laboratory with any expectation that accurate phase-equilibrium data will result. Carrying out polybaric, adiabatic melting experiments is just too difficult. As

for any complex natural process, the path of modern science out of this dilemma is to construct a computer model for the phase equilibria that will enable this aspect of the partial melting process to be integrated into a holistic description of the whole process. Such models are being developed, notably the MELTS algorithm (e.g., Ghiorso et al., 2002), and similar parameterizations (e.g., Walter et al., 1995; Herzberg and O'Hara, 2002) The experimental petrology of basalt generation should now appropriately be directed towards the goal of supplying the necessary phase equilibrium information to improve these models.

6. Conclusions

The K_2O method developed in Chapter 2 of this thesis has been successfully applied in the present study and partial melting experiments displaying a full Sp-lherzolite have been carried out in the system CMASCr at 11 kbar. The major results are:

1. The relationship of Cr and Al in pyroxene is not a simple substitution process of one for the other and the crystal structure might have important constraint on it. The Cr fraction increases with the decrease of Al at low Cr content conditions but decreases with the decrease of Al at high Cr content conditions after it reaches a maximum value. Only at extremely high Cr conditions can the Cr content in Opx overtake the Al content;
2. Cr affects the Al content in pyroxenes so that the geothermometers related to the Al content in pyroxenes in the literature have to be used with great caution. My calculation suggests the performance of all these geothermometers depends to some extent on Cr;
3. While the Ca/(Ca+Mg) ratio of Opx is independent of the chemical system, this ratio in Cpx isn't. Cpx becomes poor in Di much more rapidly in the system CMASCr than in the system CMS and the system CMAS as temperature increases. The geothermometers based on the CaO equilibrium between Opx and Cpx, therefore, should be used with great caution.
4. Cr^{3+} strongly increases the partial melting temperature and the increase is not linear, strong at low $Cr\#_{sp}$, weak at mediate $Cr\#_{sp}$ and strong again at high $Cr\#_{sp}$.
5. Cr^{3+} has a very strong effect on melt composition in the stability field of Sp-lherzolite.

6. The partitioning coefficient between the solid phase and the melt suggests that Cr^{3+} is extremely compatible during partial melting process. The effect of chromium on melt compositions, therefore, is not readily apparent from the melts themselves.

7. References

Baker, M. B. & Stolper, E. M. (1994). Determining the composition of high-pressure mantle melts using diamond aggregates. Geochimica. et. Cosmochimica. Acta 58, 2811-2827.

Barnes, S. J. & Roeder, P. L. (2001). The range of spinel compositions in terrestrial mafic and ultramafic rocks. J. Petrol. 42, 2279-2302.

Barsdell, M. (1988). Petrology and petrogenesis of clinopyroxene-rich tholeiitic lavas, Merelava volcano, Vanuatu. J. Petrol. 29, 927-964.

Barsdell, M. & Berry, R. F. (1990). Origin and evolution of primitive island arc ankaramites from Western Epi, Vanuatu. J. Petrol. 31, 747-777.

Berry, A. J., O'Neill, H. St. C., Shelley, J. M. G. & Foran, G. (2001). Spectroscopic evidence for chromium (II) in silicate melts. In Eleventh Annual V.M. Goldschmidt Conference, Abstract #3566 (2001). LPI Contribution No. 1088, Lunar and Planetary Institute, Houston, USA.

Bose, K. & Ganguly, J. (1995). Quartz-coesite transition revisited: Reversed experimental determination at 500-1200°C and retrieved thermochemical properties. Am Mineral 80, 231-238.

Boyd, F. R. & England, J. L. (1960). Apparatus for phase-equilibrium measurements at pressures up to 50 kbar and temperatures up to 1750°C. J. Geophy. Res. 65, 741-748.

Brey, G. P., Kohler, T. & Nickel, K. G. (1990). Geothermobarometry in four-phase lherzolites I. Experimental results from 10 to 60 kb. J. Petrol. 31, 1313-1352.

Brey, G. P. & Kohler, T. (1990). Geothermobarometry in four-phase lherzolite II: new thermobarometers, and practical assessment of existing thermobarometers. J. Petrol. 31, 1353-1378.

Danyushesky, L. V., Sobolev, A. V. & Dmitriev, L. V. (1987). Low-titanium orthopyroxene-bearing tholeiite, a new type of ocean-rift tholeiite. Transactions (Doklady) of the USSR Academy of Sciences 292, 102-105.

Danyushevsky, L. V., Sololev, A. V. & Dmitriev, L. V. (1996). Estimation of the pressure of crystallisation and H_2O content of MORB and BABB glasses: calibration of an empirical technique. Mineral. Petrol. 57, 185-204.

Dick, H. J. B. & Bullen, T. (1984). Chromian spinel as a petrogenetic indicator in abyssal and alpine-type peridotites and spatially associated lavas. Contrib. Mineral. Petrol. 86, 54-76.

Donaldson, C. H. & Brown, R. W. (1977). Refractory megacrysts and magnesium-rich melt inclusions within spinel in oceanic tholeiites: indicators of magma mixing and parental magma compositions. Earth Planet. Sci. Lett. 37, 81-89.

Dunn, R. & Forsyth, D. (2001). Short-period Love waves reveal the transition from broad mantle upwelling to the narrow crustal magmatic system beneath the southern East Pacific Rise. EOS Trans. Am. Geophys. Union 82, 1113.

Falloon, T. J. & Green, D. H. (1987). Anhydrous partial melting of MORB pyrolite and other peridotite compositions at 10 kbar: Implications for the origin of MORB glasses. Miner. Petrol. 37, 181-219.

Falloon, T. J., Green, D. H., Hatton, C. J. & Harris, K. L. (1988). Anhydrous partial melting of a fertile and depleted peridotite from 2 to 30 kbar and application to basalt petrogenesis. J. Petrol. 29, 1257-1282.

Falloon, T. J. & Green, D. H. (1988). Anhydrous partial melting of peridotite from 8 to 35 kbars and the petrogenesis of MORB. J. Petrol. Special Issue, 379-414.

Falloon, T. J., Green, D. H., Danyushevsky, L. V & Faul, U. H. (1999). Peridotite melting at 1.0 and 1.5 Gpa: an experimental evaluation of techniques using diamond aggregates and mineral mixes for determination of near-solidus melts. J. Petrol. 40, 1343-1375.

Falloon, T. J. & Danyushevsky L. V. (2000). Melting of refractory mantle at 1.5, 2 and 2.5 GPa under anhydrous and H_2O-undersaturated conditions: implications for the petrogenesis of high-Ca boninites and the influences of subduction components on mantle melting. J. Petrol. 41, 257-283.

Falloon, T. J., Danyushevsky, L. V. & Green, D. H. (2001). Peridotite melting at 1 GPa: reversal experiments on partial melt compositions produced by peridotite-basalt sandwich experiments. J. Petrol. 42, 2363-2390.

Ford, C. E., Russell, D. G., Graven, J. A. & Fisk, M. R. (1983). Olivine-liquid equilibria: temperature, pressure and composition dependence of the crystal/liquid cation partition coefficients for Mg, Fe^{2+}, Ca and Mn. J. Petrol. 24, 256-265.

Fujii, T. & Scarfe, C. M. (1985). Composition of liquids coexisting with spinel lherzolite at 10 kbar and the genesis of MORBs. Contrib. Mineral. Petrol. 131, 323-346.

Gasparik, T. (1984). Two-pyroxene thermobarometry with new experiment data in the system CaO-MgO-Al_2O_3-SiO_2. Contrib. Mineral. Petrol. 87, 87-97.

Ghiorso, M. S. & Carmichael, I. S. E. (1985) Chemical mass transfer in magmatic processes. II. Applications in equilibrium crystallization, fractionation and assimilation. Contrib. Mineral. Petro. 90, 121-141.

Ghiorso, Mark S.; Hirschmann, Marc M.; Reiners, Peter W.; Kress, Victor C (2002). The pMELTS: A revision of MELTS for improved calculation of phase relations and major element partitioning related to partial melting of the mantle to 3 GPa. GEOCHEM. GEOPHY. GEOSY. 3, No. 5, 10.1029/2001GC000217.

Green, D. H. & Falloon, T. J. (1998). Pyrolite: a Ringwood concept and its current expression. In: Jackson, I. (ed.), "The Earth's Mantle: its Origin, Structure and Evolution". Cambridge University Press. 311-378.

Green, D. H., Falloon, T. J., Eggins, S. M. & Yaxley, G. M. (2000). Primary magmas and mantle temperatures. Eur. J. Mineral. 13, 437-451.

Green, T. H., Ringwood, A. E. & Major, A. (1966). Friction effects and pressure calibration in a piston-cylinder high pressure-temperature apparatus. J. Geophy. Res. 71, 3589-3594.

Gudfinnsson, G. H. & Presnall, D. C. (1996). Melting relations of model lherzolite in the system CaO-MgO-Al_2O_3-SiO_2 at 2.4-3.4 Gpa and the generation of komatiites. J. Geophy. R. 101, 27701-27709.

Gudfinnsson, G. H. & Presnall, D. C. (2000). Melting behaviour of model lherzolite in the system CaO-MgO-Al_2O_3-SiO_2-FeO at 0.7-2.8 Gpa. J. Petrol. 41, 1241-1269.

Hanson, B. & Jones, J. (1998). The systematics of Cr^{3+} and Cr^{2+} partitioning between olivine and liquid in the presence of spinel. Am. Mineral. 83, 669-684.

Herzberg, C. T. & O'Hara, M. J. (1998). Phase equilibrium constraints on the origin of basalts, picrites, and komatiites. Earth Sci. Rev. 44, 39-79.

Herzberg, C. T. & O'Hara, M. J. (2002). Plume-associated ultramafic magmas of phanerozoic age. J. Petrol. 43, 1857-1883

Hess, P. C. (1992). Phase equilibria constrains on the origin of ocean floor basalts. In Geophysical Monograph 71: Mantle flow and melt generation at mid-ocean ridge. American Geophysical Union.

Hess, P. C. (1989). Origins of igneous rocks. Harvard Press, Cambridge, MA.

Hibberson, W. O. (1978). High pressure and high temperature techniques as applied to experimental petrology. Science and Technology 15-5, 22-23.

Irvine, T. N. (1977). Chromite crystallisation on the join Mg_2SiO_4-$CaMgSi_2O_6$-$CaAl_2Si_2O_8$-$MgCr_2O_4$-SiO_2. Carnegie Inst. Yearbook 76, 465-472.

Jochum, K. P., Dingwell, D. B., Rocholl, A., Stoll, B., Hofmann, A. W., Becker, S., Besmehn, A., Bessette, D., Dietze, H.-J., Dulski, P., Erzinger, J., Hellebrand, E., Hoppe, P., Horn, P., Janssens, K., Jenner, G. A., Klein, M., McDonough, W. F., Maeetz, M., Mezger, K., Munker, C., Nikogosian, I. K., Pickhardt, C., Raczek, I., Rhede, D., Seufert, H. M., Simakin, S. G., Sobolev, A. V., Spettel, B., Straub, S., Vincze, L., Wallianos, A., Weckwerth, G., Weyer, S., Wolf, D. & Zimmer, M. (2000). The preparation and preliminary characterisation of eight geological MPI-DING reference glasses for in-situ microanalysis. J. Geostand. Geoanaly. 24, 87-133.

Johannes, W., Bell, P. M., Mao, H. K., Boettcher, A. L., Chipman, D. W., Hays, J. F., Newont, R. C., Seifert, F. (1971). An interlaboratory comparison of piston-cylinder pressure calibration using albite-breakdown reaction. Contrib. Mineral. Petrol. 32:24-38.

Kamenetsky, V. S. (1996). Methodology for the study of melt inclusions in Cr-spinel, and implications for parental melts of MORB from FAMOUS area. Earth Planet. Sci. Lett. 142, 479-486.

Kamenetsky, V. S. Crawford, A. J., Eggins, S. M. & Muhe, R. (1997). Phenocrysts and melt inclusion chemistry of near-axis seamounts, Valu Fa Ridge, Lau Basin: insight into mantle wedge melting and the addition of subduction components. Earth Planet. Sci. Lett. 151, 205-223.

Kamenetsky, V. S.& Crawford, A. J. (1998). Melt-peridotite reaction recorded in the chemistry of spinel and melt inclusions in basalt from 43°N, Mid-Atlantic Ridge. Earth Planet. Sci. Lett. 164, 345-352.

Kamenetsky, V. S., Eggins, S. M., Crawford, A. J., Green, D. H., Gasparon, M. & Falloon, T. J. (1998). Calcic melt inclusions in primitive olivine at 43°N MAR: evidence for melt-rock reaction/melting involving clinopyroxene-rich lithologies during MORB generation. Earth Planet. Sci. Lett. 160, 115-132.

Kamenetsky, V. S., Crawford, A. J. & Meffre, S. (2001). Factors controlling chemistry of magmatic spinel: an empirical study of associated olivine, Cr-spinel and melt inclusions from primitive rocks. J. Petrol. 42, 655-671.

Klemme, S. & O'Neill, H. St. C. (2000). The effect of Cr on the solubility of Al in orthopyroxene: experiments and thermodynamic modelling. Contrib. Mineral. Petrol. 140, 84-98.

Kogiso, T. & Hirschmann, M. M. (2001). Experimental study of clinopyroxenite partial melting and the origin of ultra-calcic melt inclusions. Contrib. Mineral. Petrol. 142, 347-360.

Kushiro, I. (1979). Fractional crystallization of basaltic magma. In: The evolution of the igneous rocks: fiftieth anniversary perspectives. Princeton University Press.

Liang, Y. & Elthon, D. (1990). Evidence from chromium abundances in mantle rocks for extraction of picrite and komatiite melts. Nature 343, 551-553.

Libourel, G. (1991). Chromium in basalts: an experimental study. EOS Trans. Am. Geophys. Union 72, 547.

Li, J. P., O'Neill, H. St. C. & Seifert, F. (1995). Subsolidus phase relations in the system MgO-SiO_2-Cr-O in equilibrium with metallic Cr, and their significance for the petrochemistry of chromium. J. Petrol. 36, 107-132.

Lindsley, D. H. & Dixon, S. A. (1976). Diopside-enstatite equilibria at 850 to 1400oC, 5 to 35 kbar. Am. J. Sci 276, 1285-1301.

Longhi, J. & Bertka, C. M. (1996). Graphical analysis of pigeonite-augite liquidus equilibria. Am. Mineral. 81, 685-695.

McKenzie, D. & Bickle, M. J. (1988). The volume and composition of melt generated by extension of the lithosphere. J. Petrol. 29, 625-679.

Melt Seismic Team (1998). Imaging the deep seismic structure beneath a mid-ocean ridge: the melt experiment. Science 280, 1215-1218.

Mori, T. & Green, D. H. (1976). Subsolidus equilibria between pyroxenes in the CaO-MgO-SiO2 system at high pressures and temperatures. Am. Mineral. 61, 616-625.

Nagata, J., Goto, A., Obata, M. (1983). The parabolic pattern of chromium partitioning observed between pyroxenes and spinel from ultramafic rocks and its petrologic significance. Contrib. Mineral. Petrol. 82, 42-51.

Nickel, K. G., Brey, G. P. (1984). Subsolidus orthopyroxene-clinopyroxene systematics in the system CaO-MgO-SiO2 to 60 kb: a re-evaluation of the regular solution model. Contrib. Mineral. Petrol 87, 35-42.

Nickel, K. G., Brey, G. P. & Kogarto, L. (1985). Orthopyroxene-clinopyroxene equilibria in the system CaO-MgO-Al_2O_3-SiO_2. Contr. Miner. Petrol. 91: 44-53.

Nickel, K. G. (1986) Phase equilibria in the system SiO_2-MgO-Al_2O_3-CaO-Cr_2O_3 (SMACCr) and their bearing on spinel/garnet lherzolite relationships. Neues Jahrbuch fur Minerologie, Abhandlungen 155, 259-287.

O'Neill, H. St. C. (1981). The transition between spinel lherzolite and garnet lherzolite, and its use as a geobarometer. Contr. Mineral. Petrol. 77, 185-194.

O'Neill, H. St. C. & Nell, J. (1997). Gibbs free energies of formation of RuO2, IrO2, and OsO2: A high-temperature electrochemical and calorimetric study. Geochim. Cosmochim. Acta 61, 5279-5293.

O'Neill, H. St. C. & Palme, H. (1998). Compositions of the Silicate Earth: Implications for accretion and core formation. In: Jackson, I. (ed.) " The Earth's Mantle: Composition, Structure and Evolution", 3-126. Cambridge University Press. Cambridge.

Pichering, J. W. & Johnston, A. D. (2000). The effects of variable bulk composition on the melting systematics of fertile peridotitic assemblages. Contrib. Mineral. Petrol. 140, 190-211.

Presnall, D. C., Dixon, J. R., O'Donnell T. H. & Dixon, S. A. (1979). Generation of mid-ocean ridge tholeiites. J. Petrol. 20, 3-36.

Presnall, D. C. & Hoover, J. D. (1984). Composition and depth of origin of primary mid-ocean ridge basalts. Contrib. Mineral. Petro. 87, 170-178.

Presnall, D. C. & Hoover, J. D. (1987). High pressure phase equilibrium constraints on the origin of mid-ocean ridge basalts. In: Mysen, B. O. (ed.), "Magmatic Processes: Physicochemical Principles". Geochemical Soc. Spec. Pub. 1, 75-89.

Presnall, D. D., Gudfinnsson, G. H. & Walter, M. J. (2002). Generation of mid-ocean ridge basalts at pressures from 1 to 7 GPa. Geochim. Cosmochim. Acta 66, 2073-2090.

Robinson, J. A. C., Wood, B. J. & Blundy, J. D. (1998). The beginning of melting of fertile and depleted peridotite at 1.5 Gpa. Earth Planet. Sci. Lett 155, 97-111.

Schiano, P., Eiler, J. M., Hutcheon, I. D. & Stolper, E. M. (2000). Primitive CaO-rich, silica-undersaturated melts in island arcs: evidence for the involvement of clinopyroxene-rich lithologies in the petrogenesis of arc magmas. Geochem. Geophys. Geosys., 1:1999GC000032.

Schwab, B. E. & Johnston, A. D. (2001). Melting systematics of modally variable, compositionally intermediate peridotites and the effects of mineral fertility. J. Petrol. 42, 1789-1811.

Sen, G. (1982). Composition of basaltic liquids generated from a partially depleted lherzolite at 9 kbar pressure. Nature 299, 336-338.

Sen, G. (1985) Experimental determination of pyroxene compositions in the system CaO-MgO-Al2O3-SiO2 at 900-1200 °C and 10-15 kbar using PbO and H_2O fluxes. Am. Mineral. 70, 678-695.

Sigurdsson, I. A., Steinthorsson, S. & Gronvold, K. (2000). Calcium-rich melt inclusions in Cr-spinels from Borgarhraun, nothern Iceland. Earth Planet. Sci. Lett. 183, 15-26.

Slater, J., McKenzie, D., Gronvold, K. & Shimizu, N. (2001). Melt generation and movement beneath Theistareykir, NE Iceland. J. Petrol. 42, 321-354.

Sours-Page, R., Johnson, K. T. M., Nielsen, R. L. & Karsten, J. L. (1999). Local and regional variation of MORB parent magmas: evidence from melt inclusions from the Endeavour Segment of the Juan de Fuca Ridge. Contrib. Mineral. Petrol. 134, 342-363.

Stolper, E. (1980). A phase diagram for mid-ocean ridge basalts: preliminary results and implications for petrogenesis. Contrib. Mineral. Petrol. 74, 13-27.

Takahashi, E. & Kushiro, I. (1983). Melting of a dry peridotite at high pressures and basalt magma genesis. Am. Mineral. 68, 859-879.

Walter, M. J. & Presnall, D. C. (1994). Melting behaviour of simplified lherzolite in the system CaO-MgO-Al_2O_3-Na_2O from 7 to 35 kbar. J. Petrol. 35, 329-359.

Walter, M. J., Sisson, T. W. & Presnall, D. C. (1995). A mass proportion method for calculating melting reaction and application to melting of model upper mantle lherzolite. Earth Planet. Sci. Lett. 135, 77-90.

Ware, N. G. (1991). Combined energy-dispersive-wavelength-dispersive quantitative electron microprobe analysis. X-ray Spectrometry 20, 73-79.

Wilson, M. (1994). Igneous petrogenesis: a global tectonic approach. Chapman & Hall.

Witt-Eickschen, G. & Seck, H. A. (1991). Solubility of Ca and Al in orthopyroxene from spinel peridotite: an improved version of an empirical geothermometer. Contrib. Mineral. Petrol. 106, 431-439.

Chapter 4

The effects of H_2O and CO_2 on the partial melting of spinel lherzolite in the system CaO-MgO-Al_2O_3-SiO_2-H_2O-CO_2 at 11 kbar

1. Introduction

The amounts of H_2O in mantle peridotite compositions range from approximately 250 ppm in depleted MORB-source mantle to ~1160 ppm in the hypothetical primitive mantle (O'Neill & Palme, 1998), while the range of CO_2 contents is about 230-550 ppm (Zhang & Zindler, 1993; Jambon, 1994). H_2O and CO_2 are the most abundant and important magmatic volatile species (Bowen, 1928; Ingerson, 1960; Gill, 1981; McMillan, 1994; Blank & Brooker, 1994) and have a large influence on a large number of first order geological processes, including the formation of the oceans and the atmosphere (Rubey, 1951; Allegre et al., 1987), crust formation and evolution (Green, 1971; Ringwood, 1982; Hess, 1989), and the generation of basaltic magma in the upper mantle (Yoder & Tilley, 1962; Ringwood, 1975; Kushiro, 1975; Kushiro, 1990; Green & Falloon, 1998; Schmidt & Poli, 1998; Gaetani & Grove, 1998; Ulmer, 2001).

Extensive experimental studies have been carried out to study the effect of H_2O on mantle melting relations, both in simplified analogue systems (Kushiro et al., 1968a; Kushiro, 1969; Yoder, 1971; Kushiro, 1972), and with natural rock compositions (Kushiro et al., 1968b; Nicholls & Ringwood, 1972; Kushiro et al., 1972; Nicholls & Ringwood, 1973; Green, 1973; Mysen & Boettcher, 1975a, 1975b; Green, 1976; Kushiro, 1990; Hirose & Kawamoto, 1995; Hirose, 1997; Gaetani & Grove, 1998; Muntener et al., 2001). It is now rather clear that water substantially decreases the melting point of natural peridotite; as to its effect on the melt composition, however, there is still considerable disagreement. An early debate was whether hydrous melting of peridotite produced andesitic or basaltic magma (Nicholls & Ringwood, 1972; Green, 1973; Nicholls & Ringwood, 1973; Mysen & Boettcher, 1975a, 1975b; Green, 1976); this debate still continues (Kushiro, 1990; Hirose & Kawamoto, 1995; Hirose, 1997; Gaetani & Grove, 1998; Muntener et al., 2001). The only thermodynamic analysis so far, performed by Gaetani & Grove (1998), indicated a positive correlation between the

activity coefficient of SiO_2 and the H_2O content of melt; this disagrees with long recognised SiO_2-H_2O mixing model (Warner, 1973; Kushiro, 1975; Stolper, 1982a).

In experiments in the simple systems enstatite (En)-H_2O (Kushiro et al., 1968a), forsterite (Fo)–diopside (Di)–En–H_2O (Kushiro, 1969), Fo–Di–Silica (Qz)–H_2O (Kushiro, 1972) and Fo–nepheline (Ne)–Qz–H_2O (Kushiro, 1972), quartz-normative melt rather than olivine-normative melt were produced under water-saturated condition at pressures up to at least 17 kbar. These results support the hypothesis that subduction-related andesites represent primary partial melts of hydrous mantle peridotite (O'Hara, 1965). However, there are two major shortcomings in those experiments. Firstly, no spinel was added into these systems and its effect on partial melting can not be assessed. Yoder (1971) declared that the phase assemblage of Fo+Sp+Ox+Cpx+H_2O (Opx: Orthopyroxene; Cpx: Clinopyroxene) generated Qz-normative melts but did not report any experimental details or compositional data. Secondly, nearly all experiments, with only a few exceptions, were carried out under the extremes of either H_2O-free or H_2O-saturated conditions, making the thermodynamic evaluation of the effects of intermediate amounts of water uncertain. Considering the rapid increase of H_2O solubility in silicate melt with pressure (e.g., McMillan, 1994), the effect of water on melt composition under water-undersaturated conditions should form the most important part of a hydrous partial melting study.

The effect of CO_2 on partial melting in peridotites has been less extensively studied, either in simple systems or natural compositions. Most experimental studies have focused on the petrogenesis of carbonatitic - kimberlitic magmas (Mysen & Boettcher, 1975b; Mysen et al., 1976; Wyllie & Huang, 1976; Wyllie, 1977; Eggler, 1978; Eggler & Wendlandt, 1979; Green & Wallace, 1988; Wallace & Green, 1988; Falloon & Green, 1989; Ringwood et al., 1992; Dalton & Presnall, 1998a, 1998b). Due to the difficulty in analysing CO_2 content, experiments have been mostly carried out under fluid-saturated conditions. The solubility of CO_2 in silicate melts increases strongly with pressure (reviewed by Blank & Brooker 1994). Experimental data at relatively low pressures pertinent to the genesis of mid-ocean ridge basalt and island arc magma rock are few.

Only a few studies have been carried out to assess the combined effects of H_2O and CO_2 under fluid-saturated conditions (Mysen & Boettcher, 1975a, 1975b; Mysen, 1976; Taylor & Green, 1988, 1989). The only experimental study of mantle melting of which I am aware that treats both CO_2 and H_2O under fluid-absent conditions is the

recent work of Gaetani & Grove (1998), in which CO_2 was observed as an accidental contaminant in the product melt and its influence was ignored.

It follows that a partial melting experimental study with a simplified lherzolite phase assemblage in system CaO-MgO-Al_2O_3-SiO_2-H_2O-CO_2 (CMAS-H_2O-CO_2) at relatively low pressure is highly desirable. It will create a link between the anhydrous experimental studies and the fluid-saturated experimental studies thus potentially resolving some of the long-lasting discrepancies

2. Piston-cylinder experiments

2.1 Starting materials

Fine-grained mineral mixes adsorb moisture from the atmosphere quite readily. Therefore, because of the desirability of controlling the amounts of H_2O loaded into the capsules, glass starting materials were used in this study, rather than pre-crystallized mineral mixes as in my study on the system CMAS-K_2O (Chapter 2 of this thesis). The danger of using glass as the starting material is that it may crystallize initially to minerals with non-equilibrium compositions, for example, to pyroxenes with alumina contents that are too high. Once crystallised, such pyroxenes could fail to re-equilibrate. Here I can check for this problem rigorously, as the equilibrium compositions expected of the pyroxenes are well known (See Chapter 2 of this thesis). In addition, my previous work has shown that pyroxene compositions do change to their equilibrium values on the time scales used in this study, in the presence of melt (Chapter 2 and Chapter 3 of this thesis).

Table 1 lists the compositions of the starting materials. High-purity oxides (SiO_2, Al_2O_3 and MgO), carbonates ($CaCO_3$ and Na_2CO_3) and hydroxides ($Mg(OH)_2$ and $Al(OH)_3$) were used to prepare these mixtures.

Mixture SEM02-1 was made by melting the decarbonated oxide mix at 1600°C, 1 atm for 15 minutes. The composition was designed to crystallize to Fo:Sp:Opx:Cpx = 1:1:1:1 (by weight), assuming that Fo and Sp have their pure end-member compositions, while Opx and Cpx compositions were from run 116-3 in Table 2 of Walter & Presnall (1994).

SEM02-6 is the composition of the isobaric invariant melt for a simplified spinel lherzolite (Sp-lherzolite) in the system CMAS at 11 kbar, as obtained from the

Table 1 Starting materials

	SEM02-1	SEM02-6	SEM02-7*		SEM02-9*		SEM02-11*		SEM02-12		SEM02-14	SEM02-15
			1	2	1	2	1	2	1	2		
SiO_2	36.95	49.17	47.69	47.69	48.68	48.68	49.23	49.23	48.65	48.65	48.68	48.36
Al_2O_3	22.63	20.14	19.54	19.54	19.94	19.94	20.25	20.22	20.80	20.68	19.94	19.81
MgO	35.06	15.35	14.89	14.73	15.20	15.14	14.75	14.75	13.43	13.43	15.20	15.10
CaO	5.36	15.34	14.88	14.88	15.19	15.19	14.89	14.89	14.14	14.14	15.19	16.01
Na_2O	0.00	0.00	0.00	0.00	0.00	0.00	0.00	0.00	0.00	0.00	1.00	0.00
H_2O	0.00	0.00	3.00	2.77	1.00	0.92	0.87	0.82	2.97	2.78	0.00	0.00
CO_2	0.00	0.00	0.00	0.39	0.00	0.13	0.00	0.09	0.00	0.32	0.00	0.72
Total	100.00	100.00	100.00	100.00	100.00	100.00	100.00	100.00	100.00	100.00	100.00	100.00

*: 1 input; 2 calculated composition using the detected contents of H_2O and CO_2 in $Mg(OH)_2$ and $Al(OH)_3$.

Table 2 Testing experiments for starting materials and assembly arrangements at 11 kbar

Run #	SM	AA	T(°C)	Time(h)	Phase	Probe #	Thickness (cm)	FTIR #	H_2O (wt%)	CO_2(wt%)
C-1621*	SEM02-6	AA1	1340	24	Pure glass	8	0.1009	6	0.013(0.003)**	0.000(0.000)
C-1809	SEM02-6	AA2	1350	0.33	Pure glass	8	0.0227	6	0.058(0.005)	0.000(0.000)
C-1810	SEM02-11	AA2	1350	0.33	Pure glass	9	0.0088	6	0.720(0.012)	0.093(0.019)
C-1811	SEM02-9	AA2	1350	0.33	Pure glass	8	0.0080	6	0.858(0.011)	0.129(0.025)

*: from Chapter 2 of this thesis. 0.013(0.003)** should be read as 0.013 ± 0.003. SM: Starting materials. See Fig. 1 for assembly arrangement (AA).

experimental study in the system CMAS-K_2O (Chapter 2 of this thesis). The glass was prepared at 1400°C, 1 atm for 20 minutes before quenching. In order to produce SEM02-7, SEM02-9, SEM02-11 and SEM02-12, volatile-free glasses with appropriate composition were made first (also 1400°C, 1 atm and 20 minutes) and then the required amounts of $Mg(OH)_2$ or $Al(OH)_3$, both previously dried at 150°C for 24 hours, were added. SEM02-15 was generated by adding ~ 1.64% $CaCO_3$ powder, dried at 340°C and stored in a desiccator, to glass SEM02-6. The reason for using hydroxides as the source of H_2O was to control the amounts of H_2O accurately, given the very low levels of H_2O required in the experiments. Unfortunately, the subsequent analysis of the run product showed that these hydroxides were contaminated by considerable amount of carbonate. This will be discussed more fully below. In order to disentangle the effect of CO_2 from that of H_2O, some additional runs were therefore also done with H2O added as distilled H_2O.

In order to investigate the influence of small amounts of Na_2O in the other compositions, apparently present as impurities in the chemicals, glass SEM02-14, with 1 wt% Na_2O, was synthesised at 1400°C and 1 atm for 20 minutes.

All these mixtures were stored in an oven at 150°C during the time this study was carried out.

2.2 Experimental procedures

Experiments at 11 kbar were made in a conventional 12.7 mm diameter piston-cylinder apparatus (Boyd & England, 1960), using a NaCl-pyrex assembly, either with or without an Fe_2O_3 sleeve enclosing the capsule (Fig. 1). These assemblies have low friction and no pressure correction is thought to be required for the long run times and high temperatures of this study (Green et al., 1966; Bose & Ganguly, 1995; Klemme & O'Neill, 1997). Pt was used as the capsule material. The starting materials were packed into the capsule as layers in the sandwich or half-sandwich geometry.

The mass of the charge material in these experiments ranged from 11.6 mg to 19.1 mg. For the hydrous experiments, Pt capsules were welded immediately after loading. Wet tissue was used to blanket the capsule in order to prevent any water loss during the welding process (Hibberson, 1978). For anhydrous runs, loaded capsules were stored at 150°C for 6-8 hours first and later held in a steel block which had been pre-heated to 750°C while they were welded (Robinson et al., 1998; Chapter 2 and Chapter 3 of this thesis).

All experiments were performed using the 'piston-out' method, i. e. the pressure was first raised to a few kilobars, then the temperature was increased to 450°C to soften the pyrex sleeve, later the pressure was increased up to 0.5 kbar higher than the desired pressure, the temperature was increased to the nominal temperature of the run and finally the pressure was lowered to the required pressure (Johannes et al., 1971). The pressures were continuously monitored and adjusted, if necessary. The continual adjustment of pressure allowed each run to be controlled to within ± 0.2 kbar of the nominal pressure. Temperature was measured and controlled with $Pt_{94}Rh_6$-$Pt_{70}Rh_{30}$ thermocouple (type B) which was previously calibrated against the melting point of gold at 1 atm. Possible pressure effects on the emf of the thermocouple were ignored. The tip of the thermocouple, the upper ruby disc and at least the uppermost 2/3 of the Pt capsule containing the experimental charge were all carefully placed in the ~ 5 mm long hot spot of the experimental assembly. The systematics of the results both in this present study and in closely related previous work (Chapter 2 of this thesis) are consistent with temperature uncertainties of less than ± 10°C.

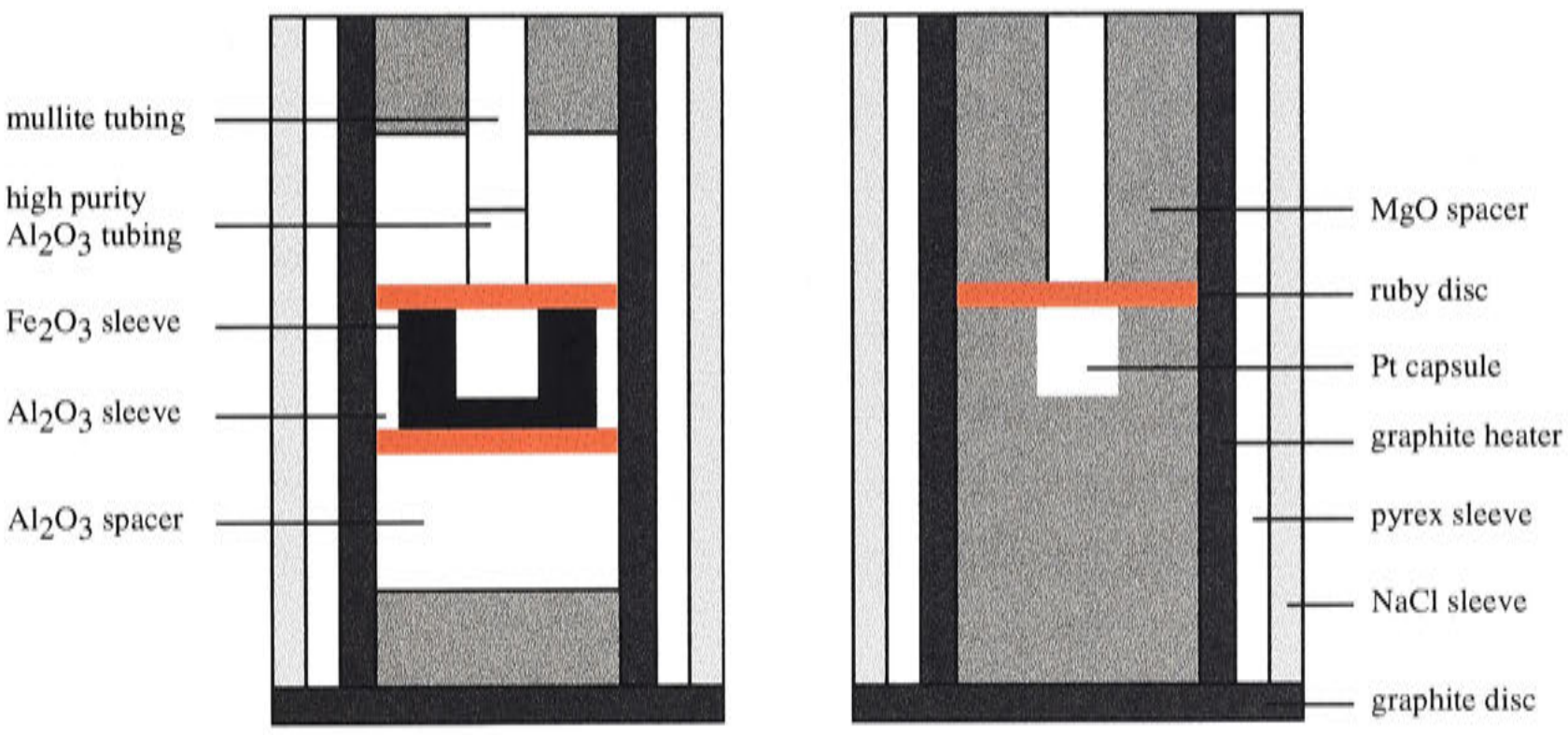

Fig. 1 Experimental assembly arrangement (AA1 and AA2) used in this study (not to scale).

2.3 Analytical conditions - Electron microprobe

At the end of a run, the sample was sectioned longitudinally, mounted in epoxy and polished using a series of diamond pastes. Run products were carbon-coated and analysed on a JEOL 6400 scanning electron microprobe in energy dispersive mode

(EDS) at the Electron Microprobe Unit (EMU) at ANU. Coexisting phases in all run products were carefully identified by back-scattered electron imaging. Beam current was 1 nA, accelerating voltage was 15 keV and analyses were reduced using the ZAF correction procedure (Ware, 1991). A beam spot size of 1 μm was used for all crystalline phases while both 1-μm and 10-μm beam spot sizes were used for glass analyses. Analytical accuracy and precision was tested by replicate measurements of two internationally-recognised glass standards, GOR132G and KL2G which have comparable composition to the phases present in this study (Jochum et al., 2000), as reported in Chapter 2 of this thesis.

Besides the expected major component oxides CaO, MgO, Al_2O_3, SiO_2, all analyses routinely sought Na_2O, FeO, Cr_2O_3 and K_2O. The latter three oxides were below the limits of detection and are not considered further, but significant amounts of Na_2O were detected in the melt in all runs (0.4 to 1.1 wt%, see Table 4). The origin of this Na_2O is enigmatic. Being an incompatible component, Na_2O is concentrated in the melt phase, so that it is below the detection limit in the analyses of the glass starting materials, and in various test runs designed to check for volatile contents (Table 2). It could be either from impurities in the oxides, hydroxides or carbonate from which the starting material glasses were prepared, or from contamination during the melting of these to glasses. To check that the Na_2O was not an analytical artefact, several runs were also analysed by WDS using the Cameca Camebax electron microprobe, at the Research School of Earth Sciences, ANU. Although analysed Na_2O contents were lowered by ~ 20%, this is likely due to the higher beam current used in WDS. Because of the good agreement between the EDS analyses and the recommended values of the secondary standards, I believe that the EDS results are more reliable.

2.4 Attainment of equilibrium

Several lines of evidence can be used to evaluate the approach to equilibrium of my experiments. These are as follows:

(1) The result of previous work in the system CMAS (Presnall et al., 1978; Sen & Presnall, 1984; Liu & Presnall, 1990) suggested that a period of several hours is adequate for the phases observed in this study to establish reversals of phase boundaries at liquidus temperatures. Experiments in the system CMAS+Na_2O (Walter & Presnall, 1994) and in the system CMAS+FeO (Gudfinnsson & Presnall, 2000) found that 48 hours was long enough for the attainment of equilibrium at temperatures close to the solidi. Most of my experiments ran for a longer time.

(2) Duplicate experiments at 1240°C and 1220°C demonstrate that pyroxene compositions are the same after 24 hours as for 94 hours, even at these relatively low temperatures (Table 3).

(3) The solid solutions, Opx and Cpx, in all experiments except the nominally anhydrous experiment C-1812 and two "two-stage" experiments (C-1807 and C-1808) show very good homogeneity in composition and demonstrate excellent internal consistency and consistency with previous work (Table 4). The compositions of the rims of the pyroxenes in C-1807 and C-1808 are also in excellent agreement with the other data, in fact only a few core compositions on larger crystals appear slightly anomalous. The most heterogeneous component, Al_2O_3, in the most heterogeneous phase (Cpx) for most experiments has one standard deviation < 0.5 wt.%, often just ~ 0.3 wt.%. The average difference between the calculated temperatures using the geothermometer of Nickel et al. (1985) and the nominal experimental temperatures is 17 K, further suggesting that Opx and Cpx are in mutual equilibrium.

(4) Almost perfect stoichiometry was found for all the solid phases by charge-balance calculation.

(5) A pair of "two-stage "reversal experiments (C-1807 and C-1808) have been conducted at 1295°C following the procedure of Presnall et al. (1978), Liu & Presnall (1990) and Baker & Stolper (1994). The melt compositions and rim pyroxene compositions from this pair are consistent with each other and with the other experiments.

3. FTIR analyses

Due to the availability of reliable analytical technique, the small size of experimentally prepared sample and the difficulty in sample preparation, the melt products of most hydrous experimental study were not analysed for H_2O. It is a pretty recent thing that FTIR spectroscopy, ion probe and oxygen-evaluating method are applied to nominal anhydrous and hydrous experimental study (Gaetani & Grove, 1998; Falloon et al., 1999; Falloon & Danyushevsky, 2000; Muntener et al., 2001; Falloon et al., 2001). The comparison study made by King et al. (2002) suggested that FTIR spectroscopy and ion probe are the best available techniques for volatile analysis.

In this study, the content of H_2O and CO_2 in the hydrous melt is detected by FTIR spectroscopy.

Table 3 Experimental conditions and phase assemblages

Run #	T(°C)	T(h)	Starting material	Assembly	ML	H_2O[a]	CO_2[a]	Phase observed	T-NBK85	T-BK90-1	T-BK90-2	T-F83
Experiment in system CMAS+H_2O+CO_2+Na_2O(trace)												
Experiment using $Mg(OH)_2$												
C-1601	1310	68	SEM02-1+SEM02-9	AA2	13.30	0.26	0.04	Fo+Sp+Melt				1395
C-1616	1310	49	SEM02-1+SEM02-9	AA2	11.60	0.10	0.01	Fo+Sp+Opx+Cpx+Melt	1298	1339	1232	1387
C-1602	1300	67	SEM02-1+SEM02-9	AA2	12.20	0.31	0.04	Fo+Sp+Opx+Cpx+Melt	1281	1325	1242	1381
C-1611	1280/1290	22/48	SEM02-1+SEM02-9	AA2	12.20	0.37	0.05	Fo+Sp+Opx+Cpx+Melt	1280	1324	1223	1380
C-1615	1280	75	SEM02-1+SEM02-9	AA2	12.80	0.46	0.06	Fo+Sp+Opx+Cpx+Melt	1270	1313	1228	1370
C-1623	1260	90	SEM02-1+SEM02-7	AA2	12.80	0.69	0.10	Fo+Sp+Opx+Cpx+Melt	1252	1296	1189	1369
C-1622[b]	1240	94	SEM02-1+SEM02-7	AA2	12.20	0.91	0.13	Fo+Sp+Opx+Cpx+Melt	1219	1262	1204	1362
C-1789	1240	24	SEM02-1+SEM02-7	AA2	14.20	0.74	0.10	Fo+Sp+Opx+Cpx+Melt	1247	1291	1204	1355
C-1633	1220	100	SEM02-1+SEM02-7	AA2	12.10	1.19	0.17	Fo+Sp+Opx+Cpx+Melt	1200	1243	1164	1355
C-1636	1200	117	SEM02-1+SEM02-7	AA2	12.10	1.53	0.21	Fo+Sp+Opx+Cpx+Melt	1183	1224	1143	1335
Experiment using $Al(OH)_3$												
C-1750	1310	49	SEM02-1+SEM02-11	AA2	15.60	0.06	0.01	Fo+Sp+Melt				1411
C-1716	1310	63	SEM02-1+SEM02-11	AA2	12.50	0.10	0.01	Fo+Sp+Opx+Melt			1223	1405
C-1729	1310	70	SEM02-1+SEM02-11	AA2	15.60	0.07	0.01	Fo+Sp+Opx+Melt			1214	1403
C-1759	1305	49	SEM02-1+SEM02-6+SEM02-11	AA2	18.40	0.02	0.00	Fo+Sp+Opx+Cpx+Melt	1320	1364	1255	1393
C-1719	1300	78	SEM02-1+SEM02-11	AA2	12.40	0.13	0.02	Fo+Sp+Opx+Melt			1232	1404
C-1747	1300	53	SEM02-1+SEM02-11	AA2	17.50	0.08	0.01	Fo+Sp+Opx+Melt			1228	1387
C-1734	1295	70	SEM02-1+SEM02-11	AA2	19.10	0.10	0.01	Fo+Sp+Opx+Cpx+Melt	1306	1349	1246	1394
C-1807	1300/1295	24/33	SEM02-1+SEM02-11	AA2	13.40	0.21	0.02	Fo+Sp+Opx+Cpx+Melt	1324	1363	1251	1386

C-1808	1280/1295	7/15	SEM02-1+SEM02-11	AA2	15.10	0.21	0.02	Fo+Sp+Opx+Cpx+Melt	1313	1355	1246	1392
C-1723	1290/1280	42.5/48	SEM02-1+SEM02-11	AA2	12.00	0.20	0.02	Fo+Sp+Opx+Cpx+Melt	1310	1352	1237	1383
C-1724	1270	92	SEM02-1+SEM02-11	AA2	13.00	0.25	0.03	Fo+Sp+Opx+Cpx+Melt[c]	1282	1326	1209	
C-1739	1260	88	SEM02-1+SEM02-12	AA2	14.30	0.60	0.07	Fo+Sp+Opx+Melt			1223	1381
C-1754	1260	94	SEM02-1+SEM02-12	AA2	14.90	0.54	0.06	Fo+Sp+Opx+Cpx+Melt	1285	1323	1218	1374
C-1741	1240	95	SEM02-1+SEM02-12	AA2	17.50	0.73	0.08	Fo+Sp+Opx+Cpx+Melt	1231	1275	1169	1354
C-1744[b]	1220	94	SEM02-1+SEM02-12	AA2	14.20	1.00	0.11	Fo+Sp+Opx+Cpx+Melt	1222	1264	1204	1333
C-1803	1220	24	SEM02-1+SEM02-12	AA2	14.50	0.98	0.11	Fo+Sp+Opx+Cpx+Melt	1241	1282	1242	1314
C-1742	1200	117	SEM02-1+SEM02-12	AA2	13.80	1.41	0.16	Fo+Sp+Opx+Cpx+Melt	1197	1239	1179	1323
Experiment using distilled H_2O												
C-1817	1335/1200	0.25/65	SEM02-1+SEM02-6+H2O	AA2	14.50	2.07	0.00	Fo+Sp+Opx+Cpx+Melt	1232	1275	1169	1353
Experiment using $CaCO_3$												
C-1812	1317	24	SEM02-1+SEM02-15	AA1	15.70	0.00	0.23	Fo+Sp+Opx+Cpx+Melt	1340	1385	1273	1375
Experiment in system CMASN												
C-1780	1314	70	SEM02-1+SEM02-14	AA1	-	-	-	Fo+Sp+Opx+Cpx+Melt	1347	1367	1286	1365
C-1773	1310	62	SEM02-1+SEM02-14	AA1	-	-	-	Fo+Sp+Opx+Cpx+Melt	1339	1359	1273	1369

AA, assembly arrangement; ML, material loaded (mg); [a], content in weight percent; [b], sample lost when making FTIR thin section; [c], too small to be accurately analysed. T-NBK85, temperature calculated by using the geothermometer in Nickel et al., (1985); T-BK-90-1, temperature calculated using equation 9 in Brey & Kohler (1990); T-BK-90-2, temperature calculated using equation 10 in Brey & Kohler (1990); T-F83, temperature calculated using the geothermometer of Ford et al. (1983).

Table 4 Phase composition on a volatile-free basis

Run #	Phase	CaO	MgO	Al_2O_3	SiO_2	Na_2O
Experiment in system CMAS+H_2O+CO_2+Na_2O(trace)						
Experiment using $Mg(OH)_2$						
C-1601, 1310°C	Fo(13)	0.28(0.04)	56.62(0.16)	0.18(0.06)	42.92(0.14)	-
	Sp(13)	0.08(0.03)	28.70(0.17)	70.97(0.17)	0.25(0.11)	-
	Melt(16)	14.02(0.14)	15.57(0.10)	20.64(0.08)	49.25(0.14)	0.51(0.05)
C-1616, 1310°C	Fo(12)	0.29(0.09)	56.61(0.20)	0.22(0.08)	42.97(0.12)	-
	Sp(12)	0.07(0.05)	29.03(0.10)	70.58(0.15)	0.32(0.12)	-
	Opx(15)	2.03(0.12)	34.81(0.16)	8.68(0.21)	54.48(0.26)	-
	Cpx(17)	19.14(0.29)	20.46(0.26)	8.59(0.25)	51.81(0.22)	-
	Melt(16)	14.13(0.15)	14.93(0.11)	20.50(0.14)	49.68(0.21)	0.75(0.05)
C-1602, 1300°C	Fo(16)	0.25(0.05)	56.61(0.20)	0.18(0.06)	42.95(0.16)	-
	Sp(17)	0.10(0.06)	29.10(0.11)	70.54(0.06)	0.26(0.04)	-
	Opx(28)	2.07(0.14)	34.85(0.19)	8.56(0.27)	54.52(0.20)	-
	Cpx(24)	19.49(0.23)	20.25(0.23)	8.65(0.23)	51.61(0.18)	-
	Melt(16)	14.89(0.12)	14.89(0.09)	20.14(0.11)	49.58(0.14)	0.49(0.05)
C-1611, 1290°C*	Fo(12)	0.28(0.04)	56.56(0.15)	0.22(0.08)	42.94(0.12)	-
	Sp(12)	0.08(0.05)	28.69(0.11)	70.93(0.15)	0.30(0.09)	-
	Opx(21)	1.96(0.20)	35.01(0.21)	8.49(0.38)	54.54(0.27)	-
	Cpx(22)	19.49(0.28)	20.28(0.23)	8.46(0.34)	51.77(0.23)	-
	Melt(16)	14.94(0.19)	14.80(0.12)	20.32(0.11)	49.40(0.19)	0.53(0.06)
C-1615, 1280°C	Fo(10)	0.29(0.04)	56.54(0.14)	0.20(0.10)	42.97(0.13)	-
	Sp(12)	0.15(0.04)	29.04(0.18)	70.50(0.20)	0.32(0.13)	-
	Opx(14)	1.99(0.11)	35.13(0.24)	8.37(0.31)	54.51(0.33)	-
	Cpx(22)	19.75(0.37)	20.23(0.33)	8.30(0.32)	51.73(0.24)	-
	Melt(16)	15.10(0.10)	14.40(0.11)	20.39(0.12)	49.62(0.13)	0.49(0.04)
C-1623, 1260°C	Fo(12)	0.22(0.04)	56.72(0.10)	0.16(0.07)	42.89(0.16)	-
	Sp(12)	0.07(0.03)	28.69(0.10)	71.00(0.10)	0.25(0.07)	-
	Opx(20)	1.78(0.19)	35.17(0.20)	8.25(0.37)	54.80(0.24)	-
	Cpx(22)	20.06(0.30)	19.90(0.31)	8.19(0.36)	51.85(0.28)	-
	Melt(16)	14.39(0.11)	14.30(0.13)	20.94(0.10)	49.72(0.16)	0.64(0.07)
C-1622, 1240°C	Fo(12)	0.23(0.06)	56.78(0.20)	0.12(0.06)	42.87(0.17)	-
	Sp(14)	0.07(0.05)	29.08(0.12)	70.66(0.14)	0.18(0.08)	-
	Opx(16)	1.85(0.36)	35.33(0.35)	8.07(0.35)	54.75(0.31)	-
	Cpx(17)	20.74(0.45)	19.58(0.25)	7.88(0.32)	51.80(0.20)	-
	Melt(16)	14.86(0.14)	13.93(0.14)	20.64(0.13)	49.81(0.20)	0.76(0.12)
C-1789, 1240°C	Fo(9)	0.22(0.04)	56.67(0.17)	0.36(0.16)	42.76(0.20)	-
	Sp(12)	0.06(0.04)	28.74(0.15)	70.83(0.23)	0.37(0.11)	-
	Opx(19)	1.86(0.35)	35.08(0.45)	8.65(0.46)	54.41(0.49)	-
	Cpx(23)	20.20(0.47)	19.58(0.32)	8.49(0.59)	51.73(0.38)	-
	Melt(12)	14.27(0.12)	13.76(0.17)	21.33(0.10)	20.03(0.18)	0.61(0.04)
C-1633, 1220°C	Fo(12)	0.21(0.05)	56.62(0.12)	0.17(0.08)	42.99(0.14)	-

Table 4 continued

	Sp(14)	0.10(0.06)	28.61(0.14)	70.95(0.24)	0.34(0.13)	-
	Opx(15)	1.65(0.18)	35.55(0.22)	7.90(0.19)	54.90(0.19)	-
	Cpx(26)	21.03(0.25)	19.36(0.18)	7.72(0.42)	51.89(0.31)	-
	Melt(16)	14.49(0.16)	13.76(0.07)	21.31(0.13)	49.84(0.16)	0.60(0.05)
C-1636, 1200°C	Fo(11)	0.22(0.04)	56.68(0.06)	0.12(0.05)	42.98(0.16)	-
	Sp(10)	0.05(0.04)	28.68(0.10)	71.08(0.12)	0.18(0.09)	-
	Opx(16)	1.53(0.06)	35.65(0.12)	7.88(0.17)	54.94(0.19)	-
	Cpx(18)	21.31(0.37)	19.22(0.34)	7.64(0.34)	51.83(0.26)	-
	Melt(15)	14.62(0.11)	13.08(0.10)	21.68(0.12)	50.18(0.18)	0.45(0.06)
Experiment using $Al(OH)_3$						
C-1750, 1310°C	Fo(11)	0.29(0.05)	56.57(0.25)	0.30(0.24)	42.83(0.22)	-
	Sp(12)	0.07(0.05)	28.79(0.11)	70.86(0.14)	0.27(0.12)	-
	Melt(13)	12.68(0.15)	16.20(0.10)	20.77(0.11)	49.72(0.13)	0.62(0.04)
C-1716, 1310°C	Fo(12)	0.27(0.04)	56.48(0.17)	0.23(0.06)	43.03(0.16)	-
	Sp(14)	0.11(0.05)	28.68(0.09)	70.93(0.10)	0.28(0.09)	-
	Opx(6)	1.98(0.25)	34.45(0.35)	9.10(0.22)	54.48(0.21)	-
	Melt(10)	13.39(0.10)	15.84(0.18)	20.46(0.12)	49.70(0.23)	0.62(0.05)
C-1729, 1310°C	Fo(15)	0.29(0.04)	56.51(0.09)	0.19(0.05)	43.02(0.08)	-
	Sp(11)	0.07(0.04)	28.77(0.15)	70.94(0.18)	0.22(0.12)	-
	Opx(20)	1.91(0.09)	34.93(0.17)	8.48(0.32)	54.69(0.26)	-
	Melt(12)	13.36(0.07)	15.64(0.08)	20.55(0.09)	49.72(0.11)	0.73(0.06)
C-1759, 1305°C	Fo(14)	0.30(0.06)	56.48(0.12)	0.20(0.08)	43.02(0.14)	-
	Sp(12)	0.06(0.04)	28.71(0.12)	70.98(0.11)	0.24(0.09)	-
	Opx(16)	2.15(0.14)	34.80(0.41)	8.25(0.52)	54.80(0.40)	-
	Cpx(22)	18.47(0.33)	20.79(0.26)	8.86(0.42)	51.88(0.31)	-
	Melt(16)	13.96(0.17)	15.25(0.09)	20.38(0.16)	49.73(0.19)	0.68(0.04)
C-1719, 1300°C	Fo(11)	0.27(0.06)	56.42(0.14)	0.22(0.06)	43.09(0.15)	-
	Sp(16)	0.08(0.05)	28.63(0.14)	70.99(0.11)	0.29(0.08)	-
	Opx(8)	2.04(0.11)	34.67(0.18)	8.72(0.19)	54.58(0.16)	-
	Melt(13)	13.59(0.16)	15.78(0.09)	20.41(0.12)	49.58(0.15)	0.64(0.03)
C-1747, 1300°C	Fo(11)	0.31(0.07)	56.46(0.15)	0.22(0.08)	43.02(0.16)	-
	Sp(13)	0.06(0.05)	28.60(0.06)	71.14(0.11)	0.20(0.10)	-
	Opx(19)	1.99(0.07)	34.65(0.10)	8.76(0.23)	54.61(0.22)	-
	Melt(16)	14.24(0.20)	14.95(0.16)	20.31(0.14)	49.79(0.13)	0.72(0.04)
C-1734, 1295°C	Fo(15)	0.30(0.06)	56.31(0.17)	0.19(0.06)	43.21(0.16)	-
	Sp(9)	0.11(0.06)	28.60(0.10)	70.96(0.11)	0.33(0.06)	-
	Opx(17)	2.10(0.15)	34.76(0.23)	8.38(0.44)	54.76(0.38)	-
	Cpx(12)	18.88(0.43)	20.47(0.37)	8.67(0.31)	51.97(0.21)	-
	Melt(16)	13.82(0.14)	15.16(0.10)	20.48(0.11)	49.77(0.13)	0.76(0.05)
C-1807, 1295°C	Fo(12)	0.29(0.05)	56.73(0.11)	0.25(0.05)	42.73(0.12)	-
	Sp(13)	0.07(0.05)	28.76(0.13)	70.94(0.09)	0.23(0.10)	-

Table 4 continued

	Opx(17)	2.14(0.12)	34.75(0.24)	8.66(0.46)	54.45(0.29)	-
	Cpx(18)	18.47(0.28)	20.84(0.32)	8.79(0.38)	51.90(0.31)	-
	Melt(11)	14.36(0.11)	15.12(0.09)	20.31(0.12)	49.64(0.13)	0.57(0.05)
C-1808, 1295°C	Fo(12)	0.30(0.04)	56.67(0.13)	0.24(0.08)	42.80(0.14)	-
	Sp(13)	0.06(0.03)	28.75(0.09)	70.93(0.19)	0.25(0.11)	-
	Opx(19)	2.11(0.13)	34.90(0.25)	8.49(0.63)	54.51(0.40)	-
	Cpx(19)	18.72(0.40)	20.75(0.35)	8.65(0.41)	51.87(0.33)	-
	Melt(17)	14.17(0.16)	15.53(0.10)	20.33(0.11)	49.57(0.17)	0.41(0.05)
C-1723, 1280°C	Fo(14)	0.27(0.05)	56.42(0.12)	0.25(0.12)	43.06(0.11)	-
	Sp(15)	0.11(0.06)	28.53(0.12)	71.06(0.13)	0.30(0.07)	-
	Opx(17)	2.06(0.09)	34.67(0.17)	8.58(0.38)	54.69(0.32)	-
	Cpx(26)	18.80(0.34)	20.33(0.27)	8.81(0.37)	52.06(0.24)	-
	Melt(15)	14.02(0.17)	14.38(0.08)	20.59(0.11)	49.90(0.13)	1.11(0.05)
C-1724, 1270°C	Fo(11)	0.31(0.12)	56.40(0.21)	0.33(0.13)	42.96(0.15)	-
	Sp(13)	0.08(0.05)	28.65(0.13)	71.10(0.13)	0.18(0.08)	-
	Opx(19)	1.88(0.12)	34.89(0.15)	8.51(0.37)	54.73(0.32)	-
	Cpx(25)	19.42(0.31)	20.09(0.27)	8.59(0.41)	51.90(0.28)	-
	Melt**					
C-1739, 1260°C	Fo(15)	0.29(0.03)	56.44(0.15)	0.17(0.05)	43.09(0.15)	-
	Sp(13)	0.07(0.03)	28.61(0.09)	71.05(0.12)	0.27(0.07)	-
	Opx(20)	1.97(0.11)	34.64(0.18)	8.94(0.32)	54.45(0.27)	-
	Melt(14)	14.15(0.11)	14.77(0.10)	20.69(0.15)	49.80(0.17)	0.59(0.04)
C-1754, 1260°C	Fo(14)	0.25(0.05)	56.61(0.15)	0.16(0.06)	42.99(0.11)	-
	Sp(13)	0.07(0.04)	28.75(0.11)	71.01(0.13)	0.17(0.09)	-
	Opx(22)	1.95(0.13)	34.84(0.20)	8.71(0.32)	54.51(0.23)	-
	Cpx(22)	19.51(0.23)	20.30(0.35)	7.96(0.53)	52.23(0.36)	-
	Melt(16)	14.32(0.15)	14.36(0.07)	20.65(0.10)	49.88(0.16)	0.79(0.05)
C-1741, 1240°C	Fo(12)	0.20(0.03)	56.48(0.11)	0.19(0.09)	43.13(0.09)	-
	Sp(13)	0.04(0.04)	28.60(0.10)	71.04(0.14)	0.32(0.06)	-
	Opx(22)	1.67(0.09)	35.22(0.28)	8.11(0.42)	55.00(0.25)	-
	Cpx(22)	20.47(0.38)	19.60(0.40)	7.93(0.43)	51.99(0.33)	-
	Melt(15)	14.04(0.12)	13.53(0.12)	21.31(0.18)	50.41(0.22)	0.71(0.05)
C-1744, 1220°C	Fo(14)	0.26(0.05)	56.63(0.10)	0.12(0.06)	43.09(0.14)	-
	Sp(10)	0.08(0.05)	28.65(0.09)	71.07(0.13)	0.20(0.12)	-
	Opx(22)	1.86(0.21)	34.99(0.30)	8.47(0.43)	54.68(0.27)	-
	Cpx(22)	20.73(0.17)	19.35(0.27)	8.06(0.49)	51.87(0.32)	-
	Melt(16)	14.39(0.14)	12.82(0.09)	21.67(0.05)	50.54(0.14)	0.58(0.06)
C-1803, 1220°C	Fo(11)	0.31(0.07)	56.56(0.13)	0.21(0.08)	42.92(0.16)	-
	Sp(10)	0.12(0.09)	28.60(0.17)	71.02(0.21)	0.25(0.14)	-
	Opx(22)	2.09(0.24)	34.89(0.27)	8.51(0.63)	54.51(0.41)	-
	Cpx(19)	20.42(0.35)	18.56(0.44)	8.07(0.60)	51.96(0.33)	-
	Melt(13)	13.91(0.14)	12.04(0.08)	22.38(0.08)	51.06(0.19)	0.61(0.05)

Table 4 continued

C-1742, 1200°C	Fo(13)	0.23(0.05)	56.58(0.14)	0.10(0.05)	43.09(0.12)	-
	Sp(14)	0.07(0.03)	28.65(0.12)	70.95(0.18)	0.33(0.12)	-
	Opx(26)	1.73(0.24)	35.20(0.36)	8.22(0.41)	54.85(0.30)	-
	Cpx(26)	21.12(0.22)	19.16(0.31)	7.87(0.65)	51.85(0.40)	-
	Melt(14)	14.27(0.18)	12.50(0.09)	21.88(0.12)	50.81(0.18)	0.54(0.04)
Experiment using distilled H_2O						
C-1817, 1200°C	Fo(12)	0.18(0.06)	56.82(0.21)	0.23(0.29)	42.77(0.14)	-
	Sp(10)	0.08(0.04)	28.66(0.09)	71.18(0.09)	0.08(0.06)	-
	Opx(22)	1.67(0.11)	35.55(0.23)	8.07(0.47)	54.71(0.28)	-
	Cpx(22)	20.46(0.41)	19.73(0.38)	7.88(0.71)	51.93(0.46)	-
	Melt(14)	14.26(0.14)	13.90(0.09)	21.56(0.12)	49.87(0.13)	0.41(0.04)
Experiment using $CaCO_3$						
C-1812, 1317°C	Fo(10)	0.30(0.04)	56.71(0.08)	0.47(0.15)	42.52(0.09)	-
	Sp(15)	0.08(0.04)	28.85(0.11)	70.74(0.18)	0.33(0.14)	-
	Opx(16)	2.28(0.11)	34.76(0.36)	8.52(0.60)	54.45(0.41)	-
	Cpx(20)	17.79(0.78)	21.04(0.80)	9.94(0.74)	51.23(0.67)	-
	Melt(13)	14.91(0.31)	14.80(0.08)	20.37(0.12)	49.52(0.13)	0.40(0.04)
Experiment in system CMASN						
C-1780, 1314°C	Fo(13)	0.30(0.05)	56.63(0.17)	0.19(0.07)	42.87(0.14)	-
	Sp(13)	0.11(0.07)	28.71(0.11)	70.99(0.15)	0.19(0.12)	-
	Opx(18)#	2.35(0.23)	34.34(0.38)	8.89(0.46)	54.37(0.26)	0.06(0.04)
	Cpx(21)#	17.97(0.42)	21.08(0.40)	8.83(0.54)	51.90(0.38)	0.22(0.06)
	Melt(16)	14.67(0.18)	13.79(0.24)	20.50(0.19)	50.01(0.16)	1.03(0.04)
C-1773, 1310°C	Fo(11)	0.28(0.05)	56.53(0.16)	0.25(0.11)	42.94(0.14)	-
	Sp(11)	0.08(0.05)	28.64(0.12)	71.09(0.15)	0.19(0.14)	-
	Opx(21)	2.28(0.25)	34.21(0.36)	9.15(0.51)	54.15(0.35)	0.22(0.06)
	Cpx(21)	18.12(0.43)	20.49(0.41)	9.17(0.50)	51.79(0.34)	0.43(0.06)
	Melt(15)	13.61(0.15)	12.96(0.51)	20.92(0.50)	50.44(0.14)	2.07(0.10)

*, only the final experimental temperature listed here for the "two-stage" experiments; **, too small to be accurately analysed; #: Na_2O content checked by WDS technique on a Cameca electron microprobe at RSES, ANU. The Na_2O content given by EDS might be higher than the real value by ~ 0.1% at high content conditions (> 1%?) but by ~ 0.2% at low content conditions (< 1%?).

3.1 Sample preparation

After analysing all phases by electron probe, I made the thin sections for FTIR analysing. Sample was first removed from the epoxy and then sawed to appropriate thickness by a diamond saw. It was later mounted to a piece of glass by using crystal-bond, reduced to desirable thickness by manually grinding against a series of silicon carbide abrasive films (3-9 μm) under ethanol or water, and finally polished on both sides using a 1 μm silicon carbide abrasive film. After removed from the glass at a

temperature of 125 °C, thin section was thoroughly washed in acetone for 30 minutes in order to dissolve away all crystal-bond.

Sample water content and sample thickness are crucial to the success of FTIR analysis because they affect the absorbance of infrared light by the sample (Ihinger et al., 1994). There are a number of absorbance peaks which can be used to quantify the fluid contents in a silicate melt. I decided to use the absorbance peak at ~ 3550 cm^{-1} to analyse H_2O and the absorbance peaks at 1300-1700 cm^{-1} to analyse CO_2 due to the availability of more information about them in the literature (fluid content, sample thickness and the absorbance). The water content of melts in the samples was roughly calculated by mass-balance skills and the appropriate thickness range was estimated for each sample, based on Stolper (1982b) and Fine & Stolper (1985/1986). Effort was finally put in making the sample thickness into the estimated thickness ranges.

26 thin sections were successfully made from the samples of the 28 hydrous experiments which contained large and quench-free melts. Their thickness was directly measured by a micrometer and ranges from 14 μm to 223 μm (Table 5) and the thickness uncertainty was estimated as ~ ± 2 μm, similar to Stolper (1982b).

3.2 Analysing condition

Measurements were carried out using a Bruker IFS-28 infrared spectrometer with attached Bruker A590 infrared microscope and Bruker Opus/IR reduction software, hosted in RSES, ANU. The entire system was purged with dry N_2 to reduce possible background contributions from atmospheric H_2O and CO_2. FTIR samples were directly put over apertures in an aluminium plate. Diameters of analysed areas varied from 30 μm to 105 μm, dependent to the sizes of the quench-free melt pools. During each analysis 100 scans were collected with the resolution of four wavenumbers between 5500 cm^{-1} and 600 cm^{-1}.

3.3 Infrared spectroscopy

Transmission infrared spectra in the 5500-600 cm^{-1} frequency range were collected for all samples. All spectra were plotted as absorbance versus wavenumber and these plots were used for measurements of background-subtracted absorption intensities; the background line was determined by drawing straight line through the minimums at the high and low wavenumber ends of the absorption peaks (Fig. 2). The

background-subtracted spectra for those experiments displaying melt coexisting with a Sp-lherzolite phase assemblage are shown in Fig. 3. The heights of the related absorption peaks are summarised in Table 5.

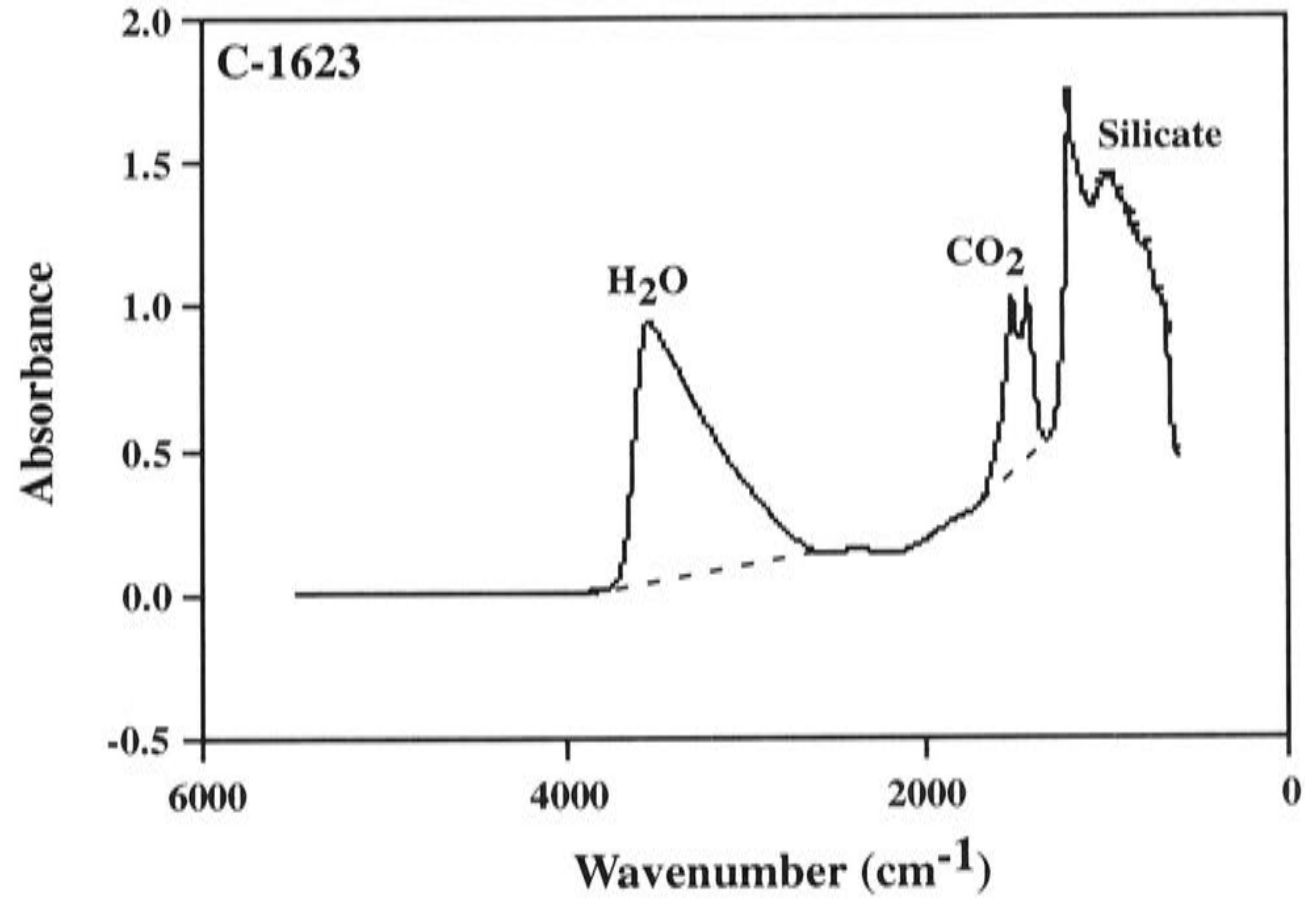

Fig. 2 Infrared spectrum of C-1623 with background to show the background-subtraction process. For information about the thin section, see Table 5.

The peak at ~ 3550 cm^{-1} is caused by the fundamental OH-stretching vibration and used to determine the water content in melts. The peaks at ~ 1515 cm^{-1} and ~ 1415 cm^{-1} are caused by the asymmetric stretch of distorted carbonate groups and I used these two peaks to measure the CO_2 content in melts.

In all cases no absorbance peak is observed for crystal-bond or epoxy, which has intense and characteristic absorbance bands in the C-H region. Also no peak is observed in the 2985-2600 cm^{-1} range and this agrees with Stolper (1982b). A peak in this region was attributed by Scholze (1959) to strong hydrogen-bonding of Si-OH groups to non-bridging oxygens. Only occasionally small positive or negative peak at ~ 2350 cm^{-1} is observed and I believe that it is caused by the background CO_2 in the air. Carbon should present in these melts entirely as carbonate (Fine & Stolper, 1985/1986; Pan et al., 1991; Pawley et al., 1992; King & Holloway, 2002).

Several samples are sufficiently parallel that their spectra show oscillation which may be used to measure the sample thickness, provided that the index of refraction of the melts is appropriately measured (more on this topic later).

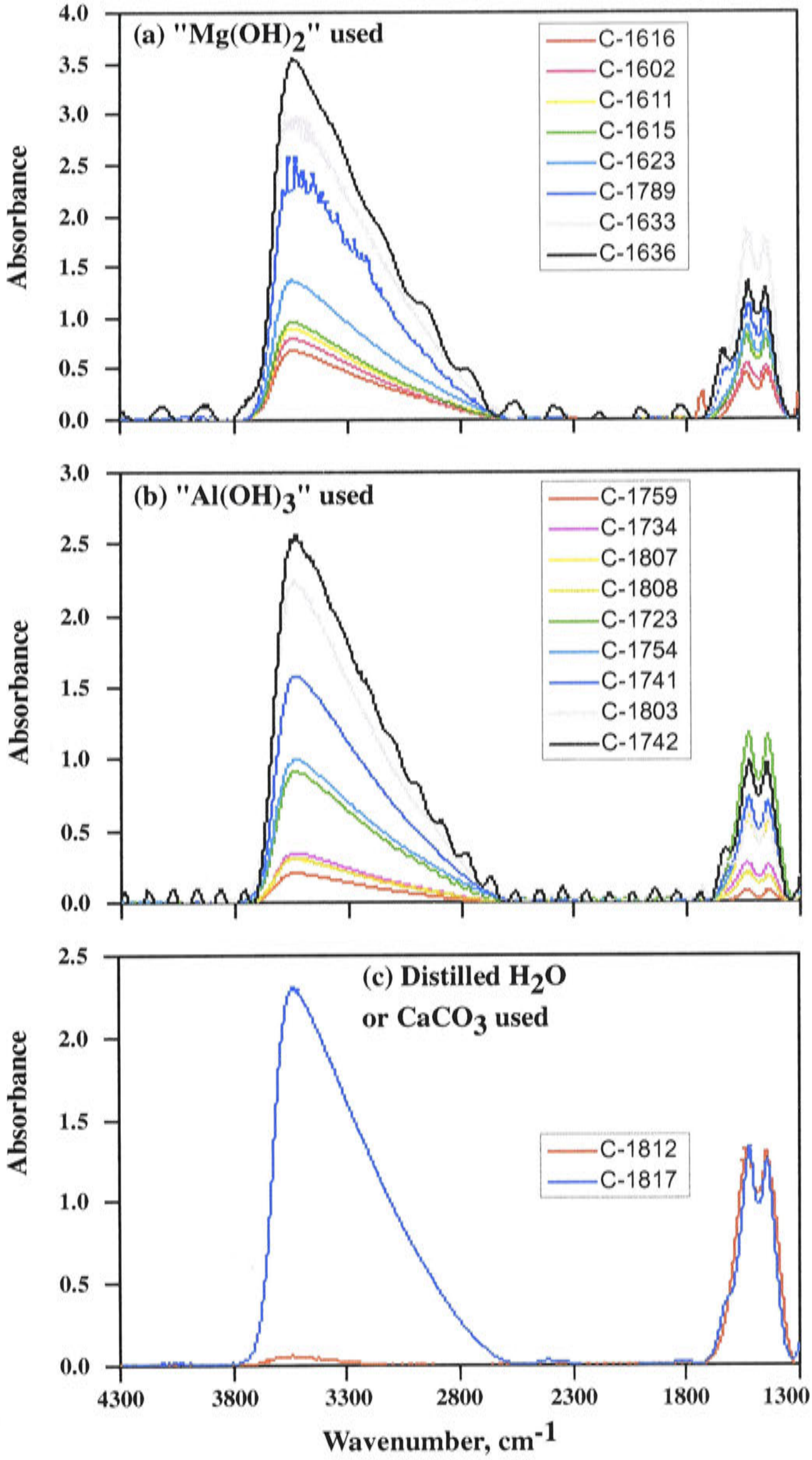

Fig. 3 FTIR spectra taken on doubly-polished run products for experiments using $Mg(OH)_2$ (a), for experiments using $Al(OH)_3$ (b), and for experiments using $CaCO_3$ or distilled H_2O (c). Spectra have been scaled to a constant sample thickness of 100 μm.

Three small problems are observed here. One sample (C-1633) has its absorbance peak at ~ 3550 cm^{-1} truncated and its water content can not be accurately measured. This sample is relatively thick and its peak at ~ 3550 cm^{-1} is slightly higher (~ 1.9) than the detection limit (0.1-1.8; Ihinger et al., 1994). Spectra taken on the sample of C-1789 show sharp peaks at ~ 3550 cm-1 position rather than smooth rounded curves. Sharp peaks usually indicate crystalline ordered structures (Pan et al., 1991); thus, a small amount of crystals might have been incorporated in the spectra and the water content of the melt in this sample may be not very accurate. The third small problem is the spectra of C-1616 show a strange peak at ~ 1700 cm^{-1}. It is possible that this peak might be due to the HOH bending vibration (Ihinger et al., 1994; King et al., 2002), indicating the presence of molecular water.

3.4 H_2O and CO_2 in melt

The Beer-Lambert law is used to quantitatively relate absorbance intensity to the concentration of the absorbing species, here H_2O and CO_2:

$$C = (M * A) / (D * \rho * \varepsilon) \quad (1)$$

where C is the concentration of H_2O or CO_2 (weight percent), M is molecular weight of H_2O (18.02) or CO_2 (44.01), A the height of the absorbance peak, D the thickness of sample (cm), ρ the density of melts (g/l) and ε the calibration factor for H_2O (67 from Stolper, 1982b) or for CO_2 (375 from Fine & Stolper, 1985/1986).

In order to use the Beer-Lambert law to determine the content of H_2O and CO_2 in melts, the density, ρ, must be determined first. Due to the limitation of sample size and the difficulty separating melt from solid phases, direct density measurement is not possible. Rather than assuming a density to carry on the calculation like Stolper & Holloway (1988), Pan et al. (1991) and Pawley et al. (1992), I used the software Magma2 (Wohletz, 1996) to calculate the density of the melt for each sample. Before conducting the calculation, I used the available density-composition data in the literature to check the software. Fig. 4 suggests Magma2 can accurately reproduce the density of the glasses with low FeO content, regardless of their formation condition (pressure and temperature). The study system here contains no iron and the uncertainty in the density calculation is probably ~ ± 2 %. The calculation procedure is: (a) making an initial guess of the melt density; (b) using the Beer-Lambert law to calculate the H_2O content of the melt; (c) renormalising the melt composition using the calculated H_2O

content and the electron probe data; (d) calculating the melt density using the software Magma2 (CO_2 is ignored in this step). If the newly calculated density matches the initial guess, calculation stops; otherwise, another round of calculation is needed. The calculated density is summarised in Table 5. The relative difference between the maximum density (2776 g/l, C-1812) and the minimum density (2555 g/l, C-1636) is less than 10%, so that the assumption of Stolper & Holloway (1988), Pan et al. (1991) and Pawley et al. (1992) is reasonable.

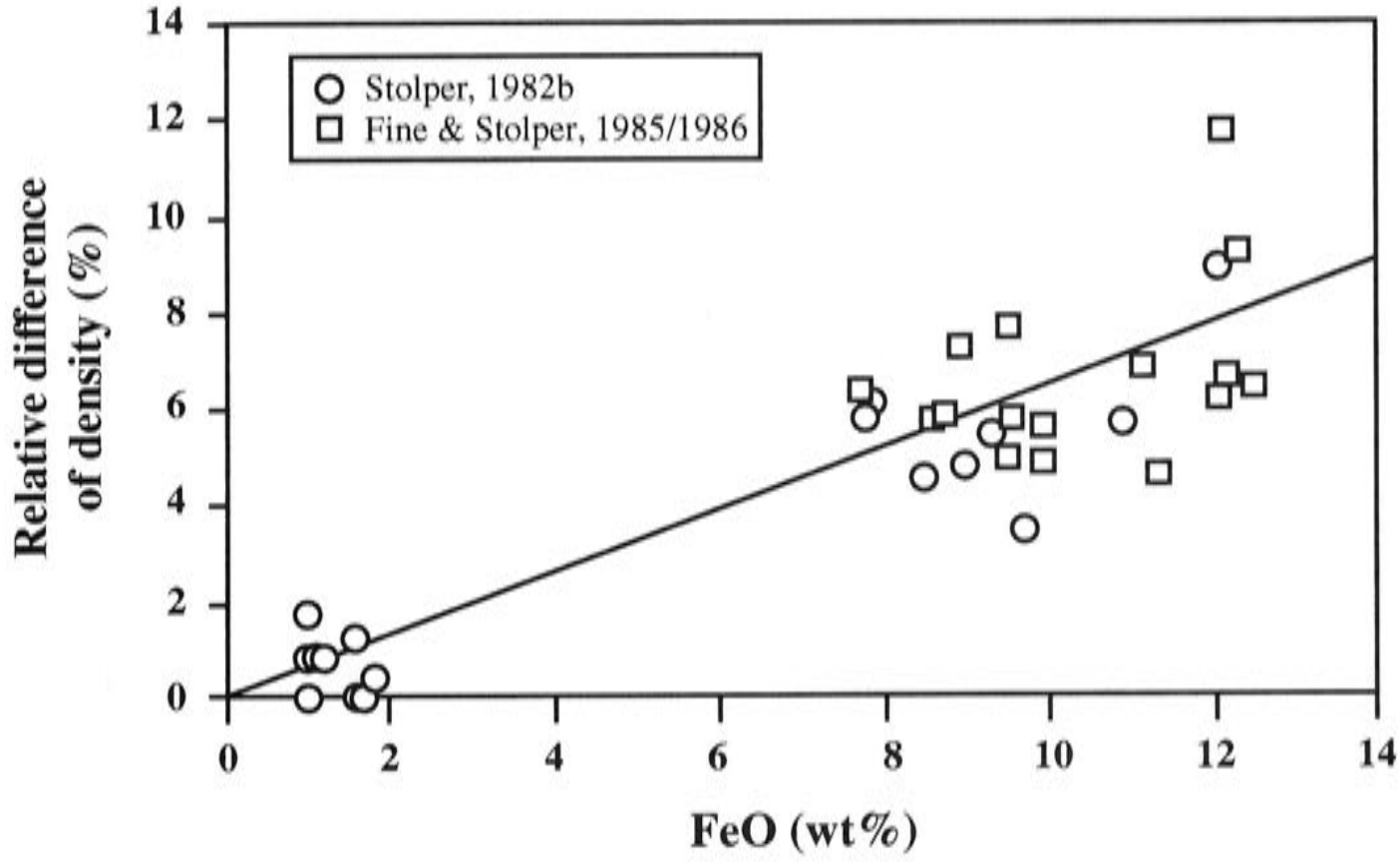

Fig. 4 Correlation of the FeO content in glasses to the relative difference of density between directly measured density and calculated density using software Magma2. For the technique used in direct density measurement, see the references cited.

The H_2O contents of melts calculated in this procedure are summarised in Table 5. It seems likely there is a linear relationship between the density and the H_2O content of the melt (Fig. 5) and 1 wt% H_2O decreases the density of the melt by ~ 56 g/l.

With the calculated density data, the CO_2 content of the melt is straightforwardly calculated by the Beer-Lambert law and is summarised in Table 5.

With some simple assumptions (Table 5), the uncertainty of the concentration of H_2O and CO_2 has been assessed. The results show that the uncertainty in thickness measurement is very important to the accuracy of the FTIR technique when the sample is very thin. It would be desirable to put some independent constraints on the thickness measurement.

Table 5 FTIR data

Run #	Thickness (cm)	ρ (g/liter)	A. #	H_2O Absorbance	H_2O (wt%)	CO_2 Absorbance	CO_2(wt%)
Experiment using $Mg(OH)_2$							
C-1601	0.0136	2748	5	0.843(0.011)	0.61(0.02)	0.418(0.022)	0.13(0.01)
C-1616	0.0169	2754	4	0.685(0.004)	0.40(0.01)	0.478(0.016)	0.12(0.01)
C-1602	0.0152	2734	3	0.955(0.005)	0.62(0.02)	0.636(0.022)	0.18(0.01)
C-1611	0.0070	2734	4	0.633(0.007)	0.89(0.04)	0.579(0.015)	0.35(0.02)
C-1615	0.0068	2729	3	0.654(0.014)	0.95(0.04)	0.542(0.019)	0.34(0.02)
C-1623	0.0067	2703	4	0.900(0.047)	1.33(0.09)	0.589(0.026)	0.38(0.02)
C-1789	0.0047	2630	5	1.199(0.125)	2.31(0.30)	0.490(0.068)	0.47(0.07)
C-1633	0.0065	2619	5	1.914(0.020)	2.98(0.13)	1.157(0.030)	0.80(0.04)
C-1636	0.0014	2555	8	0.552(0.031)	4.16(0.65)	0.216(0.015)	0.71(0.11)
Experiment using $Al(OH)_3$							
C-1750	0.0103	2751	3	0.490(0.008)	0.46(0.02)	0.300(0.009)	0.12(0.01)
C-1716	0.0223	2763	4	0.638(0.021)	0.28(0.01)	0.373(0.052)	0.07(0.01)
C-1729	0.0124	2764	7	0.259(0.003)	0.20(0.01)	0.156(0.007)	0.05(0.00)
C-1759	0.0222	2766	6	0.472(0.011)	0.21(0.01)	0.187(0.024)	0.04(0.00)
C-1719	0.0158	2764	6	0.556(0.012)	0.34(0.01)	0.382(0.021)	0.10(0.01)
C-1747	0.0192	2763	3	0.493(0.019)	0.25(0.01)	0.085(0.006)	0.02(0.00)
C-1734	0.0164	2758	6	0.581(0.015)	0.35(0.01)	0.443(0.019)	0.11(0.01)
C-1807	0.0079	2765	5	0.248(0.005)	0.30(0.01)	0.451(0.014)	0.24(0.01)
C-1808	0.0054	2769	5	0.178(0.010)	0.33(0.02)	0.112(0.011)	0.09(0.01)
C-1723	0.0060	2718	6	0.546(0.006)	0.90(0.11)	0.696(0.007)	0.50(0.02)
C-1739	0.0087	2725	5	0.937(0.040)	1.06(0.16)	0.543(0.017)	0.27(0.01)
C-1754	0.0080	2726	7	0.767(0.030)	0.94(0.05)	0.548(0.020)	0.29(0.02)
C-1741	0.0058	2666	10	1.062(0.064)	1.85(0.14)	0.476(0.038)	0.36(0.03)
C-1803	0.0037	2623	1	0.831	2.30	0.228(0.005)	0.28(0.02)
C-1742	0.0025	2626	8	0.623(0.035)	2.55(0.26)	0.225(0.017)	0.40(0.05)
Experiment using distilled H_2O							
C-1817	0.0024	2643	7	0.630(0.041)	2.67(0.29)	0.350(0.025)	0.65(0.07)
Experiment using $CaCO_3$							
C-1812	0.0091	2776	6	0.050(0.006)	0.05(0.01)	1.213(0.074)	0.56(0.04)

0.843(0.011), average followed by one standard deviation, should be read as 0.843 ± 0.011. A. #, number of analyses. The one standard deviation of H_2O and CO_2 is the square root of variance (Var), which is approximated by a Taylor expansion:

$$Var(C) = \left(\frac{MA}{D\rho\varepsilon}\right)^2 \left[\frac{Var(A)}{A^2} + \frac{Var(D)}{D^2} + \frac{Var(\rho)}{\rho^2}\right].$$

All these variables of the right hand side of the above equation are assumed to be independent. No uncertainty is assumed for the molecule weight of H_2O and CO_2, and for the calibration factor (ε) while the one standard deviation is assumed to be 2 μm for thickness measurement (D), 3% for density calculation (ρ). The uncertainty in the content of H_2O and CO_2 in the melt of C-1636 is mainly (relatively 83%) attributed by the 2-μm uncertainty in thickness measurement.

As shown above, several FTIR spectra display oscillation which can be used to measure sample thickness (C-1636 in Fig. 3a and C-1723 and C-1742 in Fig. 3b).

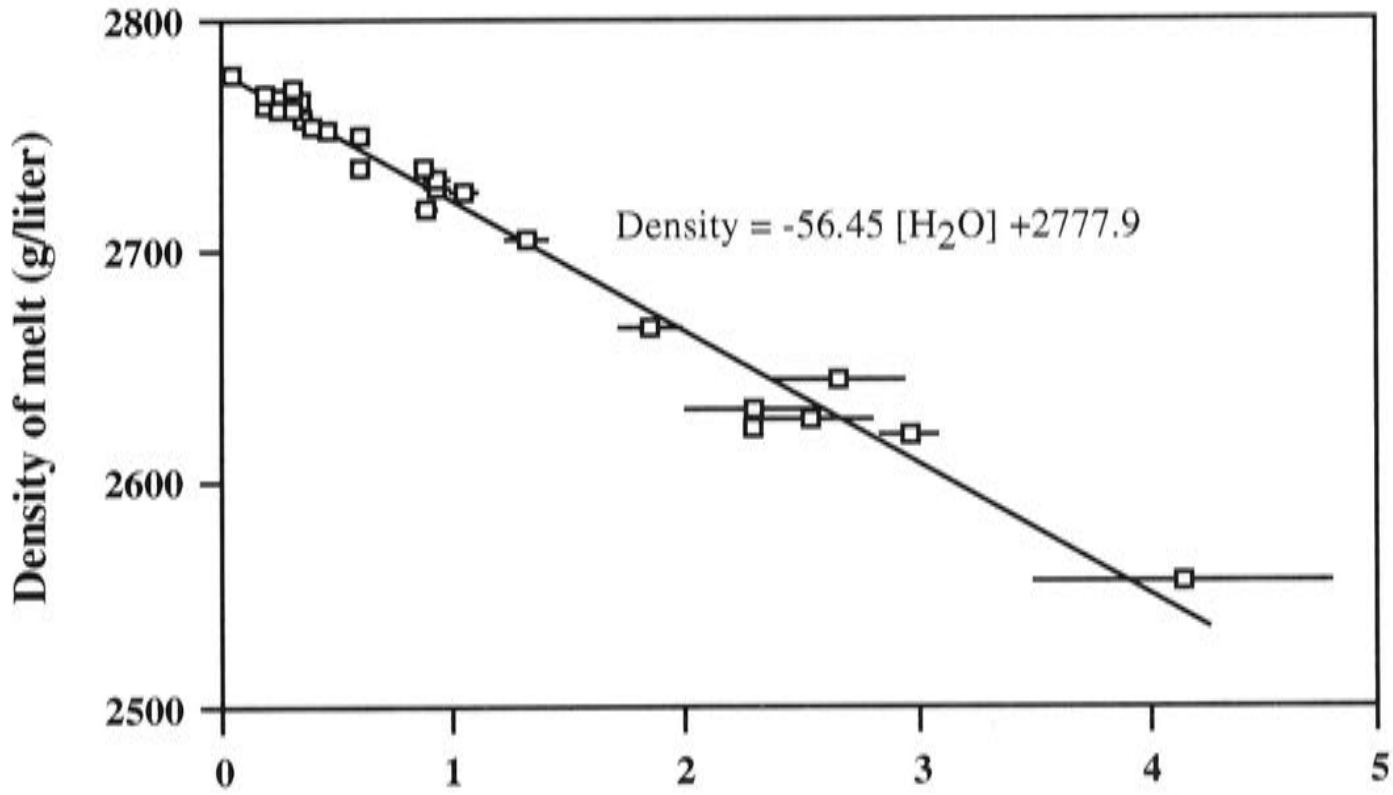

Fig. 5 Correlation of the H_2O content of melt to the calculated density using software Magma2. Error bar in this diagram and others in this study indicates one standard deviation.

The refractive index of the melt is calculated by the method of Church & Johnson (1980) which ignores H_2O and CO_2. Due to the missing mass of H_2O and CO_2, the calculated refractive index should be lower than the real refractive index, so that larger calculated thickness than real thickness should be expected and the difference between them should be positively correlated with the missing mass. These expectations are confirmed by the calculation result (Table 6 and Fig. 6).

Table 6 Thickness of sample and refractive index of glass

Sample #	Thickness-1	H_2O+CO_2	RI	Thickness-2
C-1636	14(2)	4.87(0.91)	1.547	18.7(1.2)
C-1742	25(2)	2.95(0.44)	1.556	28.2(2.4)
C-1723	60(2)	1.40(0.17)	1.568	61.7(0.4)

Thickness-1: direct measurement by micrometer (μm); H_2O+CO_2: mass of H_2O and CO_2 in the glass (weight percent; from Table 5); Thickness-2, calculated thickness (μm); RI, refractive index.

Thickness-2 is calculated by the following equation:

$$\text{Thickness(cm)} = 1/(2*n*\upsilon)$$

where n is the refractive index (RI) calculated by the method of Church & Johnson (1980) and υ is the wave length shown by the oscillation of the spectra.

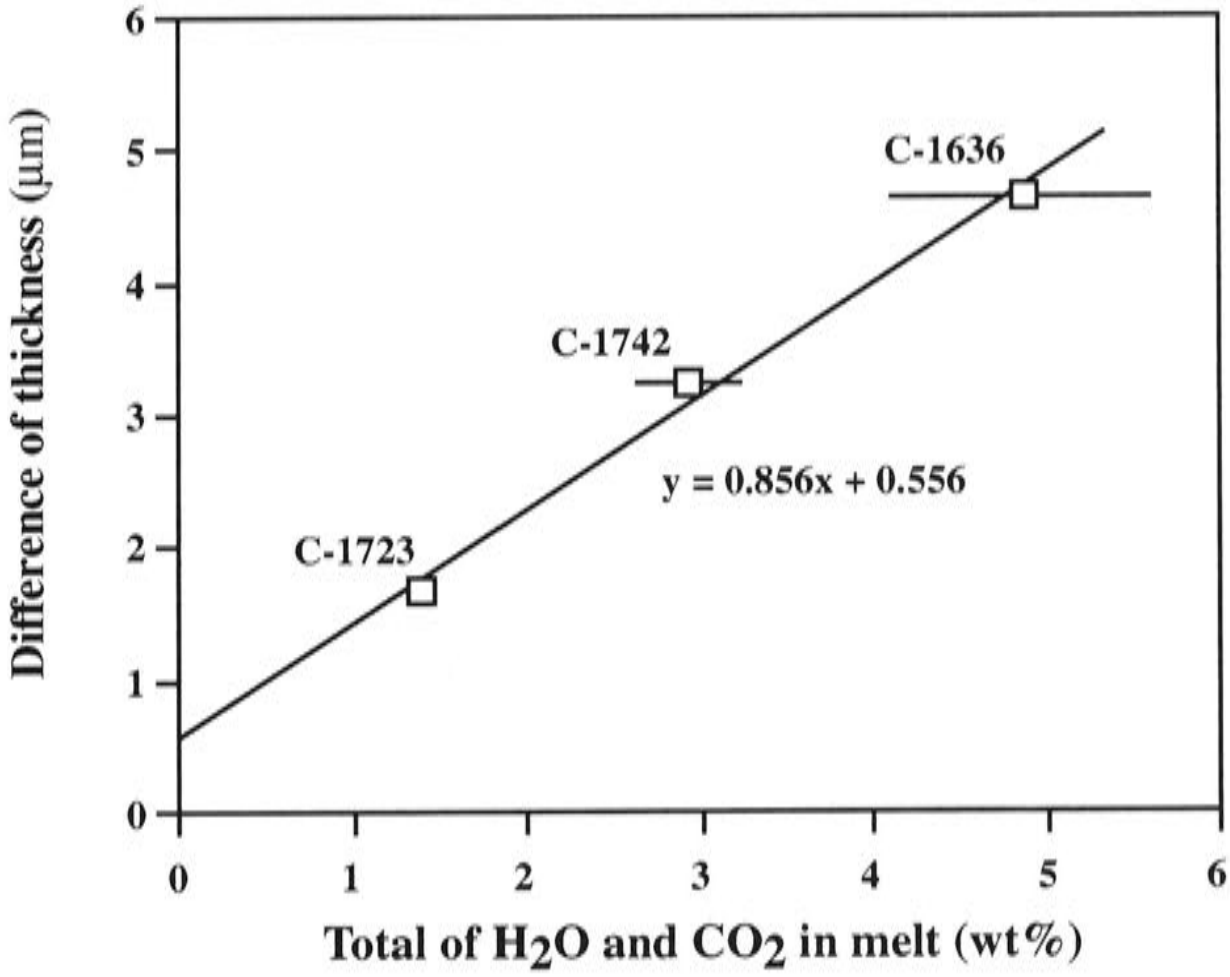

Fig. 6 Correlation of the difference in thickness between that determined from the interference oscillation using refractive index calculated from Church & Johnson (1980) and direct measurement, and the mass ignored in the calculation of the refractive index of the melt (H_2O and CO_2 in the melt from Table 5).

4. Experimental results

Table 3 summarises the starting materials, the piston-cylinder pressure assemblies used, the run conditions and the phases observed in the experiments. The mass of the charge loaded and the initial water and estimated carbon dioxide contents are also given. The temperature range covered in this study is from 1200 to 1317 °C, with run durations from 24 to 117 hours; most runs were longer than 48 hours. Out of 28 experiments with added water, 21 have melt coexisting with the Sp-lherzolite phase assemblage (Fo+Opx+Cpx+Sp), five experiments display melt coexisting with Fo+Opx+Sp, and in the remaining two experiments melt coexists with Fo+Sp only.

In order to assess the effect of Na_2O impurities on the solidus, two experiments were carried out in the system CMAS-Na_2O, and to constrain better the effect of CO_2, one experiment with only CO_2 and no initial H_2O was also performed.

The compositions of all phases from electron microprobe analyses are presented in Table 4. Melt compositions are given renormalized to 100% on a volatile-free basis. Volatile contents from FTIR spectroscopy are given in Table 5.

4.1 Compositions of crystalline phases

Fo and Sp have almost the pure end-member compositions, although Fo has ~ 0.3 wt% CaO, approximately consistent with the amounts expected from previous work (e.g., Kohler & Brey, 1990; Libourel, 1999; Chapter 3 of this thesis). The amount of CaO held in olivine at near-solidus temperatures is an important part of the whole-rock budget of CaO in depleted mantle peridotites, and should not be overlooked.

Pyroxenes were homogenous, except in two "two-stage" reversal experiments C-1807 and C-1808, where occasionally the cores of larger pyroxene crystals returned anomalous compositions, and in C-1812 (CO_2 only, no initial H_2O), which was run for just 24 hours, the alumina content of the Cpx appears slightly high. Na_2O in clinopyroxene is close to the limit of detection in most experiments (~ 0.1 wt%), and is not reported except in a few experiments where it is clearly above 0.1 wt%.

The Ca exchange geothermometer between Opx and Cpx calibrated by Nickel et al. (1985) reproduces the nominal experimental temperature very well, with an average difference of 17 degrees (Fig. 7). Of other two-pyroxene geothermometers, equation (9) in Brey & Kohler (1990) gives systematically higher and more scattering calculated temperatures with an average difference of 47 degrees, while equation 10 in Brey & Kohler (1990) gives systematically lower calculated temperatures, with an average difference of 51 degrees. These results are similar to that found in my previous study of the system CMAS-K_2O (Chapter 2 of this thesis).

4.2 Compositions of partial melts

Although quench Cpx, present as overgrowths, usually 1-2 μm thick, mainly rimming pre-existing stable Cpx and Opx, was observed in all experiments, pockets of melt with a diameter commonly > 100 μm were observed in all experiments except C-1724 and C-1773. Such pockets are sufficiently large that their middle portions are unaffected by this quench modification. The extent of partial melting in C-1724 is very low and good analysis of the melt was not possible. The melt in C-1773 was analysed and the result appears consistent with that from other experiments, although observed standard deviations are larger. All other experiments produce homogeneous melt, with typical one standard deviations ranging from ±0.04% for Na_2O to ±0.20% for SiO_2.

The compositions of melts are plotted in Fig. 8 in the projection from Diopside (Di: $CaMgSi_2O_6$) onto the plane Jd+CaTs-Fo-Qz (Jd = $NaAlSi_2O_6$; CaTs = $CaAl_2SiO_6$) (Falloon & Green, 1988). The melt at the invariant point Fo+Sp+Opx+Cpx+Melt in the system CMAS at 11 kbar is an olivine tholeiite. The effect of Na_2O is to shift the

composition towards the silica-undersaturated plane Di-Fo. The effect of H_2O is to shift the composition of melts in the opposite direction in this projection, towards the Ab+An-En (Ab = $NaAlSi_3O_8$; An = $CaAl_2Si_2O_8$; En = $Mg_2Si_2O_6$) plane; the melts becoming quartz-normative at ~ 3% H_2O. It should be noted that I have not corrected the experimental melt compositions for the small amounts of Na_2O and CO_2 present.

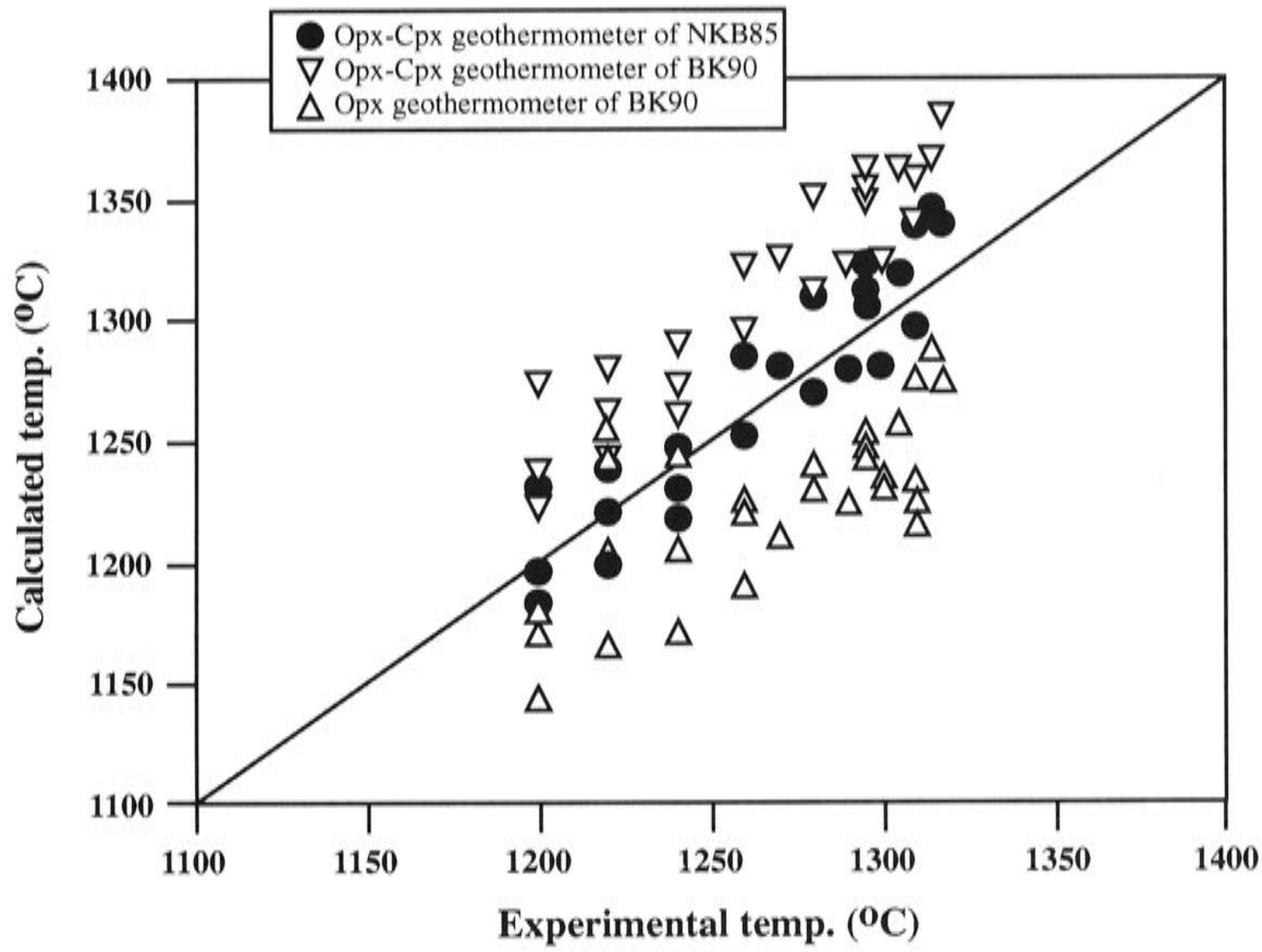

Fig. 7 A comparison diagram of experimental temperatures and calculated temperatures using different geothermometers. NKB85, Nickel et al., 1985; BK90, Brey and Kohler (Equation 9 and Equation 10; 1990).

4.3 Contamination and other mass balance issues for H_2O and CO_2 in the experiments

The diffusion rates of H_2 through Pt capsules are so rapid (e.g., Chou, 1986) that the amounts of H_2O in the capsule could potentially change significantly during the run. To minimise this, it is desirable to balance fH_2 as far as possible between the inside of the capsule and the outside; for this reason, runs were performed without an Fe_2O_3 sleeve as an H_2 getter, unless they were intended to be anhydrous.

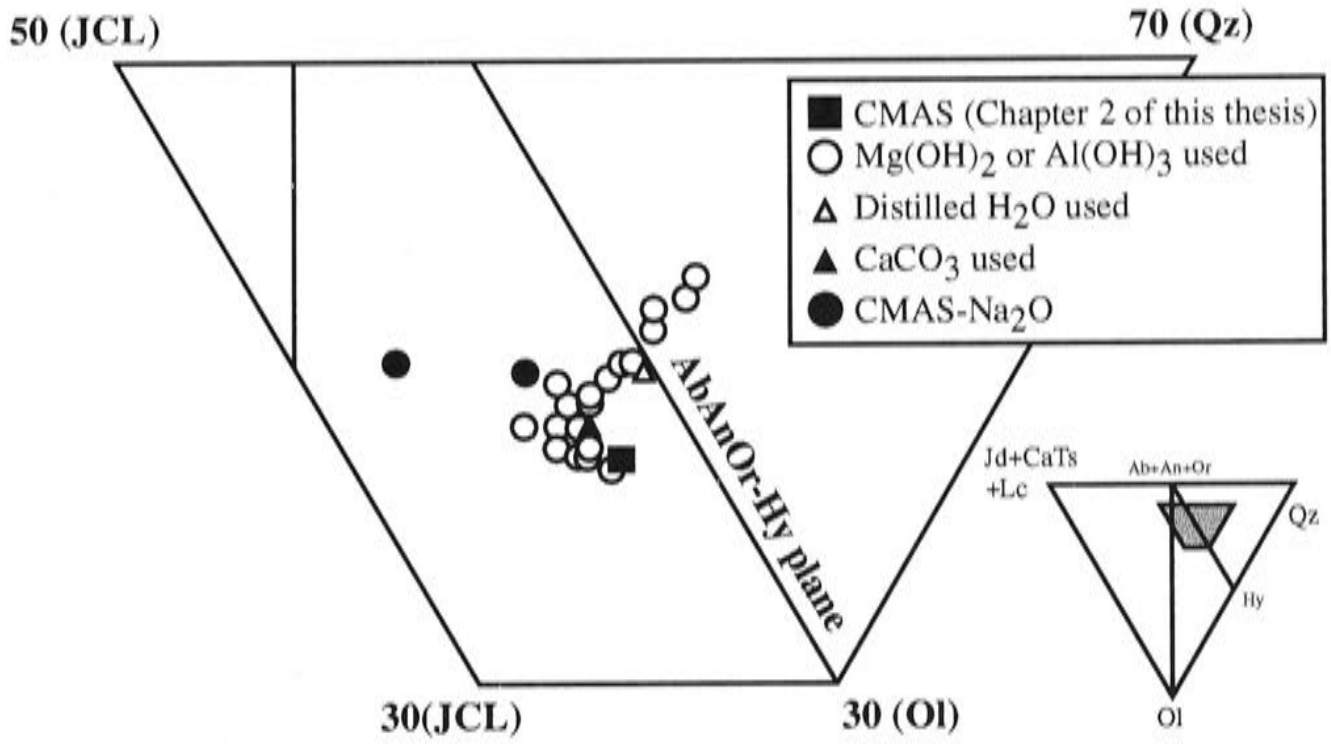

Fig. 8 Experimentally produced melt plotted onto the plane JdCaTsLc-Ol-Qz from Di. For plotting procedure, see Falloon & Green (1988). This plotting procedure is followed in Fig. 16, Fig. 17 and Fig. 18 as well. The isobarically invariant melt composition for a Sp-lherzolite in the system CMAS at 11 kbar is from Chapter 2 of this thesis.

The possibility of H_2 entering or leaving the capsule also means that the H_2O contents in the melt phase of the run products need to be determined after the run. For this, I used FTIR spectroscopy, which also revealed that the melt contained CO_2. The initial experiments, which used $Mg(OH)_2$ as the source of H_2O, showed that the amounts of CO_2 correlated with H_2O (Fig. 9), suggesting that the $Mg(OH)_2$ was the source of the CO_2. This appeared plausible, since finely divided MgO notoriously absorbs CO_2 from the atmosphere. Hence I switched to $Al(OH)_3$, on the grounds that aluminium carbonate, unlike $MgCO_3$, is not stable. However, these runs also contained CO_2 (Fig. 9), and subsequently I discovered from the Merck Index, 12th edition (Budavari, 1996) that $Al(OH)_3$, like $Mg(OH)_2$, is known to absorb CO_2. Calculation suggests that the hydroxides contained ~ 3.98 wt% CO_2 in $Mg(OH)_2$ and 3.70 wt% in $Al(OH)_3$.

In order to avoid CO_2, I then tried a run in which H_2O was added simply as distilled water (C-1817). Unfortunately, this run also contained considerable CO_2; in fact, the ratio of CO_2 to H_2O is indistinguishable from the runs starting with $Mg(OH)_2$ or $Al(OH)_3$ (Fig 9). The origin of this CO_2 is a mystery; one possibility is that C may diffuse through Pt capsules in piston-cylinder experiments, as observed by Watson et al. (1982), Watson (1987) and Brooker et al. (1998). To test whether this might be an additional problem here, three ancillary experiments were then performed. Both run conditions and results are given in Table 2, along with a relevant experiment from

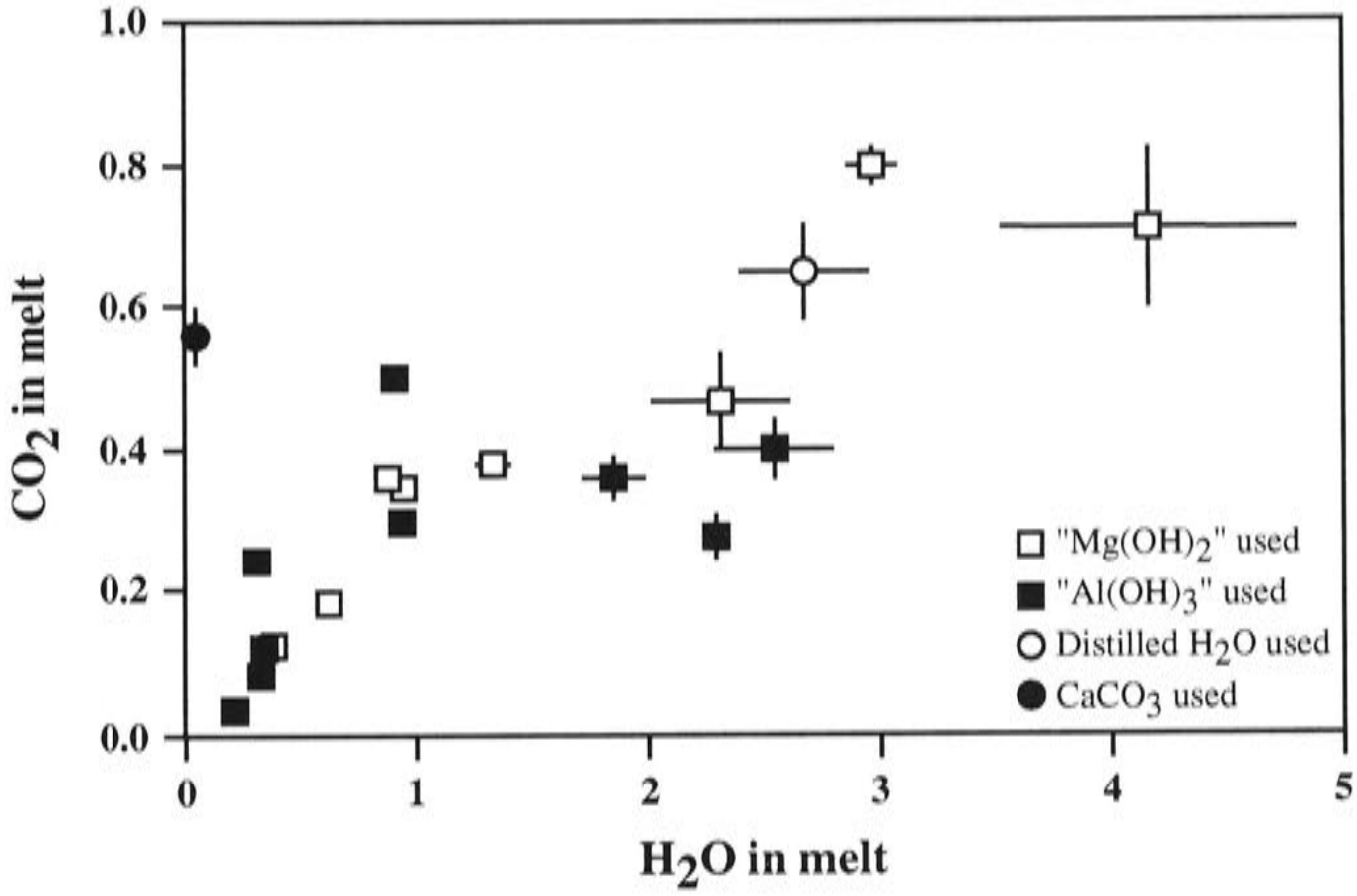

Fig. 9 The relationship of H_2O and CO_2 in the experimentally produced melts.

Chapter 2 of this thesis. Run C-1621 shows that use of the Fe_2O_3 sleeve controls the water content to a negligible level, as found by Robinson et al. (1998), and also, not surprisingly, prevents C entering the experimental charge. Run C-1809 suggests that H_2 ingress is considerably higher without the Fe_2O_3 sleeve, even in a short run time. However, there is no sign of C in the experimental charge after running the experiment for 20 minutes. The CO_2 detected in C-1810 and C-1811, which were run under the same conditions (pressure, temperature, duration, capsule material and assembly arrangement) must therefore come from the starting materials. The compositions of the starting materials SEM02-7, SEM02-9, SEM02-11 and SEM02-12 were recalculated accordingly, assuming ~ 3.98 wt% CO_2 in $Mg(OH)_2$ and 3.70 wt% in $Al(OH)_3$ (Table 1).

4.4 The effect of Na_2O: partial melting in system CMAS-Na_2O

The trace of Na_2O apparently present in the starting materials is concentrated into the melt, reaching levels as high as ~ 1 wt% (Table 4). This is too high an amount to ignore in the present context, and it is necessary to assess what effects Na_2O has on the partial melting process, so that an appropriate correction may be applied. Accordingly, two experiments were performed adding small amounts of Na_2O under anhydrous conditions, using the sandwich technique as in my previous work on the system CMAS-

K_2O (Chapter 2 of this thesis). A much more extensive study of partial melting in CMAS-Na_2O was undertaken by Walter & Presnall (1994), from 7 to 35 kbar.

The results in Walter & Presnall (1994), as parameterised by them in the form of equations describing the effect of Na_2O on temperature and melt composition, are compared to my data at 11 kbar in Fig 10. It may be seen that there is substantial agreement as regards the compositional effects, but the parameterisation of Walter and Presnall (1994) appears to show a substantially greater decrease in solidus temperature. This may be an experimental artefact caused by the solidus temperature of Walter and Presnall (1994) for the pure CMAS system being slightly too high, as I have previously argued from independent evidence (Chapter 2 of this thesis). The reason is as follows. The solidus temperature in CMAS of Walter and Presnall (1994) is constrained at 11 kbar by experiment 116-3 from the earlier work of Presnall et al. (1979). This earlier work used W-Re thermocouples, which (amongst their other problems) may oxidize in the piston-cylinder apparatus at relatively low pressures, since the alumina thermocouple tubing does not collapse completely unless pressures are greater than about 10 to 15 kbar; this allows oxygen from the air to leak in and attack the hot end of the thermocouple (e.g., Falloon et al., 2001). Oxidation causes drift to higher apparent temperatures. Walter and Presnall (1994) guarded against this oxidation by flowing N_2 around the thermocouple, but this was not done in the earlier work. It is possible, therefore, that there is a systematic offset in temperature measurement between the new experiments in CMAS-Na_2O reported by Walter and Presnall (1994), which appear to be consistent with my work, and the older experiments in the pure CMAS system from Presnall et al. (1979), below about 15 kbar. When the two sets of experiments are spliced together, this offset results in an artificially large effect of small amounts of Na_2O on the solidus temperature. Here I find that the effect of Na_2O in depressing the solidus at 11 kbar is ~ 4 ± 5 degrees per weight percent Na_2O (Fig. 10a), as compared with ~ 10 degrees in Walter & Presnall (1994).

5. Discussions

5.1 Data fitting: deconvoluting the effects of H_2O from Na_2O and CO_2 on the solidus of spinel lherzolite in CMAS at 11 kbar.

Since the system CMAS contains four components, melt coexists with four solid phases at an isobaric invariant point. Adding one component to the system (such as

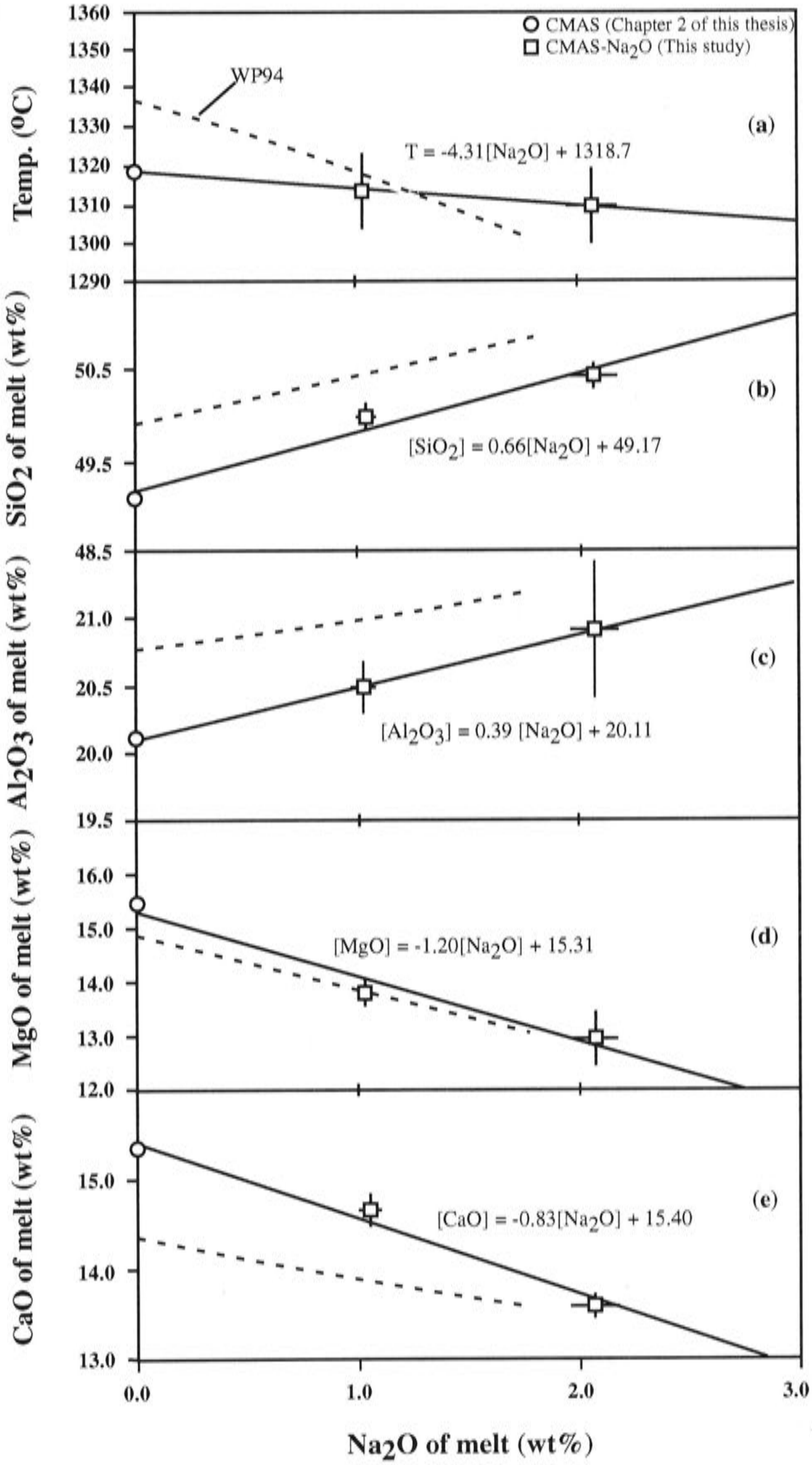

Fig. 10 A comparison diagram of Na_2O effect on solidus and melt composition at 11 kbar between this study and WP94 (Walter & Presnall, 1994). The data for the isobarically invariant point of the Sp-lherzolite in system CMAS at 11 kbar is from Chapter 2 of this thesis and used in the new regression.

H_2O) produces just one degree of freedom, hence the depression of the temperature of the solidus depends only on the amount of this extra component in one of the phases (such as H_2O in the melt). Here I need to consider three components, Na_2O and CO_2 as well H_2O, but since they are present in small amounts, I assume they are independent of each other. I also assume, for the small amounts involved, that the relationship between solidus temperature and the extra components is linear, giving the equation

$$T_{solidus} = T_{solidus}^{CMAS} + A_{Na_2O}^{T}[Na_2O] + A_{H_2O}^{T}[H_2O] + A_{CO_2}^{T}[CO_2] \quad (2)$$

We then fit the experimental data (Tables 4 and 5) to this equation, assuming the compositional uncertainties given in these tables, and an uncertainty in experimental temperature of ± 5 degrees (all uncertainties in this study are one standard deviation). I assumed $T_{solidus}^{CMAS}$ was 1319°C from Chapter 2 of this thesis. The first attempt returned a coefficient A_{CO_2} that was nominally positive but with a large uncertainty (actually 7 ± 7 degrees per wt%). Since CO_2 is concentrated into the melt phase, the sign of $A_{CO_2}^{T}$ must be negative. Clearly the current experimental technique is not sufficiently accurate to constrain $A_{CO_2}^{T}$; previous work on the effects of CO_2 on the solidi of other systems showed that it has only a small effect (Eggler, 1978), and therefore $A_{CO_2}^{T}$ is arbitrarily set to zero. With this, I obtained:

$$A_{Na_2O}^{T} = -6.3\ (1.8)\ ^{\circ}C/wt\% \quad (3)$$

and

$$A_{H_2O}^{T} = -38.2\ (1.2)\ ^{\circ}C/wt\% \quad (4)$$

The reduced chi-squared (χ_{ν}^{2}) for the regression is 2.65, indicating a reasonable fit to the data with the assumed uncertainties. The effect of small amounts of Na_2O on the solidus temperature is thus similar on a wt% basis to that of K_2O (-5.8 °C/wt% from Chapter 2 of this thesis), although it is not well constrained by the present experiments (note that adding higher amounts of Na_2O to the system at 11 kbar would tend to cause plagioclase to crystallize, as shown by Walter and Presnall, 1994). The effect of H_2O is

much larger (also when considered on a molar basis), and is very well constrained by the experiments (Fig. 11).

I adopted a similar empirical approach to disentangle the effects of H_2O from Na_2O and CO_2 on the composition of the melt at the solidus, i.e., by fitting the data in Tables 4 and 5 to empirical equations of the type:

$$[X] = [X]_{CMAS} + B^X_{Na_2O}[Na_2O] + B^X_{H_2O}[H_2O] + B^X_{CO_2}[CO_2] + C^X_{H_2O/CO_2}[H_2O][CO_2] \quad (5).$$

Results are given in Table 7 for the oxides on a volatile-containing basis.

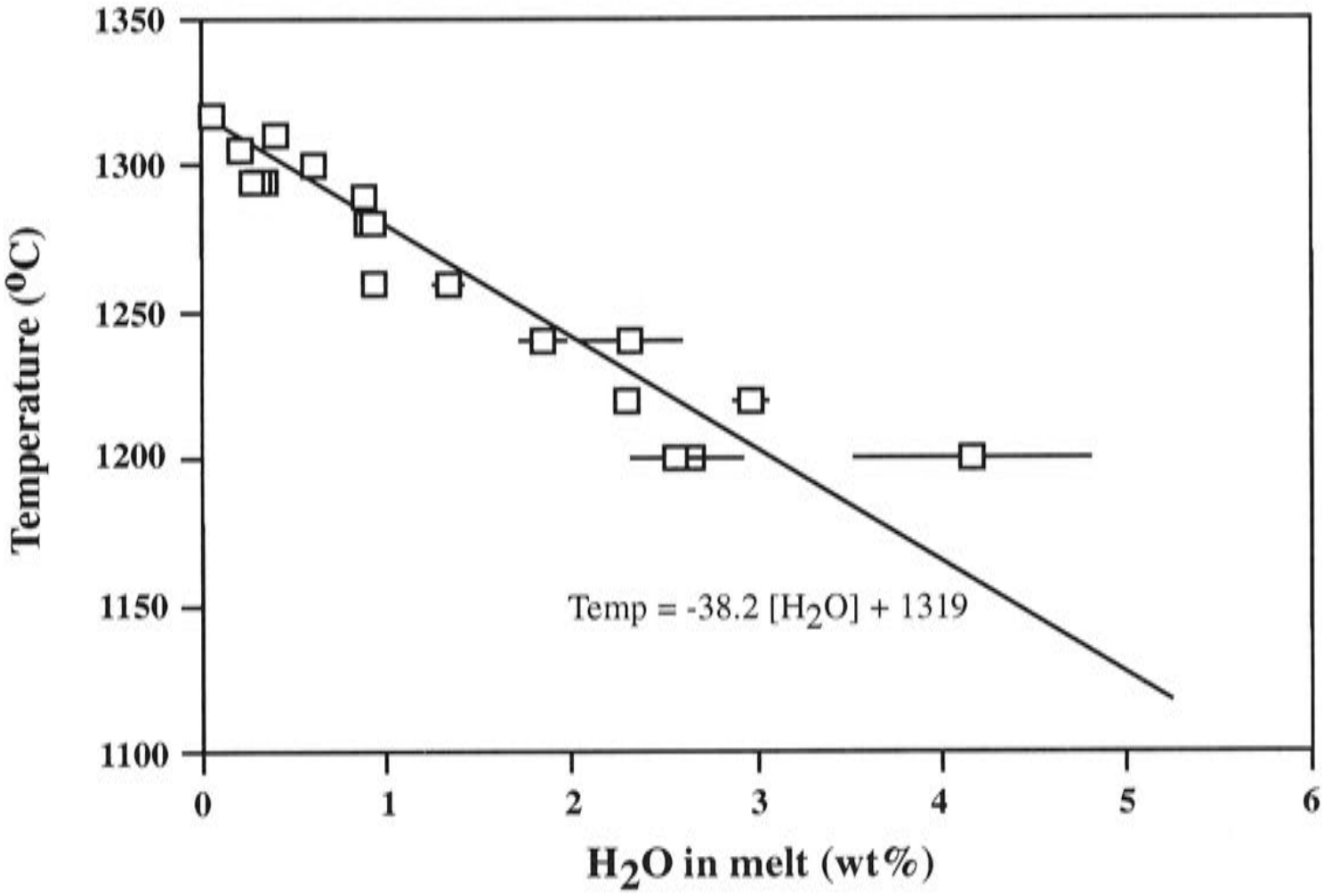

Fig. 11 H_2O effect on melting temperature in the simple system CMAS-H_2O at 11 kbar. Line is drawn according to Equation 4 in the text.

The regressed melt composition with 0% Na_2O and 0% CO_2 is plotted in Fig. 12. When H_2O is regarded as a component of the melt, increase of water increases SiO_2 and Al_2O_3, but decrease MgO and CaO. This variation pattern supports most of the observations and interpretations made by Gaetani & Grove (1998) in natural rock composition systems, except for their observation that Al_2O_3 is unaffected by water addition. The effect of water is very strong on MgO (1.49% decrease caused by 1% water increase), strong on Al_2O_3 (0.67% increase caused by 1% water increase), weak

on CaO (0.39% decrease caused by 1% water increase) and very weak on SiO_2 (0.11% decrease caused by 1% water increase). When melt composition is plotted on a water-free basis, however, the SiO_2 content of melt increases rapidly. That is simply because renormalization to 100% affects the most abundant oxide, SiO_2, the most. Similarly, the water effect on other oxides is also changed: its effect on Al_2O_3 is enhanced but its effect on MgO and CaO is depressed.

In order to show the effect of CO_2 on melt composition, I calculated the melt composition at 0% CO_2, 0.5% CO_2 and 1% CO_2 using the regression coefficients in Table 7, and the result is shown in Fig. 13. It is obvious that the CO_2 effect on melt composition is not constant but changes with the H_2O content: this effect generally increases as the water content increases. The CO_2 effect on the MgO content even changes its sign at about 1.2% H_2O. At high water conditions, the CO_2 effect on the content of all these oxides is in an opposite direction to that of H_2O.

Table 7 Results of regression analysis of the composition of melts in equilibrium with Fo+Sp+Opx+Cpx in the system CMAS with small additions of Na_2O, H_2O and CO_2.

	$[X]_{CMAS}$	$B^X_{Na_2O}$	$B^X_{H_2O}$	$B^X_{CO_2}$	$C^X_{H_2O/CO_2}$	χ^2_ν
CaO	14.77(12)	-0.65(12)	-0.39(7)	0.90(31)	-	5.1
MgO	16.27(11)	-1.01(12)	-1.49(11)	-1.27(22)	1.30(16)	6.5
Al_2O_3	19.80(12)	0.43(11)	0.67(10)	-0.25(25)	-0.57(16)	3.4
SiO_2	49.17(15)	0.61(11)	0.11(12)	-0.79(28)	-0.54(19)	1.5

For the experimentally observed melt compositions, see Table 4 and Table 5. These data were fitted to Equation 5. H_2O and CO_2 are retained as components in the melts

The generally opposite effect of CO_2 on melt composition to that of H_2O observed here may suggest that the experimental result in Gaetani & Grove (1998) has to be used with caution. Typically ~ 1.2% CO_2 was observed in their melt but its effect was ignored. My observation made above suggests that the most of the SiO_2 decrease which was assigned to H_2O by them was actually caused by CO_2 (Fig. 13a). The H_2O effect on Al_2O_3 in their experiments, however, may have been essentially masked by the presence of CO_2 so that the nominal observation is a constant Al_2O_3 content in melts (note the almost horizontal line with 1% CO_2 in Fig. 13b). Although the CO_2 effect on MgO and CaO is also opposite to that of H_2O, the H_2O effect should be preserved because its higher concentration and its stronger (in the case of MgO) or identical (in the case of CaO) effect to that of CO_2.

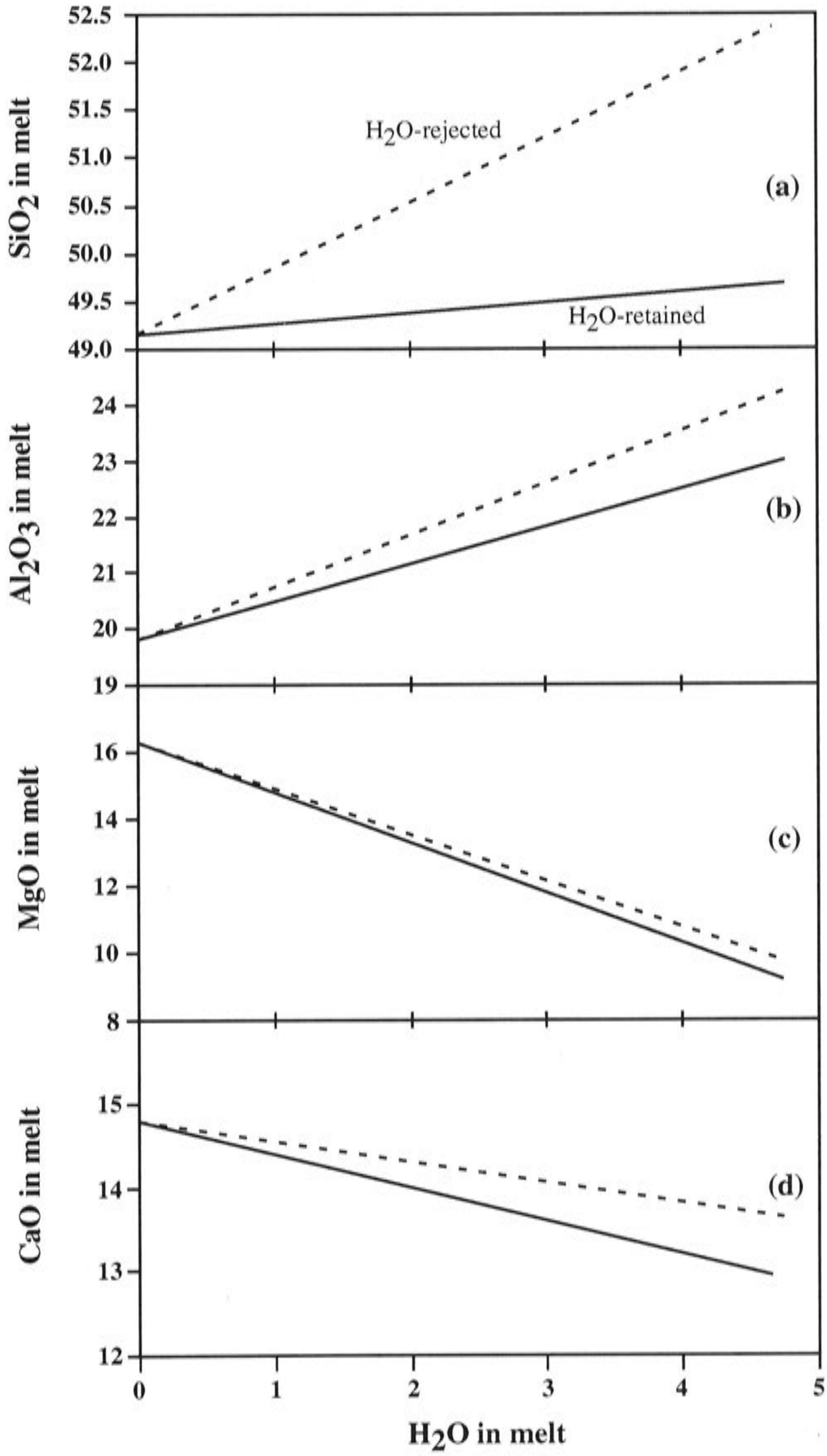

Fig. 12 The effect of H_2O on the contents of SiO_2 (a), Al_2O_3 (b), MgO (c) and CaO (d) in silicate melt at CO_2-free conditions (Equation 5 and Table 7). Solid lines: H_2O retained as a component in the melt; broken lines: Melt compositions renormalized to 100% on an anhydrous basis.

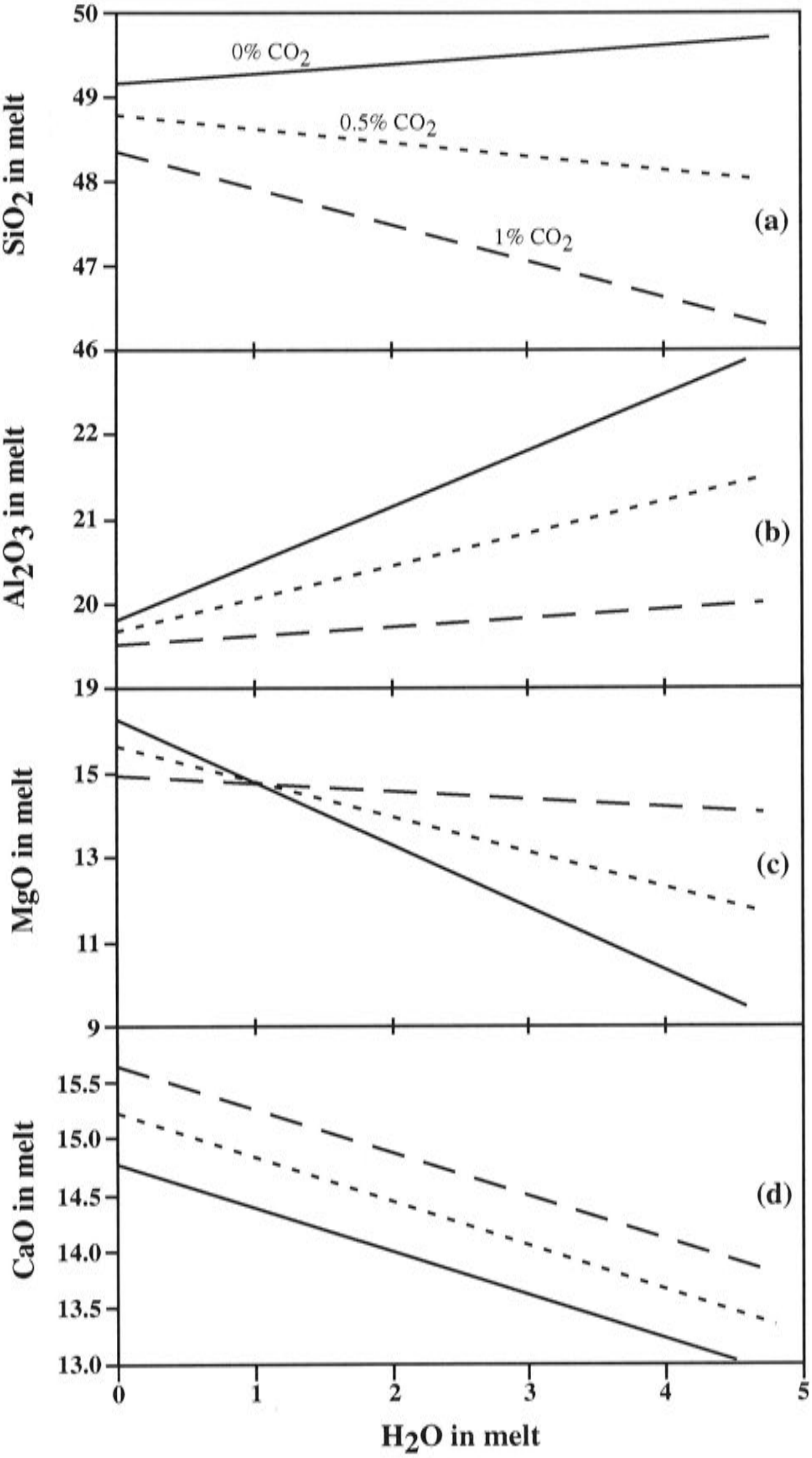

Fig. 13 The effect of CO_2 on the contents of SiO_2 (a), Al_2O_3 (b), MgO (c) and CaO (d) in silicate melt at H_2O-dominant conditions (Equation 5 and Table 7).

5.2. Water effect on melting temperature

It has been a long time since people recognised that water has a strong effect on the melting temperature of upper mantle lherzolite (Kushiro et al., 1968b; Kushiro,

1972; Green, 1973; Mysen & Boettcher, 1975a, 1975b; Green, 1976; Falloon & Danyushevsky, 2000; Ulmer, 2001). What is unknown is how much a certain amount of H_2O in melt can affect the melting temperature. In the literature, fluid-unsaturated or fluid-saturated experiments are very limited (Ulmer, 2001 and references therein) and only Gaetani & Grove (1998), Falloon & Danyushevsky (2000), Muntener et al. (2001) and Pichavant et al. (2002) analysed the H_2O content in melts using FTIR, ion microprobe, O-method or a "by-difference" method using electron microprobe. The different analysing methods, the presence of CO_2 caused by experimental technique and the various phase assemblages involved prevent people making any rigorous analysis of the H_2O effect on the melting temperature. The only model, empirical in nature, proposed by Falloon & Danyushevsky (2000), suggests an exponential correlation between H_2O content and its temperature depression. In contrast, the result here suggests that the correlation between H_2O and temperature is linear (Fig. 11): every percent of H_2O increase depresses the melting temperature by ~ 38 degrees.

According to my experience in different fluid-analysing techniques, the data from Gaetani & Grove (1998) is the most reliable data in the literature despite the CO_2 in their melts. Hence I tentatively removed the CO_2 effect on SiO_2, Al_2O_3, MgO, CaO and H_2O in the melt in those experiments which were analysed both for H_2O and for CO_2, and plotted the corrected data in Fig. 14a. Remarkably, a linear relationship between H_2O and temperature emerges and suggests that 1% H_2O decreases melting temperature by ~ 39 degrees. It is noted that my correction procedure by no means is rigorous because of the presence of other components in their melts.

Fig. 14b compares my model to that in Falloon & Danyushevsky (2000). At low H_2O content, their model suggests larger temperature depression while at high H_2O content, their model suggests smaller temperature depression.

The Falloon & Danyushevsky (2000) model was built on the relationship between the H_2O contents of experimentally produced melts and the differences of the experimental temperatures (as hydrous temperatures) and the calculation temperatures (as anhydrous temperatures) with the geothermometer of Ford et al. (1983). Since the melt composition as input into the Ford et al. (1983) geothermometer has been affected by H_2O, it is obvious that the calculated temperatures are hydrous melting temperatures rather than anhydrous melting temperatures. The above relationship on which their H_2O-temperature model was built, therefore, is essentially just an independent examination on the accuracy of the Ford et al. (1983) geothermometer at hydrous

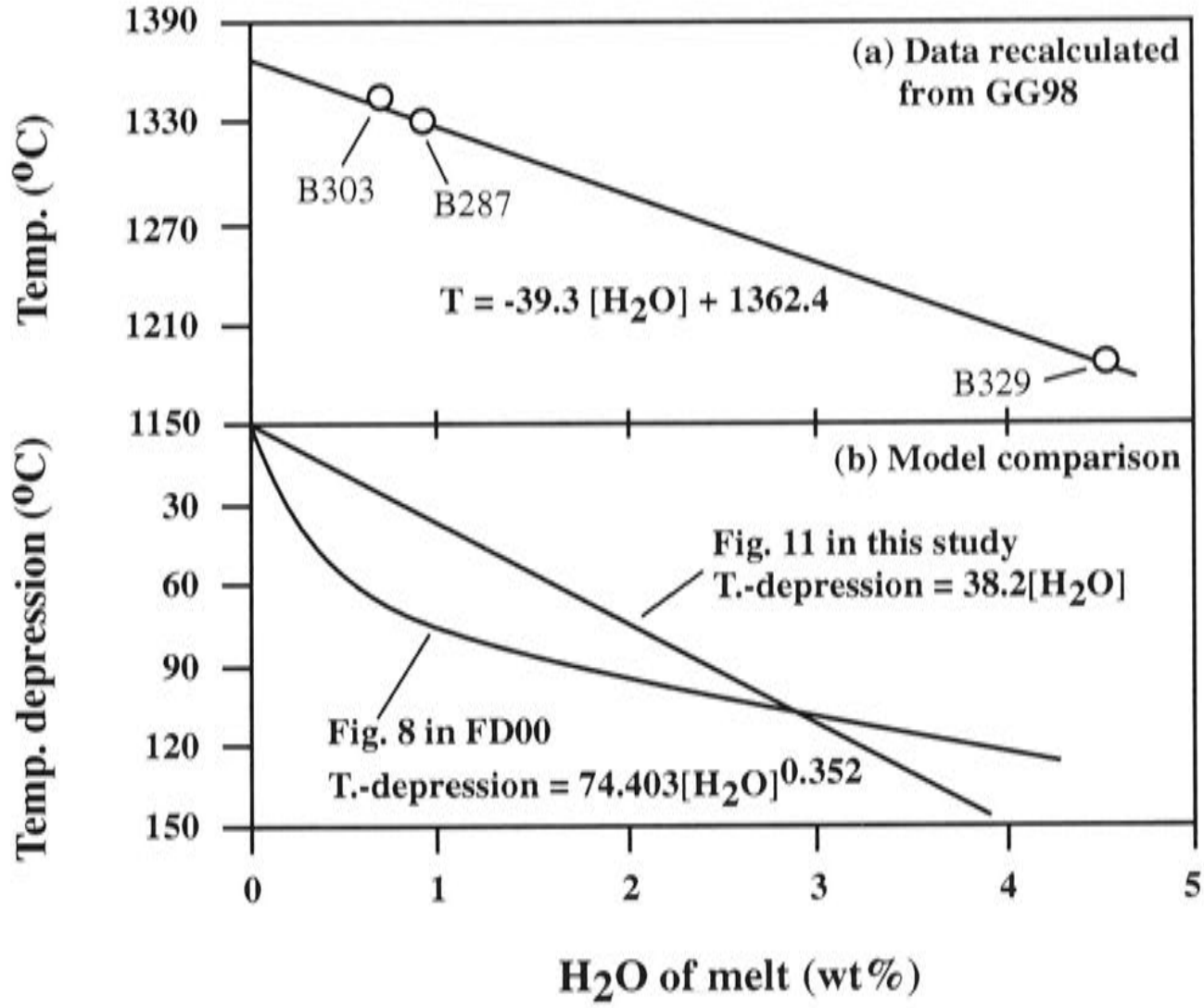

Fig. 14 The effect of H_2O on melting temperature in natural rock composition system at 12 kbar (a) and a comparison of the new model shown in Fig. 11 and the Falloon & Danyushevsky (2000) model. GG98, Gaetani & Grove (1998); FD00, Falloon & Danyushevsky (2000). In order to remove the CO_2 effect on the H_2O content, simple correction based on the preceding regression is applied to the melt compositions from Gaetani & Grove (1998). The CO_2 content in one of the melt compositions (B-329) was not reported but it is assumed to be 1%, based on the information from B305 (1.27% CO_2), which has similar experimental conditions, similar phase assemblage and similar water content. The high anhydrous solidus (~ 1362°C) of the natural rock composition at 12 kbar is partly due to the pressure difference and partly due to the contamination of the W-Re thermocouples at this pressure, according to Chapter 2 of this thesis, Chapter 3 of this thesis and Falloon et al. (2001).

condition. It follows that the Falloon & Danyushevsky (2000) model is in fact not a model about the effect of H_2O on partial melting temperature.

Fig. 15a shows that the Ford et al. (1983) geothermometer can not accurately reproduce the temperatures of my hydrous experiments, resulting in much higher calculated temperatures. Fig. 15b shows that the difference between the calculated temperature and the experimental temperature is not a simple linear function of the H_2O content. The similar curvature of the temperature difference to H_2O displayed in Fig. 15b and the "model" of Falloon & Danyushevsky (2000) displayed in Fig. 14b argues again that their model is indeed not a model about the effect of H_2O on partial melting temperature. My model built here, which suggests a simple correlation between H_2O contents and partial melting temperatures, is the only one.

It is suggested that great caution is necessary when the Ford et al. (1983) geothermometer is applied to calculate hydrous melting temperature.

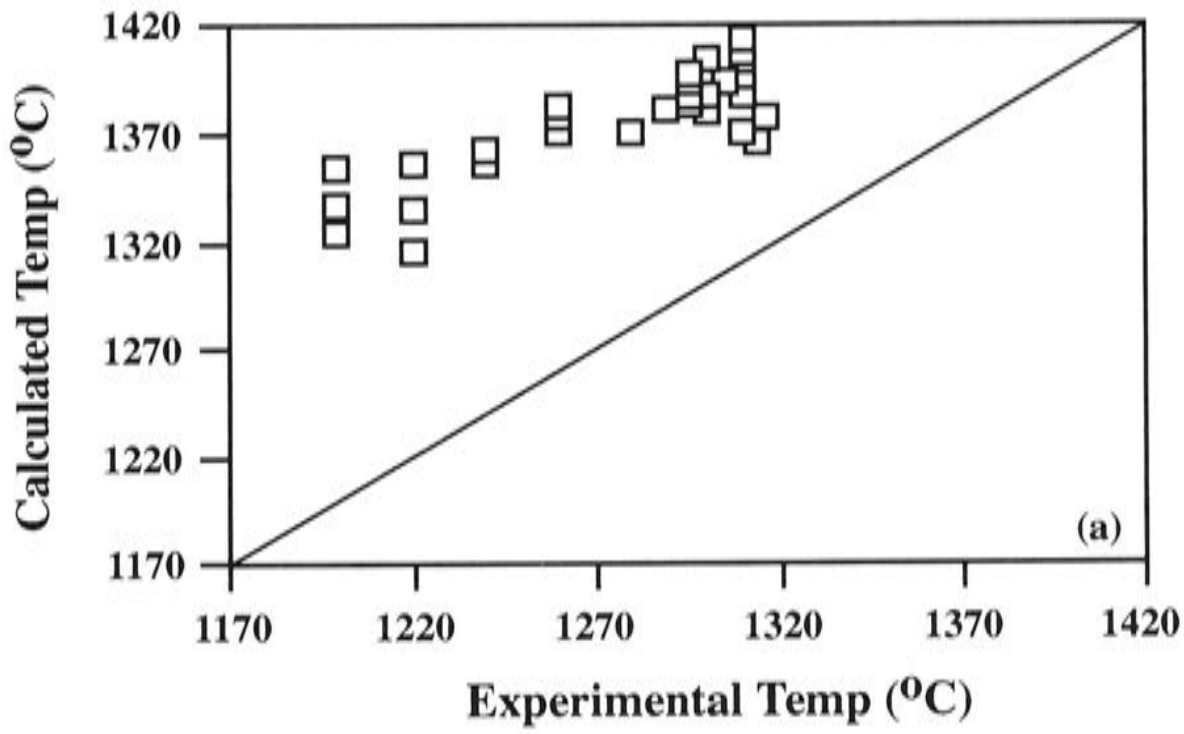

Fig. 15 Comparison of calculated temperature using the Ford et al. (1983) geothermometer and experimental temperature (a) and the relationship of the difference between calculated temperature and experimental temperature to water content (b). The curve in b is hand-drawn.

5.3. Melt property in system CMAS-H_2O-CO_2

Using the regression coefficients in Table 7, I have regressed the melt compositions from 0% H_2O to 5% H_2O at conditions of 0% CO_2, 0.5% CO_2 and 1% CO_2. The regressed melt composition is shown in Fig. 16.

When the system is H_2O-free and CO_2-free, the product melt is essentially olivine basalt (Presnall et al., 1979; Walter & Presnall, 1994; Chapter 2 of this thesis). As water adds in, Al_2O_3 in melts increases so that melts become An-richer. That leads to less CaO left to form Di. Since CaO has already been decreased by the addition of H_2O, Di should decrease rapidly, as shown by the 0% CO_2 melt trend in Fig. 16a. When H_2O increases to ~ 5%, CaO is consumed but Al_2O_3 is left by forming An so that melt

becomes Di-free and corundum-normative. Since H_2O increases the SiO_2 content but decreases the MgO content (Fig. 12), melts become more Hy-normative. With ~ 1.5% water in the melt, melt becomes quartz-normative (Fig. 16b). As H_2O increases to ~ 5%, the melt is very rich in quartz. The observation that H_2O saturated melt is rich in quartz made by Yoder (1971) and Kushiro (1972), therefore, is confirmed by the new observation.

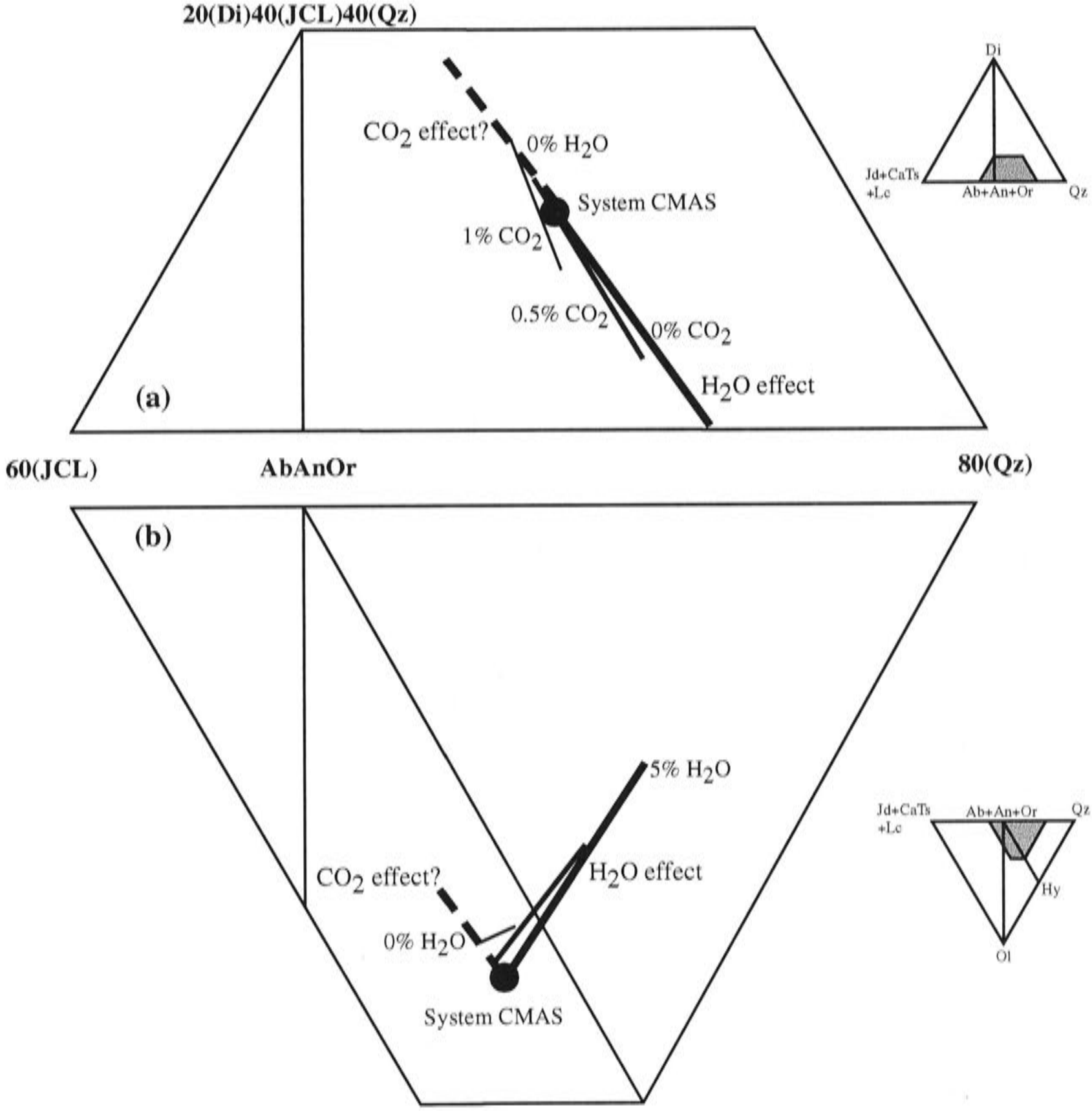

Fig. 16 Melt property shown on the plane Di-JdCaTsLc-Qz from Ol (a) and the plane Ol-JdCaTsLc-Qz from Di (b). Melt composition data is regressed for a Sp-lherzolite phase assemblage in the system CMAS-H_2O-CO_2 at 11 kbar. The isobarically invariant melt composition for a Sp-lherzolite in the system CMAS at 11 kbar is from Chapter 2 of this thesis.

CO_2 makes the melt Di-richer (Fig. 16a) and shifts the melt towards the AbAnOr-Ol plane (Fig. 16b). This observation indirectly confirms the study of Eggler (1978) in the system CMAS-Na_2O-CO_2, in which the CO_2-saturated melt melts was observed to be Ne-normative.

Fig. 16 also demonstrates the opposite effect of CO_2 on melt property to that of H_2O. At CO_2-free condition, an addition of 5% H_2O can cause a large shift of melt composition; this shift of melt composition is much counteracted by 1% CO_2.

The possibility of forming corundum-normative melts by direct partial melting of the lherzolite upper mantle is interesting. Gill (1981) found that ~ 15% of andesites around the world is corundum normative. Several explanations for the origin of corundum normative melts in calc-alkaline magma series exist: pelite assimilation, hornblende fractionation at low pressure and garnet+amphibole-spinel fractionation at high pressure (Muntener et al., 2001, and references therein). My study suggests that at water-rich conditions, direct partial melting of a lherzolite upper mantle is also a possible mechanism.

5.4. Hydrous unsaturated melt in natural rock composition system

Agreement has been consistently reached on the melt property among the hydrous partial melting studies in simple systems (Kushiro et al., 1968b; Kushiro, 1969; Yoder, 1971; Kushiro, 1972; Kushiro, 1975; Sisson & Grove, 1993; this study), the hydrous melt property in natural rock composition system, however, is still a question open to debate. There were extensive discussions about the nature of the water-saturated melt and about the possibility of andesitic magma as a primary melt generated by direct partial melting of hydrous upper mantle in the 1960s and 1970s (Kushiro et al., 1968; Kushiro & Yoder, 1972; Nicholls & Ringwood, 1972; Green, 1973; Nicholls & Ringwood, 1973; Mysen et al., 1974; Mysen & Boettcher, 1975b; Green, 1976). These discussions have continued themselves towards today (Kushiro, 1990; Hirose & Kawamoto, 1995; Hirose, 1997a; Gaetani & Grove, 1998; Falloon & Danyushesky, 2000) and no agreement has been reached so far (Ulmer, 2001).

Fig. 17 shows the melt compositions from Hirose & Kawamoto (1995) at 10 kbar, Hirose (1997a) at 10 kbar and Gaetani & Grove (1998) at 12 kbar with or without a simple correction for the CO_2 effect on SiO_2, Al_2O_3, MgO, CaO and H_2O. For those experiments in Gaetani & Grove (1998) in which both H_2O and CO_2 data are available, empirical correction was directly applied to their melt composition. For those experiments without CO_2 data, I firstly estimated the effective H_2O content by using the

linear relationship between melting temperature and water content (Fig. 11), secondly split their analysed nominal H_2O content into two parts: the effective H_2O content and the ineffective H_2O content which was counteracted by CO_2, thirdly calculated the CO_2 content required to counteract the ineffective H_2O, finally removed the CO_2 effect on the melt composition. Similar correction procedure plus a new assumption, 1% CO_2 in the melts of the experiments using Ag-Pd or Au-Pd capsule, was applied to the experiments in Hirose & Kawamoto (1995). Hirose (1997a) used Au as capsule material in his experiments, so that his experimental data was not corrected for CO_2. The graphite diffusion rate through Au at high temperature-high pressure conditions is unknown but, by analogy with H_2, it may be significantly lower than the diffusion rate through Pt and Pd (Brooker et al., 1998).

Fig. 17 suggests that the CO_2 correction process does bring forth some differences. The most notable change is the original melt data of Gaetani & Grove (1998) clouding around the Di-AbAnOr-Ol plane has been spread toward Qz. The second change is one of the two nepheline-normative melts has crossed the Di-AnAnOr-Ol plane while the other one (B287) has not. Gaetani & Grove (1998) showed that the melt in B287 contains just 0.07 wt% CO_2, so that not much CO_2 correction has been actually applied to this melt. The third change is the melts in two experiments in Hirose & Kawamoto (1995), marginally quartz-normative before the correction, become definitely quartz-normative after the correction.

The corrected composition data define a cotectic which is completely different from the 10 kbar anhydrous cotectic (Falloon et al., 1999) and also completely different from the 10 kbar hydrous cotectic tentatively drawn by Ulmer (2001), but similar to my observation in the simple system (Fig. 16). Similarly, Falloon & Danyushevsky (2000) observed a cotectic for hydrous partial melting of assemblage Ol+Opx+Sp, which is very different from that for anhydrous partial melting of the phase assemblage Ol+Opx+Sp. It must be noted that, because of the high degrees of variation in the hydrous or anhydrous natural rock composition system, the cotectic actually should be a volume in the multiple-dimension composition-temperature space and thus not unique. The general trend of melt composition from low temperature to high temperature or from high water content to low water content, however, should remain.

It follows hydrous partial melting in the natural rock composition system is almost completely controlled by two factors, water content and temperature. At high temperatures ($> \sim 1150^{\circ}C$ at $\sim$ 11 kbar), the product melt should be olivine-normative while at low temperatures ($< \sim 1150^{\circ}C$ at $\sim$ 11 kbar), the product melt should be quartz-

normative. If a certain amount of water is kept in the system and temperature is let to vary, hydrous partial melting should start from a H_2O-saturated point (stable amphibole or fluid?) at very low temperature and produce water-rich and highly quartz-normative melt (with most Na_2O locked in amphibole or fluid?). When temperature increases, partial melting extent should increase and melts move along the hydrous cotectic, becoming less water-rich and less quartz-normative. If temperature increases further, water-poor olivine-normative basaltic melt should be eventually produced. How far melt can move along the cotectic, how much melt can be produced and also what phase will be melted out first (Cpx, Opx or Sp?) are mostly dependent to how much water is in the bulk composition. In order to fully understand the behaviour of hydrous partial melting of upper-mantle, more experiments at different temperatures with different bulk water contents are required.

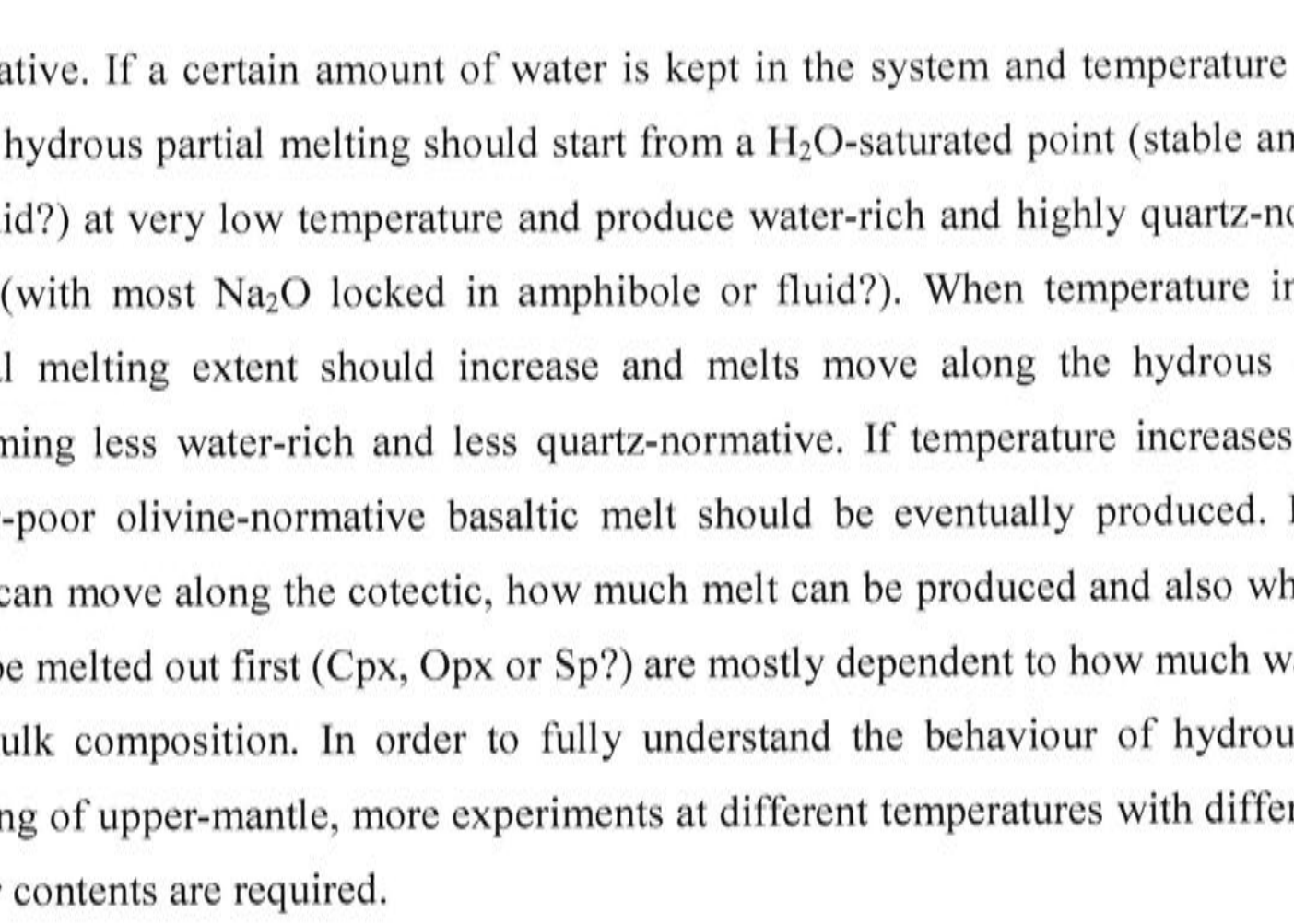

Fig. 17 Melt property shown on plane Di-JdCaTsLc-Qz from Ol (a) and plane Ol-JdCaTsLc-Qz from Di (b) at water-undersaturated condition. GG98, Gaetani & Grove, 1998; HK95, Hirose & Kawamoto, 1995; H97, Hirose, 1997a; F99, Falloon et al., 1999; U01, Ulmer, 2001. Only those experimental data for a Sp-lherzolite phase assemblage are shown. Arrows point to the direction of temperature increase (e.t., H_2O decrease).

5.5. Water-saturated melt at ~ 11 kbar

The previous subsection implies that the water-saturated melt (stable amphibole or fluid?) is one of the most important endmembers in the partial melting study of upper mantle. Although some studies have been carried out (Green, 1973; Mysen & Boettcher,

1975b; Green, 1976; Ulmer, 2001), no agreement about the compositions of the water-saturated melts has been reached so far.

Despite there is a possibility that those melts experimentally observed in Green (1973) and Mysen & Boettcher (1975b) were affected by CO_2, I plot their original data, along with the calculated melt compositions from Green (1973; 1976), in Fig. 18 without making any correction. The shown data from Mysen & Boettcher (1975b) cover wide ranges of bulk composition (B, C, and D), hydrogen fugacity (buffered by magnetite-hematite, iron-wustite, nickel-nickel oxide or the cell) and pressure (either 7.5 kbar or 15 kbar). The experimental pressure for those data from Green (1973; 1976) is 10 kbar.

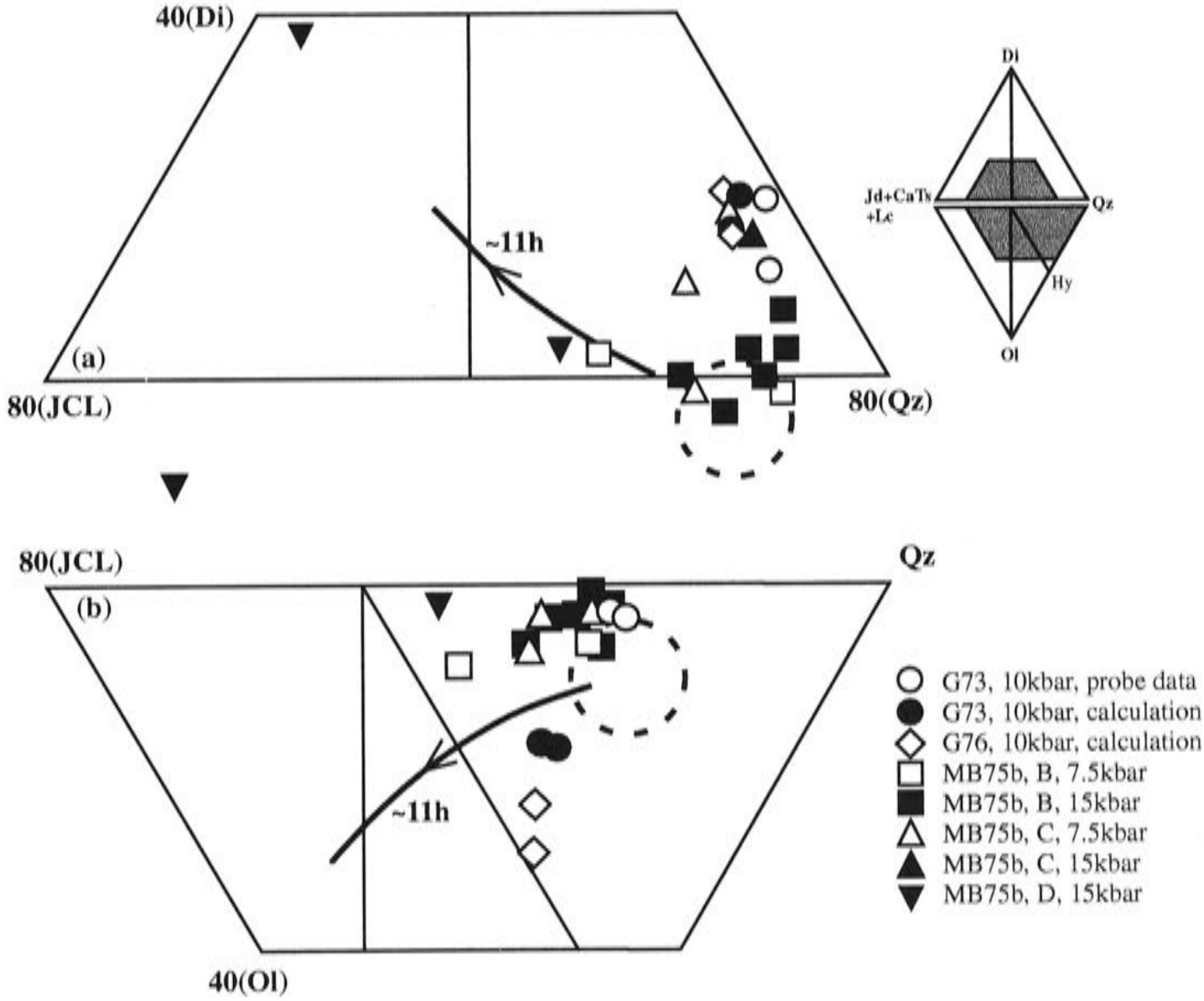

Fig. 18 Melt property shown on plane Di-JdCaTsLc-Qz from Ol (a) and plane Ol-JdCaTsLc-Qz from Di (b) at water-saturated condition. G73, Green, 1973; G76, Green, 1976; MB75b, Mysen & Boettcher (1975b). Solid curve: cotectic at water-undersaturated condition which is from Fig. 17. Arrows point to the direction of temperature increase (e.t., H_2O decrease).

Fig. 18 illustrates that the water-saturated melts spread widely and one melt composition from Mysen & Boettcher (1975b) is apparently at odd. No any obvious dependence of the water-saturated melt composition to pressure, bulk composition and hydrogen fugacity is displayed by these data.

Compared to the water-unsaturated cotectic at ~ 1.1 kbar, these experimentally defined melts are poor in Ol component but rich in Di component. Green (1973; 1976) noted the Ol-poor nature of these melts and argued that quench crystallising had affected their composition. Hence he deliberately made correction to those melts. Fig. 18b, however, suggests that he possibly over-corrected the data and the corrected melts may be too rich in Ol component. The Di-richer nature of these melts, which is the first time to be recognised, was possibly caused by those special experimental conditions: short run time (one to several hours) and very low temperature (950-1200°C). Close equilibrium in these experiments may have not been achieved and some "quenching" phases, like the quenching "Cpx" and "Amph" observed by Green (1973), may actually be crystallising phases. Due to the very short experimental time and the very low temperature, they were just not well crystallised. The melt, hence, should be too rich in those components which would be used to make these crystallising phases. Apparently, Di is one of those components.

Combining all these messages, I suggest that the H_2O-saturated melts at a pressure around 11 kbar, either coexisting with amphibole or fluid, are corundum-normative and contain about 20 wt% normative quartz (indicated by the broken circles in Fig. 18). Several melt compositions from Mysen & Boettcher (1975b) in fact are very close to the speculated melt compositions.

5.6. CO_2 and petrogenesis of special melt inclusions from island arcs

Primitive melt inclusions were documented in Ol from island arcs (Schiano et al., 2000; and references therein) and their major features are low SiO_2 content (down to 44%), nepheline-normative and high CaO contents (up to 19%). Schiano et al. (2000) suggested that these melt inclusions can not simply explained by melting of a metasomatized peridotitic mantle wedge above subducting oceanic lithosphere but they may be produced by 10-30% partial melting of a Cpx-rich lithology at lower crustal to upper mantle pressures. Recent partial melting study (Kogiso & Hirschmann, 2001) showed that the SiO_2 contents of the melt generated by partial melting of clinopyroxenite are much higher than those of the arc melt inclusions, and the partial melting temperature is much higher than that likely to be prevailing in the island arc region. The petrogenesis of these melt inclusions, thus, remains unsolved.

The SiO_2 content of the solidus melt of a Sp-lherzolite in the system CMAS at 11 kbar is ~ 49%. Studies in simple systems suggested that it can be elevated by K_2O (Chapter 2 of this thesis), Na_2O (Presnall & Hoover, 1987; Walter & Presnall, 1994; this

study), Cr_2O_3 (Chapter 2 of this thesis) and H_2O (this study), but slightly depressed by FeO (Gudfinnsson & Presnall, 2000). The effect of TiO_2 and P_2O_5 are not clear but possibly they decrease the SiO_2 content (Kushiro, 1975; Hirschmann et al., 1998). Combining the effect of these components and their abundances in the island-arc melt inclusions, it is reasonable to get a SiO_2 content of ~ 49% or even higher, in agreement with Kogiso & Hirschmann (2001). The very low SiO_2 content (down to ~ 44%) in the island-arc melt inclusions, thus, must be caused by other missing components rather than by a change of lithology from lherzolite to clinopyroxenite. Schmidt et al. (2001) suggested that CO_2 may be one important candidate.

Previous experimental studies showed that melting of lherzolite plus CO_2 (or plus CO_2+H_2O, with X-CO_2 > 0.5) produces SiO_2-poor melt with high CaO contents, high CaO/Al_2O_3 ratios and nepheline-normative nature (Huang & Wyllie, 1974; Eggler, 1978; Hirose, 1997a; Dalton & Presnall, 1998a; Dalton & Presnall, 1998b). These signatures are well preserved in those island-arc melt inclusions. However, Schiano et al. (2000) argued that CO_2 alone can not explain the petrogenesis of these melt inclusions. One argument which favours the view of Schiano et al. (2000) is that the CO_2 solubility in anhydrous basaltic melts at low pressures is so low (~ 0.5% at 11 kbar; see later discussion) that its effect on the composition of melts is not significant at all.

Two possible mechanisms to solve these problems are CO_2-dominant partial melting under hydrous conditions at relatively low pressures (Mechanism 1) and CO_2-bearing partial melting of peridotite at relatively high pressures (Mechanism 2).

Mechanism 1

It is clear from Fig. 13a, Fig. 13d and Fig. 19 that the participation of CO_2 in the H_2O-dominant partial melting at relatively low pressures cannot explain the petrogenesis of these island-arc melt inclusions which have very low SiO_2 content, but have very high CaO content and very high CaO/Al_2O_3 ratios. Thus, CO_2-dominant conditions should be sought.

The solubility of CO_2 in nominally anhydrous basaltic melt was suggested to be ~ 0.85% at 11 kbar (Pan et al., 1991; ~ 0.2% H_2O in their melts). My observation here (C-1812) shows that the CO_2 solubility is ~ 0.56 ± 0.07% at H_2O = 0.05 ± 0.01% (Table 5). The real anhydrous CO_2 solubility in basaltic melts multiply-saturated with Ol+Sp+Opx+Cpx at 11 kbar, thus, should be close to 0.5%. As H_2O adds in, due to the opposite effect of H_2O to that of CO_2, more CO_2 is needed in order to meet the requirements imposed on the melt structure and the melt composition by the solid

phases. Hence, the CO_2 solubility has to increase. This argument is further supported by the much higher CO_2 content observed in several hydrous experiments in this study (Table 5) and in Gaetani & Grove (1998).

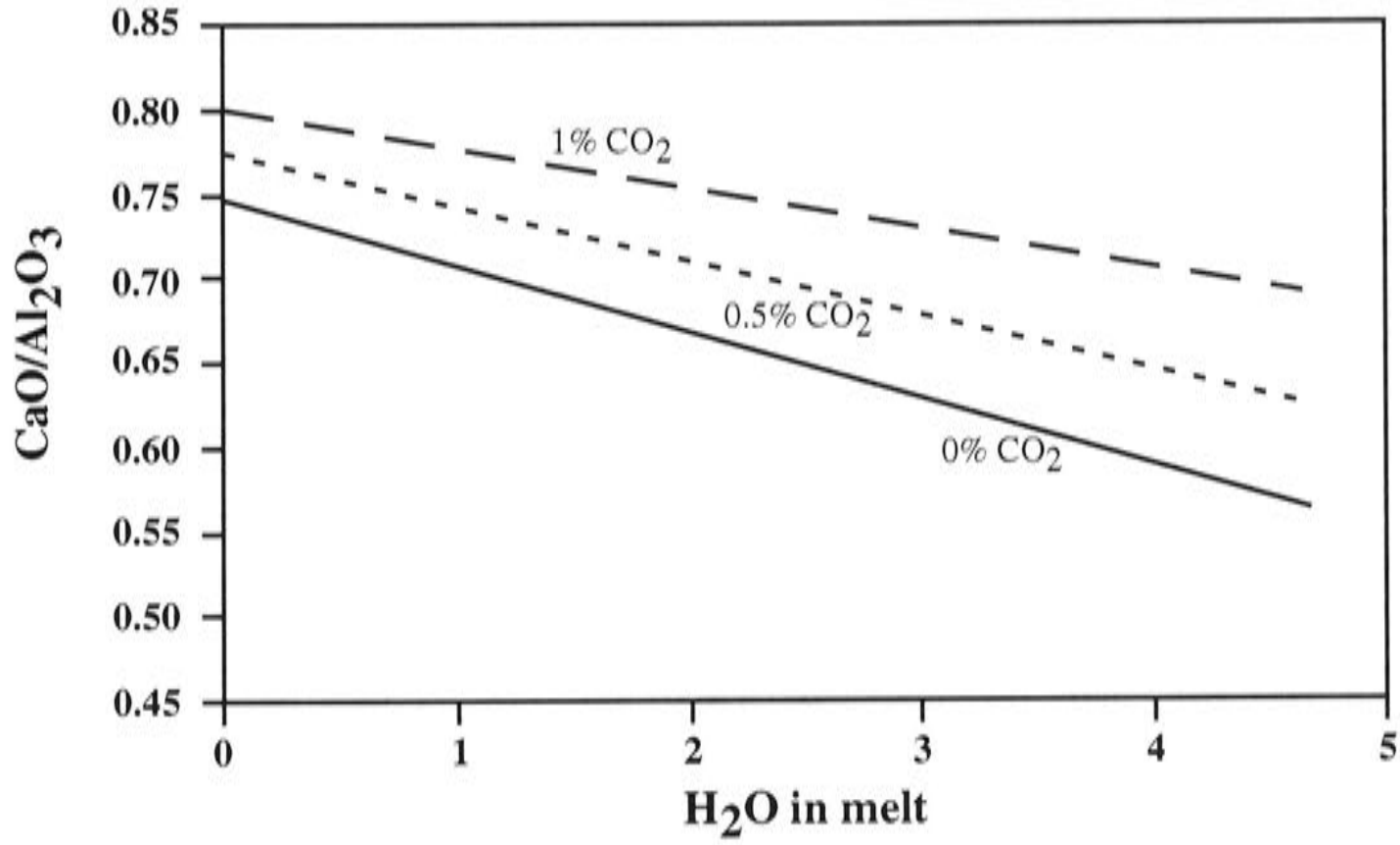

Fig. 19 CaO/Al_2O_3 ratios of the regressed melt compositions at H_2O-dominant conditions (Equation 5 and Table 7).

The CO_2 solubility in the multiply-saturated basaltic melts under hydrous conditions, thus, is directly related to the H_2O content. Previous researches argued that the water solubility in basaltic melt (on a water-containing basis) is in the range of 10-15 wt% at ~ 10 kbar (Sakuyama & Kushiro, 1979; Tatsumi, 1981; Hirose, 1997a).

Adding H_2O not only increases the CO_2 solubility in the multiply-saturated basaltic melts, it also modifies the melt composition. Taking water into account, Fig. 7 in Schiano et al. (2000) needs revision: the MgO content of the experimentally produced anhydrous melt should be reduced while the SiO_2 content and the Al_2O_3 content should be increased (Fig. 12 and Fig. 13). Their arguments on major elements against the CO_2 participation in the petrogenesis of these island-arc melt inclusions, thus, are not supported by my new experimental data.

Mechanism 2

If these melt inclusions from the island-arc region were formed at relatively higher pressures (> 25 kbar?), the second argument against the possible role of CO_2 (i.e.

the solubility limitation) doesn't exist any more. Pressure strongly increases the CO_2 solubility (Blank & Brooker, 1994; Dalton & Presnall, 1998b).

The first argument can also be easily solved. The melt compositions from Dalton & Presnall (1998a), used by Schiano et al. (2000; Fig. 7), are for near solidus melts at 60 kbar; the melt compositions from Hirose (1997b; 30 kbar), however, are not for near solidus melts (Dalton & Presnall, 1998b). It follows that the CO_2 contents in those melts from Dalton & Presnall (1998a) should be much higher (14-45% CO_2) and their compositions should be more severely modified by CO_2. In Fig. 7 of Schiano (2000), a pattern is clearly shown for the content of MgO, SiO_2, Al_2O_3 in the melts, with the melt inclusions from island-arc region locating at one end, the melts from Hirose (1997b) in the middle and the melts from Dalton & Presnall (1998a) at the other end. This simply suggests that these melt inclusions were formed under relatively CO_2-poor conditions at relatively low pressures.

6. Conclusions

The effect of H_2O and CO_2 on the partial melting of a Sp-lherzolite in the system CMAS-H_2O-CO_2 has been successfully studied here. The fluid-detecting technique, FTIR, was applied to analyse the content of H_2O and CO_2 in the melts. The major conclusions are:

1. H_2O has a strong effect on the partial melting temperature while CO_2 has a negligible effect. 1 wt% H_2O depresses the partial melting temperature by ~ 38 degrees.
2. H_2O can strongly affect the melt composition. When the system is CO_2-free and H_2O is treated as a component of the melt, 1 wt% H_2O decreases MgO by 1.49 wt% and CaO by 0.39 wt%, but increases Al_2O_3 by 0.67 wt% and SiO_2 by 0.11%.
3. CO_2 also affects the melt composition. Its effect is much stronger than and generally opposite to that of H_2O: the increase of SiO_2 caused by 5 wt% H_2O, for example, can be fully cancelled by 1 wt% CO_2. The effect of CO_2 on the melt composition, however, is not constant but changes with the H_2O content in the melt. It increases as H_2O increases.
4. H_2O affects the melt property. When the system is fluid-free, the melt is an olivine basalt. As H_2O gradually adds in, the melt gradually becomes Qz-rich and Di-poor. With ~ 1.5 wt% H_2O in the melt, the melt is Qz-normative; with ~ 5 wt% in it, it is very Qz-rich and also corundum-normative.

5. The effect of CO_2 the melt property is much stronger than that of H_2O. A shift of melt composition caused by 5 wt% H_2O can almost be counteracted by 1 wt% CO_2. At CO_2-rich conditions, nepheline-normative melt might be produced.

7. Reference

Allegre, C. J., Staudacher, T. & Sarda, P. (1987). Rare gas systematics: formation of the atmosphere, evolution and structure of the earth's mantle. Earth Planet. Sci. Lett. 81, 127-150.

Baker, M. B. & Stolper, E. M. (1994). Determining the composition of high-pressure mantle melts using diamond aggregates. Geochimica. et. Cosmochimica. Acta 58, 2811-2827.

Blank, J. G. & Brooker, R. A. (1994). Experimental studies of carbon dioxide in silicate melts: solubility, speciation, and stable carbon isotope behaviour. In: Carroll, M. R. & Holloway, J. R. (eds), "Volatiles in magmas". Mineralogical Society of America, Reviews in Mineralogy 30, 157-186.

Bose, K. & Ganguly, J. (1995). Quartz-coesite transition revisited: Reversed experimental determination at 500-1200°C and retrieved thermochemical properties. Am Mineral 80, 231-238.

Bowen, N. L (1928). The evolution of the igneous rocks. Glass Technol 16, 20-24.

Boyd, F. R. & England, J. L. (1960). Apparatus for phase-equilibrium measurements at pressures up to 50 kbar and temperatures up to 1750°C. J. Geophy. Res. 65, 741-748.

Brey, G. P. & Kohler, T. (1990). Geothermobarometry in four-phase lherzolite II: new thermobarometers, and practical assessment of existing thermobarometers. J. Petrol. 31, 1353-1378.

Brooker, R., Holloway, J. R., Hervig, R. (1998). Reduction in piston-cylinder experiments: the detection of carbon infiltration into platinum capsules. Am. Mineral. 83, 985-994.

Budavari, S. (1996). The Merck index: an encyclopedia of chemicals, drugs, and biologicals (12th ed.). Whitehouse Station, N. J. Merck.

Chou, I. M. (198). Permeability of precious metals to hydrogen at 2 kb total pressure and elevated temperatures. Am. J. Sci. 286, 638-658.

Church, B. N. & Johnson, W. M. (1980). Calculation of the refractive index of silicate glasses from chemical composition. Geol. Soc. Am. Bull. 91, 619-625.

Dalton, J. A. & Presnall, D. C. (1998a). The continuum of primary carbonatitic-kimberlitic melt compositions in equilibrium with lherzolite: data from the system CaO-MgO-Al_2O_3-SiO_2-CO_2 at 6 GPa. J. Petrol. 39, 1953-1964.

Dalton, J. A. & Presnall, D. C. (1998b). Carbonatitic melts along the solidus of model lherzolite in the system CaO-MgO-Al_2O_3-SiO_2-CO_2 from 3 to 7 GPa. Contrib. Mineral. Petrol. 131, 123-135.

Eggler, D. H. (1978). The effect of CO_2 upon partial melting of peridotite in the system Na_2O-CaO-Al_2O_3-MgO-SiO_2-CO_2 to 35 kb, with an analysis of melting in a peridotite-H_2O-CO_2 system. Am. J. Sci. 278, 305-343.

Eggler, D. H. & Wendlandt, R. F. (1979). Experimental studies on the relationship between kimberlite magmas and partial melting of peridotite. In: Boyd, F. R. & Meyer, H. O. A. (eds) Kimberlites, diatremes and diamonds: their geology, petrology and geochemistry. Am. Geophys. Union, Washington DC, 330-338.

Falloon, T. J. & Green, D. H. (1988). Anhydrous partial melting of peridotite from 8 to 35 kbar and the petrogenesis of MORB. J. Petrol. Special Issue 379-414.

Falloon, T. J. & Green, D. H. (1989). The solidus of carbonated, fertile peridotite. Earth Planet. Sci. Lett. 94, 364-370.

Falloon, T. J., Green, D. H., Danyushevsky, L. V & Faul, U. H. (1999). Peridotite melting at 1.0 and 1.5 Gpa: an experimental evaluation of techniques using diamond aggregates and mineral mixes for determination of near-solidus melts. J. Petrol. 40, 1343-1375.

Falloon, T. J. & Danyushevsky L. V. (2000). Melting of refractory mantle at 1.5, 2 and 2.5 GPa under anhydrous and H_2O-undersaturated conditions: implications for the petrogenesis of high-Ca boninites and the influences of subduction components on mantle melting. J. Petrol. 41, 257-283.

Falloon, T. J., Danyushevsky, L. V. & Green, D. H. (2001). Peridotite melting at 1 GPa: reversal experiments on partial melt compositions produced by peridotite-basalt sandwich experiments. J. Petrol. 42, 2363-2390.

Fine, G. J. & Stolper, E. M. (1985/1986). Dissolved carbon dioxide in basaltic glasses: concentrations and speciation. Earth Planet. Sci. Lett. 76, 263-278.

Ford, C. E., Russell, D. G., Graven, J. A. & Fisk, M. R. (1983). Olivine-liquid equilibria: temperature, pressure and composition dependence of the crystal/liquid cation partition coefficients for Mg, Fe2+, Ca and Mn. J. Petrol. 24, 256-265.

Gaetani, G. A. & Grove, T. L. (1998). The influence of water on melting of peridotite. Contrib. Mineral. Petrol. 131, 323-346.

Gill, J. B.(1981). Orogenic andesites and plate tectonics. Springer, Berlin Heidelberg New York.

Green, D. H. (1971). Magmatic activity as the major process in the chemical evolution of the earth's crust and mantle. In: Ritsema, A. R. (eds) In the upper mantle. Tectonopys. 13, 47-71.

Green, D. H. (1973). Experimental melting studies on a model upper mantle composition at high pressure under water-saturated and water-undersaturated conditions. Earth Planet Sci. Lett. 19, 37-53.

Green, D. H. (1976). Experimental testing of equilibrium partial melting of peridotite under saturated, high pressure conditions. Can. Mineral. 14, 255-268.

Green, D. H. & Wallace, M. E. (1988). Mantle metasomatism by ephemeral carbonatite melts. Nature 336, 459-462.

Green, D. H. & Falloon, T. J. (1998). Pyrolite: a Ringwood concept and its current expression. In: Jackson, I. (eds), "The Earth's Mantle: its Origin, Structure and Evolution". Cambridge University Press. 311-378.

Green, T. H., Ringwood, A. E. & Major, A. (1966). Friction effects and pressure calibration in a piston-cylinder high pressure-temperature apparatus. J. Geophy. Res. 71, 3589-3594.

Gudfinnsson, G. H. & Presnall, D. C. (2000). Melting behaviour of model lherzolite in the system CaO-MgO-Al_2O_3-SiO_2-FeO at 0.7-2.8 Gpa. J. Petrol. 41, 1241-1269.

Hess, P. C. (1989). Origins of igneous rocks. Harvard Press, Cambridge, MA.

Hibberson, W. O. (1978). High pressure and high temperature techniques as applied to experimental petrology. Science and Technology 15-5, 22-23.

Hirose, K.& Kawamoto, T. (1995). Hydrous partial melting of lherzolite at 1 GPa: the effect of H_2O on the genesis of basaltic magmas. Earth Planet. Sci. Lett. 133, 463-473.

Hirose, K. (1997a). Melting experiments on lherzolite KLB-1 under hydrous conditions and generation of high-magnesian andesitic melts. Geology 25, 42-44.

Hirose, K. (1997b). Partial melt compositions of carbonated peridotite at 3 GPa and role of CO_2 in the alkali-basalt magma generation. Geophys. Res. Lett. 24, 2837-2840.

Hirschmann, M. M., Baker, M. B. & Stolper, E. M. (1998). The effect of alkalis on the silica content of mantle-derived magmas. Geochimi. Cosmochimi. Acta 62 (5), 883-902.

Huang, W. L. & Wyllie, P. J. (1974). Eutectic between wollastonite II and calcite contrasted with thermal barrier in MgO-SiO2-CO2 at 30 kilobars, with applications to kimberlite-carbonatite petrogenesis. Earth Planet. Sci. Lett. 24, 305-310.

Ihinger, P. D., Hervig, R. L. & McMillan, P. F. (1994). Analytical methods for volatiles in glasses. In: Carroll, M. R. & Holloway, J. R. (eds), "Volatiles in magmas". Mineralogical Society of America, Reviews in Mineralogy 30, 67-121.

Ingerson, E. (1960). The water content of primitive granitic magma. Am. Mineral. 35, 806-815.

Jambon, A. (1994). Earth degassing and large-scale geochemical cycling of volatile elements. In: Carroll, M. R. & Holloway, J. R. (eds), "Volatiles in magmas". Mineralogical Society of America, Reviews in Mineralogy 30, 479-517.

Jochum, K. P., Dingwell, D. B., Rocholl, A., Stoll, B., Hofmann, A. W., Becker, S., Besmehn, A., Bessette, D., Dietze, H.-J., Dulski, P., Erzinger, J., Hellebrand, E., Hoppe, P., Horn, P., Janssens, K., Jenner, G. A., Klein, M., McDonough, W. F., Maeetz, M., Mezger, K., Munker, C., Nikogosian, I. K., Pickhardt, C., Raczek, I., Rhede, D., Seufert, H. M., Simakin, S. G., Sobolev, A. V., Spettel, B., Straub, S., Vincze, L., Wallianos, A., Weckwerth, G., Weyer, S., Wolf, D. & Zimmer, M. (2000). The preparation and preliminary characterisation of eight geological MPI-DING reference glasses for in-situ microanalysis. J. Geostand. Geoanaly. 24, 87-133.

Johannes, W., Bell, P. M., Mao, H. K., Boettcher, A. L., Chipman, D. W., Hays, J. F., Newont, R. C., Seifert, F. (1971). An interlaboratory comparison of piston-cylinder pressure calibration using albite-breakdown reaction. Contrib. Mineral. Petrol. 32:24-38.

King, P. L. & Holloway, J. R. (2002). CO_2 solubility and speciation in intermediate (andesitic) melts: the role of H_2O and composition. Geochimi. Cosmochimi. Acta 66 (9), 1627-1640.

King, P. L., Vennemann, T. W., Holloway, J. R., Hervig, R. L., Lowenstern, J. B. & Forneris, J. F. (2002). Analytical techniques for volatiles: a case study using intermediate (andesitic) glasses. Am. Mineral. 87, 1077-1089.

Klemme, S. & O'Neill, H. St. C. (1997). The reaction $MgCr_2O_4 + SiO_2 = Cr_2O_3 + MgSiO_3$ and the free energy of formation of magnesiochromite ($MgCr_2O_4$). Contrib. Mineral. Petrol. 130, 59-65.

Kogiso, T. & Hirschmann, M. M. (2001). Experimental study of clinopyroxenite partial melting and the origin of ultra-calcic melt inclusions. Contrib. Mineral. Petrol. 142, 347-360.

Kohler & Brey (1990). Calcium exchange between olivine and clinopyroxene calibrated as a geothermometer for natural peridotites from 2 to 6 kb with applications. Geochimi. Cosmochimi. Acta 54, 2375-2388.

Kushiro, I., Yoder, H. S. & Nishikawa, M. (1968a). Effect of water on the melting of enstatite. Bull. geol. Soc. Am. 79, 1685-1692.

Kushiro, I., Syono, Y. & Akimoo, S. (1968b). Melting of a peridotite nodule at high pressures and high water pressures. J. Geophys. Res. 73, 6023-6029.

Kushiro, I. (1969). The system forsterite-diopside-silica with and without water at high pressures. Am. J. Sci. 267A, 269-294.

Kushiro, I. (1972). Effect of water on the composition of magmas formed at high pressures. J. Petrol. 13, 311-334.

Kushiro, I. & Roder, H. S. (1972). Origin of calc-alkalic peraluminous andesite and dacites. Yb. Carnegie Instn. Wash. 71, 411-413.

Kushiro, I., Shimizu, N., Nakamura, Y. & Akimoto, S. (1972). Compositions of coexisting liquid and solid phases formed upon melting of natural garnet and spinel lherzolites at high pressures: a preliminary report. Earth Planet. Sci. Lett. 14, 19-25.

Kushiro, I. (1975). On the nature of silicate melt and its significance in magma genesis: regularities in the shift of the liquids boundaries involving olivine, pyroxene, and silica minerals. Am. J. Sci. 272, 411-431.

Kushiro, I. (1990). Partial melting of mantle wedge and evolution of island arc crust. J. Geophys. Res. 95, 15929-15939.

Libourel, G. (1999). Systematics of calcium partitioning between olivine and silicate melt: implications for melt structure and calcium content of magmatic olivines. Contrib. Mineral. Petrol. 136, 63-80.

Liu, T. C. & Presnall, D. C. (1990). Liquidus phase relationships on the join anorthite-forsterite-quartz at 20 kbar with applications to basalt petrogenesis and igneous sapphirine. Contrib. Mineral. Petrol. 104, 735-742.

McMillan, P. F. (1994). Water solubility and speciation models. In: Carroll, M. R. & Holloway, J. R. (eds), "Volatiles in magmas". Mineralogical Society of America, Reviews in Mineralogy 30, 131-156.

Muntener, O., Kelemen, P. B. & Grove, T. L. (2001). The role of H_2O during crystallization of primitive arc magmas under uppermost mantle condition and genesis of igneous pyroxenites: an experimental study. Contrib. Mineral. Petrol. 141, 643-658.

Mysen, B. O., Kushiro, I., Nicholls, I. A. & Ringwood, A. E. (1974). A possible mantle origin for andesitic magmas: discussion of a paper by Nicholls and Ringwood. Earth Planet. Sci. Lett. 21, 221-229.

Mysen, B. O. & Boettcher, A. L. (1975a). Melting of a hydrous mantle. I. Phase relations of natural peridotite at high P and T and with controlled addition of water, carbon dioxide and hydrogen. J. Petrol. 16, 520-548.

Mysen, B. O. & Boettcher, A. L. (1975b). Melting of a hydrous mantle. II. Geochemistry of crystals and liquids formed by anatexis of mantle peridotite at high pressure and high temperature as a function of controlled activities of water, hydrogen and carbon dioxide. J. Petrol. 16, 549-593.

Mysen, B. O., Eggler, D. H., Seitz, M. G. & Holloway, J. R. (1976). Carbon dioxide in melts of andesite, tholeiite, and olivine nephephinite composition to 30 kb pressure. Contrib. Mineral. Petrol. 53, 227-239.

Mysen, B. O. (1976). The role of volatiles in silicate melts: solubility of carbon dioxide and water in feldspar, pyroxene, and feldspathoid melts to 30 kb and 1625°C. Am. J. Sci. 276, 969-996.

Nicholls, I. A. & Ringwood, A. E. (1972). Production of silicate-saturated tholeiitic magmas in island arcs. Earth and Planet. Sci. Lett. 17, 243-246.

Nicholls, I. A. & Ringwood, A. E. (1973). Effect of water on olivine stability in tholeiites and production of silica-saturated magmas in the island arc environment. J. Geol. 81, 285-306.

Nickel, K. G., Brey, G. P. & Kogarto, L. (1985). Orthopyroxene-clinopyroxene equilibria in the system CaO-MgO-Al_2O_3-SiO_2. Contrib. Mineral. Petrol. 91, 44-53.

O'Hara, M. J. (1965). Primary magmas and the origin of basalts. Scott. J. Geol 1, 19-40.

O'Neill, H. St. C. & Palme, H. (1998). Compositions of the Silicate Earth: Implications for accretion and core formation. In: Jackson, I. (eds) "The Earth's Mantle: Composition, Structure and Evolution", 3-126. Cambridge University Press. Cambridge.

Pan, V., Holloway, J. R. & Hervig, R. L. (1991). The pressure and temperature dependence of carbon dioxide solubility in tholeiitic basalt melts. Geochimica. et. Cosmochimica. Acta 55, 1587-1595.

Pawley, A. R., Holloway, J. R. & McMillan, P. F. (1992). The effect of oxygen fugacity on the solubility of carbon-oxygen fluids in basaltic melt. Earth Planet. Sci. Lett. 110, 213-225.

Pichavant, M., Mysen, B. O. & Macdonald, R. (2002). Source and H2O content of high-MgO magmas in island arc settings: An experimental study of a primary calc-alkaline basalt from St. Vincent, Lesser Antillers arc. Geochimica et Cosmochimica Acta 66: 2193-2209.

Presnall, D. C., Dixon, S. A., Dixon, J. R., O'Donnell, T. H., Brenner, N. L., Schrock, R. L. & Dycus, D. W. (1978). Liquidus phase relations on the joint diopside-forsterite-anorthite from 1 atm. to 20 kbar: their bearing on the generation and crystallization of basaltic magma. Contrib. Mineral. Petrol. 66, 203-220.

Presnall, D. C., Dixon, J. R., O'Donnell T. H. & Dixon, S. A. (1979). Generation of mid-ocean ridge tholeiites. J. Petrol. 20, 3-36.

Presnall, D. C. & Hoover, J. D. (1987). High pressure phase equilibrium constraints on the origin of mid-ocean ridge basalts. In: Mysen, B. O. (ed.), "Magmatic Processes: Physicochemical Principles". Geochemical Soc. Spec. Pub. 1, 75-89.

Ringwood, A. E. (1975). Composition and petrology of the Earth's mantle. McGraw-Hill, New York.

Ringwood, A. E. (1982). Phase transformations and differentiation in subducted lithosphere: implications for mantle dynamics, basalt petrogenesis, and crustal evolution. J. Geol. 90, 611-643.

Ringwood, A. E., Kesson, S. E., Hibberson, W. & Ware, N. (1992). Origin of kimberlites and related magmas. Earth Planet. Sci. Lett. 113, 1746-1782.

Robinson, J. A. C., Wood, B. J. & Blundy, J. D. (1998). The beginning of melting of fertile and depleted peridotite at 1.5 Gpa. Earth Planet. Sci. Lett. 155, 97-111.

Rubey, W. W. (1951). Geological history of sea water: an attempt to state the problem. Geol. Soc. Am. Bull. 62, 1111-1147.

Sakuyama, M. & Kushiro, I. (1979). Vesiculation of hydrous andesitic melt transport of alkalis by separated vapor phase. Contrib. Mineral. Petrol. 71, 61-66.

Schiano, P., Eiler, J. M., Hutcheon, I. D. & Stolper, E. M. (2000). Primitive CaO-rich, silica-undersaturated melts in island arcs: evidence for the involvement of clinopyroxene-rich lithologies in the petrogenesis of arc magmas. Geochem. Geophys. Geosys., 1:1999GC000032.

Schmidt, M. W. & Poli, S. (1998). Experimentally based water budgets for dehydrating slabs and consequences for arc magma generation. Earth Planet. Sci. Lett. 163, 361-379.

Scholze (1959). Der Einbau des Wassers in Galsern. Glastech Ber 32, 81-88, 142-145 and 278-281.

Sen, G. & Presnall, D. C. (1984). Liquidus phase relationships on the join anorthite-forsterite-quartz at 10 kbar with applications to basalt petrogenesis. Contrib. Mineral. Petrol. 85, 404-408.

Sisson, T. W. & Grove, T. L. (1993). Experimental investigations of the role of H2O in calc-alkaline differentiation and subduction zone magmatism. Contrib. Mineral. Petrol. 113, 143-166.

Stolper, E. M. (1982a). The speciation of water in silicate melts. Geochim. Cosmochim. Acta 46, 2609-2620.

Stolper, E. M. (1982b). Water in silicate glasses: an infrared spectroscopic study. Contrib. Mineral. Petrol. 81, 1-17.

Stolper, E. M. & Holloway, J. R. (1988). Experimental determination of the solubility of carbon dioxide in molten basalt at low pressure. Earth Planet. Sci. Lett. 87, 397-408.

Tatsumi, Y. (1981). Melting experiments on a high-magnesian andesite. Earth Planet. Sci. Lett. 54, 357-365.

Taylor, W. R. & Green, D. H. (1988). Measurement of reduced peridotite-C-O-H solidus and implications for redox melting of the mantle. Nature 332, 239-352.

Taylor, W. R. & Green, D. H. (1989). The role of reduced C-O-H fluids in mantle partial melting. In: Ross, J. (eds), "Kimberlites and related rocks-their occurrence, origin and emplacement 1", 592-602.

Ulmer, P. (2001). Partial melting in the mantle wedge - the role of H_2O in the genesis of mantle-derived 'arc-related' magmas. Physics of the Earth and Planetary Interiors 127, 215-232.

Wallace, M. E. & Green, D. H. (1988). An experimental determination of primary carbonatite magma composition. Nature 335, 343-346.

Walter, M. J. & Presnall, D. C. (1994). Melting behaviour of simplified lherzolite in the system $CaO-MgO-Al_2O_3-Na_2O$ from 7 to 35 kbar. J. Petrol. 35, 329-359.

Ware, N. G. (1991). Combined energy-dispersive-wavelength-dispersive quantitative electron microprobe analysis. X-ray Spectrometry 20, 73-79.

Warner, R. D. (1973). Liquidus relations in the system CaO-MgO-SiO_2-H_2O at 10 kb PH_2O and their petrologic significance. Am. Jour. Sci. 273, 925-946.

Watson, E. B., Sneeringer, M. A. & Ross, A. (1982). Diffusion of dissolved carbonate in magmas: experimental results and applications. Earth Planet. Sci. Lett. 61, 346-358.

Watson, E. B. (1987). Diffusion and solubility of C in Pt. Am. Mineral. 72, 487-490.

Wohletz, K. (1996). Magma2: an estimation of magma physical and chemical properties with IUGG classification. The University of California.

Wyllie, P. J. & Huang, W. L. (1976). Carbonation and melting reactions in the system CaO-MgO-SiO_2-CO_2 at mantle pressures with geophysical and petrological applications. Contrib. Mineral. Petrol., 54, 79-107.

Wyllie, P. J. (1977). Mantle fluid compositions buffered by carbonates in peridotite-CO_2-H_2O. J. Geol. 85, 187-207.

Yoder, H. S. & Tilley, C. E. (1962). Origin of basalt magmas: an experimental study of natural and synthetic rock systems. J. Petrol. 3, 342-532.

Yoder, H. S. (1971). The join diopside-pyrope-H_2O at 10 kb: its bearing on the melting of peridotite, the ACF metamorphic facies, and the gedrite-hornblende miscibility gap. Yb. Carnegie Instn. Wash. 69, 176-181.

Zhang, Y. & Zindler, A. (1993). Distribution and evolution of carbon and nitrogen in Earth. Earth Planet. Sci. Lett. 117, 331-345.

Chapter 5

Conclusions and future work

1. Conclusions of this thesis

1.1 Partial melting study in the system CMAS±K_2O

In this study, I have developed a new experimental method (the K_2O method) which can be used to determine isobarically invariant/pseudo-invariant solidus temperature and solidus melt composition. This method, when applied to the system CMAS at 11 kbar, gives a solidus temperature and solidus phase compositions in agreement with most literature data. Reversal experiments with and without the addition of Ol justify this new approach.

The effect of K_2O on the composition of the melt generated by partial melting of a Sp-lherzolite in the system CMAS+K_2O at 11 kbar is to increase SiO_2 and Al_2O_3 but decrease MgO and CaO. Thus, the effect of K_2O on the melt composition is in the same direction to that of Na_2O, but it is much stronger. Like Na_2O, K_2O also depresses the solidus, but to a greater extent. Despite these similarities between the effects of K_2O and Na_2O, there are differences: K_2O decreases the Di component of the melt while Na_2O has not any apparent effect; K_2O makes the melt Qz-normative while Na_2O makes it Ne-normative; K_2O can make the melt corundum-normative while Na_2O can not. Hence, the role of K_2O and Na_2O in changing the melt property is significantly different, in disagreement with traditional views.

The partial melting reaction of a Sp-lherzolite in the system CMAS+K_2O is always peritectic. At high temperatures, Ol is the only phase in reaction relationship with melt while it is joined by Sp at low temperatures. At high temperatures, Cpx is the largest contributor to the melt-generating process but is overtaken by Opx at low temperatures.

1.2 Partial melting study in the system CMAS-Cr_2O_3

The effect of Cr_2O_3 on the partial melting of a Sp-lherzolite in the system CMAS-Cr_2O_3 has been studied successfully. The experimental technique (the K_2O method), designed and justified in the study in the system CMAS ± K_2O, was applied here. This

method helps to broaden the temperature interval of the phase assemblage Ol+Sp+Opx+Cpx+Melt and to make the melt quenchable. An external Fe_2O_3 sleeve was used in these experiments to minimise both the hydrogen fugacity and the likelihood of possible redox reaction which may convert Cr^{3+} to Cr^{2+} or even chromium metal.

During the partial melting process Cr_2O_3 tends to retain in the solid phases and the distribution coefficient of Cr_2O_3 is 0.84 between Ol and Melt, 165.8 between Sp and Melt, 7.2 between Opx and Melt, and 8.7 between Cpx and melt. Hence, Cr_2O_3 is highly compatible in the early stages of the partial melting of a Sp-lherzolite but becomes incompatible when all Sp, Opx and Cpx in the source are about to melt out during the late stages of the partial melting.

Cr_2O_3 increases the solidus in a complicated way: the temperature increase is very strong at low Cr_2O_3 contents, relatively weak at median Cr_2O_3 contents and strong again at high Cr_2O_3 contents.

The temperature increase caused by Cr_2O_3 provides us a unique opportunity to assess the relationship of pyroxenes at high temperatures. The result suggests that low Ca-Cpx and high Ca-Cpx can not coexist in the system CMAS-Cr_2O_3 at 11 kbar and the stable pyroxene assemblage at high temperature is Opx and a supercritical Cpx, the latter decreasing its Ca content rapidly but continuously with increasing temperature.

Cr_2O_3 also changes the melt composition. It substantially decreases the Al_2O_3 content but strongly increases the MgO content. It increases the SiO_2 content at a relatively weaker level. Its effect on the CaO content, however, is negligible. As Cr_2O_3 increases, thus, the CaO/Al_2O_3 ratio of the melt increases sharply and the melt progressively becomes more Di-normative. Another interesting effect of Cr_2O_3 on the melt composition is that a small amount of Cr_2O_3 makes the melt Qz-normative but more Cr_2O_3 does not make the melt more Qz-normative. Instead, the melt moves towards Hy and remains only marginally Qz-normative.

The excellent agreement (high SiO_2, high CaO/Al_2O_3, high Di component and Hy-normative) between the experimentally produced melts at high Cr_2O_3 conditions in the system CMAS-Cr_2O_3 and the melt inclusions in Sp and Ol from mid-ocean ridge basalt and oceanic island basalt suggests that the upper mantle from which magma is generated is very refractory. The much lower Di component of the most primitive melts assembled by Presnall & Hoover (1987) possibly indicate that these melts might have been modified by high pressure fractional crystallisation of Cpx. The much lower Di component of the experimentally produced melts using natural rock compositions in the

literature, however, suggests that the used starting compositions are too fertile (poor in Cr_2O_3).

1.3 Partial melting study in the system CMAS-H_2O-CO_2

Numerous experiments have been carried out to study the effect of H_2O and CO_2 on the partial melting process of the upper mantle. Due to the complex inherited in this kind of experiments, the difficulty of determining the volatile contents of small samples, the H_2O and CO_2 contents of the product melts were unknown and the effects of these volatiles could not be fully determined or parameterised.

In this study electron microprobe and Fourier transform infrared spectroscopy were used to analyse the melt for all components, producing the first complete set of melt compositional data. Hence, the effect of H_2O and CO_2 on partial melting of a Sp-lherzolite can be assessed.

H_2O decreases the partial melting temperature sharply: 1 wt% H_2O reduces it by ~ 38 degrees. CO_2, however, does not have any apparent effect.

The effect of H_2O on melt composition is 1 wt% H_2O decreases MgO by 1.49 wt% and CaO by 0.39 wt%, but increases Al_2O_3 by 0.67 wt% and SiO_2 by 0.11%. With this effect, high H_2O should make melt corundum-normative and quartz normative. The speculation in the literature that H_2O-saturated melt should be nepheline normative is thus not supported by the result here.

The effect of CO_2 on melt composition is much stronger than and generally opposite to that of H_2O: the increase of SiO_2 caused by 5 wt% H_2O, for example, can be fully cancelled by 1 wt% CO_2. The effect of CO_2 on the melt composition, however, is not constant but changes with the H_2O content of the melt. It increases as H_2O increases. At CO_2-rich conditions, nepheline-normative melt might be produced.

The strong effect of CO_2 on melt composition casts doubt on partial melting studies using natural rock compositions in the literature. In these studies, inner graphite capsule was used and considerable amount of CO_2 might be present in the melts and modify the melt composition. Since the effect of CO_2 on melt composition increases as H_2O increases, the problem would be more severe under hydrous conditions.

2. Future work

This work, having produced important and valuable knowledge, has been carried out only at 11 kbar. It is apparent that another study at different pressures is necessary in order to reveal how pressure functions.

With the completion of this study, TiO_2 is the only component that remains unstudied but abundant enough to exert important influence on the partial melting process of the upper mantle. An experimental study on the partial melting behaviour of a lherzolite phase assemblage in the system CMAS+TiO_2 is therefore desirable.

Other important research directions suggested by this study include experimental evaluation of the diamond aggregate method in the system CMAS and determination of the effect of H_2O on the solubility of CO_2 in basaltic melt buffered by a lherzolite phase assemblage.